Ab Initio Computational Methodologies for Investigation of Excited State Processes: Structural-Functional Relations in Electron Transfer Reactivity in Organic Molecules

---

Dissertation

for

the partial fulfillment of the requirements for
a natural sciences doctorate
(Dr. sc. nat.)

presented by

the Mathematics and Natural Sciences Department

of the

Universität Zürich

by

Limor Shenar-Jackson

from

Ireland

Doctoral Committee

Prof. Dr. Kim Baldridge (Principal Investigator)
Prof. Dr. Jay Siegel
Prof. Dr. Peter Hamm

Zürich, 2016

Ab Initio Computational Methodologies for Investigation of Excited State Processes: Structural-Functional Relations in Electron Transfer Reactivity in Organic Molecules

---

Dissertation

zur

Erlangung der naturwissenschaftlichen Doktorwürde
(Dr. sc. nat.)

vorgelegt der

Mathematisch-naturwissenschaftlichen Fakultät

der

Universität Zürich

von

Limor Shenar-Jackson

aus

Irland

Promotionskomitee

Prof. Dr. Kim Baldridge (Vorsitz)
Prof. Dr. Jay Siegel
Prof. Dr. Peter Hamm

Zürich, 2016

Abstract

Electron transfer (ET) is one of the most fundamental and important chemical reaction processes, with applications spanning from organic optoelectronic devices on the one hand, to important fundamental biological processes on the other. Electron transfer (ET) reactivity may be described in terms of donor-bridge-acceptor (DBA) systems, in which a donor and acceptor orbitals, or states, are coupled to one another through a series of bridge states. As such, a detailed understanding of through space and through bond interactions components of the electronic coupling interactions for bridge-mediated systems, as well as their influences on the electron tunneling pathways and transfer integrals, greatly facilitates the understanding of the mechanistic aspects of the ET process. Over the last decades, great interest has emerged in the in-depth clarification of the mechanisms of electron transfer, and the factors that control the reaction rates, thereby motivating more robust and reliable theoretical methods for applications in this area. Theoretical models have become important tools contributing to details of the electron transfer process not available to experimental studies. As well, quality experimental measurements provide feedback for the development of more accurate theoretical models. In this work, motivated by shortcomings of methods based on more traditional LR-TDDFT approaches, a new charge-constraint C-DFT first-principles methodology has been implemented into the *ab initio* computational suite GAMESS, for the calculation of the electronic coupling between donor and acceptor states of organic molecular systems with electron transfer reactivity. The C-DFT methodology is developed using direct diabatic states construction. Through the development and associated validation, it is demonstrated that, with careful partitioning and choice of donor, acceptor, and spacer, the effective Hamiltonian is able to form diabats with localized molecular orbitals, representing the constraints in demand. The methods and implementations are demonstrated on model organic donor-acceptor systems, which provide a systematic comparison for through bond and through space interactions associated with electron transfer mechanisms. Calculated electronic coupling and associated decay attenuation factor results are shown to meet experimental expectations for bridgeless systems as well as for bridge-mediated systems, including saturated and unsaturated bridges. This methodology provides the necessary underlying ability for better understanding of the details of the rate process in ET reactions, which ultimately aid in the development of future applications.

Zusammenfassung

Elektronentransferreaktionen zählen zu den grundlegenden und wichtigsten chemischen Reaktionen. Sie finden sich in der ganzen Bandbreite wieder, die von optoelektronischen Bauteilen auf Basis organischer Moleküle bis zu grundlegenden biologischen Prozessen, wie etwa der Photosynthese, reicht.
Elektronentransfermechanismen lassen sich als eine Donor-Brücke-Akzeptor-Kette auffassen. Ein Donor und ein Akzeptor Orbital sind über eine Reihe von verbrückenden (Energie-)zuständen verbunden. Für ein tieferes Verständnis der Elektronentransferreaktion und ihres Mechanismus ist daher entscheidend, die Wechselwirkung der Elektronen sowohl durch den Raum als auch über die Bindungen des Brückensystems zu kennen, ebenso wie Tunneling-Pfade und die Kopplung zwischen den Elektronen (transfer integral). In den letzten Jahrzenten wuchs das Interesse an einer tiefschürfenden und genauen Beschreibung der Elektronentransferreaktion und ihrer Reaktionskinetik, was die Entwicklung von zuverlässigen und stabilen theoretischen Modellen anstiess. Solche Modelle geben auch Aufschluss zu experimentell nicht zugängliche Zwischenschritten. Im Gegenzug konnten präzise Messungen die theoretischen Modelle weiter verbessern. Die vorliegende Arbeit versucht vorhandene Schwächen des traditionellen LR-TDDFT Ansatzes zu überwinden. Dazu wurde eine «charge-constraint C-DFT first-principle» Methode entwickelt und in das ab-initio Softwarepaket «GAMESS» implementiert. Sie berechnet die Elektronen-Kopplung zwischen den Donor und Akzeptor-Zuständen eines organischen Moleküls, welches zu Elektronentransferreaktionen fähig ist. Die Methode basiert auf der Einführung direkter diabatischer Zustände.

Die Entwicklung und die damit einhergehende Validierung zeigen, dass die effektive Hamilton-Funktion, nach sorgfältiger Partitionierung des Systems in Donor-, Akzeptor- und Spacerkomponenten, mit lokalisierten Molekülorbitalen diabatische Zustände bildet und dadurch die erforderlichen Randbedingungen hervorbringt.

Ausarbeitung und Implementation der Methode wurde anhand von organischen donor-akzeptor Modellverbindungen verifiziert, welche einen systematischen Vergleich der Wechselwirkungen durch den Raum als auch über die Bindung in Zusammenhang mit dem Elektronentransfermechanismus erlauben. Die berechneten

Elektronen-Kopplungseffekte und zugehörigen Dämpfungsfaktoren stimmen mit experimentell erwarteten Werten überein. Das betrifft nicht verbrückte ebenso wie verbrückte Systeme, wobei die Brückenglieder gesättigte wie ungesättigte Bindungen enthalten können. Die erarbeitete Methode erhellt, die Details, die der Elektronentransferreaktion zugrunde liegen.

Table of Contents page

1. Introduction

1.1 Challenges

The superior accuracy-to-cost ratio of density functional theory (DFT) has made it a method of choice for practical calculations. The formulation of linear-response time-depended DFT (LR-TDDFT) for obtaining excited-states laid the groundwork for excited states applications in organic compounds and transition metal complexes.[1] However traditional functionals in DFT and also in LR-TDDFT suffer from self-interaction error (SIE), which result in erroneous delocalization or in some cases localization of the density. These errors are responsible for some failures of properties such as energies and structures of long-ranged-charge separated states. Therefore, LR-TDDFT approach may work well for some types of excited states than for others. For instance, LR-TDDFT calculations tend to underestimate the energies of charge-transfer excitations, and they fail in double excitations.[1,2] This project's central aim is addressing these shortcomings without affecting the favorable accuracy-to-cost ratio.

1.2 Project aims

In this thesis, shortcomings of LR-TDDFT have motivated consideration of directions in constrained density functional theory (C-DFT). This thesis reports on the effort of creating from scratch a complete C-DFT program within the context of the computational chemistry package, GAMESS[3]. As a primary focus, all code implementation is carried out with considerations of efficiency and optimization in mind. The constrained density functional theory (C-DFT) is applicable to all calculations of excited states involving all available density functionals in the code. The theory takes advantage of the underlying Kohn-Sham (KS) SCF procedure as a platform for diabatic electronic states.

The implementation of C-DFT code into GAMESS[3] is done completely from scratch, resulting in a new version of GAMESS with code integrated into a standard version, which will be available for the public to use. For practical calculations, the new C-DFT implementation capabilities are validated on various test systems as well as research systems. Capabilities include the ability to carry out single point energy calculations at a defined geometry, and for both closed shell systems (paired electrons) as well as for open shell systems (not all electrons are paired). Careful considerations of smooth and efficient convergence capabilities are addressed via both economical methods (e.g., Newton's method of optimization) as well as with possible convergence accelerators.

The primary aims of this project include the following:

Aim 1: Implement from scratch a charge C-DFT code into the quantum chemistry code, GAMESS. This will be carried out in stages as follows:
   a) Single closed shell electron SCF for energetics and properties.
   b) Open shell SCF for energy and properties.

Aim 2: Enable inclusion of solvation in the model.

Aim 3: Enable inclusion of various orbital localization schemes.

Aim 4: Considerations for code efficiency and optimization.

Aim 5: Validation of results for energy and charge distribution for test sets.

Aim 6: Implement a component for calculating electronic coupling matrix element between two diabatic states utilizing output information from C-DFT code.

Aim 7: Validation of electron-transfer Marcus theory parameters, in particular, electronic coupling matrix element values.

2. Background

2.1 Constrained Density Functional Theory (C-DFT)

The Constrained Density Functional Theory methodology capability is the primary focus of this work. This C-DFT method is a density functional theory (DFT) based approach that will enable investigation of diabatic states with applications in electron transfer theory. The method is programmed into the computational chemistry program General Atomic Molecular Electronic Structure Systems, GAMESS[3], which our group develops and supports. In what follows, the fundamental principles of DFT and C-DFT will be highlighted to the extent important for the development of the new theory, including a discussion of the Self-Interaction Error, which is a fundamental issue when considering these DFT-based theories for investigations of excited states.

2.1.1 Fundamental Principles of DFT

Density functional theory (DFT) is a theoretical approach amenable to static electronic many-body problems. The exceptional balance between accuracy and low computational cost has led to a steady growth in popularity of DFT to the point of being the method of choice for practical calculations.

The main idea of DFT involves description of a molecular system via its density and not via its many-body wave function. According to the **first Hohenberg-Kohn theorem**, there is one-to-one correspondence between the potential and the ground-state electron

density. Thus it asserts that any property of the system of interacting particles can be viewed as a functional of the ground state density *ρ(r)*. Within the framework of Kohn-Sham (KS) DFT, the many-body problem of interacting electrons is reduced to a problem of fictitious non-interacting electrons moving in an effective potential. The non-interacting system is constructed in such a way, that its density is the same as that of the interacting electrons.

The total energy of the interacting many-body system can be expressed by

$$E[\rho] = 2\sum_{i}^{N/2}\langle\phi_i| -\frac{1}{2}\nabla^2|\phi_i\rangle + \int dr\, v_n(r)\rho(r) + J[\rho] + E_{XC}[\rho] \quad (1)$$

where the first term describes the electronic kinetic energy. The other three terms represent the electron-nuclear attraction (external potential), coulomb energy, and exchange-correlation energy, respectively.

The second **Hohenberg-Kohn theorem** asserts that there exists a Variational principle for the above energy expression, thus the exact ground-state density is found by minimization of the energy functional

$$E_0 = \min_{\rho}\big[E[\rho(r)]\big] \quad (2)$$

2.1.2 Fundamental Principles of C-DFT

Constrained-DFT is based on time-independent ground state DFT. This focus of this method is on a system whose ground-state density is forced to satisfy some specific constraint(s). This enables the user to impose a charge or a spin density on a group of atoms, while the constrained electronic ground state can be identified with the diabatic states. A diabatic state is an electronic state that does not change character as a function of molecular geometry, [4] in contrast to the adiabatic, or Born-Oppenheimer electronic states. The significant role of the diabatic state will be discussed more extensively below.

Recently a C-DFT approach was proposed by Wu and Van Voorhis, [5] which relies on the addition of an external potential to the usual KS potential. This external potential leads to a constrained electronic ground state. The charge constraint is defined as the integral of the electron density multiplied by a weight function that specifies the region of interest

$$\int w_c(r)\rho(r)d^3r = N_c \quad (3)$$

Accomplishing the constrained electronic ground state relies on the addition of an external potential to the usual KS, using the Lagrange multiplier scheme for optimization as,

$$W[\rho, V_c] = E[\rho] + V_c(\int w_c\,(r)\rho(r)d^3r - N_c) \quad (4)$$

where V_c is the Lagrange multiplier to enforce the constraint, which is unique for a given constraint. Furthermore, $W(V_c)$ is a concave function of V_c, with stationary point when the first derivative (Eqn. 5) is zero, which restores the constraint of Equation 3, and the second derivative (Eqn. 6) is nonpositive. As in the KS scheme, the occupied orbitals are chosen as the lowest eigenstates, thus $\epsilon_i - \epsilon_a < 0$. This implies that the function is at a maximum

$$\frac{dW}{dV_c} = \int w_c\,(r)\rho(r)d^3r - N_c \quad (5)$$

$$\frac{\partial^2 W}{\partial^2 V_c} = 4\ \sum_i^{occ} \sum_a^{unocc} \frac{\langle\phi_i|w_c|\phi_a\rangle^2}{\epsilon_i - \epsilon_a} \leq 0 \quad (6)$$

Accordingly, the desired solution is a minimum with respect to the density and a maximum with respect to V_c:

$$E = \min_\rho \max_{v_c} [E[\rho(r)] + V_c(\int w_c\,(r)\rho(r)d^3r - N_c)] \quad (7)$$

2.1.3 Self-Interaction Error (SIE) in DFT

In Hartree-Fock theory, the form of the many-particle Hamiltonian is such that an electron does not interact with itself. The self-interaction term included by the Coulomb potential is exactly cancelled out by a similar term in the exchange potential. In DFT, on the other hand, the exchange term is represented by one of a variety of developed exchange functionals, but only in an approximated way. In this way, the Coulomb self-interaction and exchange self-interaction of an electron do not cancel each other exactly, leading to a self-interaction error. The SIE results in density localization errors, in general leading to increased charge delocalization, and is believed to be the origin of many qualitative and quantitative failures in DFT calculations. Such failures include, for example, poor description of charge transfer, inaccuracies of binding energies, underestimation of activation energy barriers, and inaccuracies of band gaps of solids. [1,4]

Strategies for addressing the SIE can be roughly grouped into the following categories [1]:

(1) Design of better approximations to the exact density functional.

(2) The use of other *ab initio* techniques other than DFT. However, other *ab initio* techniques that also include the ability to treat weak interactions, are typically computationally demanding especially for the size systems that one would like to deal with in electron transfer theory.

(3) Develop new DFT-based methodologies on top of existing DFT traditional functionals, which also manage the known SIE shortcomings.

(4) Use of a combination of standard DFT methods with *ab initio* methods for hybrid methods that can avoid the SIE.

Approaches to reduce the self-interaction error by designing density functionals, (1), are known as self-interaction correction (SIC) methods.[5] The first self-interaction correction method was proposed by Perdew and Zunger[6], where the self-interaction is corrected on an orbital by orbital basis.[78] Even though the Perdew and Zunger SIC method significantly improves the Kohn-Sham eigenvalues for molecules, the scheme is computationally demanding and tends to significantly decrease reliability of thermochemistry and sometimes geometries.[54] Several other attempts to correct for the presence of self-interaction have been suggested, including for example the development of the B05[9] and MCY[10] density functionals, which contain 100% exact exchange, and a scheme recently proposed by d'Avezac, Calandra, and Mauri [11] for systems with a single unpaired electron. In this latter scheme, a correction is applied only to the singly occupied orbital within a restricted open shell calculation. Unfortunately, no fully satisfactory scheme has yet emerged to solve the problem of SIE. [54,78]

The present thesis effort focuses on the development of an accurate C-DFT method. Because the C-DFT method is based on the underlying density functional that is applied, the method will inherently have issues of SIE coming from the third category, (3), listed above. Of particular interest, however, the C-DFT method in general offers a means of managing some of the detrimental effects of the SIE error.[1] In C-DFT, the specified constraints imposed on the density enforce charge localization and thereby inherently minimize the charge delocalization associated with the SIE. In fact, the C-DFT methodology provides a direct route to diabatic electronic states, enabling construction of physically motivated effective Hamiltonians for a variety of problems for which a truly satisfactory XC functional does not yet exist.

3. Perspective of this Project

Much effort has been extended in the last decade towards achieving accurate predictions of electronic coupling and mechanistic details in bridge-mediated electron transfer (ET) reactions. Of prime interest are models based on quantum mechanical (QM) and density functional theory (DFT) schemes. For large systems and associated reaction processes, directions have turned towards the latter schemes, due to more

efficient computational costs. With the use of efficient strategies such as the present topic of C-DFT, our understanding of specific processes in electron transfer (ET) theory can be pursued with a reasonable computational cost. With electron transfer reactions being one of most fundamental and important chemical processes in nature, and the many technologies and extensive range of applications in both biological as well as materials directions, C-DFT enables further advancements to be made given more understanding of the accuracy, quality, and range of applicability. As such, the current effort is not only directed towards implementation of an efficient computational C-DFT scheme, but to present the various underlying factors that control accuracy and efficiency of electronic coupling factors in electron transfer theory, including wavefunction type or density functional type, basis set, orbital localization scheme, effects of solvation, and convergence schemes.

3.1 Electron Transfer (ET) Theory

3.1.1 Importance of ET reactions

Electron transfer (ET) is clearly one of the most fundamental and important chemical processes, which lies at the heart of a variety of chemical systems. Long-range ET is a key energy step occurring in disciplines ranging from biology, chemistry, and physics to materials science, such as in natural photosynthesis, where light is converted into chemical energy by a series of step-wise electron transfer processes. Over the last two decades mimicking the elementary steps of natural photosynthesis has gained much interest, driven by the potential applications of such systems, ranging from artificial photosynthesis to molecular electronics, such as in dye-sensitized solar cells and organic light emitting diodes. Nonetheless, a thorough understanding key parameters associated with controlling mechanistic aspects of the ET processes is essential. Importantly, understanding underlying theoretical methodologies that can impact predictions of electronic coupling, energetics, and ultimately kinetics, will ultimately lead to better methodologies for prediction.[1,12,13,14,15]

3.1.2 Diabatic and Adiabatic representations

There are two quite different representations of potential energy surfaces: adiabatic and diabatic (Fig. 1). Adiabatic state representations can be investigated using the Born-Oppenheimer approximation. The Born-Oppenheimer approximation is based on the rational that the nuclear mass is much larger than the electron mass, which means that the nuclei move considerably slower than the electrons. This has important

consequences in the mathematics associated with the solving of the Schrödinger equation. In particular, that the motion of the nuclei and the electrons can be solved independently, where the total molecular wavefunction (ψ) is a product of the nuclear wavefunction (ψ_N) and the electronic wavefunction (ψ_{el}), for which the nuclei are assumed to be stationary, and fixed to a given geometry Q_i (Eqn. 8)

$$\Psi(q_i, Q_i) = \Psi_{el}(q_i; Q_i)\Psi_N \tag{8}$$

where q_i and Q_i are the electrons and the nuclear coordinates respectively. The system remains an eigenfunctions of the true Hamiltonian at all times[16,17], where the nuclear potential operator in the Schrödinger Equation is diagonal, while the kinetic energy operator is not. The Born-Oppenheimer approximation leads to the non-intuitive result of an avoided crossing (Fig. 1), and since the Born-Oppenheimer approximation breaks down in the avoided crossing region, the adiabatic surfaces provide a poor description in particular in this region.

In the diabatic representation, the diabatic states should conserve as much as possible their main electronic characteristics as a function of molecular geometry. Therefore, the electronic wavefunction is effectively not changing with internuclear distance R, that is:

$$\partial/_{\partial R}\,\Psi_{el} \simeq 0 \tag{9}$$

In distinction with the adiabatic representation, in diabatic representation the electronic Hamiltonian is not diagonal, and the diabatic potential curves do cross. Therefore the diabatic representation typically provides better descriptions of situations that adiabatic presentation fail to describe.

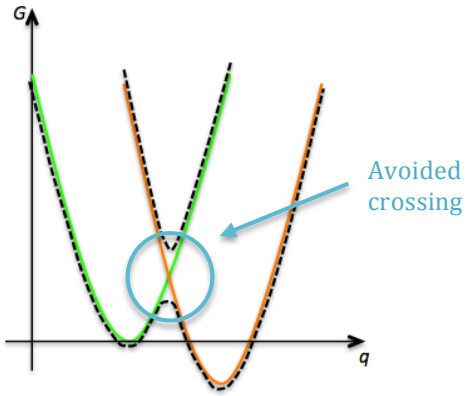

Figure 1. Schematic representation of free energy ET reaction along a reaction coordinate q. The green and orange curves represent the reactant (R) and product (P) diabatic states respectively. The black dashed lines are the adiabatic surfaces, where the resultant avoided crossing is also indicated.

3.1.3 Nonadiabatic ET

The electronic interaction between a donor (D) and an acceptor (A) in molecular systems is extremely weak compared to the energetics in bond breaking or making processes in most chemical reactions.[16] In accord with the time-dependent Schrödinger equation, there is a time element involved for the wave function to evolve from one diabatic state to another, where weaker mixing between two diabatic states leads to a longer evolution time. Therefore, different attributes are expected for varying degrees of mixing of states along the pathway, where there is a distinction between adiabatic ET reactions and diabatic ET reactions.[16] In adiabatic ET reactions, there is a strong mixing between the two diabatic states and the system remains an eigenfunction of the true Hamiltonian at all times, following the pathway shown on the right side of Fig. 2. In nonadiabatic ET reactions (Fig. 2 left), on the other hand, the mixing can be so weak that there is not enough time spent in the curve-crossing region for the wave function to evolve, and the system continues on the reactant diabatic surface with possible multiple back reflections before finally landing on the product diabatic surface.[16] The transition between two diabatic states A and B depends on the passage of nuclei through the crossing region, where the splitting, Δ, between the two adiabatic curves at the crossing point is given by

$$\Delta = 2|H_{ab}| \tag{10}$$

with H_{ab} the electronic coupling matrix element connecting the two diabatic states (discussed in more detail below). If H_{ab} is very large compared to the kinetic energy of nuclear motion, $k_b T$ (where k_b is the Boltzmann constant and T the temperature), the upper electronic state will be thermally inaccessible ($\Delta >> k_b T$), and the nuclei will move according to the lower state on the adiabatic potential curve. When $\Delta \lesssim k_b T$ thermodynamic considerations alone do not determine whether the electronic state can change. Depending on the relative time scale of electronic and nuclear motion, the system can either remain in diabatic state A, or it can undergo a transition A→B and move along the adiabatic curve.[18]

To establish a criterion for rough characterization of adiabaticity, an uncertainty relation has been derived by Wolynes *et.al*.[18] In this criterion, the energy uncertainty is given by $\hbar/\tau_{LZ}$, where $\hbar$ is the reduced Planck's constant, and τ_{LZ} is the time spent in the mixing region, the so called the Landau-Zener region. In the case of small energy uncertainty compared to the splitting, Δ, the system typically remains on the lower

surface passing through an adiabatic transition. If the system moves through the mixing region with constant velocity v, and the transition occurs over a region of length ℓ_{LZ}, then τ_{LZ} is given by

$$\tau_{\mathrm{LZ}} = {}^{\ell_{\mathrm{LZ}}}/_{\upsilon} \tag{11}$$

where ℓ_{LZ} is approximately

$$\ell_{\mathrm{LZ}} = \frac{\Delta}{|F_2 - F_1|} \tag{12}$$

with forces, F_1 and F_2 defining the slopes of the diabatic curves at the avoided crossing. The adiabaticity parameter, γ_{LZ}, defined as the ratio of the splitting Δ to the energy uncertainty, is given by

$$\gamma_{\mathrm{LZ}} = \frac{\Delta}{\hbar/\tau_{\mathrm{LZ}}} = \frac{\ell_{\mathrm{LZ}}\Delta}{\hbar\upsilon} = \frac{\Delta^2}{\hbar\upsilon|F_2 - F_1|} \tag{13}$$

If $\gamma_{\mathrm{LZ}} \gg 1$, then the transition is adiabatic. If $\gamma_{\mathrm{LZ}} \lesssim 1$, the system can remain on the diabatic surface and reach the upper state. The probability, *P,* for the system to stay on the adiabatic surface, has been calculated by Landau, Zener and Stueckelberg as

$$P = 1 - \exp\left(-\pi\gamma_{\mathrm{LZ}}/2\right) \tag{14}$$

This expression verifies that if $\gamma_{\mathrm{LZ}} \gg 1$, $P \approx 1$, and the transition is adiabatic. If $\gamma_{\mathrm{LZ}} \lesssim 1$, then

$$P = \frac{\pi}{2}\gamma_{\mathrm{LZ}} = \frac{\pi}{2}\frac{\Delta^2}{\hbar\upsilon|F_2 - F_1|} \tag{15}$$

where the probability is proportional to Δ^2.

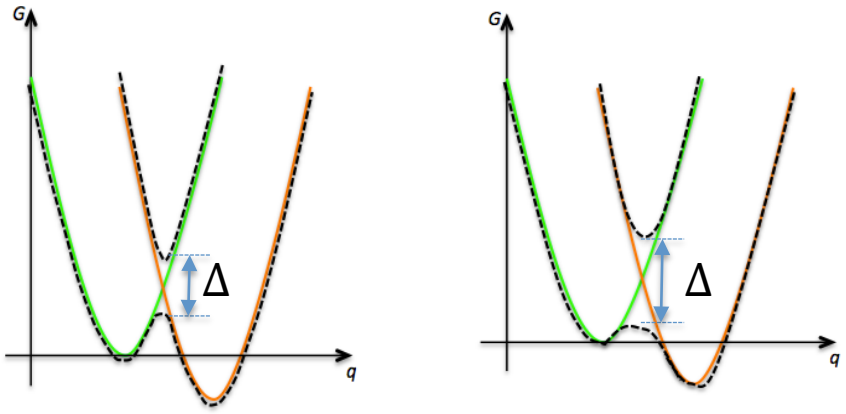

Figure 2. Schematic representation of free energy of nonadiabatic (left) and adiabatic (right) ET reactions along a reaction coordinate q. The green and orange curves represent the reactant and product diabatic states respectively. The black dashed lines are the adiabatic surfaces.

The emphasis in this thesis work is on long-ranged ET, for potential applications in biological and molecular electronics associated systems for example. Because such systems are characterized by weak, long-ranged interaction between localized donor and acceptor groups, these reactions are often nonadiabatic. In the nonadiabatic weak-coupling limit, QM or DFT treatment of electron transfer begins with the Fermi golden rule formulation for the probability of the transition between two states. In this regime, the rate expression as derived from time-dependent perturbation theory treatments is,[16,19,13,20]

$$k_{ET} = 2\pi\hbar^{-1}|H_{ab}|^2 FCWD \tag{16}$$

The rate in the above expression is given as a product of an electronic coupling matrix element H_{ab}, and the Franck-Condon-weighed density of states ($FCWD$).[16,19] $FCWD$ accounts for the conservation of energy, and describes the influence from the nuclear modes of the system, and is the sum of products of overlap integrals of the vibrational wave functions of the reactants with those of the products.[20,13] The electronic coupling matrix element, H_{ab}, reflects the strength of the interaction between the reactant and the product diabatic states at the nuclear configuration of the transition state, and is defined in terms of the effective electronic Hamiltonian matrix element that couples the initial and final states.[13,21] Because of the square dependency of the rate, $k_{ET,}$ on the electronic coupling matrix element, quantitative theoretical predictions of reaction rate are challenging due to the high sensitivity to the accuracy of the electronic coupling, such that even a 0.1 eV error can lead to large error in rate prediction.[22]

3.1.4 Marcus ET rate theory

Basic understanding of ET kinetics and associated mechanistics has represented a long lasting challenge. In the 1950s, Rudolph A. Marcus developed the first fundamental and generally accepted quantitative description of ET reactions in solution.[23,24,25] Marcus theory is a classical transition state theory (TST) of ET that assumes that the reactant and product electronic states are weakly coupled. Thus Marcus theory represents a nonadiabatic case of ET. For electron transfer, Marcus approximated the involved crossing potential surfaces by simple parabolas with equal force constants (curvature) which, when combined with transition state theory, leads to the following rate expression: [13]

$$k_{ET} = \frac{2\pi}{\hbar} \frac{|H_{ab}|^2}{\sqrt{4\pi\lambda k_B T}} \exp\left[-\frac{(\lambda + \Delta G)^2}{4\lambda k_B T}\right] \tag{17}$$

where T is the temperature, k_b is the Boltzmann constant, and $\hbar$ is the reduced Planck constant. In more detail, the three other parameters are:

1) λ – represents the reorganization energy, which specifies the free energy associated with forcing the reactant into an equilibrium configuration of the product, i.e., the energy gained by a nuclear (and solvent) relaxation after vertical excitation from the reactant to the product state.[13] The parameter λ is a sum of the solvent reorganization and the inner sphere reorganization. The solvent reorganization energy considers the reorientation of the solvent molecules after ET has taken place, and the inner sphere reorganization energy represents the changes of bond lengths and bond angles, at the redox centers while changing oxidation states.

2) ΔG – representing the driving force, which constitutes the free energy difference between reactant and product states.

3) H_{ab} – represents the electronic coupling matrix element.

The energy difference between the two adiabatic states at the crossing point equals twice the electronic coupling matrix element (Fig. 3).

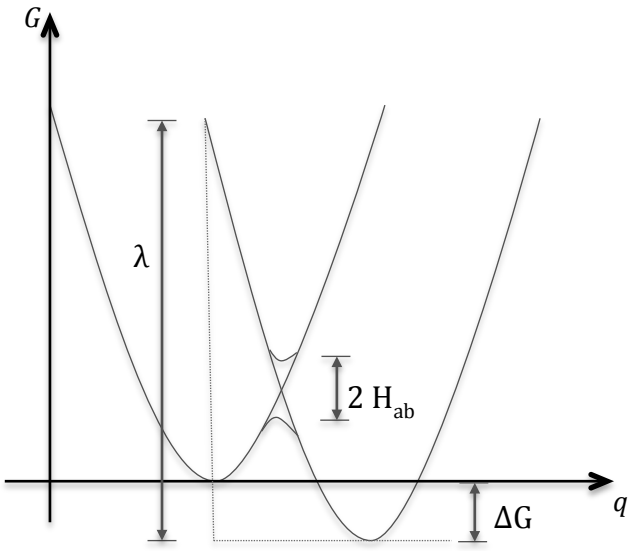

Figure 3. Marcus parabola energy diagram including reorganization energy (λ), driving force (ΔG) and electronic coupling matrix element (H_{ab}).

3.1.4.1 Marcus regimes: normal, inverted and barrierless

According to Marcus theory, there are three different regimes of the transfer energy that can be distinguished: the normal, the barrierless, and the inverted region (Fig. 4). These three regimes create the so-called Marcus-parabola, where log(k_{ET}) is plotted against the

driving force (Fig. 4 bottom). In the normal region, where -ΔG<λ , k_{ET} increases with increasing driving force (more negative ΔG) and the activation free energy $\Delta G^{\ddagger}$ decreases. In the barrierless region, -ΔG=λ, k_{ET} reaches its maximum value and the activation energy vanishes. In the Marcus inverted region, -ΔG>λ, k_{ET} decreases and $\Delta G^{\ddagger}$ increases with increasing driving force.

One of the most significant predictions of Marcus theory is that, the rate of an electron transfer reaction may decrease as the free energy of the reaction increases. The best experimental evidence for that inverted region was provided in 1984 by pioneering study[26] of Miller, Calcaterra and Closs, almost 25 years after it was predicted, followed by repeated successful experimental for other electron transfer reactions in other laboratories. As one can see in Fig. 5, Miller *et al* synthesized a series of eight homologous compounds, consisting of the same donor, the same rigid saturated hydrocarbon spacer, and with identical distances between the donor and the acceptor. [26,25] Plotting the rates against the driving force, they obtained the so-called Marcus parabola behavior. Moreover, it is now well established that nature makes profitable use of the Marcus inverted region. The inverted region effect plays an important role in photosynthesis in slowing down charge recombination, in favoring of the rate of the forward electron transfer.[27]

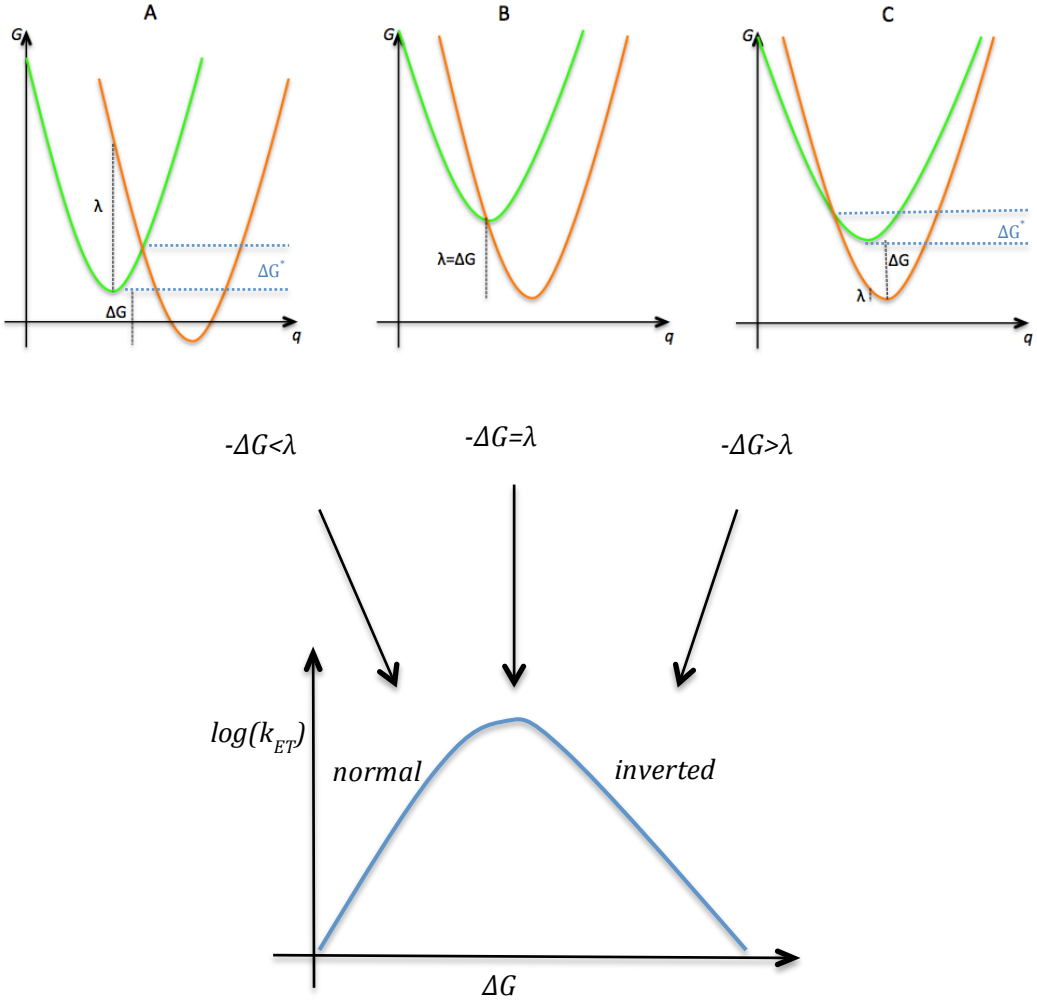

Figure 4. Top: Energy surfaces corresponding to the normal (A), barrierless (B) and inverted (C) electron-transfer reactivity regions of Marcus theory. Bottom: Marcus-parabola of logk_{ET} plotted against the driving force ΔG.

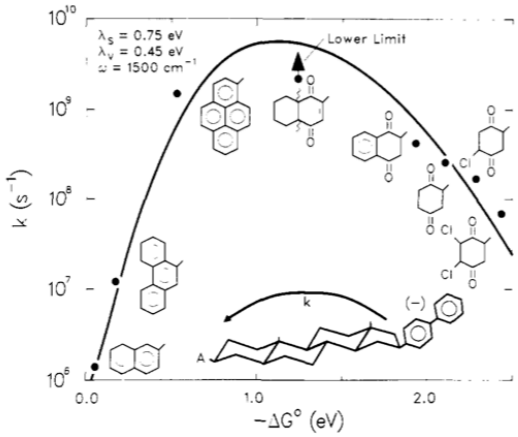

Figure 5. Marcus-parabola example Taken from *J. Am. Chem. Soc.*, **1984**, *106* (10), p 3047–3049. Pioneering study by Miller and Closs definitively proved the existence of the inverted region .[26]

3.1.5 ET in bridge mediated systems D-B-A

3.1.5.1 Bridge mediated systems: Through space (TS) and through bond (TB) interactions

For bridge-mediated ET reactions, tunneling can take place from the donor to the acceptor, over potentially large bridge distances. This occurs as a cooperatively of through-bond (TB) and/or through-space (TS) interactions (Fig. 6).[28] The rate as described by the golden rule is in the weak coupling non-adiabatic regime. The through-space interaction involves electronic coupling of the orbitals of the donor with those of the acceptor when they are in close proximity. Through-bond coupling occurs through step-wise coupling through the bridge orbitals between the donor and the acceptor.[16, 20,22,29] Since the extent of the couplings depend on the extent of the overlap integral between the participating orbitals, it follows that the direct or through space coupling is a short-range effect, negligible beyond a separation greater than ~3Å, while the through-bond coupling is a longer range phenomenon.[30,31,32] A detailed understanding of both components of the electronic coupling interactions for bridge-mediated systems as well as their influences on the electron tunneling pathways and transfer integrals greatly facilitates the understanding of the mechanistic aspects of the ET process. As such, accurate computational prediction requires methodology that can appropriately model these factors.

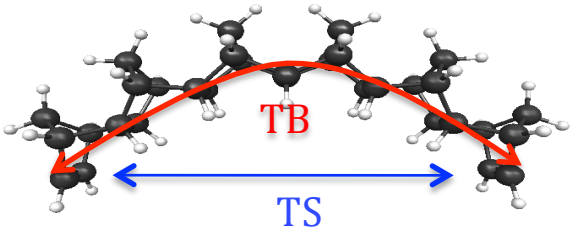

Figure 6. Schematic representation of through-space (TS) and through-bond (TB) interactions in a bridge mediated system, where the donor and the acceptor are defined as the end ethylene groups.

TB and TS interactions are responsible for the difference in energy between otherwise degenerate π orbitals separated by some distance within a molecule (e.g., Fig. 7). When a degenerate set of π orbitals, π_1 and π_2, interact through space, two combinations of orbitals result: a symmetric bonding combination $\pi^+ = \pi_1 + \pi_2$, and the anti-symmetric combination $\pi^- = \pi_1 - \pi_2$, the former lying energetically below the latter. The energy splitting between the two orbitals can be observed by photoelectron spectroscopy[19] as

well as computationally obtained. This splitting can be on the order of ~4 eV at bonding distance, and exponentially decays with increasing distance. A further through-bond interaction can result due to the bridge construction in bridge-mediated systems. In this case, the orbitals of the sigma framework of the bridge contribute to further mixing with the now nondegenerate set of π orbitals resulting in a further splitting and re-positioning of the original orbitals, as shown in the example in Figure 7.[22,31,32,28] In Fig. 7 one can see the TS interactions between the π orbitals of the end ethylene donor and acceptor groups, and further TB interactions within the σ and σ* frameworks. Depending on the nature and composition of the bridge between D and A and the extent of the coupling to the central σ system, one can observe a reordering of the energy levels even such that the symmetric combination is higher in energy than the antisymmetric combination. The ordering of the resulting symmetric/antisymmetric orbitals can become a diagnostic to the type and relative magnitude of the overall electronic coupling in a bridge-mediated system, and provide important mechanistic information in the understanding of the electronic pathways available in the system.

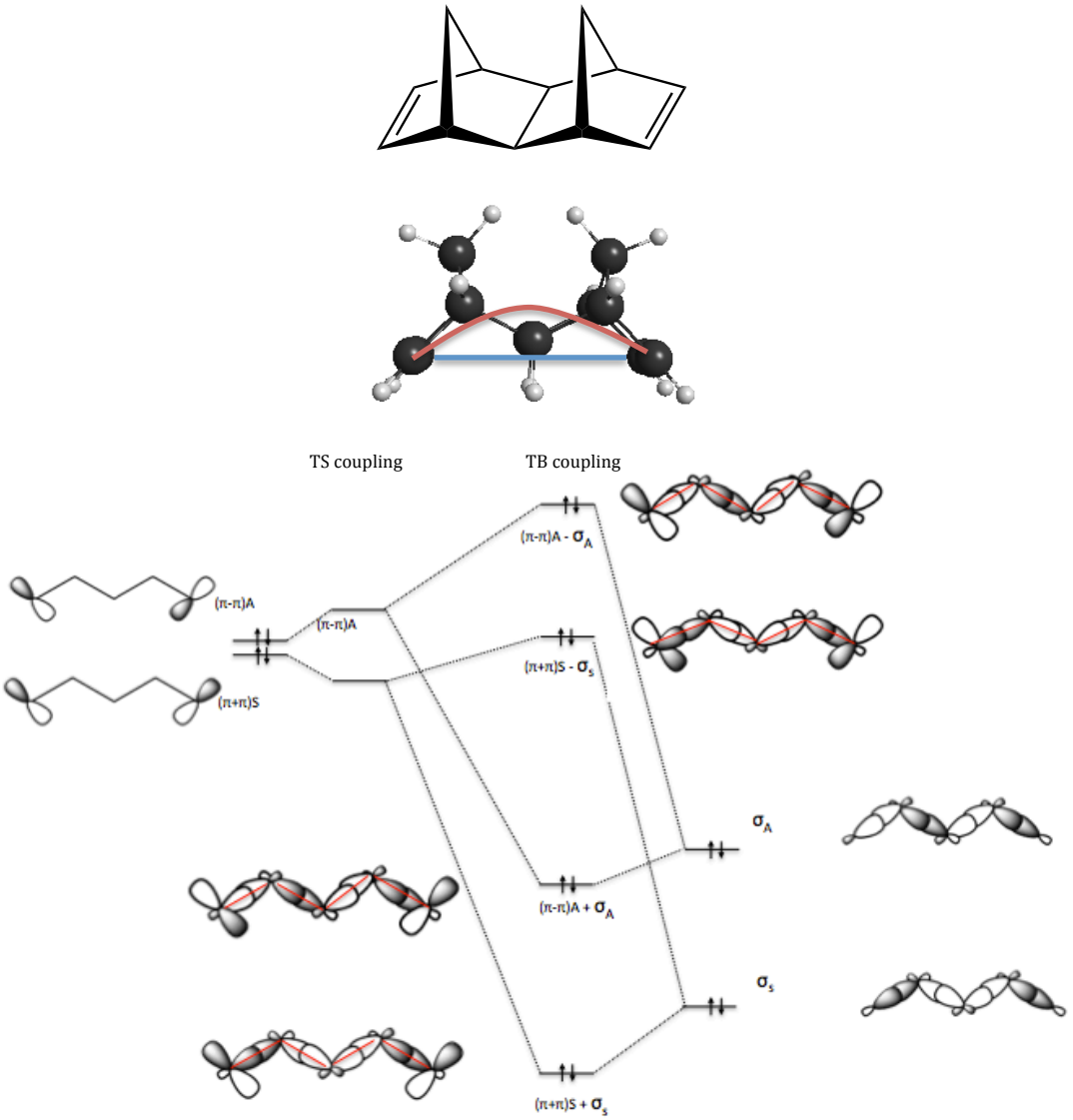

Figure 7. TS and TB coupling for a system consisting of ethylene D and A end groups with intervening σ-bonded norbornyl bridge units.

3.1.5.2. Bridged mediated ET mechanisms: Hopping and Superexchange

Electron transfer in bridged mediated systems is dictated by either of two distinguished mechanisms[13]: the coherent tunneling superexchange mechanism[33] or incoherent hopping mechanism[34,35] (Fig. 8). In the superexchange approach to nonadiabatic ET pioneered by Kramers[36], Anderson[37], Halpern and Orgel[38] and McConnell (1961)[33], the entire system, comprising of a donor, an acceptor and a bridge is treated as a supermolecule D-B-A. The theory of hopping conduction, the mechanism that takes over from superexchange in D-B-A supermolecules with longer bridges, was proposed by Miller and Abrahams[34] and extended by Mott in 1968.[35,39]

The tunneling superexchange model requires the donor and the acceptor at either ends of the bridge to be energetically well separated from the bridge states. The electron tunneling is mediated by the virtual orbitals on the connecting bridge, and the charge is at no time located on the bridge units. Therefore the bridge is neither reduced nor oxidized but it merely functions as a coupling medium for the transfer process. [33,29,24,40] The incoherent hopping mechanism, on the other hand, involves real intermediate states that actively transport the electron along the bridge. The charge is transferred by a series of short-range steps via the bridge units, which involves redox states on the bridge. Therefore the charge has a finite lifetime at the bridge. In the incoherent hopping mechanism each individual step may be conceived as a superexchange process.[33,29,13, 40,24,41,24]

In many realistic cases, the electron transfer is expected to be governed by a mixture of these two mechanisms,[13] where the energy gap between the donating state and the bridge states regulates the domination of the mechanism involved. When the bridge states lie high in energy, superexchange typically dominates, while when the bridge states are low in energy or even resonant with the donor state, hopping may dominate. Thus, it is clear that the relative energy of the frontier orbitals of the bridge unit essentially determines the main mechanism of ET.[24]

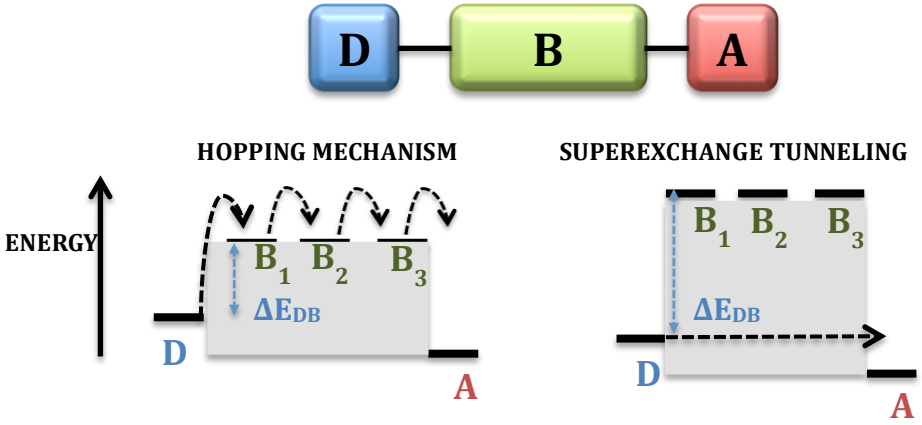

Figure 8. Schematic representation of incoherent hopping mechanism (left) and the coherent tunneling superexchange mechanism (right).

3.1.5.3 McConnell model and D-A distance dependence of ET rates

Superexchange is incorporated into nonadiabatic ET rate theory by reinterpreting the electronic coupling matrix element, H_{AB}, as the effective coupling element between a donor and an acceptor via the bridge.[39] The McConnell's model[33] for the influence of the intervening medium in the coherent tunneling superexchange mechanism invokes

perturbation theory to derive an expression for the magnitude of bridge-mediated electronic coupling H_{DA} between D and A with identical bridge units B that mediate the electronic coupling[13,33,42,43,33]

$$H_{DA} = \frac{H_{DB}H_{BA}}{\Delta E_{DB}}\left(\frac{H_{BB}}{\Delta E_{DB}}\right)^{n-1} \quad (18)$$

where the total electronic coupling H_{DA} is given in terms of the electronic coupling of the bridge to the donor H_{DB} and the acceptor H_{BA}, the interaction H_{BB} between B units of a chain composed of n identical units, and the energy gap ΔE_{DB} between the donor and the bridge states (Fig. 8).[13]

If the electronic coupling between B subunits is small compared to the energy gap between the donor and the bridge states (H_{BB}/ ΔE_{DB} << 1), the distance dependence of the electronic coupling is exponential and described by [13,42]

$$H_{DA} = H_0 exp\left[-(\frac{\beta}{2})(R - R_0)\right] \quad (19)$$

where H_0 is the coupling at the van-der-Waals contact distance R_0, R is the D-A distance, and β is the system specific attenuation factor given by[13,42]

$$\beta = \left(\frac{2}{r}\right) ln\left(\frac{\Delta E_{DB}}{H_{BB}}\right) \quad (20)$$

According to the McConnell model, three factors contribute to the expression of the attenuation factor β: the tunneling energy gap, ΔE_{DB}, the electronic coupling between individual bridge units, V_{BB}, and the length of one bridge unit r. Of these three factors, the most critical parameter is the tunneling energy gap ΔE_{DB}.[13]

Given the Golden Rule dictates that the electron-transfer rate constant k_{DA} for nonadiabatic electron transfer is proportional to the H_{DA}^2 (Eqn. 16), the distance dependent of k_{DA} via the coherent superexchange mechanism is exponential and is given by[42]

$$k_{DA} = k_0 exp[-\beta(R - R_0)] \quad (21)$$

Therefore this exponential dependence of the rate on the length is based on the exponential dependence of the coupling.[24]

To examine the effect of the tunneling energy gap ΔE_{DB} on the total electronic coupling $H_{DA,}$ Albinsson and co-workers have compared the transfer rates of a series of D–B–A systems with constant R_{DA}, which consists of the same donor–acceptor couple with

structurally similar but electronically different bridge systems. One series of D–B–A systems, ZnP–RB–AuP+, was designed with zinc porphyrin as the donor, and gold(III) porphyrin as the acceptor, where RB denotes an oligo-phenyleneethynylene (OPE)-based bridge. For the entire series, ZnP acts as an electron donor while AuP+ serves as the electron acceptor.[44,45] The electronic structure of the OPE bridge (3B) was modified by replacing the central benzene unit by either naphthalene (NB) or anthracene (AB) (Fig. 9). This enabled investigation of the variation of the tunneling energy barrier ΔE_{DB} while keeping a fixed donor-acceptor distance R_{DA}.[13]

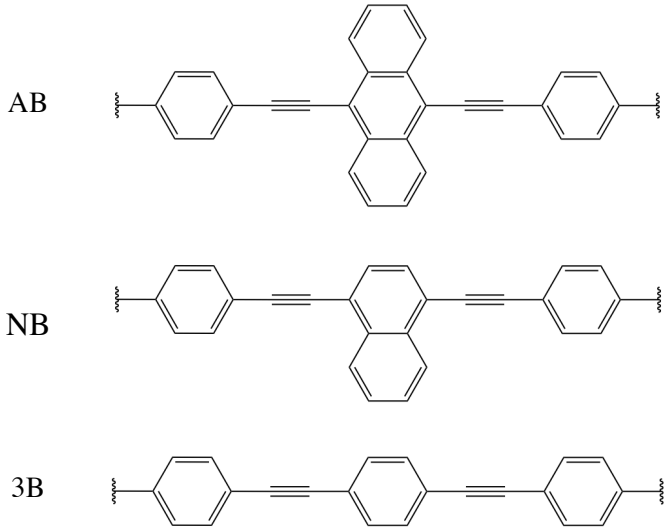

Figure 9. Molecular structures of the AB, NB and 3B bridges of the D-B-A systems ZnP-RB-AuP+.

The key finding of this work was the experimental demonstration of the linear correlation between the electronic coupling H_{DA} and the inverse of the tunneling energy gaps, $1/\Delta E_{DB}$ as predicted by the McConnell model.[46]

For both the hopping and the superexchange mechanisms, it is evident from the distance dependence of orbital overlap that the electronic coupling and, consequently, the ET rate, decreases as the distance between the donor and the acceptor increases. However, both ET mechanisms show different distance dependencies. As discussed above, the McConnell model for superexchange predicts an approximately exponential dependence of H_{DA} on the donor acceptor distance, R_{DA}, a claim consistently verified by experimental data.[47,48,49] In the case of the hopping mechanism, there is a wire-like dependence of the ET rate on the distance between the donor and acceptor redox centers, *i.e.*, charge transport is enabled over almost 'infinite' distances.[24] As the length of a bridge increases, the superexchange interaction becomes smaller, and the rate constant for

charge transfer may be dominated by the incoherent term. For long distances, the incoherent, wire-like channel generally becomes more efficient than the coherent one.[50,51,52]

3.1.5.4 Attenuation factor β values

As mentioned previously, in the nonadiabatic electron transfer limit, the distance dependent of the rate of ET, k_{DA}, via the coherent superexchange mechanism is exponential and is given by Eqn. 21[42], where the attenuation factor, β, in the rate expression could vary quite substantially for different D-B-A systems.

$$k_{DA} = k_0 exp[-\beta(R - R_0)] \quad (21)$$

The future development of effective systems for use as molecular photonic devices depends on the ability of molecular materials to conduct charge over large distances, where ideally, the mechanism for charge transfer will involve through-bond coupling in bridge distances in excess of 100 Å with high efficiency and excellent directionality.[40] Achievement of an ideal weak distance dependent wire-like behavior that enables charge transport over almost 'infinite' distances, involves systems with small attenuation β-values as closed to zero as possible. However, in cases where the β-value is very small, the distance dependence is no longer well described by the McConnell model and is no longer expected to decay exponentially.[13] Although consideration of β-values are typically only considered in mechanisms that are expected to decay exponentially in a tunneling superexchange mechanism, they have also been considered for electron transfer that occur via the incoherent hopping mechanism.[13]

The attenuation factor, β, can vary quite substantially for different D-B-A systems. As mentioned, an important determinant of electronic coupling is the makeup of the bridge connecting the D with the A or redox centers.[53] In general, β-values are larger for systems comprised of σ-bonds bridges than for systems connected by π-conjugated bridges, the latter of which typically provides more efficient long-range transfer.[13] Unsaturated bridge systems increase the electronic communication between redox centers relative to saturated bridge systems[24] due to their rigidity and rod-like structure, and more importantly, the associated electron delocalization that allows for substantial electronic communication between individual bridge units thereby mediating the charge transfer over long distances.[13,24]

A wide range of β-values, referring to the rate expression k_{ET}, for systems comprised of σ-bonds bridges as well as for π-conjugated bridges has been reported in the literature. Table 1 shows a rough break down of characteristic β range values as observed in the literature, where for bridge mediated systems the β-values reported are significantly smaller than those related to electron transfer in vacuum.

2.8-3.5 $Å^{-1}$	electron transfer in vacuum[54,55]
1.0–1.4 $Å^{-1}$	for proteins[56,54,57, 58]
<<0.2–1.4 $Å^{-1}$	for DNA[59]
0.8–1.0 $Å^{-1}$	for saturated hydrocarbon bridges[60,61]
<<0.01 – 0.8 $Å^{-1}$	for unsaturated phenylene, polyene and polyyne bridges[50,62,63,64]
Table 1. Characteristic β range values as observed in the literature.	

In Table 2, some more specific experimental attenuation β values are reported for D-bridge-A systems with both saturated as well as unsaturated bridges constructions.

β		Ref.
Saturated bridge		
0.95$Å^{-1}$	Saturated bridge Molecules: 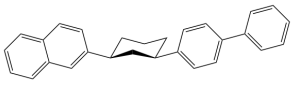 1,3ee (R_{DA}=10A) 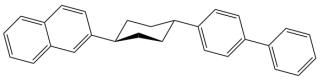 1,4ee (R_{DA}=11.8A)  2,7ee (R_{DA}=12.5A)  2,6ee (R_{DA}=14A)	16

$0.85Å^{-1}$	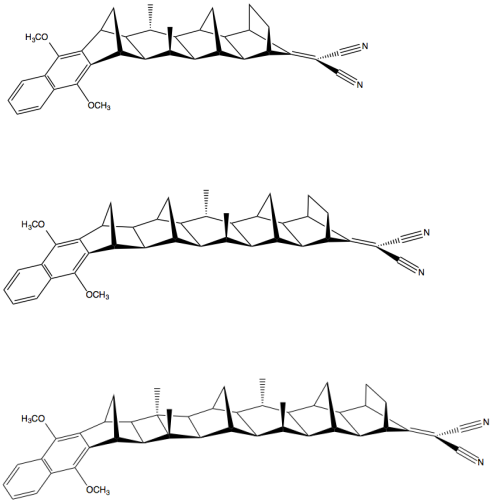	61
π-conjugate bridge		
$0.08Å^{-1}$	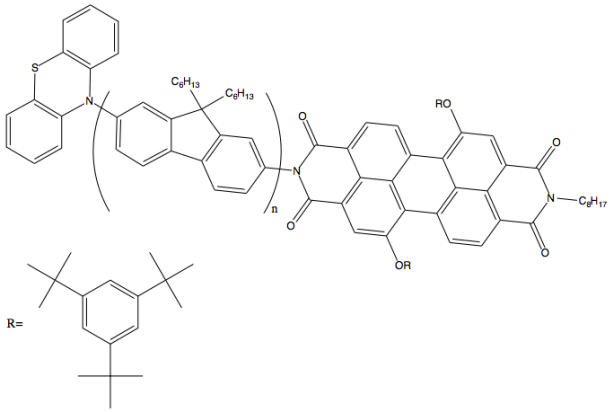	65
$0.34Å^{-1}$	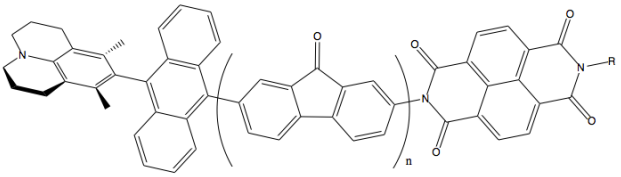	42
$0.04Å^{-1}$	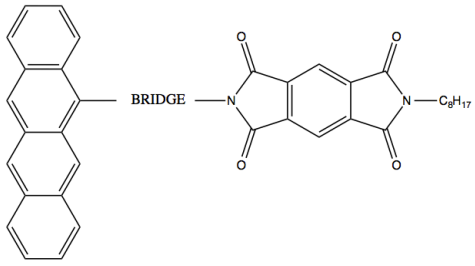	50

	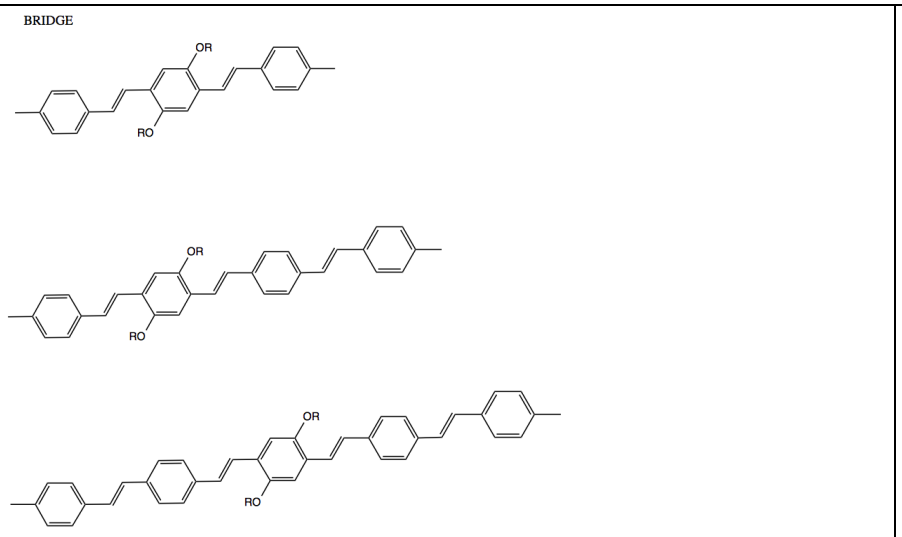	
$0.03Å^{-1}$	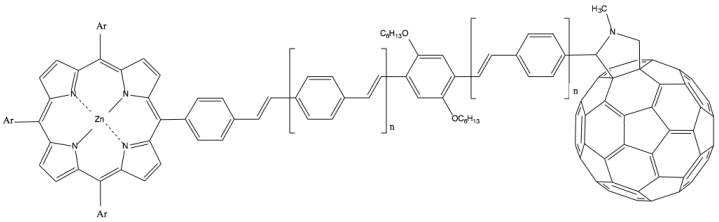	66

Table 2. Various experimental attenuation β values ($Å^{-1}$ units) for the rate expression $k_{ET.}$

4. C-DFT and Marcus ET rate theory

Investigations into electron transfer theory typically require consideration of diabatic states. This requires construction of diabatic potential energy surfaces from adiabatic surfaces. In routine *ab initio* theory, the potential energy surface is obtained within the adiabatic representation, where the Born-Oppenheimer approximation applies. In this case, the electronic and nuclear motions in a molecular are separable, leading to molecular wave functions in terms of electron and nuclear degrees of freedom. Nonseparable terms, due to nuclear kinetic energy in the Hamiltonian, may couple potential energy surfaces, and in those cases also need to be considered. This requires performing a unitary transformation from the adiabatic representation to a diabatic representation, where the nuclear kinetic energy operator is diagonal, and the coupling is due to the electronic energy, $H_{ab,}$ as diabatic states are not eigenfunctions of the electronic Hamiltonian.

When modeling electron transfer, one needs two diabatic states representing the donor state and the acceptor state of the electron transfer process. The associated diabatic states maintain electronic characteristics, and can be identified based on their electronic

density, such as one diabatic state has excess electron density on the donor, while the other diabatic state has excess electron density on the acceptor. The C-DFT approach can provide a practical and effective route for obtaining approximate diabatic states, using direct diabat construction without reference to any particular adiabatic states. Suitable diabatic states can be obtained by optimizing the wavefunction subject to constraints on the density, where the resulting Kohn-Sham determinant can represent a diabatic state. These diabatic states can constitute a starting point for calculating ET parameters within Marcus theory. One of these parameters, the electronic coupling matrix element, H_{AB}, enters as a squared parameter in the Marcus rate expression (Eqn. 17). This parameter is dominated by the overlap between the tails of the wave functions of the donor state and the acceptor state. According to McConnell[33] model mentioned above, the coupling would also fall off exponentially as the distance (R) between the donor and the acceptor increases (Eqn. 19).[1,2] In accord with the Condon approximation, H_{ab} is assumed to remain constant along the reaction coordinate.[2]

4.1 Electronic coupling matrix element H_{ab} from charge-constraint C-DFT

In this section the focus is on the use of charge constraints for the definition of diabats using the C-DFT approach. The associated theoretical steps are defined for extracting the electronic coupling matrix element, H_{ab}, between two diabatic states, a and b, following the general theory formulations of Wu and Voorhis.[2]

The electronic coupling matrix element H_{ab} between two orthogonal diabatic electronic state wavefunctions ψ_a and ψ_b is

$$H_{ab} = <\psi_a|H|\psi_b> = \int \psi_a{}^* H \psi_b d\tau \neq 0 \quad (22)$$

where H is the electronic Hamiltonian and ψ_a and ψ_b are the wavefunctions of the diabatic states a and b. When carrying out C-DFT calculations, H is approximated by the Kohn-Sham Hamiltonian, and the two diabatic wavefunctions are approximated by the Kohn-Sham determinants ψ_A and ψ_B, which are generally nonorthogonal. To distinguish these nonorthogonal states from the orthogonal states, capital subscripts are used. Following the Hohenberg-Kohn theorem, each diabatic wavefunction is determined by its density:

$$|\psi_A> \equiv |\psi(\rho_A)> \quad (23)$$
$$|\psi_B> \equiv |\psi(\rho_B)>$$

And the coupling becomes a functional of the two densities ρ_A and ρ_B

$$H_{AB}[\rho_A, \rho_B] \equiv < \psi_A|H|\psi_B > \tag{24}$$

The Hamiltonian matrix in the constrained basis is:

$$\mathrm{H} = \begin{pmatrix} H_{AA} & H_{AB} \\ H_{BA} & H_{BB} \end{pmatrix} \tag{25}$$

where the diagonal elements are the constrained-DFT energies:

$$\begin{aligned} H_{AA} &=< \psi_A|H|\psi_A >= E_A \\ H_{BB} &=< \psi_B|H|\psi_B >= E_B \end{aligned} \tag{26}$$

In C-DFT, one calculates a ground state that is imposed to satisfy specific constraints. Therefore, each diabat is an eigenstate of the Hamiltonian in its own alternative potential,

$$(H + V_c w_c)|\Psi_c >= F|\Psi_c > \tag{27}$$

where V_C is a unique constraining potential to a specific constrained state and

$$F =< \Psi_c|H + V_c w_c|\Psi_c >= E[\rho_c] + V_c \int w_c \rho_c = E + V_c N_c \tag{28}$$

where F represents the potential energy including the interaction with the constrained potential. The off-diagonal elements of H are:

$$\begin{aligned} H_{AB} &=< \psi_A|H|\psi_B >= F_B < \psi_A|\psi_B > -V_c^B < \psi_A|w_c|\psi_B > \\ H_{BA} &=< \psi_B|H|\psi_A >= F_A < \psi_B|\psi_A > -V_c^A < \psi_B|w_c|\psi_A > \end{aligned} \tag{29}$$

Since the wavefunctions are approximated, the calculated H_{AB} and H_{BA} are not identical. To preserve hermiticity one takes the average of the two.

For orthogonalizing the two states, first the overlap matrix is constructed as,

$$\mathrm{S} = \begin{pmatrix} 1 & S_{AB} \\ S_{BA} & 1 \end{pmatrix} \tag{30}$$

where

$$S_{AB} = S_{BA} =< \psi_A|\psi_B > \tag{31}$$

In the present work, the overlap between the two diabatic states, S_{AB}, is calculated as the overlap between the relevant orbitals for the ET, in particular, those that dominate the contribution to the electronic coupling. Typically, the dominant orbitals involved in the ET are the frontier orbitals.

The projector matrix is

$$\mathrm{w}_c = \begin{pmatrix} w_c^{AA} & w_c^{AB} \\ w_c^{BA} & w_c^{BB} \end{pmatrix} \tag{32}$$

where

$$w_c^{AA} =< \psi_A|w_c|\psi_A >= \int w_c \rho_A = N_c^A \tag{33}$$

$$w_c^{BB} =< \psi_B|w_c|\psi_B >= N_c^B$$

$$w_c^{AB} = w_c^{BA} =< \psi_A|w_c|\psi_B > \tag{34}$$

In order to orthogonalize ψ_A and ψ_B, the two-dimensional generalized eigenvalue problem is next solved,

$$\mathrm{w}_c\mathrm{C} = \mathrm{SCn} \tag{35}$$

where n is the diagonal matrix of generalized eigenvalues and C is the matrix of generalized eigenstates. Followed by similarity transformation,

$$\mathrm{C}^{\dagger}\mathrm{HC} \tag{36}$$

The final H_{AB} is the off-diagonal element of the resulting matrix.

5. Continuum Solvation Model for *ab initio* theory (COSab)

Accurate prediction and improved understanding of realistic biological, chemical, physical, and environmental systems normally requires inclusion of solvent effects in the underlying theory. Typically, solvent effects are considered in quantum mechanical theory using explicit solvent methods, implicit models, or a combination of the two. In particular, a cost effective and yet accurate methodology developed in our group is the

continuum solvation model (COSab),[67] a well-established continuum solvation method for introducing solvation effects into *ab initio* theory. The COSab method belongs to the class of dielectric continuum models, where the solute molecule is initially embedded in a dielectric continuum of permittivity ε and approximated as a perfect conductor, and subsequently corrected for realistic systems.[68,69,70] The solute forms a molecular shaped cavity (Fig. 10) within the dielectric and accounting for solute/solvent and solvent solvent interactions, including back-response from the solvent are all accounted for self consistently with to the usual solute/solute interactions.[67] For realistic conditions, the molecular shaped cavity is constructed as an assembly of atom-centered spheres with radii approximately 20% larger then the van der Waals radius as the optimal surface of interaction between solute and solvent wavefunctions. This has been shown to be in consistent agreement with experimental solvation energies.[67]

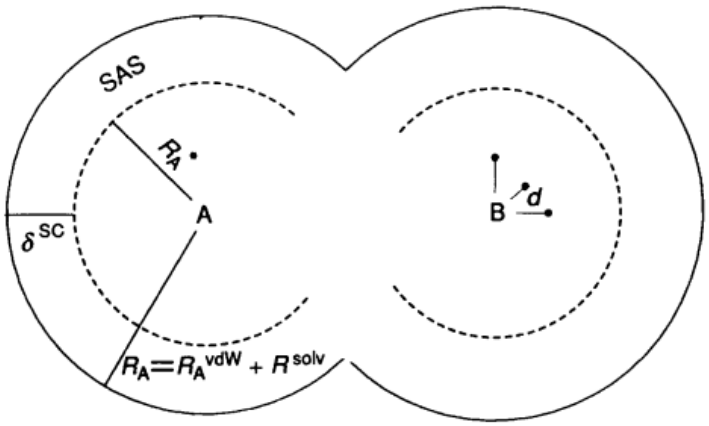

Figure 10. Construction of SAS (schematic) ; Solid circles indicate the surface accessible to the centers of solvent molecules, dashed lines the surface accessible to solvent charges. For atom B the three dipole representation points are indicated in addition. This figure is taken from reference 67.

The solute molecule is bound by the molecular shaped cavity, represented m surface segments with corresponding potential $\Phi=(\Phi_1,..., \Phi_m)$, which is related to the charge distribution of the solute, i.e., the positions and charges of the nuclei and the electron density. This potential induces screening charges, $q=(q_1,...,q_m)$, arising from the polarization of the continuum.[69]

The COSab theory is initially formulated under the assumption of screening in conductors, i.e., a medium with infinite dielectric permittivity ε. In this way, the initial formulations have relatively simple boundary conditions of vanishing total potential, resulting in a closed form for the resulting equations that can be easily solved for the

potential arising on the surface segments due to the solute and the associated screening charges.[67,71] The screening charges in a finite dielectric are then well approximated as [69]

$$q = f(\varepsilon)q^* \tag{37}$$

where the scaling factor $f(\varepsilon)$, based on the basic electrostatic idea regarding scale of dielectric screening energies for a given geometry with respect to the dielectric permittivity of the screening medium, can be written then as[23,24]

$$f(\varepsilon) = \frac{\varepsilon-1}{\varepsilon+x} \tag{38}$$

In the original COSab paper, the value of x is set to 0.5 as it is widely accepted that x = 0.5 yields the most accurate results for neutral compounds.[67]

The COSab theory allows for calculation of accurate gradients without cavity shape constraints and the self-consistent process of optimizing the solute charge density is done with the screening potential simultaneously included in the SCF cycle using directly the electrostatic potentials of the charge distribution within the cavity. Therefore, the COSab method is fully variational and accurate gradients can be readily calculated.[72]

The COSab model allows for the calculation of a comparatively simple, explicit expression for the screening energy of a molecule in a dielectric medium.[23] It has become very popular due to its algorithmic simplicity, numerical accuracy and stability, and its essential robustness with respect to artifacts resulting from the small percentage of solute electron density, which unavoidably reaches out of the cavity, the so-called outlying charge.[67,71,73,69] The outlying charge error can be quite large, especially for solute systems with rather diffuse electron density, like in anions.[73]

The first quantum chemical *ab initio* implementation[69] of COSab was carried out within the *ab initio* quantum chemistry package GAMESS[3]. In the GAMESS implementation atom centered multipole representation of the density for the calculation of the vector potential Φ_X (related to the charge distribution of the solute, i.e., the positions and charges of the nuclei and the electron density[69]) was used. As this representation treats all charges as if they were inside the cavity, it handles the problem of outlying charges.[74] A second approach for including effects of outlying charge, which has been implemented into GAMESS as well is the Double Cavity (DC) method[70], originally proposed by Klamt.[70] This method involves construction of a second molecular shaped cavity that lies outside

the primary molecular shaped cavity to effectively encompass the electron density of the solute.[70]

6. Orbital Localization Methods

In orbitals related methodologies, like in determination of electronic coupling element, which is a function of orbital overlap, one expects to find variation as a function of the set of molecular orbitals. Despite the computational potential appeal of the canonical molecular orbitals (CMOs), their tendency to delocalize through the whole system may not be appropriate to all treatments. Alternatively, localized molecular orbitals (LMOs) serve as an important bridge between chemical intuition and molecular wave functions. For ET bridged mediated systems D-B-A one should find out the most appropriate set of orbitals representing the orbital-based description of TB and TS interactions.

Localized molecular orbitals (LMOs) methods, incorporated into a theoretical description of molecules are substantial in understanding classical chemical bonding concepts, such as bonds, nonbonding electrons and core orbitals.[75,76] From classical point of view bonds are attributed to an increased probability of finding electrons between two nuclei, thus LMO methods aim to define MOs that are spatially confined to a relatively small volume, indicating the bonded atoms. [77]

A Hartree–Fock wave function can be written as a single Slater determinant, composed of a set of N orthonormal MOs[77]

$$\Phi = \frac{1}{\sqrt{N!}} \left| \begin{pmatrix} \phi_1(1) & \phi_2(1) & \cdots & \phi_N(1) \\ \phi_1(2) & \phi_2(2) & \cdots & \phi_N(2) \\ \vdots & \vdots & \ddots & \vdots \\ \phi_1(N) & \phi_2(N) & \cdots & \phi_N(N) \end{pmatrix} \right| \tag{39}$$

Where

$$\langle \phi_i | \phi_j \rangle = \delta_{ij} \tag{40}$$

For computational considerations, it is advantageous to work with canonical MOs which make the matrix of Lagrange multipliers diagonal ($\lambda_{ij}=0$ and $\lambda_{ii}=\varepsilon_i$), and that are eigenfunctions of the Fock operator at convergence. These canonical MOs commonly do not resemble the bonding orbitals of Lewis structures as they tend to be delocalized over the whole molecule.[77] However, the resulting canonical MOs represent only one of the many possible unitary bases in the SCF space, defined by the minimization of energy.[77,78] Once the SCF procedure has accomplished, other sets of orbitals may be acquired by linear combinations of the canonical MOs, while the total wave function and thus all observable properties are unaffected.[77] The single determinant many-electron

Hartree-Fock wave functions composed of N molecular orbitals $\{\phi_i$ (r), i= 1 ... N$\}$ are invariant with respect to unitary transformation U of the occupied orbitals[78,75]

$$\phi' = \boldsymbol{U}\phi \tag{41}$$

$$\phi'_i = \sum_{j=1}^{N_{orb}} u_{ij}\phi_j \tag{42}$$

$$UU^{\dagger} = 1 \tag{43}$$

All localization procedures intend to find a unitary transformed orbital set which satisfies a given optimum localization criterion.[75] The three well known localization methods, all of them are implemented into GAMESS[3], can be summarized as follows:

The **Boys** method[79] maximize the distance between centroids of the orbitals, defined by the following functional[77]

$$\langle\Omega\rangle_{Boys} = \sum_{i>j=1}^{N_{orb}} \left(\langle\phi'_i|r|\phi'_i\rangle - \langle\phi'_j|r|'\phi_j\rangle\right)^2 \tag{44}$$

The **Edmiston–Ruedenberg** (ER)[78] localization scheme uses the inverse of the distance between two electrons as the operator, and maximizes the expectation value[17]

$$\langle\Omega\rangle_{ER} = \sum_{i=1}^{N_{orb}} \langle\phi'_i\phi'_i|\frac{1}{r_1-r_2}|\phi'_i\phi'_i\rangle \tag{45}$$

This corresponds to determining a set of LMOs that maximizes the self-repulsion energy.[77]

The **Pipek–Mezey**[75] localization scheme does not localize in terms of coulombic properties as do the above two methods.[80] It corresponds to maximizing the sum of the Mulliken atomic charges. The contribution charge to atom A is[77]

$$\rho_A = \sum_{i=1}^{N_{orb}} \sum_{\alpha\in A}^{M_{basis}} \sum_{\beta}^{M_{basis}} c_{\alpha i} c_{\delta i} S_{\alpha\beta} \tag{46}$$

And the function to be maximized is[77]

$$\langle\Omega\rangle_{PM} = \sum_{A=1}^{\text{Atoms}} |\rho_A|^2 \tag{47}$$

In spite of the theoretical advantages of the Edmiston-Ruedenberg (ER) procedure, from a computational perspective the ER localization method involves a high computational effort since it requires all two-electron integrals over the occupied canonical molecular orbitals and as the ER method is an iterative process involving a series of unitary transformations where the two electron integrals are updated many times before convergence of the localization is achieved. The computational complexity of each iterative step increases like the fifth power of the number of basis orbitals n^5, while both Boys' and Pipek-Metzey's algorithms behave like n^3.[77,75,76] As a result of these computational difficulties of ER localizations, for the moment, ER method is impractical

for very large molecules, and Boys or Pipek–Mezey procedures are often used in practice.[77,76]

Pipek –Metzey localization is suitable for separating core and valence orbitals and it supports σ-π separation.[75] Its orbitals are similar to the ER orbitals, particularly in their σ-π separation, while Boys gives a set of "τ" or "banana bonds" for double bonds.[80]

7. Project implementation

7.1. General Perspective and Challenges

The development and implementation of a new C-DFT code is carried out in the *ab-initio* quantum chemistry package GAMESS[3] as the main component of this thesis work. GAMESS is one of the highest used software for carrying out quantum chemical computations in the community, and so additions to this code will be of general availability to this community. The software enables calculations at a variety of different wavefunction types, including restricted Hartree-Fock (RHF), density functional theory (DFT), configuration interaction (CI), many body perturbation theory (MP2), coupled-cluster (CC) variants, and multiconfigurational SCF (MCSCF), as well as the open shell equivalents. With this package, it is possible to investigate structure, energetics, properties, mechanism and general reaction path characteristics in ground and excited states. GAMESS has a significant variety of atom-centered basis sets, and additionally allows for external basis sets to be used.

With the underlying density functional theory in place, GAMESS is ideally set up for the implementation of the new C-DFT capabilities to be implemented. The initial stage of implementation involves enabling a single point (calculation at a single specific geometry) closed shell (all electrons are paired) energy C-DFT capability, with the ability to account for user-specified charge relocation. This capability will be termed charge C-DFT. For a single point energy calculation subject to a specified charge constraint, a diabatic state of the lowest energy state of the system is found using the following protocol:

1. Selection of specific donor and acceptor fragments.
2. Definition of a charge constraint. In the current C-DFT protocol, the Becke weighting scheme[68] is used for charge definition.
3. Constrained DFT orbital optimization following a SCF C-DFT procedure as described below and shown in flow-chart in Fig. 11.

In stage two of the implementation, a single point C-DFT capability is implemented for open shell systems, where not all electrons are paired.

7.2 SCF procedure

As discussed in 2.1.2, the desired solution in C-DFT involves criteria that ensure location of a minimum with respect to the electronic density and maximization with respect to the constraint potential, V_c. As such, a stationary point can be found via a self-consistent field procedure until these two criteria are satisfied.

The basic procedure implemented for a C-DFT single point calculation involves modification of the general self-consisted field (SCF) procedure in GAMESS for the specific criteria of the new C-DFT procedure. The SCF method is an iterative method, where one begins with a specified set of molecular coordinates and a guess set of associated molecular orbitals, and solves the Schrödinger equation iteratively to obtain an increasingly accurate set of orbitals. The final set of optimized orbitals is found through the solving of the Roothaan equations:

$$FC = SC\varepsilon \tag{48}$$

where F is the Fock matrix, S is the overlap matrix, C is the matrix of coefficients of the orbitals, and ε is a diagonal matrix of the energies of the molecular orbitals. At the *n*th iteration, the Fock matrix, F, is diagonalized using the orbitals from (n-1) iteration. When the difference between two consecutive Hamiltonians is negligible, the system is said to be self-consistent and the SCF procedure is completed.

Following the general theory formulations of Wu and Voorhis,[81] the C-DFT capability is implemented into GAMESS using a double SCF loop procedure (Fig 11). An outer loop controls the SCF procedure for solving the KS equations, where the orbitals are improved iteratively. At every SCF step, an inner loop is employed to optimize V_c keeping the Coulombic and exchange-correlation (XC) potentials unchanged. This latter condition makes the inner loop relatively cheap computationally (at least for atom-centered basis sets), although any V_c trial demands a matrix diagonalization. The optimization of V_c requires a maximization of the energy for a given Coulombic, XC, and core potentials. Once V_c is optimized, the constrained density is used to build new Coulombic and XC potentials as the starting point for a new outer loop.

In the optimization of V_c, it is necessary to implement Newton's method for optimization (Eqn. 49), which is utilized to reduce the number of inner iterations.

$$X_{n+1} = X_n - \frac{f\prime(X_n)}{f\prime\prime(X_n)} \tag{49}$$

where $f'(X_n)$ and $f''(X_n)$ are the first and second derivative of the energy with respect to V_c (Eqns. 5 and 6 respectively).

In practice a major challenge within C-DFT implementation is the complex necessity to converge concertedly the molecular orbital coefficients on one hand, and the constraining potential V_c on the other. For the purpose of efficient convergence, we have adopted various approaches. In addition of Newton's method implementation and developing adapted DIIS convergence accelerator for C-DFT calculations as described below, we have also used additional criteria and approaches for the convergence procedure. Recalling that the optimization of the constraining potential, V_C, requires a maximization of the energy, which is equivalent to a minimization of the difference between the desired charge and the actual charge, a convergence criterion (CDFTTOL) is applied in our convergence procedure on the charge difference between the desired charge and the actual charge at a given inner loop. In principle, inner loops are carried on as long as the difference between the desired and the actual charge has not reached the tolerance criterion of CDFTTOL. However we have adjusted the criterion and limited the number of inner loops in accordance with the calculation stage. During the first SCF steps, when the electronic density is far from convergence, the number of inner loops is limited and we have set a large tolerance value, while this criterion is tightened as the calculation is progressed. This not only reduces dramatically the number of matrix diagonalization steps, but also assists in the convergence procedure, since a significance change of the constraining potential, V_C, during one outer loop may influence dramatically the results of the next outer loop, leading to an oscillating V_C with large amplitude during the SCF procedure, therefore facing difficulties in convergence. For that cause we have also limited the extent of the change in V_C from one inner loop to the next inner loop.

After SCF procedure has converged, a specialized C-DFT output is created with the one-diabatic state's information required for farther calculation of the overlap S_{AB} between the two diabatic states as well as for calculation of the off diagonal element W_{AB} of the weight function matrix (Eqns. 32-34). This output contains the relevant wavefunction and weight information at each grid point.

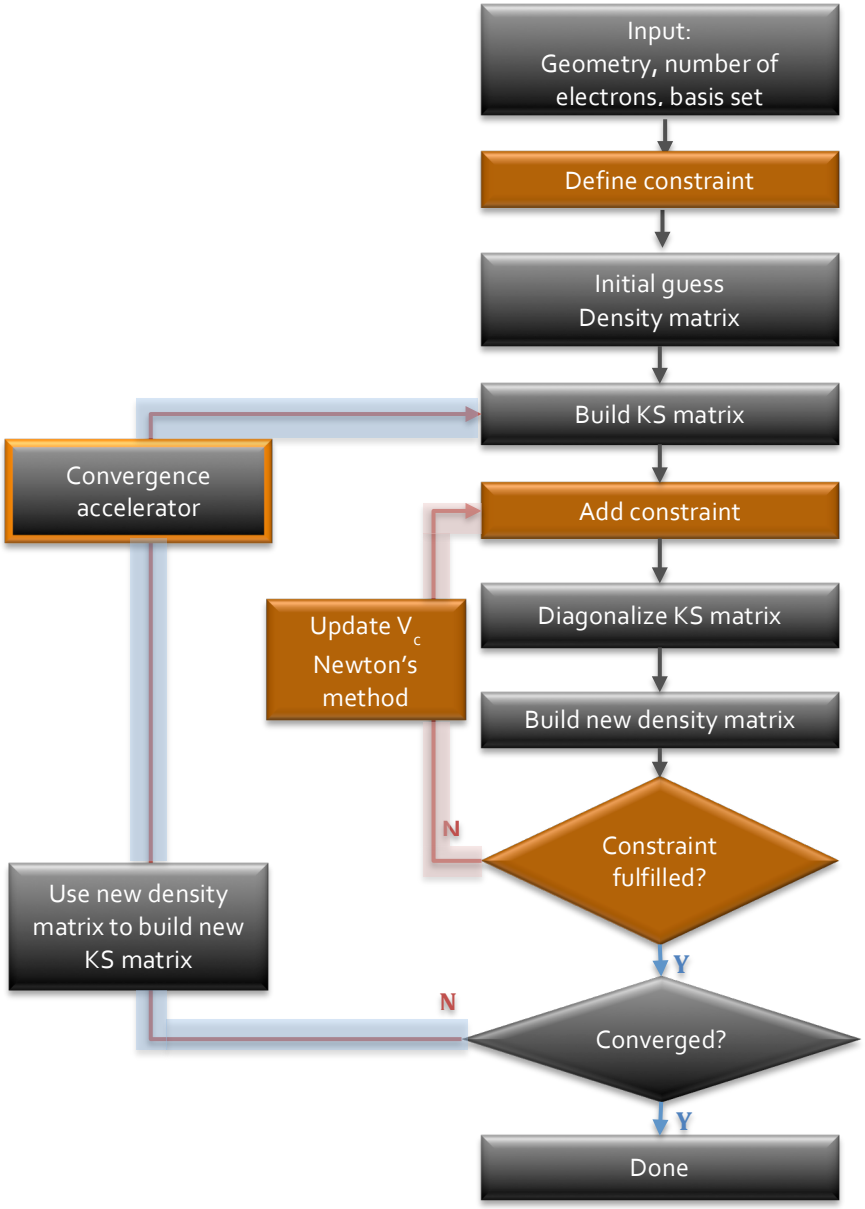

Figure 11. SCF C-DFT procedure algorithm.

7.3 H_{AB} Implementation Components

The overall procedure for the implemented C-DFT method is illustrated in Figure 12. In particular, the ultimate determination of the electronic coupling matrix element, H_{AB}, between two diabatic states, A and B, using the implemented C-DFT method results. For each diabatic state a separate C-DFT SCF procedure is required. As explained above in section 7.2, a specialized molecular orbital output has been developed for each diabatic state, which is used for determination of the overlap S_{AB} between the two diabatic states as well as for calculation of the off diagonal element W_{AB} of the weight function matrix

(Eqns. 32-34). Using these two calculated parameters, together with the energy parameters acquired for each diabatic state, the electronic coupling matrix element H_{AB} is determined in accord with Equations 22-36.

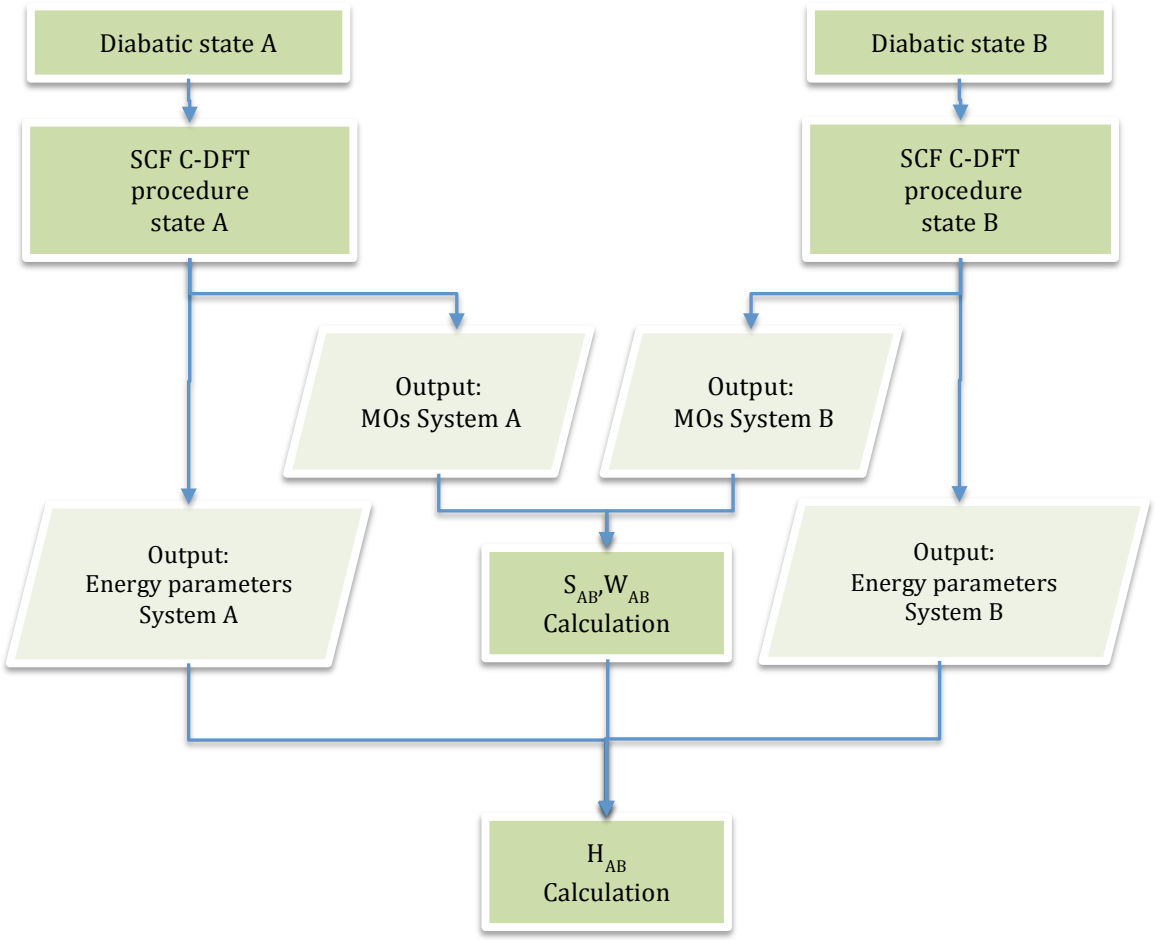

Figure 12. Implementation flow chart of H_{AB} calculation using C-DFT method.

7.4 DIIS accelerator

The use of so-called convergence accelerators may be very effective to improve SCF convergence. As discussed before (section 7.2), since in C-DFT the optimizations with respect to the density and with respect to V_C are entangled, the C-DFT SCF convergence becomes to be even more complex. Therefore, for accelerating SCF convergence, the DIIS (Direct Inversion in the Iterative Space)[82,83] accelerator had been adapted to C-DFT procedure.

DIIS is a powerful tool for an efficient convergence of SCF procedure. With DIIS the current fock matrix at the *n*th iteration is replaced by a linear combination of the previous fock matrices, refining steep changes from one iteration to the next one. Adaptation of DIIS into C-DFT should be handled carefully, as the DFT SCF loop becomes to be a nested loop, where the Fock matrix is changed within each inner loop. Therefore, in our implementation, for each outer loop we use the optimal V_c to construct the Fock matrix and save it to next outer iterations, while within an outer loop, only in the first inner loop a Fock matrix calculated by a linear combination using the optimal constrained Fock matrix of previous outer loops is saved for use of the other inner iterations.

7.5 COSab Solvation Model

For practical calculations our code includes capabilities for various systems reflecting chemical reactions. For that reason we added to our C-DFT code a solvation model capability, as in practice most chemical reactions happen in solution phase rather than in gas phase. The conductor-like screening model COSab, described in a previous section above, was adapted to our C-DFT code within the SCF procedure. While in DFT calculations the solvation energy correction is updated in each SCF iteration of the minimization with respect to the density, in C-DFT calculation the solvation energy correction is needed for every C-DFT SCF inner loop iteration (Fig. 13). Given that the inner loop is employed to optimize V_c, its value is changed within every inner iteration, therefore the electron density is changed within every inner iteration, and the solvation energy correction should be updated consequently as well.

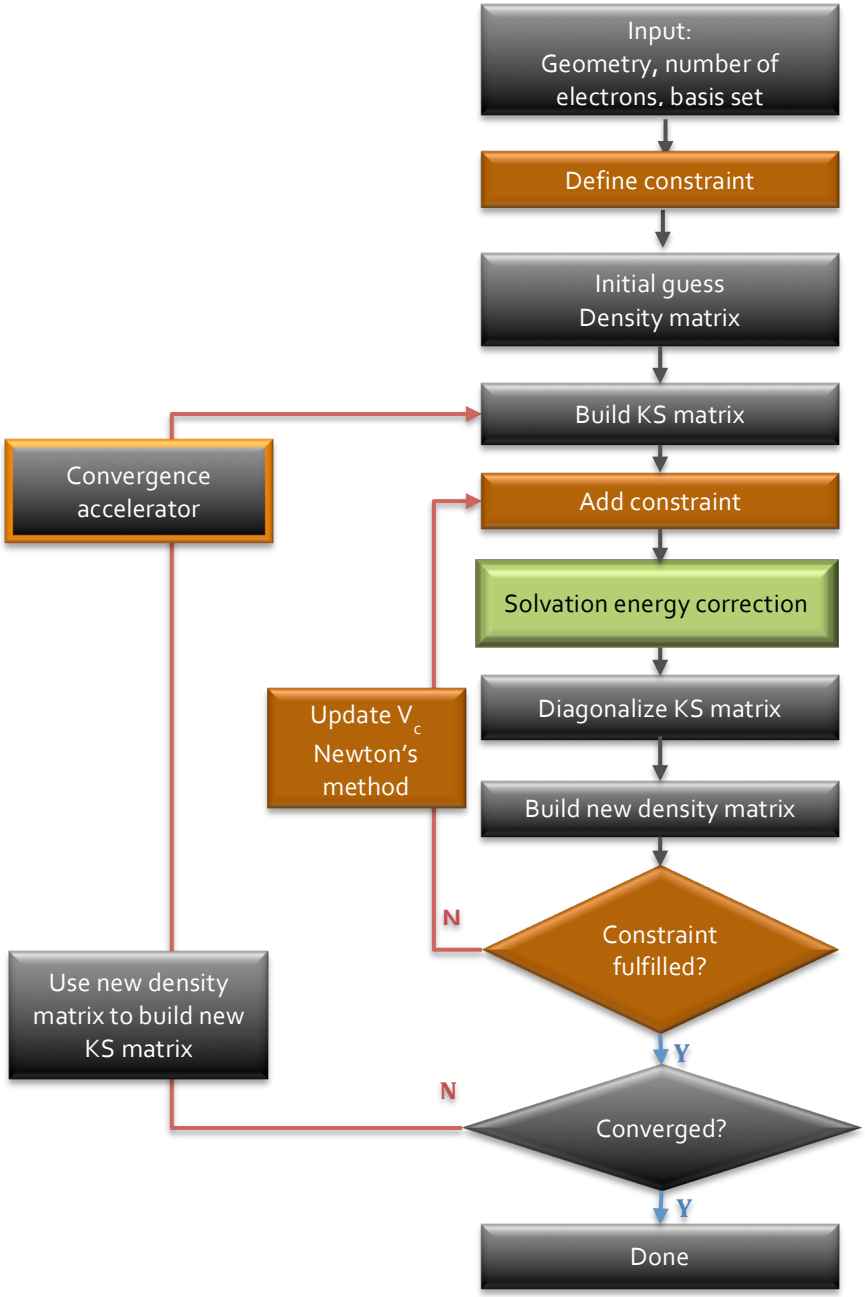

Figure 13. SCF C-DFT procedure algorithm including COSab solvation.

7.6 Localized Molecular Orbitals (LMOs)

In the present work, the following three LMOs representations are evaluated: Boys[79], Edmiston–Ruedenberg (ER)[78] and Pipek–Mezey[75], which are described in a previous section above, and are already implemented within the GAMESS[3] package for DFT calculations . Each of the representation uses different criteria together with a unitary transformation to transform standard delocalized canonical MOs into localized MOs.

To examine the effect of applying various localized MOs schemes compared to the canonical MOs set when calculating the electronic coupling matrix element H_{AB} using C-DFT method, a specialized additional C-DFT output of the LMOs is created. Similar to the specialized output described for the CMOs at section 7.2, the output contains the relevant information of the LMOs at each grid point, for farther calculation of the overlap S_{AB} between the two diabatic states as well as for calculation of the off diagonal element W_{AB} of the weight function matrix according to Eqns. 32-34 (Fig. 12). For each localization method a different procedure was developed for creating the output.

8. Results of C-DFT calculations and discussion

In the C-DFT method, diabatic states are determined for both the donor diabat and the acceptor diabat. In the donor diabatic state, an extra electron(s) or fraction of electron is constrained to be localized on a defined donor fragment. In the acceptor diabatic state, an extra electron(s) or fraction of electron is constrained to be localized on a defined acceptor fragment. In general, C-DFT is formulated such that constraints are in terms of charge and/or spin on defined molecular fragments of the ET system. As discussed, this is typically carried out by the use of one of several options of charge definition or charge population on atoms or fragments.

Atomic charges are not uniquely defined in quantum mechanics nor via experiment. However, in computational methodologies, there are several types of spatial partitioning schemes. These schemes can broadly be divided into two categories: the first category involves schemes that use basis set based partitioning (based on MO analysis), such as Mulliken or Löwdin. The second category involves separation of the electron density in real space in one of a variety of ways, for example, the Becke partitioning scheme.[84]

The Mulliken scheme is based on a partitioning of the atoms based on the nature of the atomic orbitals' contribution to the molecular wave function. In this method, the electrons are partitioned in accord with the center of molecular bonds, where ½ of the electrons go to one of the atoms of the bond and the other ½ go to the other atom. No account is taken of the electronegativity differences of the atoms in the bond, which can lead to quite severe estimates of the charges on the atoms. Another relatively severe problem is that Mulliken populations are extremely basis set dependent, which can lead to results that are in contradiction to chemical intuition. [84]

In the second category of charge partitioning schemes, the Becke approach, the real space is divided into Voronoi cells, each of them comprising all the grid points that are closer to the nucleus under consideration than to any other nucleus. The integrated number of electrons in Voronoi cells is attributed to the atom, thereby defining its charge. Each atomic integral is evaluated on a spherical grid using numerical techniques. Therefore, the Becke scheme is very well suited for C-DFT computations, and is used in the current work.

Critical to the particular study is the identification of the donor and acceptor for the studied ET system, and the establishment of the associated charge constraint that correspond to the amount of charge movement in the particular electron transfer process. Charge constrained, as implemented in this work, can be either defined as the charge on an atom or set of atoms, or, as the difference between the charges of two atoms or between the charges of two sets of fragments of atoms.

Subsequently, the associated diabatic states are calculated for the case where the charge is localized on the donor fragment, and the case where the charge is localized on the acceptor fragment. In the current investigation, the difference between the charge on the diabat associated with the acceptor fragment is set to 1 (1 electron), and the diabat associated with charge on the donor fragment, is set to -1. Therefore, the two diabats together represent the process of a particular ET reaction, where electron is transferred from a donor to an acceptor.

8.1 Restricted Hartree-Fock (RHF) level C-DFT calculations for validation sets

Prior to calculating complex systems, one should validate the basic principles of the methodology using key test systems. For this purpose, specific molecules and sets of molecules are used to test that each aspect of the implemented methodology are correctly working, as detailed below.

8.1.1 Results of charge constraining potential for N_2 symmetric system: Variation of charge constraint

For validation that the charge constraint methodology is working, a symmetric system is chosen and the results monitored as a function of constraint. For this, the N_2 molecule

was chosen, as it is a simple symmetric system, composed of only two atoms that can be identified with a single atom donor and a single atom acceptor. The strong triple bond between the nitrogen atoms provides a good test of the charge constraint methodology. The triple bond in N_2 accounts for its unusual stability, its extraordinary large bond energy (225 kcal/mol) and its very short experimentally observed bond length of 1.10 Å (compared to bond length of 1.21 Å for the double bond in O_2, and to bond length of 1.42 Å for the single bond in F_2).[85,86]

The constraining potential V_c is the Lagrange multiplier that enforces the charge constraint, as discussed in the methodology section above. When the charge constraint is large, one expects a commensurately large value of the constraining potential. In addition, for a symmetric system, one expects symmetrical results when applying the same charge constraint on the donor (N1) and on the acceptor (N2). To examine whether the results from the implemented model correctly show this expected behavior, the starting geometry for N_2 was calculated to be 1.1056729 Å, as optimized at the B3LYP/6-31G(d) level of theory. This bond length is in good agreement to the experimentally observed value of 1.10 Å.[85,86] C-DFT calculations at the same level of theory, B3LYP/6-31G(d), were carried out on the optimized geometry, for various charge separations where for each calculation with a charge constraint on the donor, a symmetrical charge constraint on the acceptor was also calculated. These calculations enabled testing of the closed shell (Restricted Hartree Fock, RHF) implementation of the C-DFT code, using a split-valence representation with d functional polarization effects.

The results of this first validation test are presented in Figure 14. The calculated external constraining potential, V_c, has increasing values as the charge separation demand is higher. This follows what is expected for the implemented model. In addition, one can also see the expected symmetrical behavior for this system, where for each charge constraint on the donor (e.g. charge of 0.6 on atom N1), the resultant constrained potential has an equivalent resultant constrained potential for the same charge constraint on the acceptor (charge of -0.6 on atom N1).

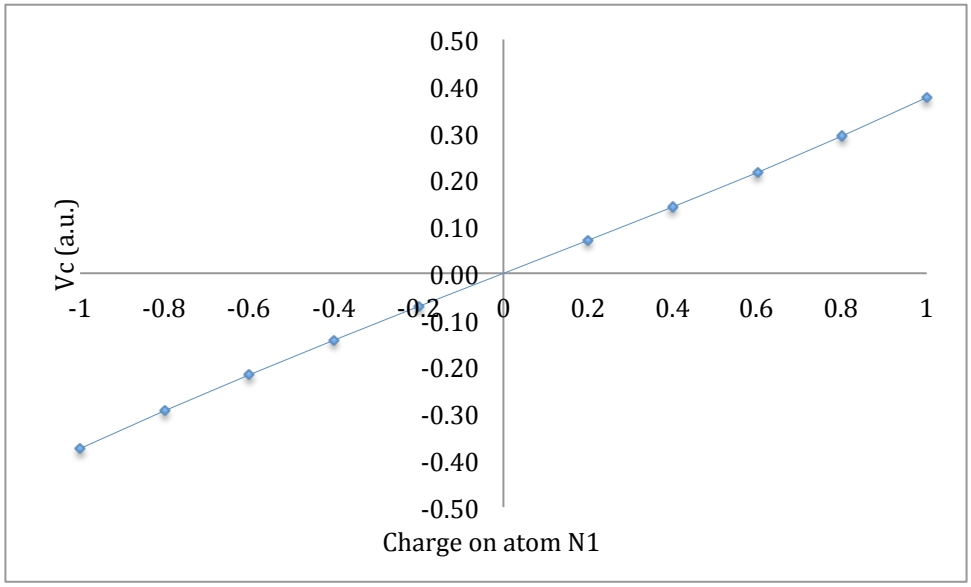

Figure 14. Constraining potential (a.u.) for N_2 molecule as against the charge on atom N1 with separation distance of 1.1056729Å.

With the basic principles of the methodology validated for a simple symmetric system with single atom donor and acceptor components, one can move to more complicated systems to validate additional aspects of the implemented methodology.

8.1.2 Results of constraining potential on C_6H_8: Varying D/A fragments

In C-DFT, the choice of donor and the acceptor fragments of the system has important implications on the extent of the electronic coupling in the electron transfer process. The choice of donor and acceptor component also has impact on the associated constraining potential. As such, careful thought must be put into choice of donor and acceptor definitions prior to carrying out the calculation of the electronic coupling.

To illustrate the effect of donor/acceptor definition, the C_6H_8 system has been investigated to show different constraining potential results. The C_6H_8 molecule was initially optimized with C_{2h} point group symmetry at the B3LYP/6-31G(d) level of theory. From the optimized geometry, three C-DFT systems were constructed with differently specified donor and acceptor components, as follows (Fig 15):

1) D and A defined to be the two CH_2 end groups,
2) D and A defined to be the two end C atoms,
3) D and A defined to be the ethylene end groups

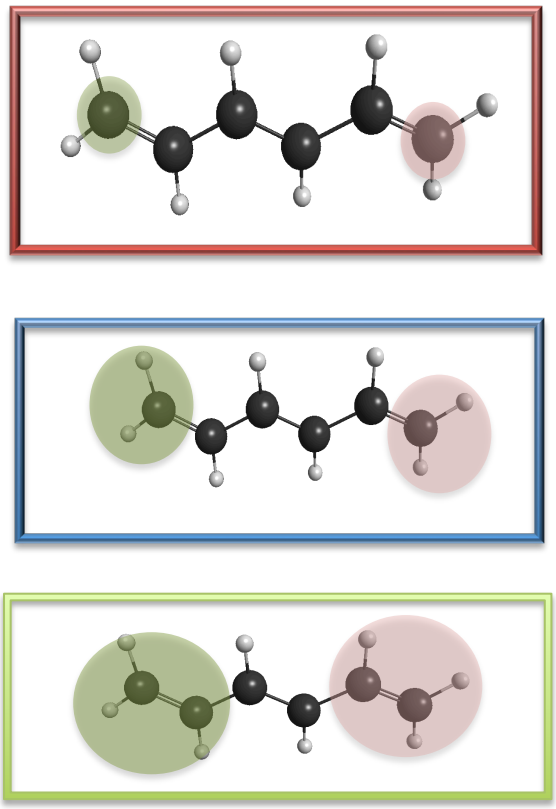

Figure 15. Middle: C_6H_8 with donor and acceptor defined as end CH_2 groups; Top: C_6H_8 with donor and acceptor defined as end C atoms; Bottom: C_6H_8 with donor and acceptor defined as end ethylene groups

Calculations were carried out as a function of charge constraint on the D-bridge-A system. Figure 16 shows the resulting calculated constraining potentials as a function of charge constraint for the three systems. One finds, as expected, that the charge constraining potential has increasing values as the charge separation demand is higher. For the system with donor and acceptor defined as end C atoms, the constraining potential trends calculated are higher, followed by the system with donor and acceptor taken as CH_2 fragment, and finally, the lowest constraining potential trends are associated with the ethylene fragment donor and acceptor component. These trends imply that more external potential is required to enforce the same constraint on a small fragment than for fragments where the constraint demand is distributed across more atoms. As a consequence, the resultant highest total energy value is associated with the D/A defined as the end C atoms (E_{ABS}= -232.818108 a.u.; E_{REL}=75.0 kcal), followed by the system with D/A taken as CH_2 end groups (E_{ABS}=-232.912944 a.u.; E_{REL}=15.5 kcal), where the lowest energy was calculated for the system associated with the ethylene end groups (E_{ABS}=-232.937608 a.u.; E_{REL}=0.0 kcal). The HOMO energy values of the first two systems (i.e., end C atoms as D/A, and CH_2 as D/A) share similar HOMO energy values

(-0.2010 a.u and -0.2026 a.u. respectively). In contrast, when the D/A are assigned as the ethylene pi systems, the calculated HOMO energy value lies significantly higher in energy (-0.1821 a.u.), associated with the reactivity of the pi systems. From an organic chemistry perspective, the most likely D/A fragment would indeed likely be associated with the higher lying pi groups of a D/A molecular construct.

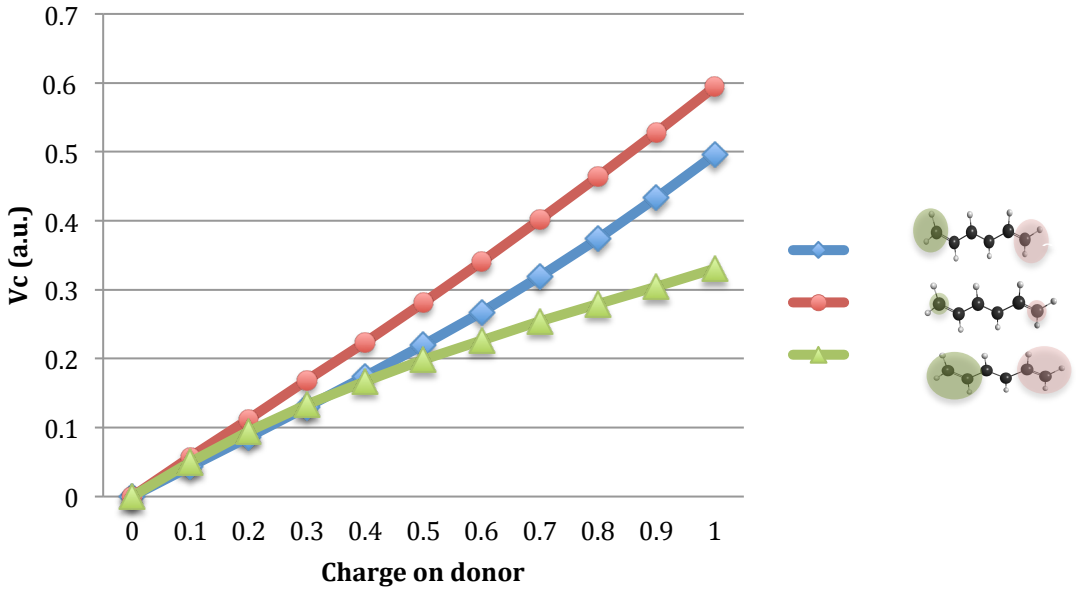

Figure 16. Constraining potential Vc (a.u.) as against the charge separation. Red circles: C_6H_8 with donor and acceptor of end C atoms; blue squares: C_6H_8 with donor and acceptor of end CH_2 groups; green triangles: C_6H_8 with donor and acceptor of end ethylene groups.

8.2 Restricted Open Shell Hartree-Fock (ROHF) level C-DFT calculations for validation sets

8.2.1 Calculated results for ethylene-dimer-cation: Creating diabatic states

To validate the implemented C-DFT methodology for open shell systems, and to validate that the methodology correctly creates the expected diabatic states, a validation test set with the ethylene dimer cation was chosen. This system is small, with clear donor and acceptor fragments definition, while the choice of this molecule reflects the interest in describing charge transport in organic semiconducting materials.

The initial geometry of the ethylene monomer was fully optimized at the B3LYP/6-31G(d) level of theory. The dimer cation was then created from two monomers with an initial fixed distance of 3.5 Å. The associated diabatic states of the ethylene-dimer-cation system were created based on a specified charge difference constraint as follows. For

the acceptor diabatic state, A, the charge (+1) was constrained to the upper dimer fragment. For the donor diabatic state, B, the charge (+1) was constrained to the lower dimer fragment. The resulting system is shown in Fig. 17.

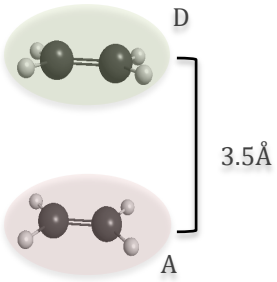

Figure 17. Ethylene-dimer-cation with distance of 3.5 Å between the donor and acceptor components.

The constraining potential calculated for these two diabatic states are both found to be 0.21 Hartree, as expected for a symmetrically designed system. The associated SOMO and SOMO-1 orbitals (Fig. 18) calculated show the excess electron on the lower fragment for state A, and the excess of an electron on the upper fragment for state B. For state A, the doubly occupied orbital SOMO-1 is localized on the lower fragment, while the singly occupied SOMO orbital is localized on the upper fragment. For state B, the opposite picture is found. As such, C-DFT methodology is adequately representing the open shell system, and, is able to create the two diabats according to the constraints. One diabatic state has excess of an electron on the donor, while the other diabatic state has excess of an electron on the acceptor. Therefore, the two diabatic states can adequately represent an electron transfer reaction from the donor to the acceptor.

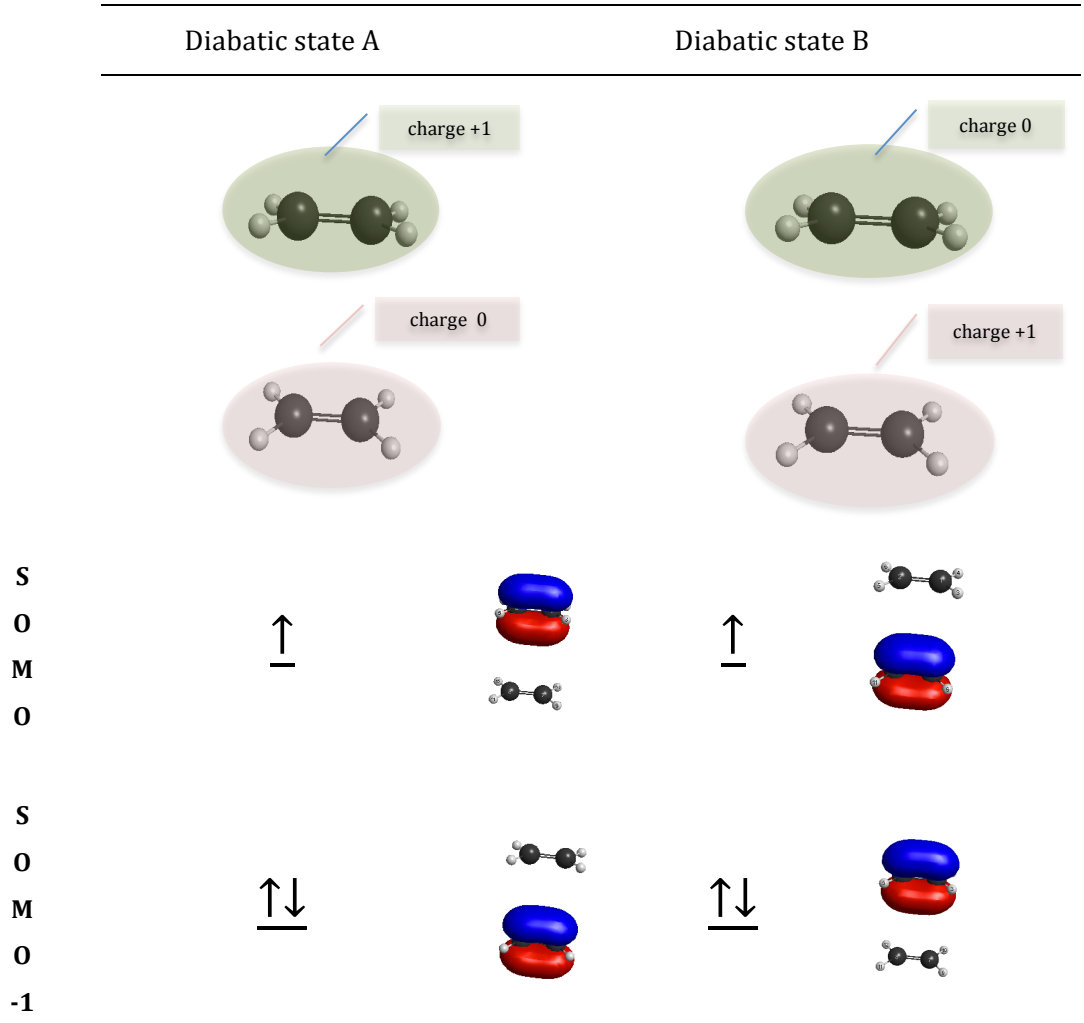

Figure 18. The two diabatic states with their charge constraints of ethylene-dimer-cation and the SOMO and SOMO-1 orbitals of those states.

8.3 Restricted Open Shell Hartree-Fock (ROHF) level C-DFT S_{AB} and H_{AB} results

8.3.1 Calculated results for anthracene-dimer-anion: S_{AB} and H_{AB} results

To investigate results of the calculated overlap and electronic coupling predicted by the implemented C-DFT methodology, the anthracene-dimer anion was chosen. This also tests the open shell implementation. The choice of the anthracene dimer anion system reflects an interest in organic semiconducting materials that possess extended π-conjugated systems, while the anthracene dimer is one of the smallest such systems. In this system, the donor and acceptor fragments were associated with each of the monomers of the anthracene dimer anion complex as shown in Figure 19. This system is classified as a non-bridged (or bridgeless) D/A system. For this validation test, associated diabatic states of the anthracene-dimer-anion were investigated as a function

of the distance between the monomers.

The initial geometry for the anthracene monomer was taken from previous work of Blumberger at the BP86/def2-TZVP level of theory.[87] From this optimized monomer, various anthracene dimer anions were created with different fixed distances between monomer units. This was followed by C-DFT calculations at the B3LYP/6-31G(d) level of theory, as in the previous validation tests. For donor diabatic state A, a charge of -1 was constrained to the upper dimer fragment, while for acceptor diabatic state B, a charge of -1 was constrained to the lower dimer fragment (Fig. 21).

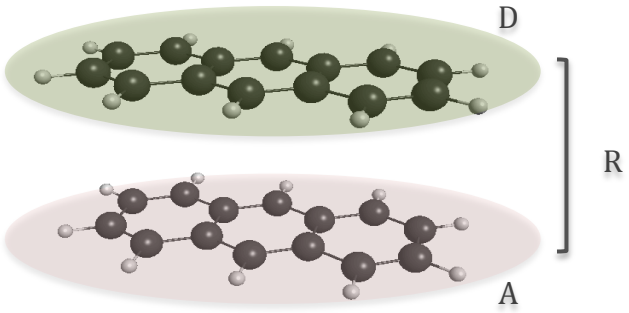

Figure 19. Anthracene-dimer-anion with distance R between the donor and acceptor monomer fragments.

The overlap between diabatic states A and B, S_{AB}, as a function of distance between the monomers was determined from the overlap of the associated SOMO orbitals (the calculated SOMO orbitals are displayed in Figure 21). As shown in Figure 20, the calculated overlap decreases exponentially with the distance between the donor and acceptor fragments ($R^2 = 0.965$). This behavior originates from the overlap between the tails of the wave functions of the donor and the acceptor. As the tails decay exponentially, the overlap is also expected to fall off exponentially as the distance (R) between the donor and the acceptor increases.

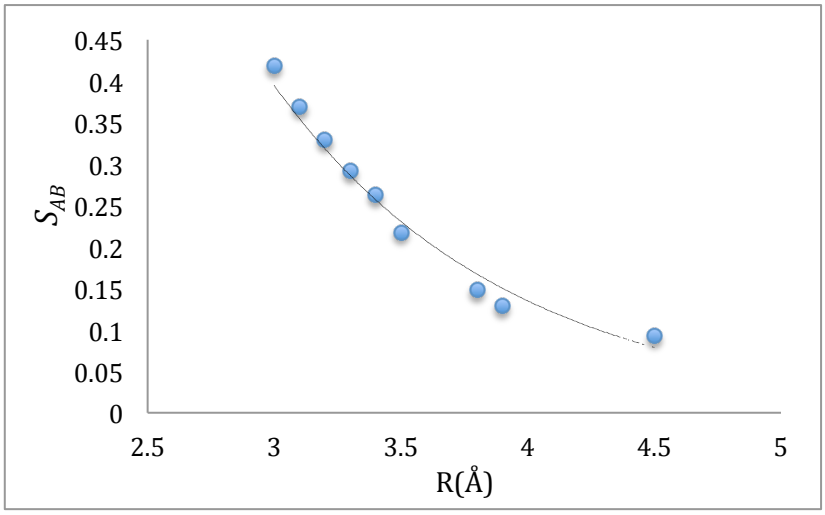

Figure 20. Overlap between diabatic states as a function of the distance R between the donor and the acceptor (Å) fragments for the anthracene dimer anion.

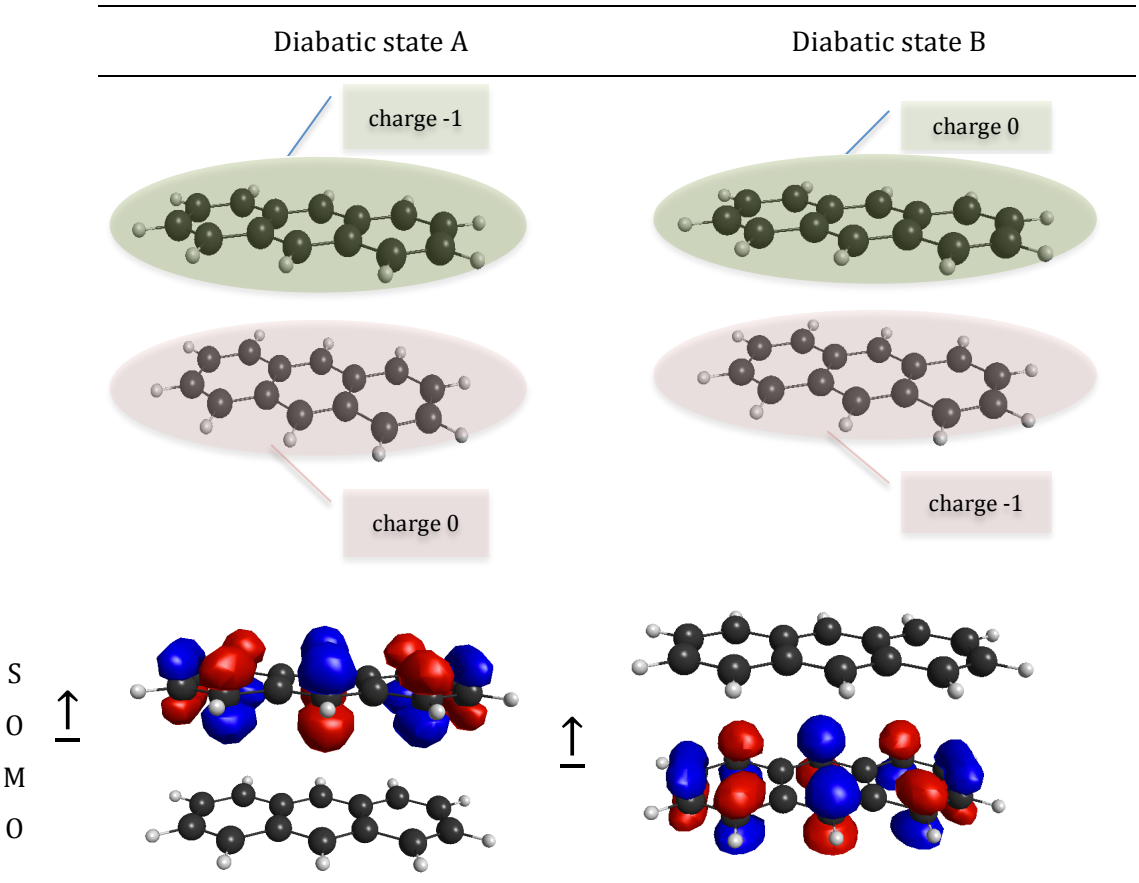

Figure 21. Two diabatic states of the anthracene dimer anion, with associated charge constraints and SOMO orbitals.

The exponential decay of the overlap S_{AB} with increasing distance between D and A fragments is also reflected in the results of calculated electronic coupling matrix element,

H_{AB}, between the two diabatic states. This is expected, as the overlap S_{AB} is used in the determination of the electronic coupling matrix element according to Eqn 29. As such, one also expects an exponential decrease in electronic coupling as the distance between the donor and acceptor components increases. The corresponding results of calculated H_{AB} for the system as a function of increasing spacing between donor and acceptor are shown in Figure 22. In this case, the exponential fit is found to be y=3.4e(-1.48x) with R^2= 0.993. As such, this system shows a β/2 attenuation rate of 1.48 Å. These results are found to be in close agreement to the high level conventional *ab initio* SCS-CC2 results obtained by Kubas *et.al*[87], as shown in Figure 22. For this bridgeless system, the calculated attenuation factor (β/2)= 1.48 $Å^{-1}$ is high and in agreement with β values characteristic for electron transfer in vacuum, for which values are typically found between 2.8 $Å^{-1}$ < β < 3.5 $Å^{-1}$.[54,55]

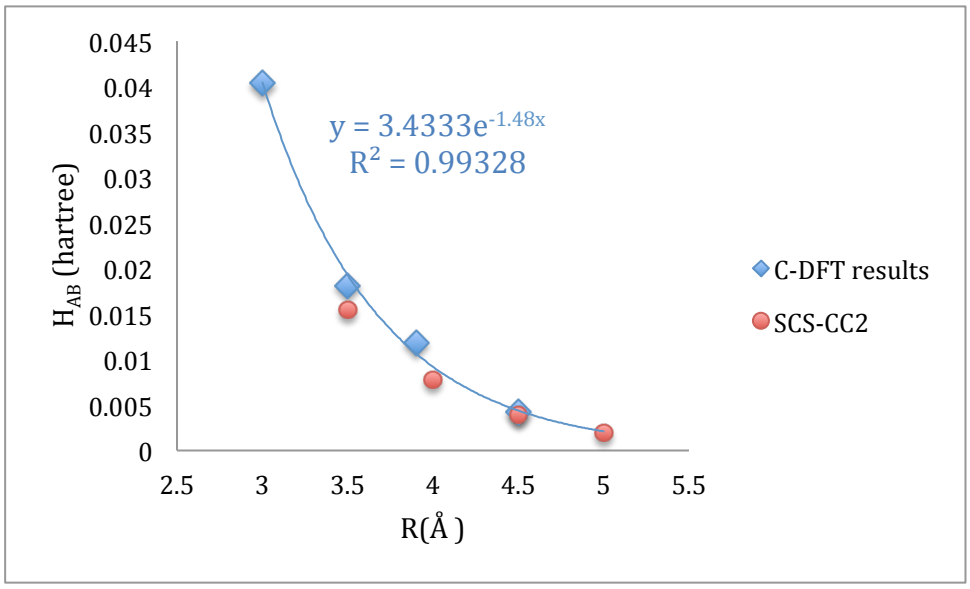

Figure 22. Electronic coupling matrix element (hartree) between diabatic states as against the distance between the donor and the acceptor (Å) as calculated with C-DFT results (blue) and compared to results of reference 87.

8.4 Electronic coupling matrix element for donor-bridge-acceptor (D-B-A) systems

For the last decade, there has been much interest in accurate predictions of electronic coupling in bridge-mediated nonadiabatic electron transfer reactions, where interaction between the donor and the acceptor orbitals can take place via through-apace (TS) and through-bond (TB) effects.[28] Detailed understanding of these interactions and their influences on the electronic coupling is essential for understanding the mechanism of bridge mediated ET reactions. In particular, electronic coupling can be shown to be

affected by the details associated with the bridge length as well as the specific nature of the bridge construction.

8.4.1 Bridge mediated systems with saturated hydrocarbon bridge

Comprehensive photoemission spectroscopy (PES) and electron transmission spectroscopy (ETS) studies on bridge mediated D–B–A systems based on saturated hydrocarbons were advocated by Paddon-Row *et al.*[19,88,89,90] for many years for the purpose of detailed understanding of bridge characteristics affecting the electronic coupling. Extensive studies have been dedicated to the set molecules **1**-**6** shown in Figure 23. This validation test series is characterized by ethylene D/A groups with intervening σ-bonded norbornyl-unit bridges of varying length.

Utilizing the experimental techniques of PES and ETS provides the energy level splittings between the adiabatic states. Computationally, this splitting is associated with twice the calculated value of electronic coupling in the C-DFT theory, $2*H_{ab}$.[19] Important development of this area is also attributed to the design, synthesis, and characterization of greater complexity series of unsymmetrical D/A with saturated bridge D-B-A series of molecules such as **7'**-**11'**, shown in Figure 24. These latter systems are characterized by a dimethoxynaphthalene donor coupled to dicyanovinyl acceptor, with varying length norbornyl-type-unit bridge.[61,19,88]

The experimental data reported[90,61] is used for comparisons in the present work where available. The results are also compared to results acquired using an alternative computational approach for determination of electronic coupling in nonadiabatic systems, developed previously in our group by Berstis.[22] That alternative approach was developed to enable accurate yet inexpensive predictions of ET parameters, in particular electronic coupling, for bridge mediated systems. The method is based on construction of an effective Hamiltonian using a Green function operator and Löwdin partitioning scheme.[22]

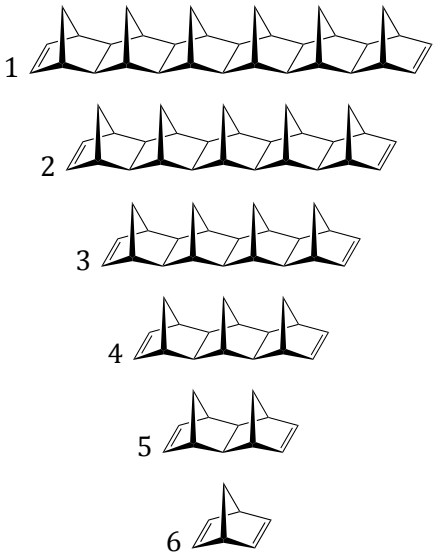

Figure 23. Molecules 1-6 of ethylene D/A groups with intervening σ-bonded norbornyl-bridge units.

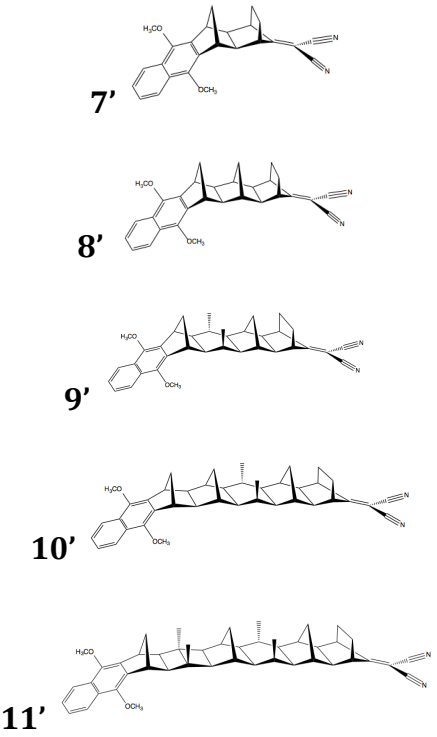

Figure 24. Molecules **7'-11'** with dimethoxynaphthalene donor coupled to dicyanovinyl acceptor, with varying length of norbornyl-based bridge.

8.4.1.1 Symmetric D-B-A saturated hydrocarbon bridge

To study the dependence of the electronic coupling on the mechanistic details through the bridge, it is of interest to investigate the details of not only the bridge length but the particular nature of the bridge in terms of pathways through the bridge. In the present test set, the central attention is on systems with saturated hydrocarbon bridges. In particular, systems **1**-**6**, consisting of ethylene groups as donor and acceptor, with intervening σ-bonded norbornyl-unit bridge units of varying length (Fig. 23). The implemented C-DFT method was employed for calculation of the associated two diabatic states for each molecule, at the B3LYP/6-31G(d) level of theory. The donor and the acceptor were defined as the ethylene end groups for all systems (Fig. 25).

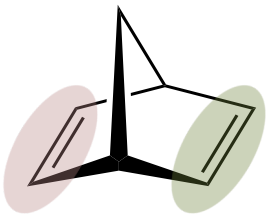

Figure 25. In the test series **1**-**6**, the ethylene end groups are defined as donor and acceptor, respectively.

In a standard DFT calculation without charge constraint, the canonical highest occupied molecular orbital (HOMO) is found to involve the π orbital of both the donor and the acceptor fragments. In a C-DFT calculation, on the other hand, the highest occupied molecular orbital for the donor and acceptor diabatic state is localized on the donor and on the acceptor fragments, respectively, in accord with the D/A fragment definition (Fig. 26).

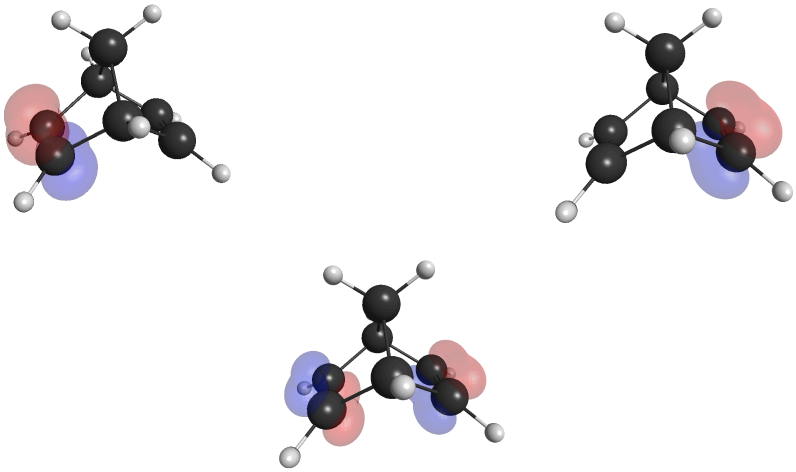

Figure 26. Top: Highest occupied molecular orbitals of each of the diabatic states for system **6**. Bottom: Highest occupied molecular orbital of standard DFT calculation of molecule **6.**

Looking at the overlap values, S_{AB}, from the C-DFT calculation for the set **1**-**6** (Table 3), one can see that, as expected, the overlap S_{AB} between the two diabatic states decreases with increasing donor-acceptor distance. The correlation shows an exponential decrease with exponential curve fitting of R^2= 0.997 (Fig. 27). This sharp decrease is associated primarily with the decay of TS interactions as the bridge length separates the D and A orbitals to the point where there is virtually no interaction. However, there is also a progressively weakening TB coupling as the bridge lengthens, as illustrated by the progressive reduction in the contribution of the bridge to the HOMO with increasing bridge units (Table 3).

Molecule	HOMO diabatic state A	S_{AB}
6	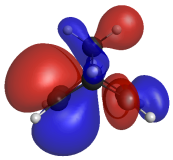	0.1912
5	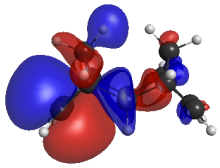	0.0911
4	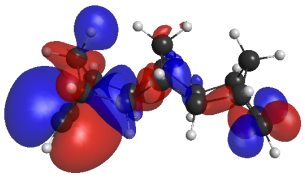	0.0247
3	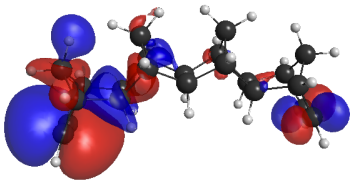	0.0081
2	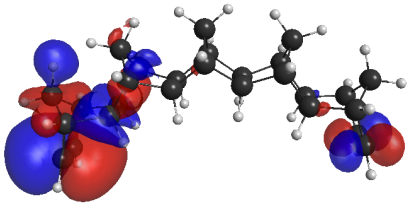	0.0029
1	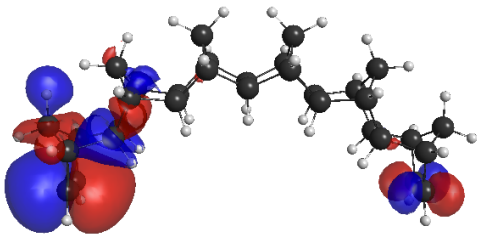	0.0010

Table 3. Highest occupied molecular orbitals for diabatic state A for molecules **1**-**6**, with the respective overlap S_{AB} values (contour value for the purpose of orbitals illustration in MacMolPlt = 0.015 a.u.).

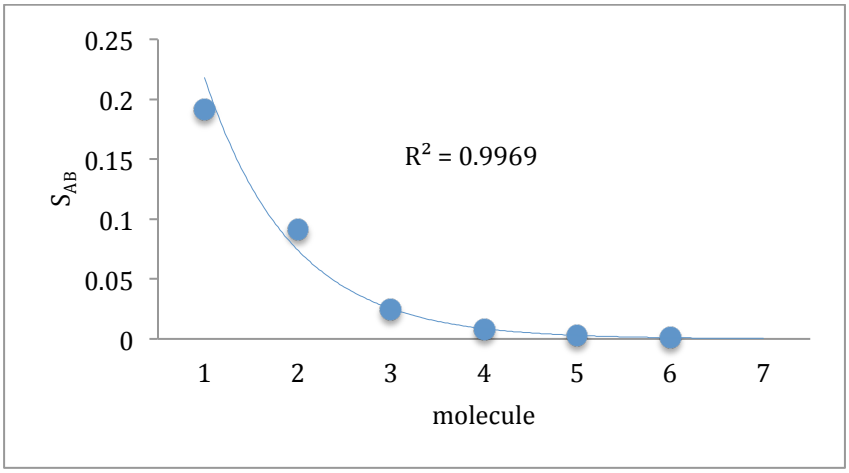

Figure 27. Overlap S_{AB} between the two diabatic states for molecules **1**-**6**.

The exponential decay of the overlap S_{AB} with increasing bridge units is again reflected in the results of calculated electronic coupling matrix element H_{AB} between the two diabatic states of molecules **1**-**6**, in accord with Eqn. 29 (Figure 28). The electronic coupling matrix element has the characteristic exponentially behavior (curve fitting R^2= 0.983) with increasing distance between the donor and the acceptor. The calculated attenuation factor (β/2) in accord with Eqn. 19 is 0.541 $Å^{-1}$, a value that is found to be in good agreement with β values characteristic for saturated hydrocarbon bridged systems.[16, 60,61]

Looking at the highest occupied molecular orbitals of systems **1**-**6** obtained with C-DFT (Table 3), one can see the progressive reduction in the contribution of the bridge with increasing bridge units, highlighting again the weakening TB coupling. The results can be compared to experimental values (Table 4) of splitting between the adiabatic states, as associated with $2*H_{ab}$. This comparison is shown for systems **5** and **4** (values for **3** were too small to be determined with these experimental techniques).[19,90] Figure 28 shows the relative agreement between the C-DFT results and those of experiment.

5 	Splitting=0.87ev H_{ab}=0.87/2=0.435ev
4 	Splitting=0.32ev H_{ab}=0.32/2=0.16ev

Table 4. Experimental values for the electronic coupling matrix element H_{AB} for **4** and **5**.[90]

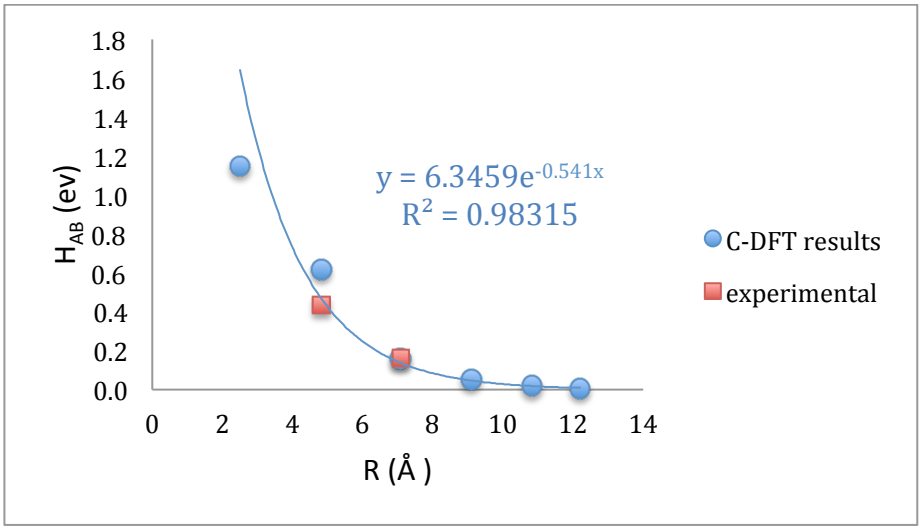

Figure 28. Electronic coupling matrix element H_{AB} (ev) against the distance R between the donor and the acceptor calculated with C-DFT method using 6-31G(d) basis set (blue) for molecules **1**-**6**, and experimental values[90] (red) for molecules **4** and **5**.

It also is of interest to investigate the quality of the electronic coupling prediction with level of theory, for example, wavefunction type and basis set extent. This is important to understand the level of theory necessary to make reliable predictions with economical cost. To further examine the effect of the basis set choice on the electronic coupling results using the C-DFT methodology, calculations were carried out using the basic STO-3G basis set, the 6-31G(d) basis set, and the 6-31G+(d) basis set. As a general observation, (Fig. 29) all three basis sets show the expected exponential decrease of the coupling with increasing D/A distance with relative consistency across the basis sets. In particular, the relatively modest STO-3G basis set results show similarity to the 6-31G(d) results, with almost the same attenuation factor (0.536 and 0.540 respectively). The basis set with the diffuse functionality, shows a faster (attenuation factor 0.609) decrease, where the significant differences appear to occur mostly in short D/A distances. The reliable results achieved with the economical STO-3G basis set can support its use for larger and more complex systems, where computational time considerations are involved.

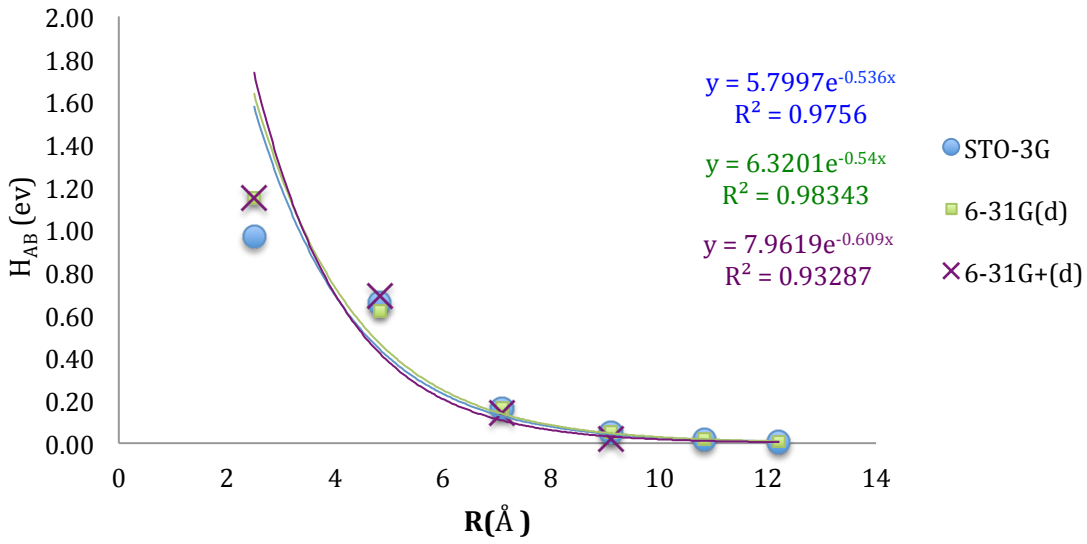

Figure 29. Electronic coupling matrix element H_{AB} (ev) against the distance R between the donor and the acceptor calculated with C-DFT method for various basis sets: STO-3G (blue circles), 6-31G(d) (green squares) and 6-31G+(d) in purple crosses.

Figure 30 also shows the trends in electronic coupling predictions as a function of basis set extent for systems **1**-**5**, with comparisons to the theory of Berstis[22] using the DFT based Green's function model, where in a general observation, one finds a relative consistency in predictions across basis set, with the exception of when diffuse functionality is incorporated into the basis set. Using diffuse functions resulted in coupling overestimation, which was suggested to be associated with the loss of locality and expansion of the D/A areas for the electron to occupy into regions too delocalized on the bridge. With respect to C-DFT, in general, one can see compatibility of results in terms of behavior as a function of basis set extent and size in a good extent between the two methods, despite the quite difference in theoretical methodology.

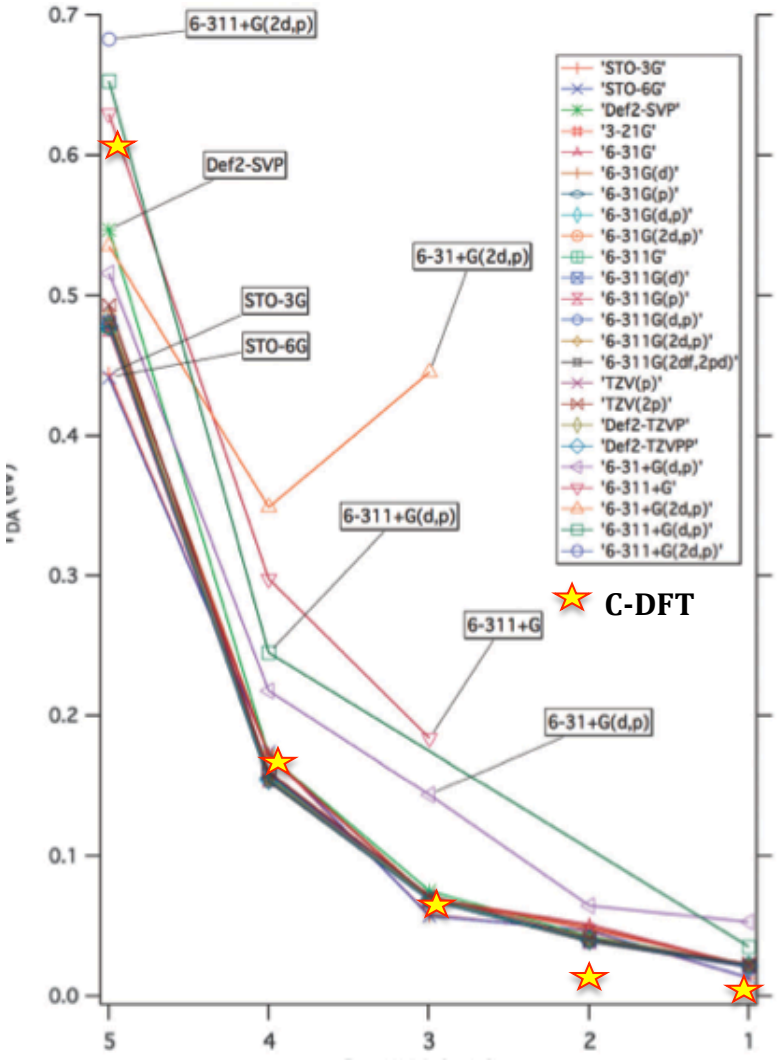

Figure 30. Electronic coupling matrix element H_{AB} (ev) for molecules **1-5** results taken from reference no. 22 for various basis sets using DFT based Green's function method, with C-DFT results using 6-31G(d) basis set added on top of that, marked with yellow-red stars symbols.

8.4.1.2 Effect of D/A fragments definition in C-DFT: D-B-A saturated hydrocarbon bridge

Unlike in the above more simplified validation set, more complicated D–Bridge–A systems can introduce difficulties in the determination of the donor and the acceptor fragments. In particular, it becomes more and more difficult to isolate the specific molecular orbital(s) that dominate the contribution to the electronic coupling. What typically becomes necessary is to investigate several possible D/A fragment choices, looking at the probability for electron transfer by way of each individual possibility in terms of the magnitude of the electronic coupling determined. In this way, one is essentially investigating different electron transfer pathways through the D/A system, and identifying the most probable path for the occurrence of an electron transfer.

To explore the effect of D/A fragments choices on prediction of electronic coupling in more complex systems than the series **1**-**6**, the series of molecules **7**-**10** (Fig. 31) was chosen. This series has been adapted from the corresponding experimental set of molecules **7'**-**10'** in Figure 24 above, to create a more consistent set for testing. This series is characterized by a dimethoxynaphthalene donor coupled to dicyanovinyl acceptor, with varying length of norbornyl-type bridge. Experimental ET reaction rate measurements using fluoresecence quenching have been determined for molecules **9'**-**11'**.[61] A three-point correlation with distance was obtained showing exponential decay with β factor of 0.85 $Å^{-1}$, which can be compared to the theoretical C-DFT predictions via Equation 21.

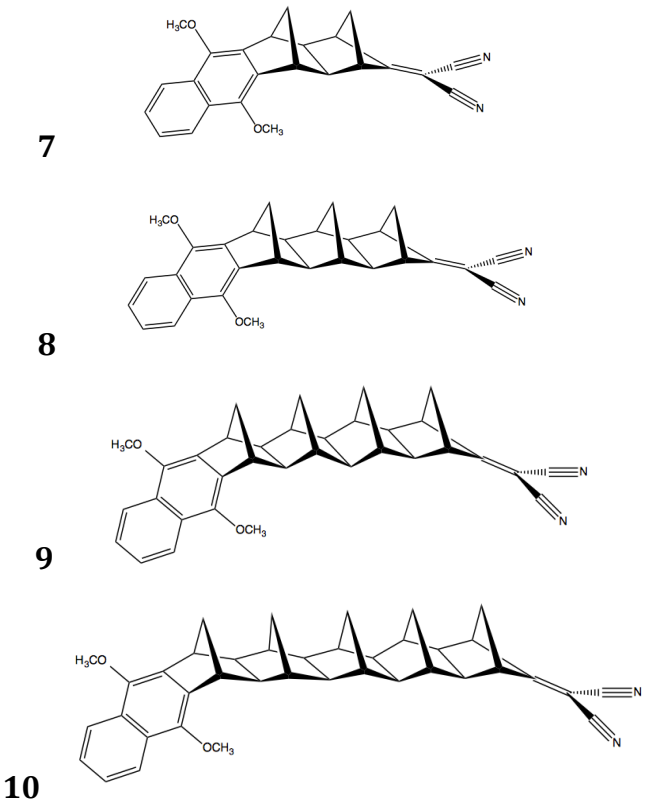

Figure 31. D-bridge-A systems **7**-**10** characterized by a dimethoxynaphthalene donor coupled to dicyanovinyl acceptor, with varying length norbornyl-type bridge.

To explore the effect of D/A fragments choice on the overall electronic coupling factor, the four different D/A fragment definitions, b1-b4, were chosen corresponding to molecules **7**-**10** respectively, as shown in Figure 32. The results for each system are discussed separately in the next sections.

	D	A
b1	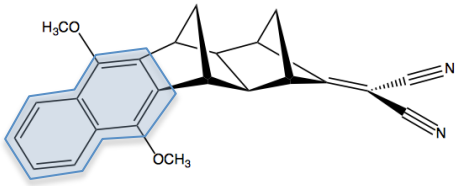	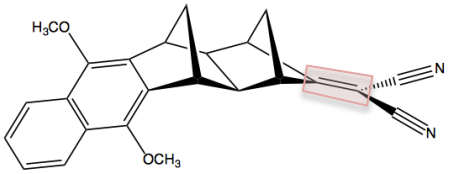
b2	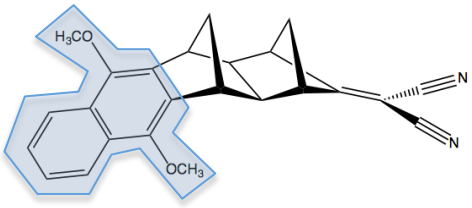	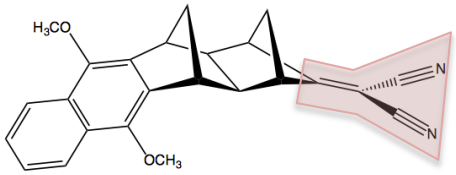
b3	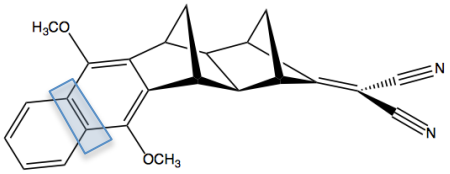	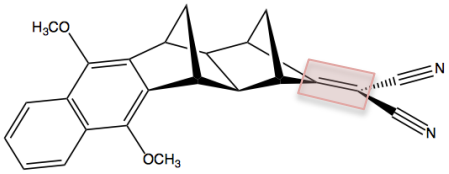
b4	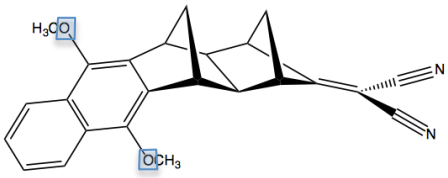	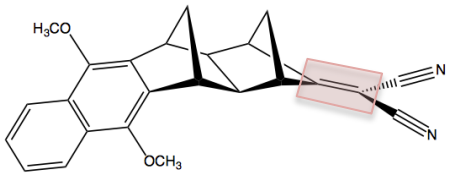

Figure 32. C-DFT various D/A fragment definitions (b1-b4) for molecules **7**-**10**, as presented by molecule **7**.

8.4.1.2.1 b1 D/A fragments choice

The D/A fragments for set b1 were defined to be all carbon atoms of the naphthalene groups as the donor, and the two carbon atoms of the vinyl group as the acceptor as illustrated in Figure 32. Motivated by reliable results, received in the former section (molecules **1**-**6**) using the B3LYP/STO-3G basis set, and for economical computation reason, the validation C-DFT calculations were carried out at the B3LYP/STO-3G level of theory for initial testing. To obtain the appropriate combination of molecular orbitals of donor diabatic state and acceptor diabatic state that are primary contributors towards the electronic coupling, it is necessary to evaluate the set of all possible π-type molecular orbitals associated with the chosen D and the A fragments (Fig. 33). Analysis

of all the possible D/A MO pairs (Table 5) reveal a particular set of MOs, one from diabatic state A (HOMO) representing the acceptor, and one from diabatic state B (HOMO-1) representing the donor. This pair in particular is found to dominate the contributions to the electronic coupling. As one can see in Figure 34, this set of MOs has non-negligible S_{AB} values, and one finds also the expected exponential behavior (exponential fit R^2=0.994) with increasing bridge length.

	Diabatic state B	Diabatic state A
HOMO (no.97)	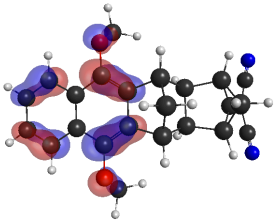	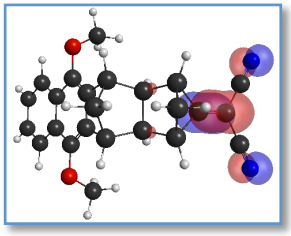
HOMO-1 (no. 96)	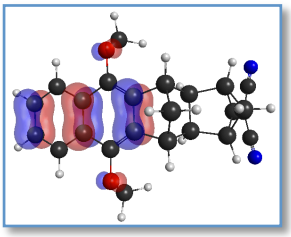	
HOMO-2 (no. 95)	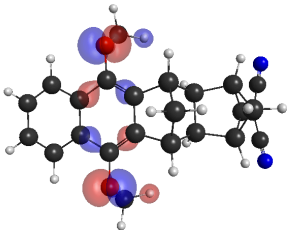	
HOMO-3 (no. 94)	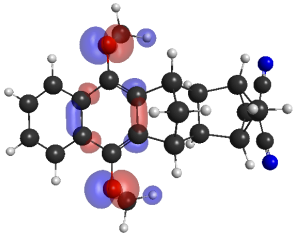	

Figure 33. The **7** highest occupied MOs for D/A definition b1. The molecular orbital contour value in MacMolPlt = 0.05 a.u.

Orbital: Diabatic State B	Orbital: diabatic state A	S_{AB} molecule 7	S_{AB} molecule 8	S_{AB} molecule 9	S_{AB} molecule 10
HOMO	HOMO	3.0E-10	8.7E-08	2.7E-08	8.0E-09
HOMO-1	HOMO	0.09841	0.03050	0.01085	0.00476
HOMO-2	HOMO	4.1E-08	2.1E-08	1.2E-09	7.2E-09
HOMO-3	HOMO	0.02643	0.00098	0.00017	0.00018

Table 5. Overlap S_{AB} of relevant MOs pairs between the two diabatic states, A and B, for D/A definition b1. The corresponding molecular orbitals are shown in Figure 33.

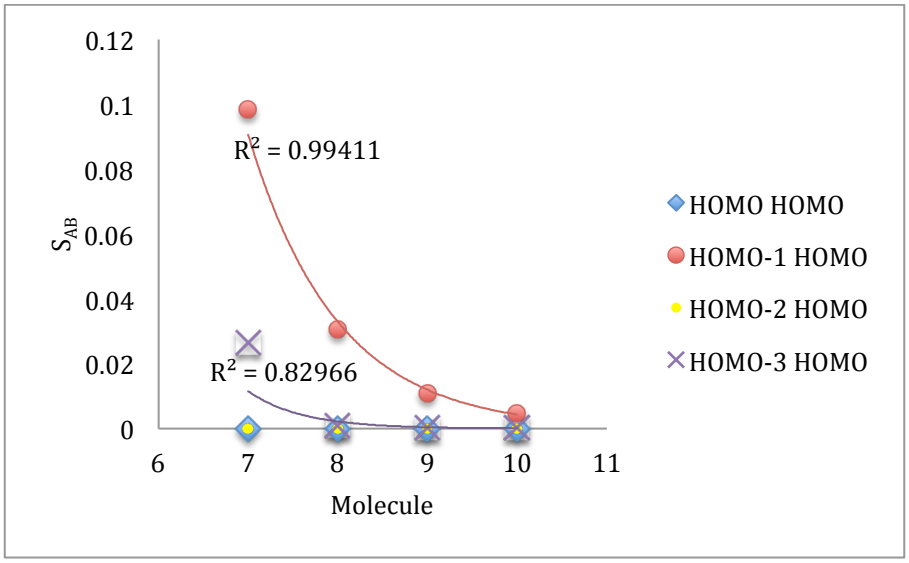

Figure 34. S_{AB} values for systems **7**-**10** using the b1 D/A definition, for various MO pairs.

The exponential decay of the overlap S_{AB} with increasing bridge units for HOMO of diabatic state A and (HOMO-1) for diabatic state B, is again also reflected in the results of the calculated electronic coupling matrix element (Fig. 35), H_{AB}, between the two diabatic states, with curve fitting R^2= 0.999 as a function of increasing distance between the donor and the acceptor units, and the attenuation factor (β/2) in accord with Eqn. 19 is found to be 0.497 $Å^{-1}$, a value which is in agreement with β values characteristic for saturated hydrocarbon bridged systems,[16, 60,61] as well as with the experimental value (β/2)=0.425 $Å^{-1}$ associated with this set of systems. Therefore, the b1 definition of D/A fragment appears to properly localize the MOs in accord with the desired constraint D-bridge-A partition.

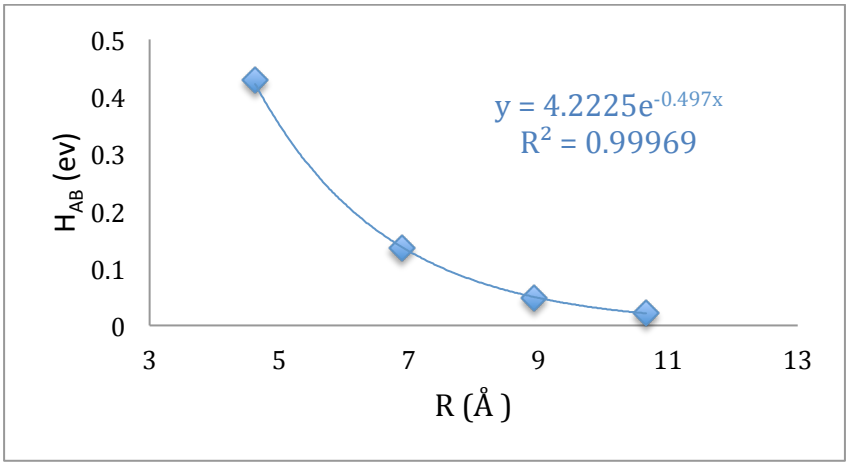

Figure 35. Electronic coupling matrix element H_{AB} (ev) against the distance R between the donor and the acceptor calculated with C-DFT method for molecules **7**-**10** b1 set.

8.4.1.2.2 b2 D/A fragments choice

The D/A fragments for b2 set were defined to be all atoms of the dimethoxynaphthalene as the donor, and all atoms of the dicyanovinyl as the acceptor (Fig. 32). The C-DFT calculations were carried out at the B3LYP/STO-3G level of theory for initial testing. In the same manner as with the b1 definition, analysis of all possible π-type D/A MO pairs (Fig. 36) failed to find any suitable pair with non-negligible values and with the expected exponential behavior (Table 6, Fig. 37).

	Diabatic state B Contour value=0.05	Diabatic state A Contour value=0.05
HOMO (no.97)	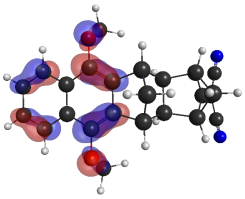	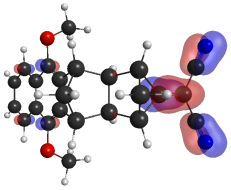
HOMO-1 (no. 96)	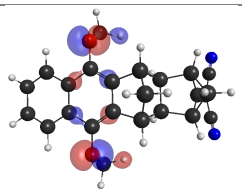	
HOMO-2 (no. 95)	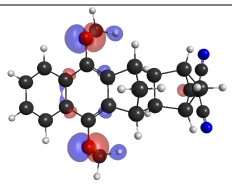	
HOMO-3 (no. 94)	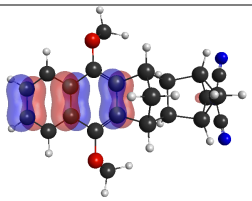	

Figure 36. b2 molecule **7** highest MOs.

Orbital: Diabatic State B	Orbital: diabatic state A	S_{AB} molecule **7**	S_{AB} molecule **8**	S_{AB} molecule **9**	S_{AB} molecule **10**
HOMO	HOMO	1.2E-07	0.04621	0.04599	0.04615
HOMO-1	HOMO	7.2E-08	0.00216	0.00199	0.00212
HOMO-2	HOMO	0.03519	0.00268	0.00229	0.00202
HOMO-3	HOMO	0.01101	0.01359	0.01878	0.02067

Table 6. Overlap S_{AB} of relevant MOs pairs between the two diabatic states, A and B, for D/A definition b2. The corresponding molecular orbitals are shown in Figure 36.

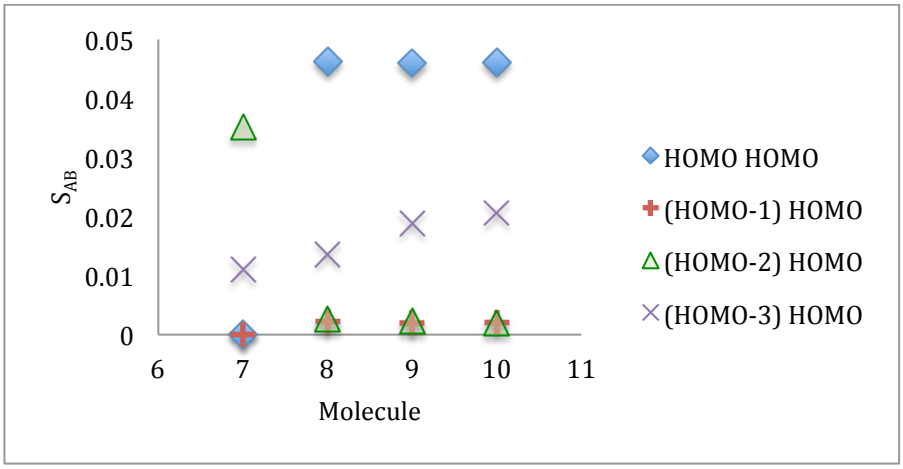

Figure 37. S_{AB} values for systems **7-10** using the b2 D/A definition, for various MO pairs.

As with the b1 definition, the analogous combination of MOs types, i.e. HOMO of diabatic state A and (HOMO-3) of diabatic state B (Fig. 36) were used to explore the electronic coupling matrix element H_{AB} between the two diabatic states, using the overlap S_{AB} for calculating the electronic coupling matrix element according to equation 29 (Fig. 38). As one can see, the S_{AB} behavior is reflected also in the results of the electronic coupling matrix element H_{AB}, showing non-exponential behavior. This behavior is not compatible with the exponential trend expected from this type of saturated hydrocarbon bridged D-B-A system.

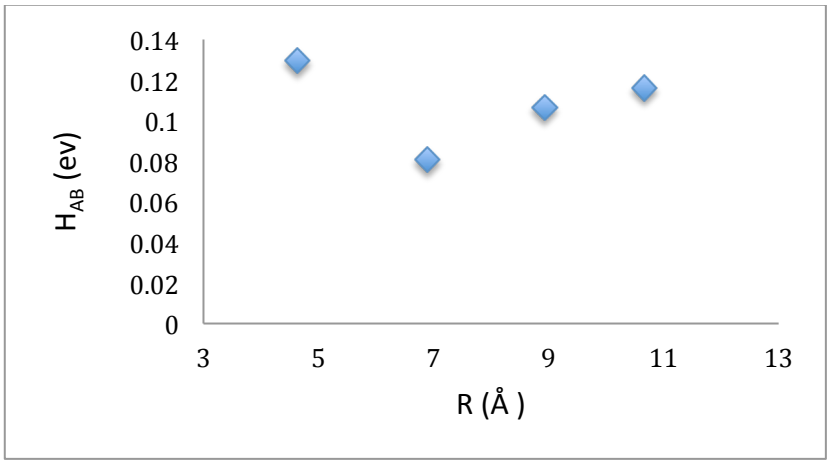

Figure 38. Electronic coupling matrix element H_{AB} (ev) against the distance R between the donor and the acceptor calculated with C-DFT method for molecules **7-10** b2 set, with combination of HOMO for diabatic state A and (HOMO-3) for diabatic state B.

For further understanding of the unexpected non-exponential behavior of the electronic coupling matrix element for the b2 definition of D/A fragments, a deeper look at the highest relevant MOs was necessary. This was carried out by setting a smaller contour

value (0.01 a.u.) for the depiction of the orbitals. In Table 7, the relevant orbitals of the b2 D/A definition set for diabatic state A compared to those of the b1 D/A definition set for diabatic stat A are presented. As one can see, the calculated orbitals with the D/A fragments choice of b2 set are not localized mainly on the acceptor as expected for diabatic state A, rather also localized on the donor. In contrast, for the b1 D/A definition set of orbitals, the diabatic state A yields orbitals located mainly on the acceptor. Therefore, the b2 set D/A fragments choice failed to localize the MOs according to the desired constraint D/B/A partition. This is likely a result of too many atoms incorporated into the acceptor fragment, with results indicating that it is not a likely electron transfer pathway. Rather, thinking about D and A fragments in terms of the most likely high energy occupied orbitals that are able to transfer an electron, once comes to a more organic chemistry view of something more like the D/A definition in b3, with two pi-bonded carbon atoms fragment.

Molecule	HOMO orbital of diabatic state A for b2 set	HOMO orbital of diabatic state A for b1 set
7	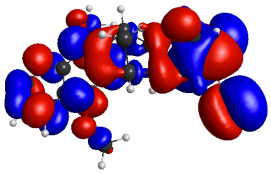	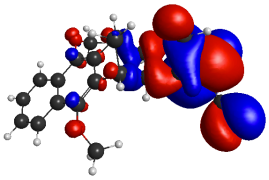
8	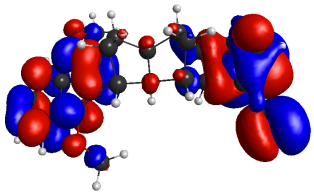	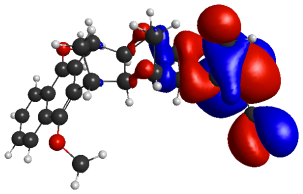
9	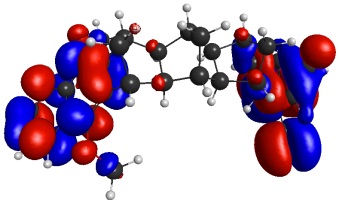	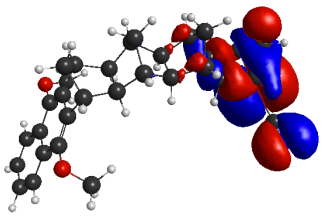
10	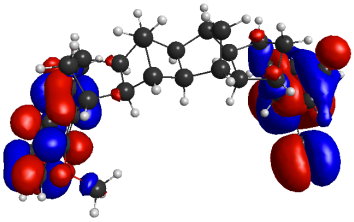	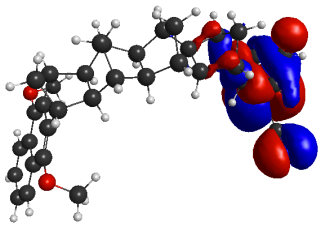

Table 7. Highest occupied molecular orbitals of diabatic state A for b1 and b2 sets for molecules **7**-**10**. The contour value for the purpose of orbitals illustration in MacMolPlt = 0.01a.u.

8.4.1.2.2.1 b2 D/A fragments choice using Localized Molecular Orbitals (LMOs)

As the b2 definition of D/A fragments choice with C-DFT calculation failed to localize the MOs according to the desired constraint for the D-bridge-A partition, further orbital localization together with the C-DFT calculation was carried out using the Pipek-Metzey method with the same b2 D/A fragments choice. The equivalent pair of MOs of the b1 D/A definition, which appeared to dominate the contributions to the electronic coupling (Table 8), were analyzed for **7**-**10**. Although for diabatic state A the relevant orbital is found to be the HOMO, for diabatic state B the relevant MO localized on the donor is not necessarily one of the highest orbitals, e.g. for molecule **7** the relevant orbital was found to be HOMO-10.

System	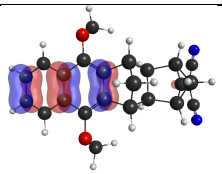 diabatic state B	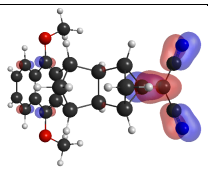 diabatic state A
7	HOMO-10	HOMO
8	HOMO-11	HOMO
9	HOMO-3	HOMO
10	HOMO-3	HOMO

Table 8. The position of the relevant orbitals for the two diabatic states A and B for molecules **7**-**10**, using the b2 D/A definition and the Pipek-Metzey orbital localization scheme.

Using the indicated pairs of LMOs shown in Table 8 for the various systems, the S_{AB} trends were determined across the set. Figure 39 shows an exponential behavior of S_{AB} with length of bridge such that already at system **10** (with 5 bridge units) the overlap drops to essentially zero (R^2=0.994).

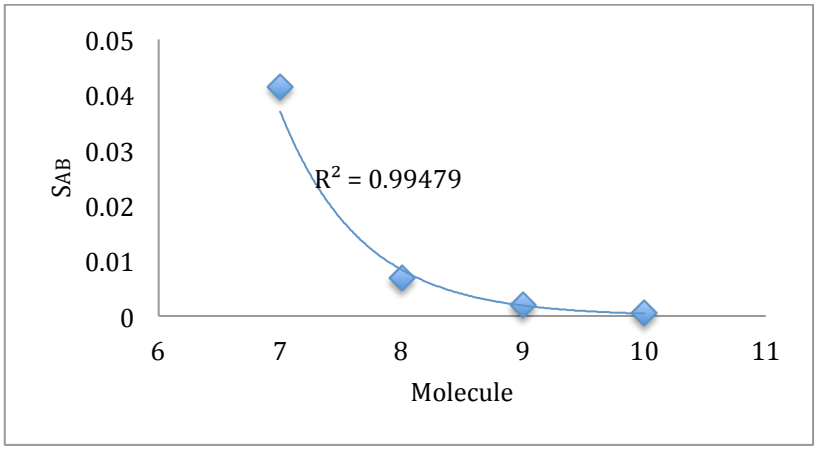

Figure 39. C-DFT calculated overlap values, S_{AB}, for molecules **7**-**10** for the b2 D/A definition using localized molecular orbitals calculated with the Pipek-Metzey localization scheme.

The exponential decay of the overlap S_{AB} with increasing bridge units for the chosen pair of the LMOs, is again reflected in the results of calculated electronic coupling matrix element H_{AB} (Fig. 40). The C-DFT calculated trend across the systems shows exponential behavior (R^2= 0.945), with calculate attenuation factor (β/2) of 0.51Å^{-1}, a value which is in agreement with β values characteristic for other saturated hydrocarbon bridged systems,[16, 60,61] and also with the experimental value (β/2)=0.425 Å^{-1}. In this case, the b2 D/A definition choice with further Pipek-Metzey orbital localization properly localizes the MOs according to the desired constraint D-bridge-A partition. One caveat is that, for diabatic state B the relevant MO localized on the donor is not one of the highest orbitals.

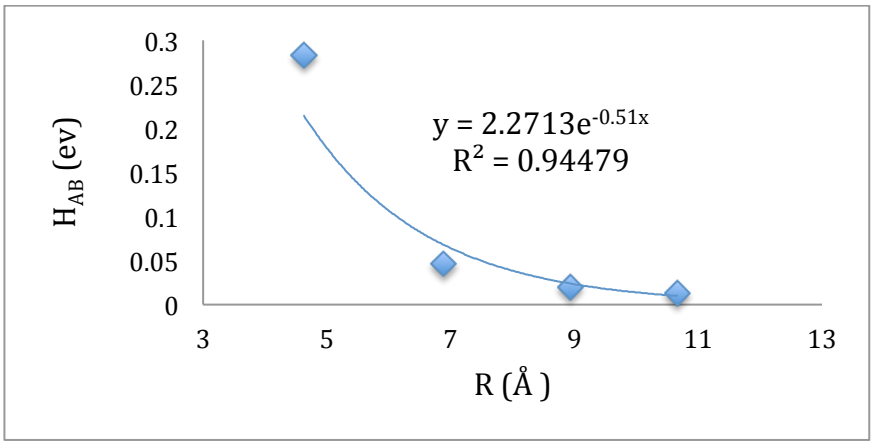

Figure 40. C-DFT calculated electronic coupling matrix elements, H_{AB}(ev), as a function of distance, R, between the donor and the acceptor for **7**-**10** using the b2 D/A definition with the Pipek-Metzey orbital localization scheme.

8.4.1.2.3 b3 D/A fragments choice

The D/A fragment choice for the b3 set were defined to be the two shared carbon atoms of the two fused rings of the naphthalene as the donor, and the two carbon atoms of the vinyl as the acceptor (Figure 32). The C-DFT calculations were carried out at the B3LYP/STO-3G level of theory for initial testing. As with the other D/A definitions, all possible π-type D/A MO pairs (Fig. 41, Table 9) were analyzed. Analogous to results found for the b1 D/A definition, HOMO-3 represents the acceptor orbital for diabatic state A, and HOMO-1 represents the donor orbital for diabatic state B. This combination dominates the contributions to the electronic coupling with the best exponential fit for S_{AB} (R^2=0.998) and non-negligible values (Fig. 42).

	Diabatic state B Contour value=0.05	Diabatic state A Contour value=0.05
HOMO (no.97)	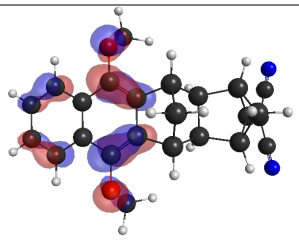	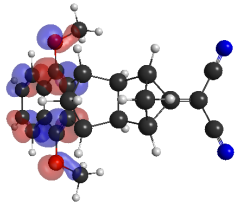
HOMO-1 (no. 96)	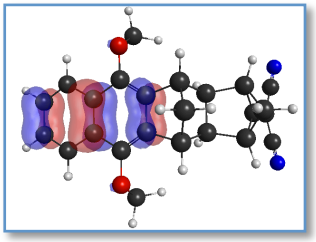	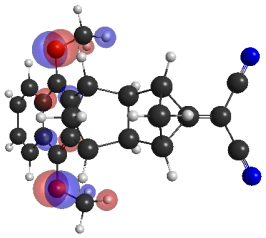
HOMO-2 (no. 95)	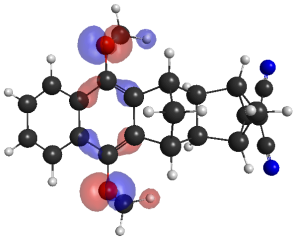	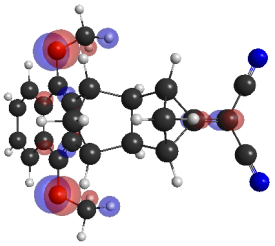
HOMO-3 (no. 94)	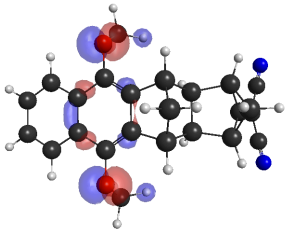	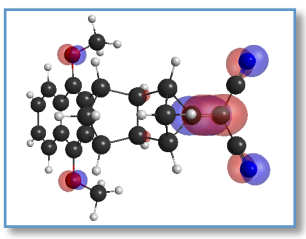

Figure 41. b3 molecule **7** highest MOs.

Orbital: Diabatic state B	Orbital: Diabatic state A	S_{AB} molecule 7	S_{AB} molecule 8	S_{AB} molecule 9	S_{AB} molecule 10
HOMO	HOMO	1.2E-07	0.0462	0.0459	0.0461
HOMO-1	HOMO	7.2E-08	0.0022	0.0019	0.0021
HOMO-2	HOMO	0.0352	0.0027	0.0023	0.0021
HOMO-3	HOMO	0.0111	0.0136	0.0187	0.0206
HOMO	HOMO-1	0.1089	0.1091	0.1107	0.1105
HOMO-1	HOMO-1	1.9E-06	4.2E-07	8.6E-07	2.4E-07
HOMO-2	HOMO-1	0.9911	0.9909	0.9907	0.9908
HOMO-3	HOMO-1	1.8E-06	0.0002	1.4E-05	1.5E-05
HOMO	HOMO-2	6.8E-07	3.8E-06	1.3E-06	1.0E-06
HOMO-1	HOMO-2	0.17982	0.1195	0.1167	0.11670
HOMO-2	HOMO-2	2.3E-06	1.8E-04	1.4E-05	1.4E-05
HOMO-3	HOMO-2	0.9319	0.9866	0.9874	0.9874
HOMO	HOMO-3	2.2E-07	3.4E-07	6.5E-08	2.3E-08
HOMO-1	HOMO-3	0.1077	0.0510	0.0194	0.0090
HOMO-2	HOMO-3	4.3E-07	6.4E-06	2.0E-07	6.5E-08
HOMO-3	HOMO-3	0.3189	0.0349	0.0098	0.0033

Table 9. Overlap S_{AB} of relevant MOs pairs between the two diabatic states, A and B, for D/A definition b3. The corresponding molecular orbitals are shown in Figure 41.

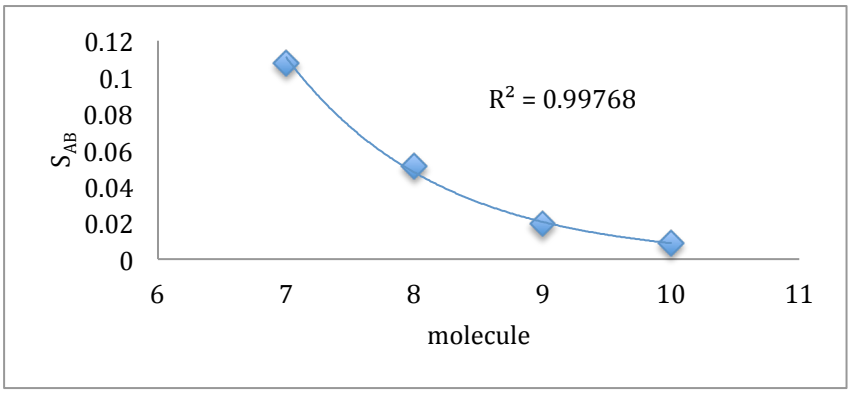

Figure 42. S_{AB} values between (HOMO-3) of diabatic state A and (HOMO-1) for diabatic state B for molecules **7**-**10** using the b3 D/A definition.

The exponential decay of the overlap S_{AB} with increasing bridge units for the pair (HOMO-3) of diabatic state A and (HOMO-1) for diabatic state B, is reflected again in the results of calculated electronic coupling matrix element H_{AB} (Fig. 43) with curve fitting R^2= 0.993 and calculate attenuation factor (β/2) of 0.418Å^{-1}, a value which is in agreement with β values characteristic for other saturated hydrocarbon bridged systems, [16, 60,61] and also with the experimental value (β/2)=0.425 Å^{-1}. In this case, the

b3 D/A definition choice also appears to properly localize the MOs according to the desired constraint D-bridge-A partition.

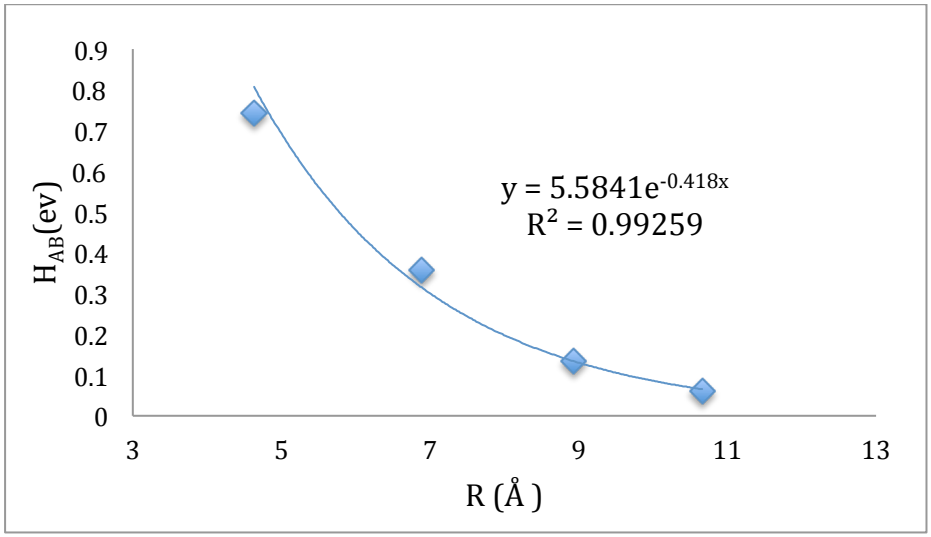

Figure 43. C-DFT calculated electronic coupling matrix elements, H_{AB} (ev), as a function of the distance R between the donor and the acceptor for systems **7**-**10** using the b3 D/A definition.

8.4.1.2.4 b4 D/A fragments choice

The D/A definition for the b4 set was defined to be the two oxygen atoms of the dimethoxynaphthalene as the donor, and the two carbon atoms of the vinyl as the acceptor (Fig. 32). The C-DFT calculations were carried out at the B3LYP/STO-3G level of theory for initial testing. In the same manner as in the previous sets, analysis of all possible π-type D/A MO pairs (Fig. 44, Table 10) was carried out. Results revealed a particular pair of MOs as found in the b1 and b3 D/A definition sets, one from diabatic state A (HOMO) that represents the acceptor, and one from diabatic state B (HOMO-3) that represents the donor. This pair of orbitals dominates the contributions to the electronic coupling, and show a good exponential fit of S_{AB} (R^2=0.992) with non-negligible values (Figure 45).

	Diabatic state B Contour value=0.05	Diabatic state A Contour value=0.05
HOMO (no.97)	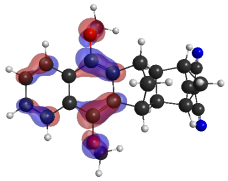	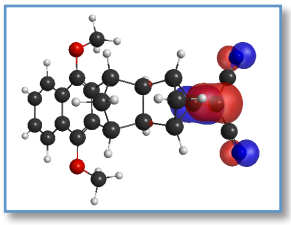
HOMO-1 (no. 96)	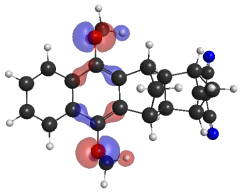	
HOMO-2 (no. 95)	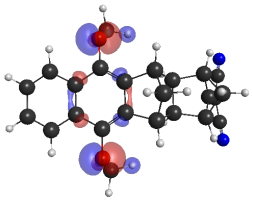	
HOMO-3 (no. 94)	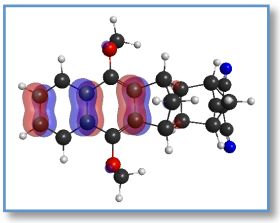	

Figure 44. b4 molecule 7 highest MOs.

Orbital: Diabatic State B	Orbital: diabatic state A	S_{AB} molecule 7	S_{AB} molecule 8	S_{AB} molecule 9	S_{AB} molecule 10
HOMO	HOMO	9.3E-09	6.7E-08	1.8E-08	5.2E-09
HOMO-1	HOMO	7.8E-08	1.0E-06	7.4E-08	3.1E-08
HOMO-2	HOMO	0.0041	0.0030	0.0011	0.0004
HOMO-3	HOMO	0.1532	0.0435	0.0151	0.0066

Table 10. Overlap S_{AB} of relevant MOs pairs between the two diabatic states, A and B, for D/A definition b4. The corresponding molecular orbitals are shown in Figure 44.

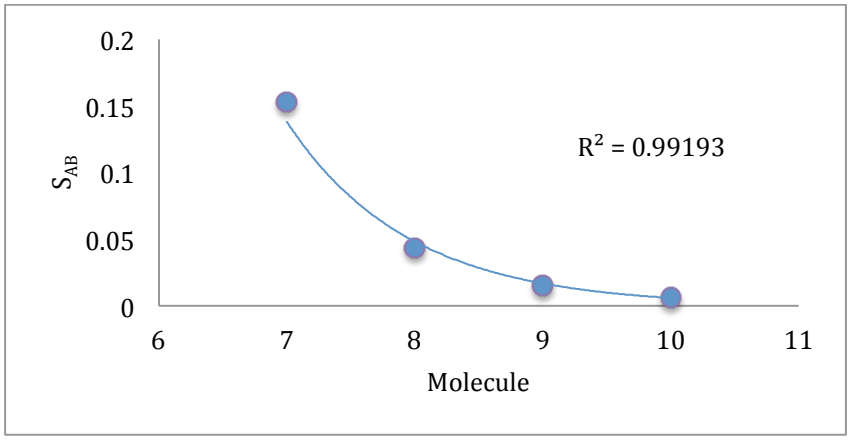

Figure 45. S_{AB} values between HOMO of diabatic state A and (HOMO-3) for diabatic state B for molecules **7**-**10** using b4 D/A definition.

The associated C-DFT calculated trends for electronic coupling matrix elements (Fig. 46) for the set of systems was also found to behave exponentially (R^2= 0.999) as a function of increasing distance between the donor and the acceptor. The calculated attenuation factor (β/2) is 0.526Å^{-1}, which is in agreement with β values characteristic for other saturated hydrocarbon bridged systems,[16,60,61] and with the experimental value (β/2)=0.425 Å^{-1}. As such, the b4 D/A definition choice also properly localizes the MOs according to the desired constraint D-bridge-A partition.

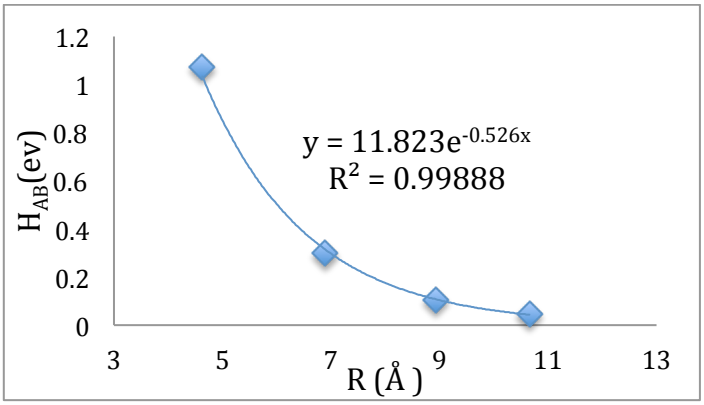

Figure 46. Electronic coupling matrix element, H_{AB} (ev), against the distance R between the donor and the acceptor calculated with C-DFT method for molecules **7**-**10** b4 set.

8.4.1.2.5 Conclusion remarks for D/A fragments choice

Deciding on the definition of the donor and the acceptor fragments within C-DFT calculation may be complex, as observed above, and may involve several choices of D/A fragment. This process only gets more complicated with increasing system size. The results of D/A choice definitions b1-b4 for the set of molecules **7**-**10** are discussed in

detail above. As can be seen, more than one set of choice of D/A fragments can be used with acceptable representation of the ET process. An important factor is that the acquired MOs of the two diabatic states should dominate the contribution to the electronic coupling, where the relevant MO of one diabatic state represents the donor, and the relevant MO of the other diabatic state represents the acceptor.

Comparison to experimental results were also made where possible, as well as to previous published results acquired by Berstis[22] using the alternate DFT based Green's function method. The experimental ET reaction rate for molecules **9'-11'** were shown to have an exponential decay with β factor of 0.85 $Å^{-1}$.[61] In the DFT based Green's function model, D/A combinations of LMOs pair were also scanned, where the selection among the various π-type LMOs on the dimethoxynaphthalene (Figure 47) revealed LMO assigned as '*k*' to dominate the contribution to the electronic coupling. In Figure 47 one can see the resemblance between the π-type MOs on the dimethoxynaphthalene acquired by the DFT based Green's function model and their equivalent MOs acquired by the C-DFT method.

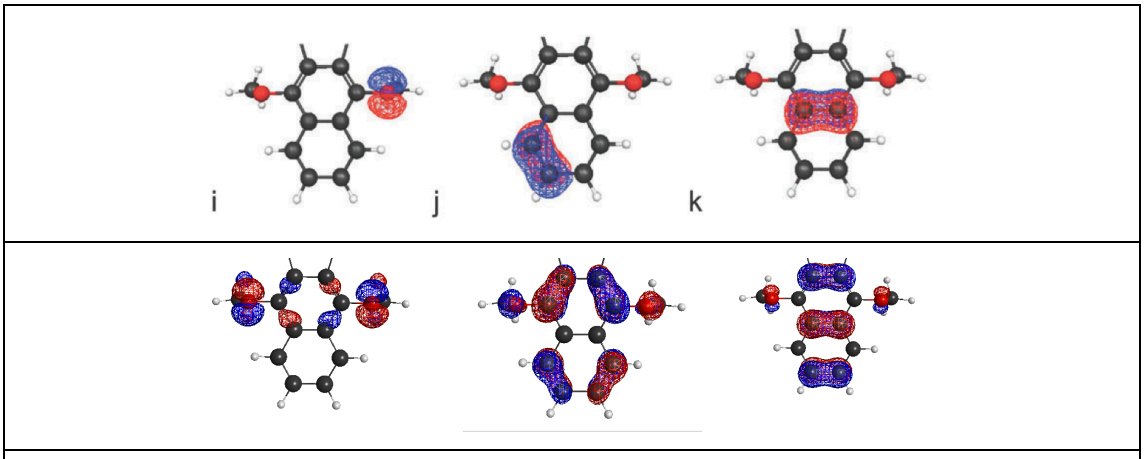

Figure 47. π-type MOs on the dimethoxynaphthalene acquired by the DFT based Green's function model[22] (top), and the equivalent MOs acquired by the C-DFT method (bottom).

All calculated and experimental results of the attenuation factor (β/2) associated with the calculated H_{AB} values are presented in Table 11 and in Figure 48. With regard to the attenuation factor, one can see that, with the exception of the D/A definition b2, all C-DFT calculation results are in the range of 0.418$Å^{-1}$-0.526$Å^{-1}$. These results correlate well with the experimentally observed decay curve as a function of increasing bridge length, as well as with β values characteristic for saturated hydrocarbon bridged systems in general.[16, 60,61] The D/A definitions b1, b3 and b4 revealed similar pairs of MOs for the donor and acceptor orbital components, one localized on the donor, and the

other on the acceptor in accord with the constraint. The D/A choice of b2, on the hand, yielded MOs not mainly localized on the donor or on the acceptors, resulting in unexpected overlap values (the overlap increase with increasing D/A distance). Only further localization in the case of the D/A choice b2 set using the Pipek-Metzey localization scheme yielded the expected exponential behavior, providing localized-MOs where one is localized mainly on the donor and the other on the acceptor. The MOs resulting from the C-DFT calculation for the b2 D/A definition are delocalized not mainly on the donor and acceptor fragments. As such, this D/A choice fails to localize the MOs according to the constraint. In this case, further localization with general LMOs schemes is seen to localize the orbitals to a point where they represent better the initial constraints.

Source		**Attenuation factor (β/2) of H_{AB}**
Experimental[61]		(0.85 $Å^{-1}$/2) = 0.425 $Å^{-1}$
Berstis[22]		0.64 $Å^{-1}$
b1		0.497 $Å^{-1}$
b2		No exponential behavior
	Using Pipek-Metzey localization scheme	0.51 $Å^{-1}$
b3		0.418 $Å^{-1}$
b4		0.526 $Å^{-1}$

Table 11. Attenuation factors (β/2) of H_{AB} for experimental systems **9'-11'**, DFT based Green's function method by Berstis, and calculated for molecules **7**-**10** for b1-b4 D/A definitions using the implemented C-DFT method.

Looking at the H_{AB} values presented in Figure 48, one can see clearly the unexpected behavior regarding the b2 definition of D/A. Although various D/A fragments choices yielded similar attenuation factors, β, the electronic coupling matrix element H_{AB} values showed a much wider range. For the b1 definition of D/A, the results obtained are essentially in agreement with results obtained by DFT-based Green's function method, where higher results were found in the cases of the b3 and b4 D/A definitions. The further localization of b2 D/A orbitals lead to reduction in the calculated H_{AB} values.

When comparing the various D/A definitions in these systems, b1-b4, one should also consider the energy level order of the relevant orbitals contributing to the electronic coupling. In general, orbitals relevant for the ET process will likely be positioned higher

in energy (e.g., HOMO, HOMO-1) rather than lower in energy (e.g., HOMO-3 and below).

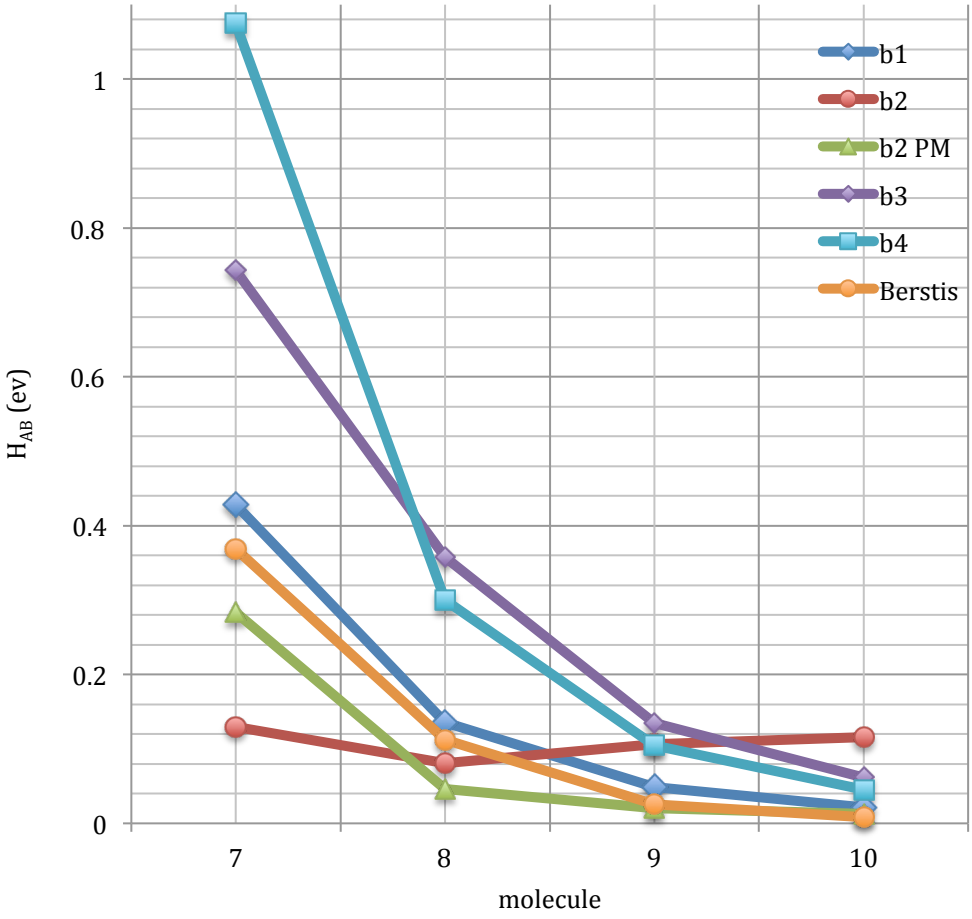

Figure 48. Electronic coupling matrix element H_{AB} (ev) for molecules **7**-**10**, with various D/A fragments definitions (b1-b4), as well as Laura Berstis' results calculated with DFT-based Green's function method.

8.5 Molecular orbital localization schemes

In C-DFT calculations for ET reactions, the density is imposed to satisfy some specific constraints according to predefined fragments distinguished as the donor and the acceptor. As a result, the calculated MOs are localized according to the constraint. To examine the effect of additional standard molecular orbital localization schemes (as described in Section 6), the three localization methods: Pipek-Metzey, BOYS, and Edmiston–Ruedenberg schemes, will be discussed here in terms of their compatibilities to the implemented C-DFT method as applied to several of the validation systems.

8.5.1 Effect of Localization Schemes: D-A systems of anthracene-dimer anion

B3LYP/6-31G(d) C-DFT calculations were carried out on the two diabatic states of anthracene-dimer-anion as a function of distance between the monomers, using the additional 3 molecular orbital localization schemes: Pipek-Metzey, BOYS, and Edmiston–Ruedenberg. One of the monomers of the anthracene-dimer-anion was defined as the donor, and the other as the acceptor, therefore this is a non-bridged system.

The calculated canonical HOMO for one diabatic state is a π-type orbital, localized on the donor dimer, and the HOMO for the other diabatic state is localized on the acceptor dimer, as shown in Figure 49.

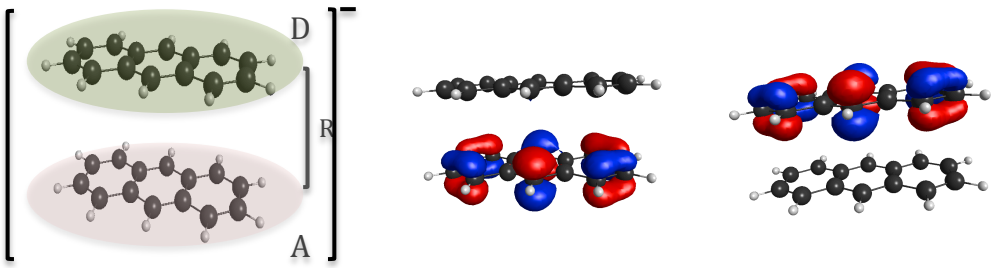

Figure 49. C-DFT calculated anthracene-dimer-anion structure (left) and the two highest occupied MOs for each of the two diabatic states.

Applying all three molecular localization schemes to this system in this particular case have no additional effect on the characterization of the highest occupied MOs, over that of the Canonical orbital representation. As such, the C-DFT calculated overlap S_{AB} values between the two diabatic states are also not affected, as can be seen in the results in Table 12.

R (Å)	S_{AB}			
	Canonical	**Pipek-Metzey**	**BOYS**	**ER**
3	0.4187	0.4187	0.4187	0.4187
3.2	0.3233	0.3233	0.3233	0.3233
3.5	0.2189	0.2189	0.2189	0.2189

Table 12. C-DFT calculated overlap values, S_{AB}, between the two diabatic states of anthracene-dimer-anion as a function of distance R between the monomers, using canonical orbitals compared with the three localized molecular localization schemes.

8.5.2 Localization Schemes: D-B-A systems with saturated hydrocarbon bridge

The series of systems **1**-**6** characterized by ethylene D/A groups with intervening σ-bonded norbornyl-unit bridges of varying length was extensively discussed previously. C-DFT results were further analyzed with the additional Pipek-Metzey and BOYS orbital localization schemes. The donor and the acceptor were defined as the end ethylene groups as before. For comparison, standard DFT calculations using the same functional and basis set were applied to these systems, also employing the additional Pipek-Metzey and BOYS orbital localization schemes.

The results of these studies are shown in Figure 50 for **5**. As one can see, with regard to the canonical orbital representation, the standard DFT calculated HOMO is symmetrical and localized on the entire molecule, while the C-DFT canonical HOMO is asymmetrical and localized primarily on the donor, with nontrivial contribution from the bridge. Further orbital localization with Pipek-Metzey or BOYS schemes, is seen in this system to further localize the orbitals. The consequence of this further orbital localization is to reduce dramatically the contribution of the bridge to the highest orbitals. In this case, the localized MOs for standard DFT compared to the C-DFT are very similar. This reduction in orbital contribution is reflected in the C-DFT calculated overlap S_{AB} between the two diabatic states using the C-DFT method (Fig. 51). The results obtained for the Pipek-Metzey localization scheme are not as dramatic as those obtained using the BOYS scheme, as observed in the orbital depiction.

	C-DFT HOMO	**DFT HOMO**
Canonical	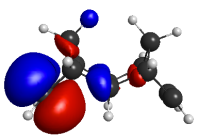	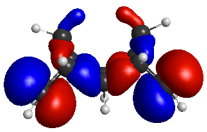
Pipek-Metzey LMOs	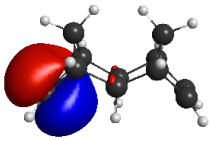	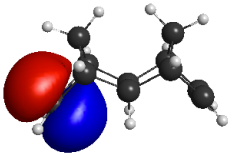
BOYS LMOs	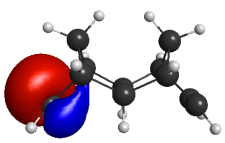	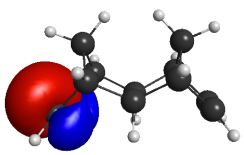

Figure 50. Canonical and localized HOMO for **5** calculated with DFT and C-DFT (contour value in MacMolPlt = 0.035 a.u.).

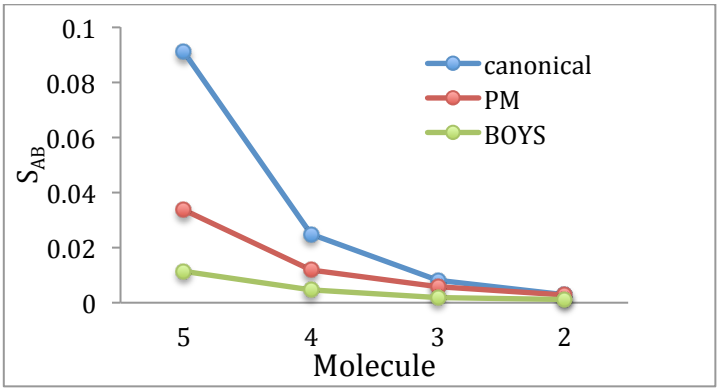

Figure 51. C-DFT calcualted overlap values, S_{AB}, for **2**-**5** calculated for the canonical orbitals, as well as for the localized Pipek-Metzey (PM) and BOYS orbitals.

8.5.3 Conclusion remarks for LMOs schemes

In C-DFT, the calculated MOs are localized according to the defined constraint. The highest occupied MOs represent the contributions of the donor and the acceptor in accord with their fragments definition, and also the contribution of the bridge. Subsequent C-DFT calculations of the S_{AB} values with those orbitals represent the system as a whole with respect to the constraints. Further orbital localization with standard procedures reduces dramatically the contribution of the bridge in this system, and also the contribution of other atoms belong to the D/A. As such, the localized MOs may no longer represent the initial constraints.

8.6 Solvation model: COSab results

To examine the effect of solvation on calculated electronic coupling matrix elements with the developed C-DFT method, the COSab method was applied. This method belongs to the class of dielectric continuum models, but with several enhancements to compensate for errors in standard continuum models. In COSab the solute molecule is embedded in a dielectric continuum of permittivity ε, which for solvation in water simulation was set to ε=80.

B3LYP/6-31G(d) C-DFT:water calculations for D-Bridge-A systems with saturated bridges for the series of **1**-**6** and **7**-**10** were carried out to investigate the effect of water environment on the prediction of overlap and electronic coupling parameters. The results of the electronic coupling matrix elements are shown for both gas-phase and in water for **1**-**6** in Figure 52, and for **7**-**10** in Figure 53. For both series, the exponential

behavior characteristic of the electronic coupling in gas-phase is maintained in water, where the attenuation factors (β/2) are almost unchanged: for **1**-**6** series (β/2) = 0.541 Å^{-1} in gas-phase and (β/2) = 0.543 Å^{-1} in water, and for **7**-**10** series with D/A fragments definition of D/A from set b1 (β/2) = 0.497 Å^{-1} in gas-phase and (β/2) = 0.482 Å^{-1} in water. However, in general, the calculated absolute values of the electronic coupling are somewhat attenuated, being smaller than those obtained in the gas-phase calculations, as might be expected.

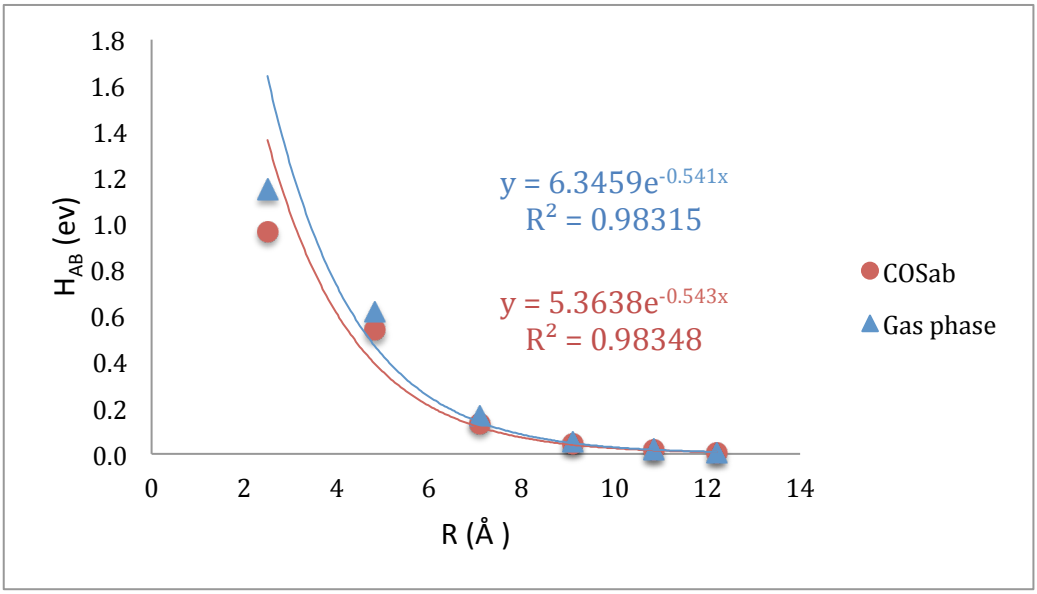

Figure 52. C-DFT electronic coupling matrix elements, H_{AB} (ev), for **1**-**6** in gas phase (blue) and in water (red) as a function of the distance R between the donor and the acceptor.

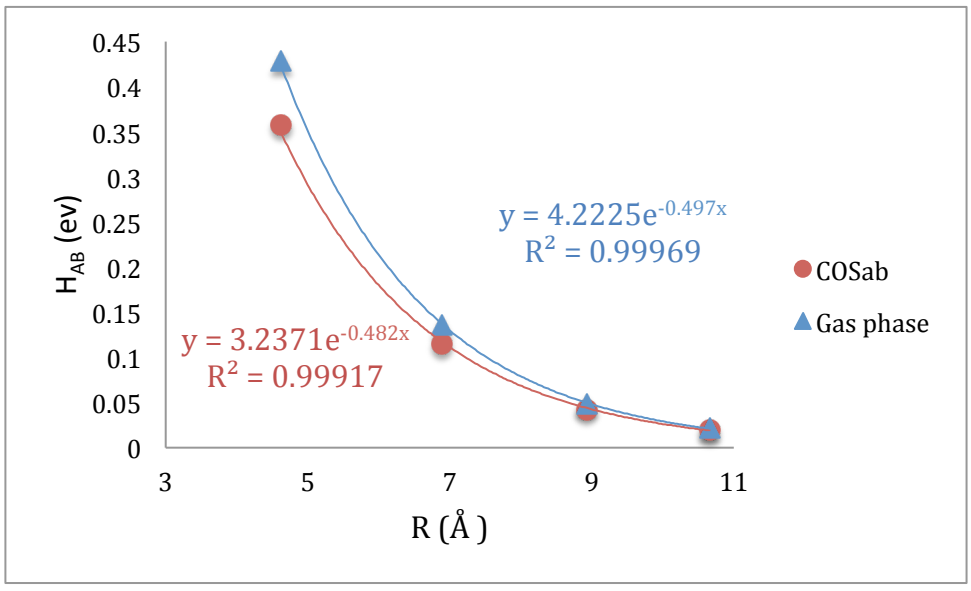

Figure 53. C-DFT electronic coupling matrix elements, H_{AB} (ev), for **7**-**10** in gas phase (blue) and in water (red) as a function of the distance R between the donor and the acceptor.

To understand the parameters affecting the general reduction in H_{AB} values in water compared to gas-phase, the overlap S_{AB} values calculated in gas-phase were compared to those in water for both series of molecules (Figure 54 and Figure 55). As one can see, the values obtained for both the gas-phase and in water are nearly identical. A further look at the highest molecular orbitals (Table 13) for a representative example, **7**, in gas-phase and in water supports the suggestion that the water environment has little to no significant influence on orbital representation and associated overlap.

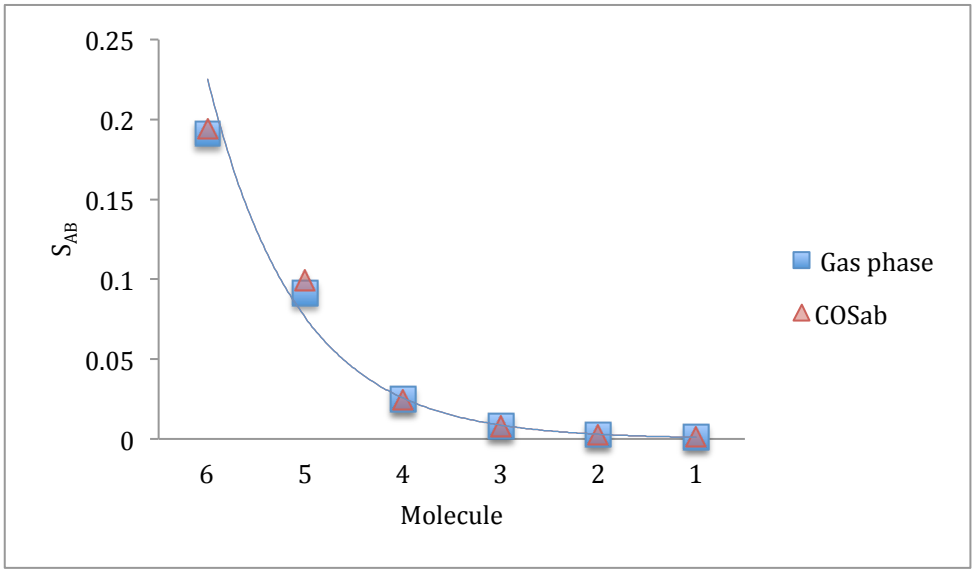

Figure 54. C-DFT calculated S_{AB} values for **1-6** in gas phase and in water.

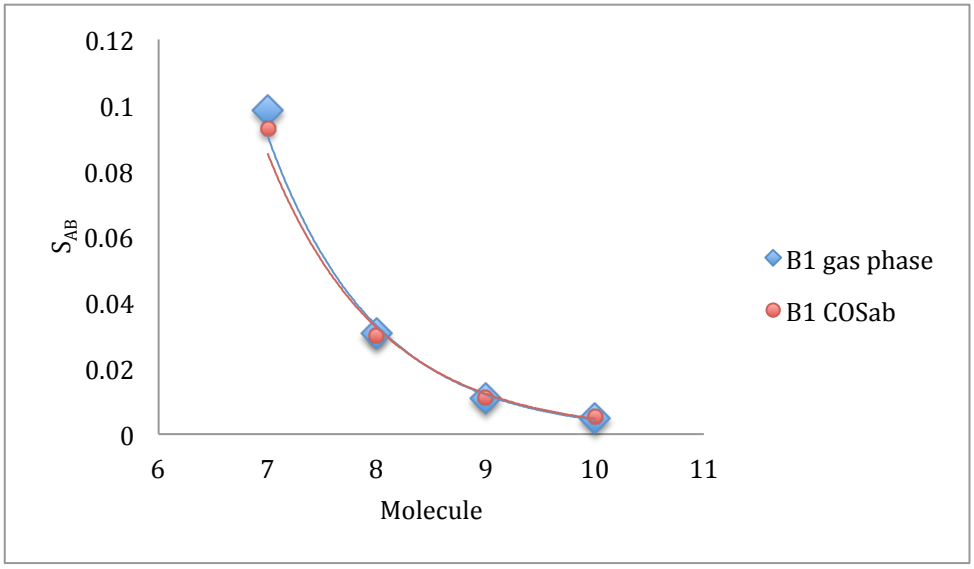

Figure 55. C-DFT calculated S_{AB} values for **7-10** for D/A definition from the b1 set in gas phase and in water.

	COSab		Gas phase	
	Diabatic state B	**Diabatic state A**	**Diabatic state B**	**Diabatic state A**
HOMO	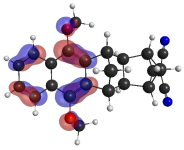	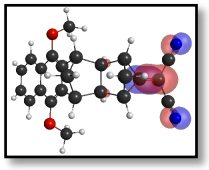	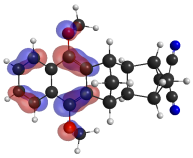	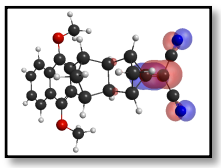
(HOMO -1)	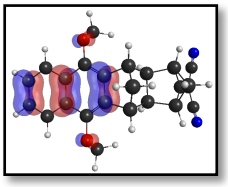		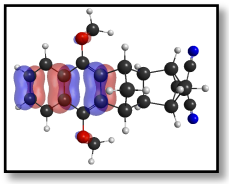	
(HOMO -2)	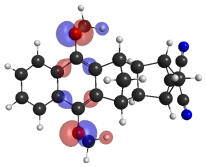		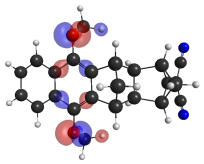	
(HOMO -3)	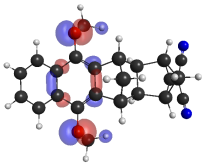		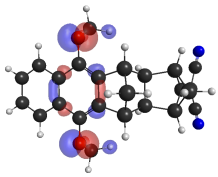	

Table 13. Highest MOs for **7** with the b1 D/A definition in gas-phase and in water (contour value=0.05 a.u.).

In fact, the reduction in the electronic coupling in solution environment is almost exclusively electronic in nature. Importantly, solvent has the most dramatic effect in the case of charged systems. In a C-DFT calculation, by enforcing charge constraints, we effectively create charged fragments. In Table 14, one can see the reduction in solvated energy for **1**-**6** compared to the respective gas-phase value.

Molecule	Energy in gas-phase	Energy in COSab
1	-1240.925660	-1240.987149
2	-1046.927635	-1046.985496
3	-852.923960	-852.991789
4	-658.926853	-658.994977
5	-464.924705	-464.995631
6	-270.971069	-271.026930

Table 14. Comparison of total energy calculated with C-DFT for **1**-**6** in gas-phase and in water environment.

9 Application of C-DFT methodology: *f*-Cor-bridge-*f*-Cor systems with materials properties

Organic semiconductors-based devices, studied continuously since late 1940th [91], have attracted widespread attention in recent years. Promising technology is being introduced in an extensive range of applications for use in electronic and optoelectronic devices[92] such as sensors[93,94,95,96], organic light-emitting diodes (OLEDs) [93,97,98,99,96], polymer light-emitting diodes (PLEDs)[100], memory elements[93,101], organic thin-film transistors (OTFTs)[91], organic photo voltaic (OPV)[93,102], organic field-effect transistors (OFETs) [103,91,96] and organic light-emitting transistors (OLETs)[104].

The interest in organic materials for electronic applications as a viable alternative to the conventional semiconductor materials, such as silicon, stems from benefiting from a few advantages, as the organic materials considered to have high photoluminescence quantum yields[98], and they can be used to make optoelectronic devices lightweight, energy-saving, flexible, large area size, low cost and printable. The processing is considered to be easy, and the organic films can be attached to a variety of very-low-cost substrates such as glass, plastic or metal foils.[97, 102] Additionally, the organic materials can be chemically functionalized via covalently bonded side groups, improving the selectivity and sensitivity of the materials, creating derivatives to obtain diversity of precursors monomers.[93,105] In particular, organic π-electron systems have received

attention as potential materials, where the semiconducting behavior being associated with the π molecular orbitals delocalization .[92,98]

Many remarkable advances have been in the design and use of organic materials in the past few years, and new capabilities and properties have been revealed, some of them cannot be duplicated by silicon based devices.[93] Organic electronics materials are beginning to be more significant in the commercial world, while the most advanced organic electronic systems already in commercial production are high efficiency, very bright and colorful thin displays based on organic light-emitting diodes (OLEDs).[97,99] Another emerging application involves photovoltaics, where also organic thin-film transistors offer great potential for applications in chemical and biological sensing for various detections in a variety of fields, such as medical, biological, environmental and homeland security.[93] Yet the future holds a great promise for organic materials based devices, where the search for the novel semiconducting material still maintains a challenge for researchers to obtain improved devices.

9.1 Corannulene based curved aromatic systems

Non-planar aromatic molecules have been synthesized by pioneering studies already by the 1950th.[96,106,107] Polycyclic aromatic hydrocarbon (PAHs) molecules can be forced into non-planar structures, e.g. by embedding non-hexagonal rings.[108] Embedding five-membered rings into an otherwise flat PAH molecule can lead to curved PAH molecules known as aromatic bowls or buckybowls.[108] The curvature imparts in these compounds unique electronic properties that are not observed in planar PAH analogues, such as pyrene or naphthalene.[105]

Corannulene, representing one third of C_{60} with chemical formula $C_{20}H_{10}$, is the smallest sub-unit of fullerenes that is described as a shallow bowl (Fig. 56), where the curvature results from the presence of a five-membered ring centered among six-membered rings. The curvature of such structures leads to a substantial dipole moment, ranging from 2.07 D for the corannulene molecule $C_{20}H_{10}$[109,110,111] and becomes even as high as 6.02 D for $C_{50}H_{10}$.[112,96] The ability to control the curvature in bowl-shaped aromatic systems contributes for the development of molecular device design with tunable function.[113, 114,115, 96]

Since its first synthesis in 1966[116] efforts have been made for investigating and understanding corannulene and corannulene derivatives properties and their potential

applications in various fields, such as molecular tweezers [117,118], solar cells[119], organic light emitting diodes (OLEDs)[115] and organic field-effect transistors (OFETs). [120]

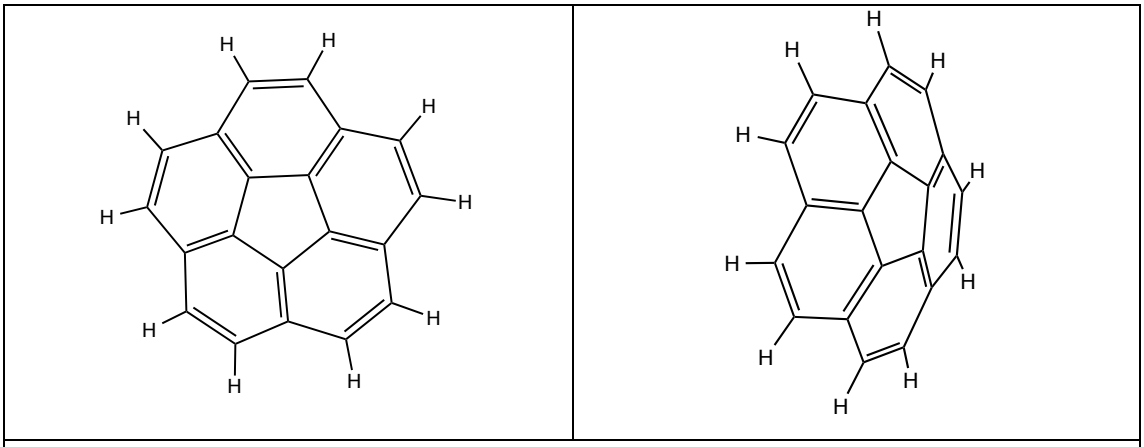

Figure 56. Corannulene structure.

Corannulene can be synthesized in a large-scale synthesis, stimulating commercially viable production. Its functionalization affects the bowl structure, therefore the electronic and dynamic properties, obtaining a diversity of precursor monomers.[121,96] This opens the possibility of creating a huge variety of derivatives.[105, 115] High variety of corannulene derivatives can contribute in obtaining novel devices for electronic applications.[122,114]

9.2 System design

The corannulene-based D-bridge-A system that has been designed by our experimental collaborators is characterized by functionalized corannulene donor and acceptor, with both saturated as well as unsaturated bridges (Fig. 57). C-DFT calculations have been carried out for a wide variety of *f*-Cor-bridge-*f*-Cor systems to investigate the variation in electron transport and mechanistic aspects of transport in this type of materials system. In particular, the main categories of *f*-Cor-bridge-*f*-Cor system include:

(a) Modification in bridge length

(b) Saturated vs. unsaturated bridge types

(c) Effect of functional groups on the D and A corannulene motifs.

The variation in bridge type enables investigation of variation in mechanism of electron transport between hydrocarbon vs. conjugated bridge types. Typically, π-conjugated

bridges provide more efficient long-range electron transfer with more substantial electronic communication between the individual bridge units.[13,24] A primary focus of this study is on systems with bridges of this nature.

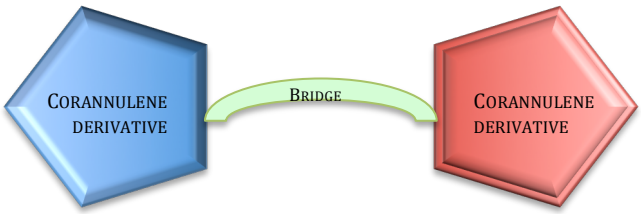

Figure 57. Schematic illustrative structure of *f*-Cor-bridge-*f*-Cor based D-Bridge-A systems.

C-DFT calculations have been carried out for sets A-F (Fig. 58). Each set member is composed of the same D/A and bridge unit B, with various number (n) of bridge units, enabling investigation of the dependence of the bridge length within each set. To study the effect of the D/A character on the electronic coupling, various corannulene derivatives are tested as discussed below. For the purpose of investigation of a wire-like behavior, the bridges of all sets except for set D have been chosen to be of π-conjugated nature.

A	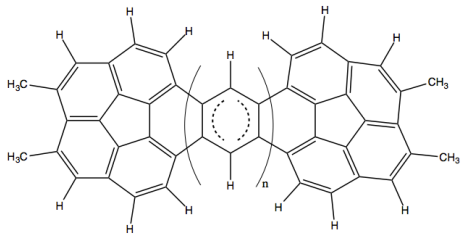
B	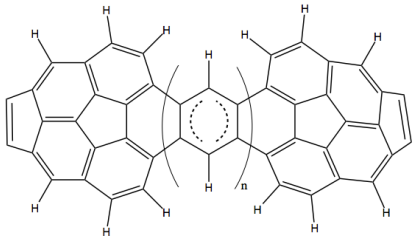
C	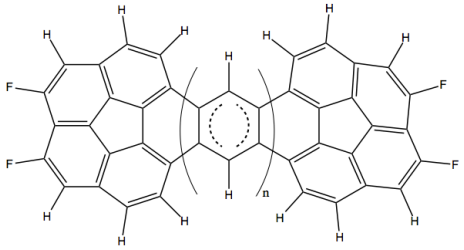
D	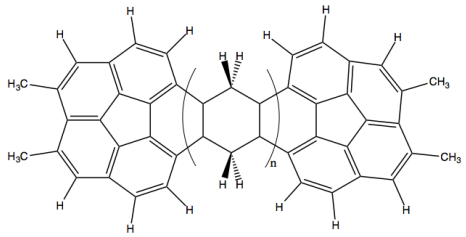
E	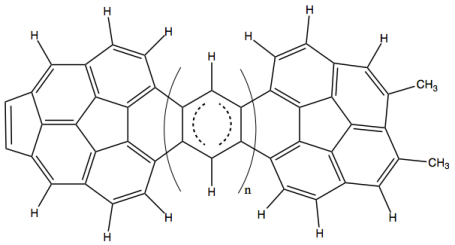
F	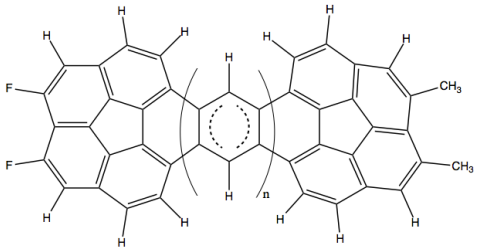

Figure 58. *f*-Cor-bridge-*f*-Cor D-bridge-A systems, **A**-**F**, with functionalized corannulene derivatives as D/A and various hydrocarbon bridges.

Initially, all geometries were fully optimized at the B3LYP/STO-3G level of theory. This was followed by C-DFT calculations at the B3LYP/STO-3G level of theory. The D/A fragments for the C-DFT calculations were defined as the entire corannulene-based derivative, in the same manner as demonstrated for set A systems in Figure 59. The distance between the donor and the acceptor is measured as the distance between the end atoms of the corannulene derivative connected to the bridge (Figure 60).

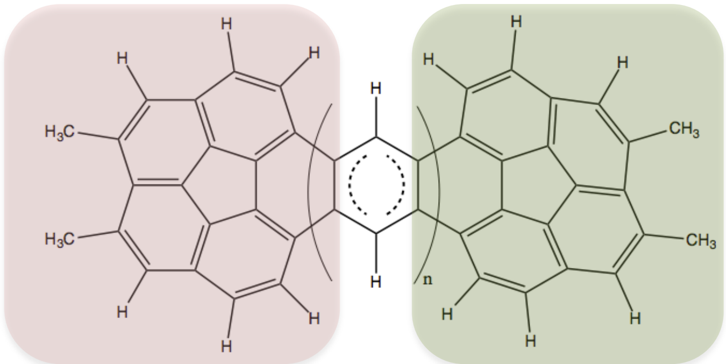

Figure 59. The donor and acceptor dimethyl-corannulene fragment end groups as defined in C-DFT calculation for set A systems.

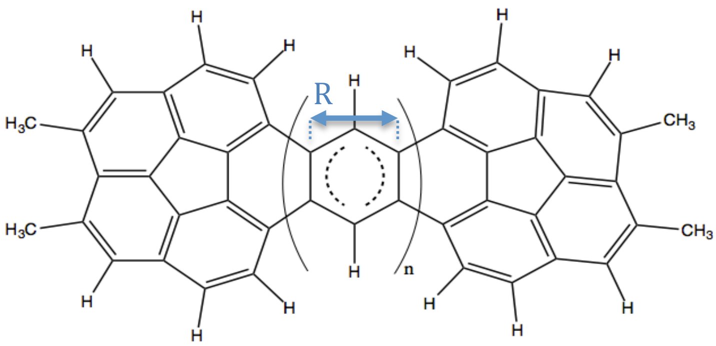

Figure 60. Set A systems measure of the distance R between the donor and the acceptor as the distance between the corannulene derivatives' end atoms connected to the bridge

9.3 1,2-dimethyl-corannulene D/A units with π-conjugated bridge of varying length

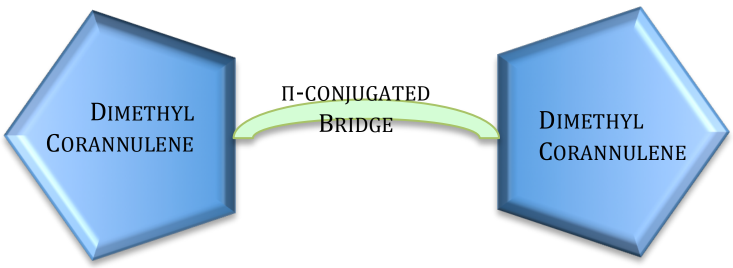

Figure 61. Schematic illustration for *f*-Cor-bridge-*f*-Cor for set A systems.

Set A is characterized by dimethyl-corannulene D/A units composed of fused benzene-like π-conjugated bridge units, with varying number of bridge units n=1-4 (Figures 58,61). The highest occupied molecular orbitals for the set A systems as obtained in standard DFT calculations are presented in Figure 62. The HOMO orbitals are seen to be symmetric, with electron density delocalization over the entire molecule. The highest occupied MOs obtained from the C-DFT, on the other hand, are not symmetric, and are more optimally localized mostly on either the donor in one diabatic state or on the acceptor in the other diabatic state (Table 15), as expected from the definition of our D/A fragments. However, one can still see a nontrivial contribution of the bridge within these D/A molecular orbitals.

n	**HOMO**
1	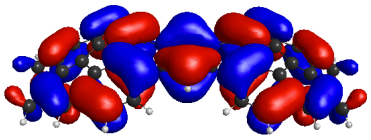
2	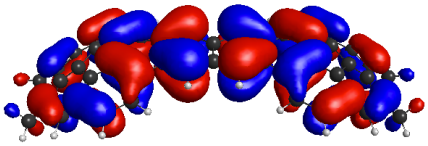
3	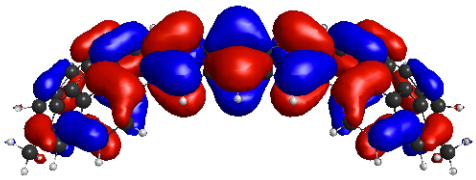
4	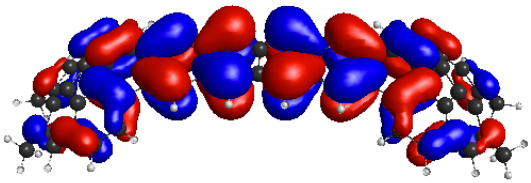

Figure 62. Highest occupied molecular orbitals as calculated in standard DFT for set A systems.

Looking at the overlap S_{AB} values for set A systems (Table 15, Fig. 63) one can see that although the value of S_{AB} is reduced as the distance between the donor and the acceptor gets larger, it decays slowly and does not show exponential behavior. This behavior may well be attributed to the significance contribution of the bridge to the overlap between the two diabatic states for all set A systems.

n	HOMO of diabatic state A	HOMO of diabatic state B	S_{AB}
1	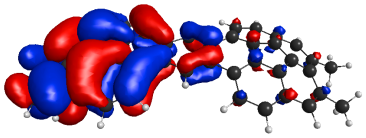	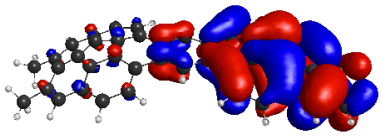	0.0174
2	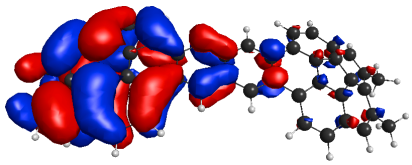	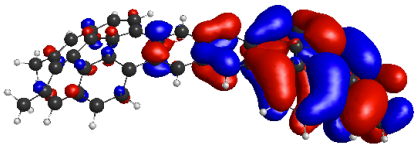	0.0154
3	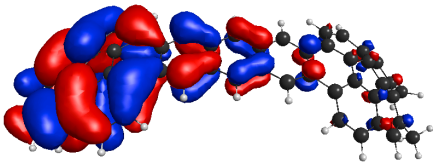	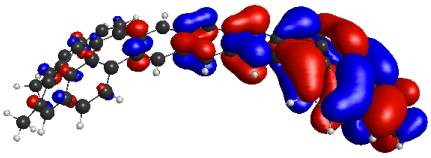	0.0142
4	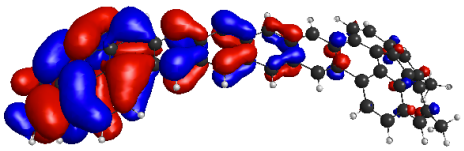	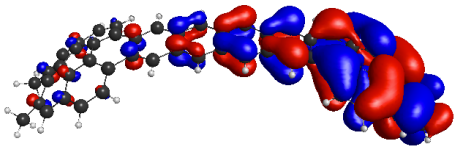	0.0108

Table 15. Highest occupied molecular orbitals of the two diabatic states for set A (n=1-4) systems with the C-DFT calculated overlap S_{AB}.

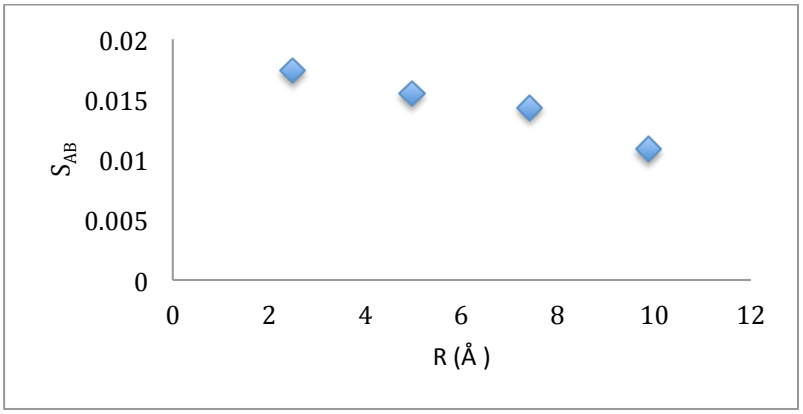

Figure 63. C-DFT calculated overlap, S_{AB}, between the two diabatic states against the distance R between the donor and the acceptor for set A systems (n=1-4).

The slow decay behavior of the overlap S_{AB} with increasing bridge units is reflected in the results of calculated electronic coupling matrix element, H_{AB}, between the two diabatic states of set A systems, using the overlap S_{AB} for calculating the electronic coupling matrix element according to Equation 29 (Table 16, Fig. 64). As previously mentioned, although β-values only apply for mechanisms that are expected to decay exponentially in a tunneling superexchange mechanism, they have been used as quality

factors for electron transfer reactions that occur via an incoherent hopping mechanism.[13] Therefore the β-value has been calculated regardless of the non-exponential behavior, and the calculate attenuation factor (β/2) determined. Here the value is found to be 0.043Å^{-1}, a relatively small value that is in agreement with β range values of other unsaturated π-conjugate bridged systems.[50,65,66]

Number of bridge units	H_{AB} (ev)
1	0.05114434
2	0.04955737
3	0.04669936
4	0.03676367

Table 16. C-DFT electronic coupling matrix elements H_{AB} (ev) calculated for set A with n=1-4.

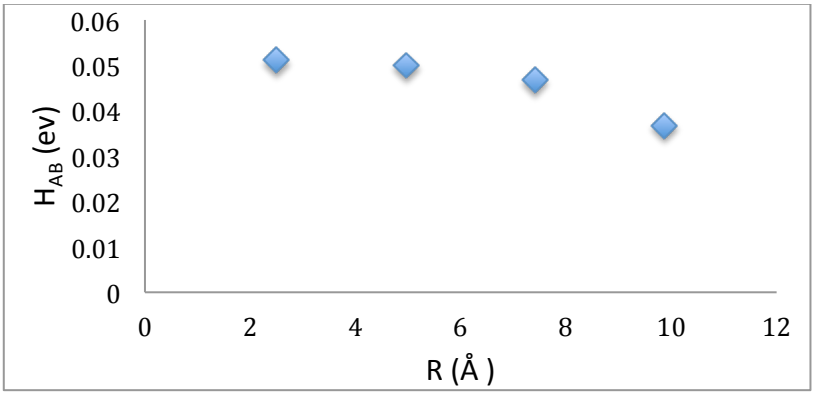

Figure 64. C-DFT electronic coupling matrix elements, H_{AB} (ev), as a function of the distance between the donor and the acceptor calculated for set A systems.

9.4 1,2-dimethyl-corannulene D/A units with saturated bridge of varying length

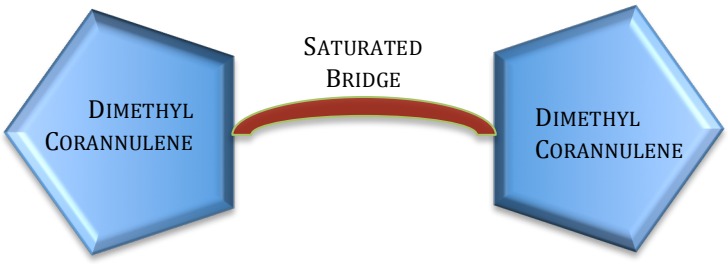

Figure 65. Schematic illustration for *f*-Cor-bridge-*f*-Cor for set D systems.

To examine further the effect of the unsaturated π-conjugate bridged on the electronic coupling matrix element characteristics, the set of systems D was investigated. This set

is composed of the same donor and acceptor as in set A systems, *i.e*. dimethyl-corannulene D/A units, but with different bridge component. In set A, the bridge is composed of fused benzene-like π-conjugated bridge units, which in set D is replaced with a saturated bridge, composed of fused cyclohexane-like bridge units ranging from n=1 to n=4 (Figure 65, Figure 58).

The donor and acceptor fragments for set D were defined in the same manner as for set A (Figure 59), and the distance between donor and acceptor units measured as in Figure 66.

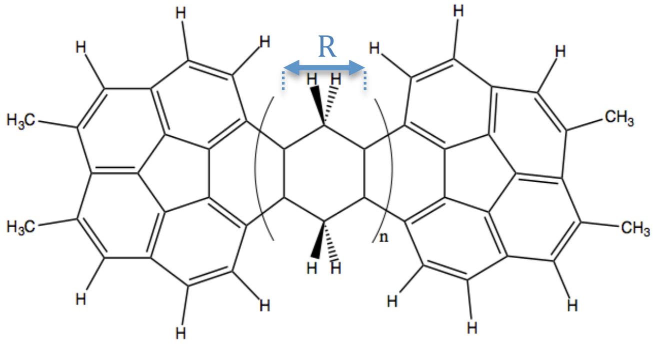

Figure 66. Set D systems measure of the distance R between the donor and acceptor fragments as the distance between the corannulene derivative end atoms connected to the bridge.

The highest occupied molecular orbitals of set D systems, as obtained in a standard DFT calculation as well as in the C-DFT calculations are presented in Figure 67. As with the A set systems, the HOMO orbitals obtained for a standard DFT calculations are symmetric, with electron density delocalization over the entire system, while the highest occupied MOs obtained in C-DFT, are not symmetric and localized primarily on either the donor in one diabatic state or on the acceptor on the other diabatic state, as per definition of D/A fragment units in the C-DFT. However, unlike the case of the unsaturated bridge set A systems, one can see that for these saturated bridge systems, the contribution of the bridge within these molecular orbitals seems to be much less significant. These results are well suited to the idea suggested before, regarding unsaturated bridges allowing for substantial electronic communication between the individual bridge units.

n	DFT Highest occupied molecular orbitals	
1	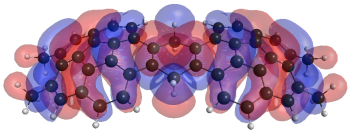	
2	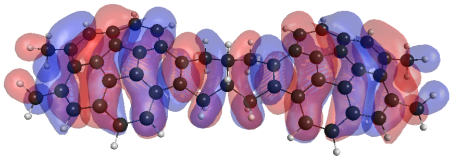	
3	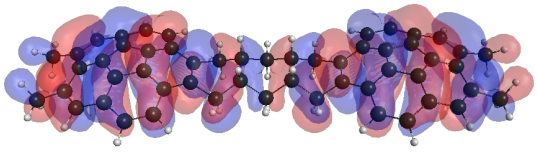	
4	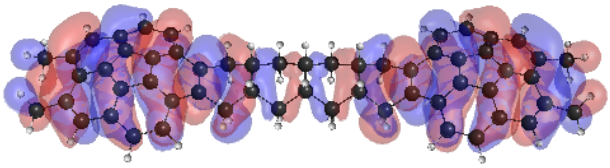	
	C-DFT Diabatic state A	**C-DFT Diabatic state B**
1	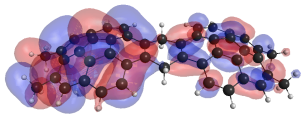	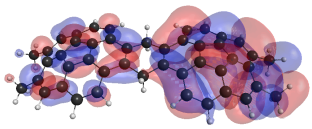
2	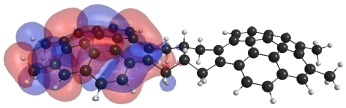	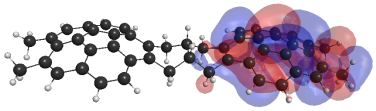
3	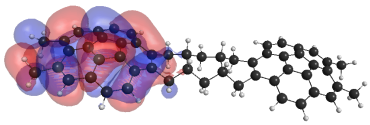	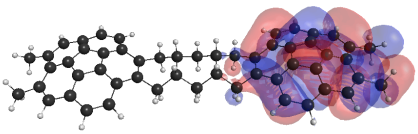
4	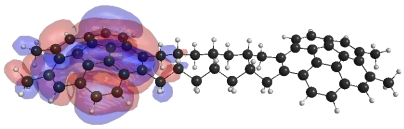	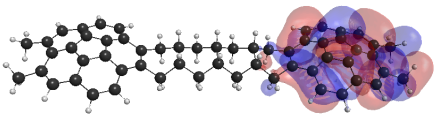

Figure 67. Highest occupied molecular orbitals obtained in DFT calculations (top set), and the highest occupied molecular orbitals obtained in C-DFT (bottom set), for the two diabatic states of set D systems.

Figure 68 shows the trends in the C-DFT calculated overlap S_{AB} values as a function of R for set D systems as compared to set A. While the overlap S_{AB} between the two diabatic

states reduces with increasing donor-acceptor distance, there are dramatic differences between the two system sets. In particular, very different attenuation is observed with the unsaturated bridge set A systems than for set D systems, where the decrease shows an exponential behavior for the latter (R^2= 0.996). In addition, across all systems, the overlap values obtained for the unsaturated bridge of set A are in general higher than those of the overlap values obtained for the saturated bridged set D. This may be attributed to a more significant contribution of TB interactions in the case of the unsaturated bridge associated with the set A systems.

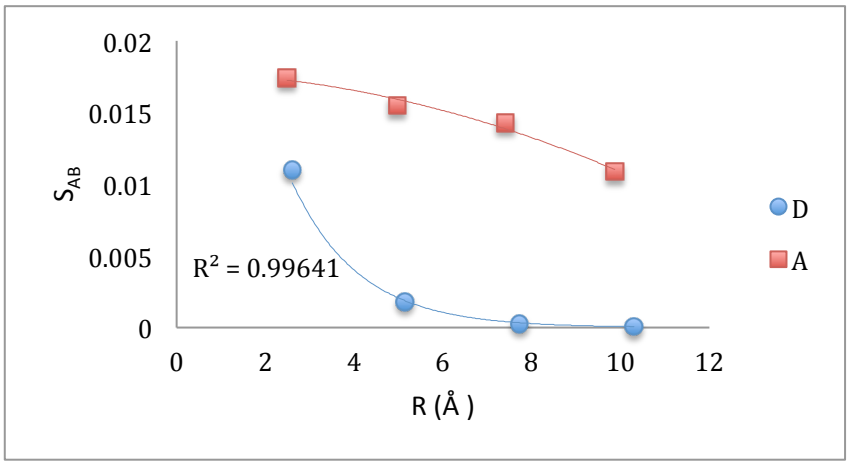

Figure 68. C-DFT calculated overlap S_{AB} values between the two diabatic states as a function of the distance R between the donor and the acceptor for set D systems (n=1-4) in blue circles, and for set A systems in red squares.

The exponential decay of the overlap S_{AB} with increasing bridge units is reflected in the results of calculated electronic coupling matrix element, H_{AB}, between the two diabatic states of set D systems as shown in Figure 69. The trend in electronic coupling matrix element is exponential (R^2= 0.997) with increasing distance between the donor and the acceptor. The calculated attenuation factor (β/2) is 0.66$Å^{-1}$, a value in agreement with β values characteristic for other saturated hydrocarbon bridged systems.[16, 60,61]

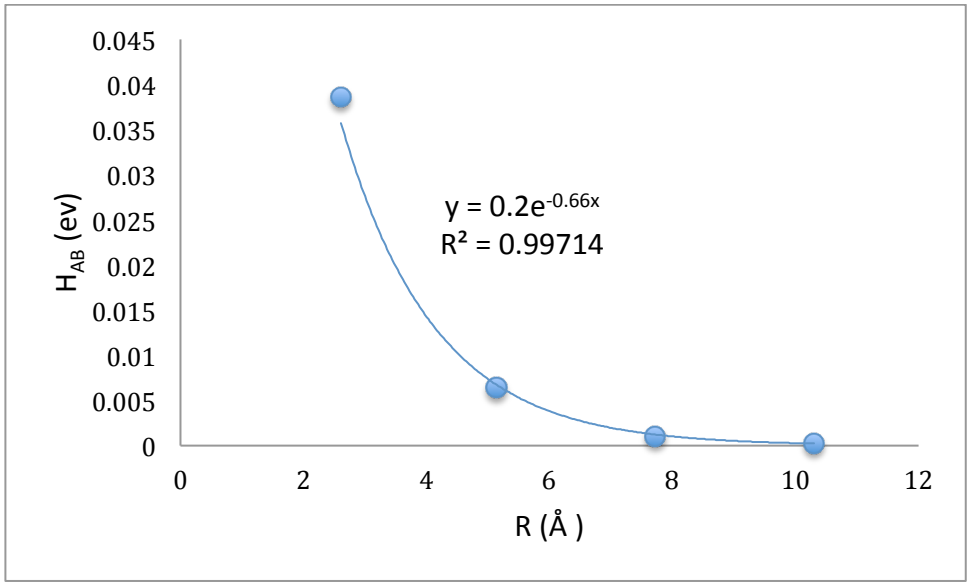

Figure 69. C-DFT electronic coupling matrix element, H_{AB} (ev), values as a function of the distance between the donor and the acceptor for set D systems.

9.5 Symmetric and Unsymmetric annulated-1,2-dimethylcorannulene D/A

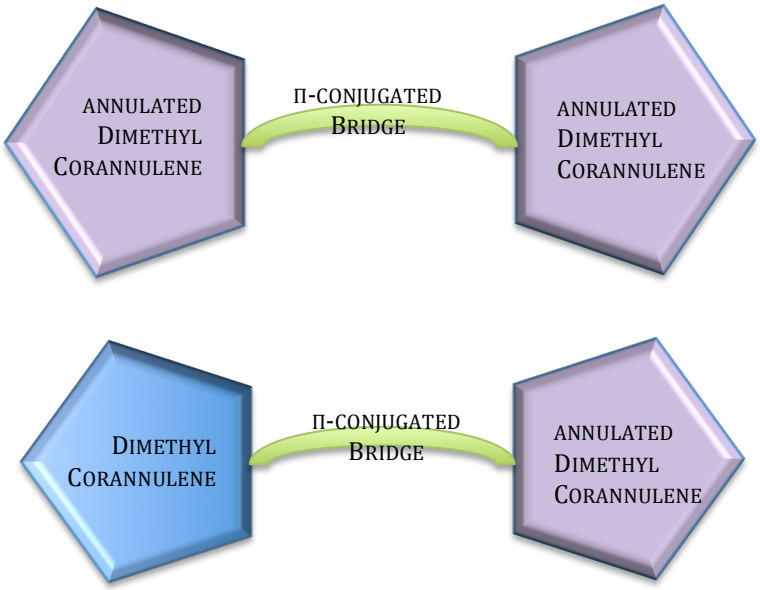

Figure 70. Schematic illustration for *f*-Cor-bridge-*f*-Cor for set B systems (top) and set E systems (bottom).

A very high variety of corannulene derivatives have already been synthesized, and the functionalization shown to affect the bowl structure, and therefore the electronic and dynamic properties.[105,115] To examine the effect of D/A corannulene derivatives characteristics on the C-DFT calculated electronic coupling, two additional *f*-Cor-bridge-*f*-Cor sets were investigated. These are characterized by annulated dimethyl-

corannulene D/A units with π-conjugated bridge of varying length with the number of bridge units n=1-4 (Figure 70, Figure 58). In set B, the systems are symmetrical, with both donor and acceptor as annulated dimethyl-corannulene, while in set E, the systems are asymmetrical, with annulated dimethyl-corannulene as the donor, and dimethyl-corannulene as the acceptor.

The optimized structures of sets B and E in comparison to set A optimized structures are presented in Figure 72. Bowl depth of corannulene derivatives is measured as the distance between the best plane fit defined by the 5 C's of the base 5 membered ring and the best plane fit defined by the 10 carbon atoms of the rim, between the centroid points on the two planes (Fig. 71). In particular, looking at the structures of A and B sets, clearly the D/A annulated dimethyl-corannulene bowl depth is significantly deeper than the bowl depth of the D/A dimethyl-corannulene. For the asymmetrical set E structures, with annulated dimethyl-corannulene as the donor, and dimethyl-corannulene as the acceptor, the bowl depth of the donor with the annulated dimethyl-corannulene is deeper than the bowl depth of the acceptor.

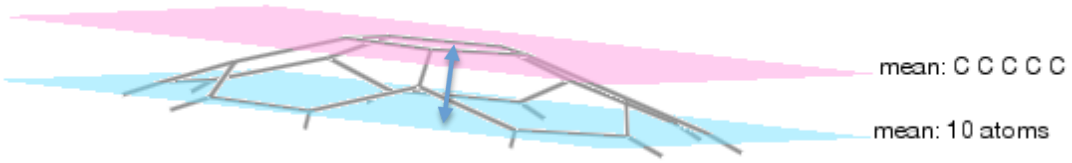

Figure 71. Corannulene derivative bowl depth measure illustration.

System	
Set A n=1	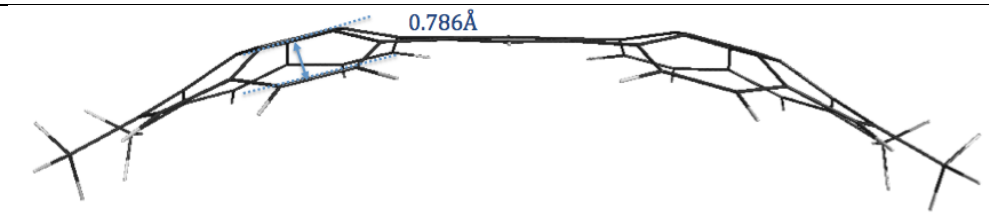
Set B n=1	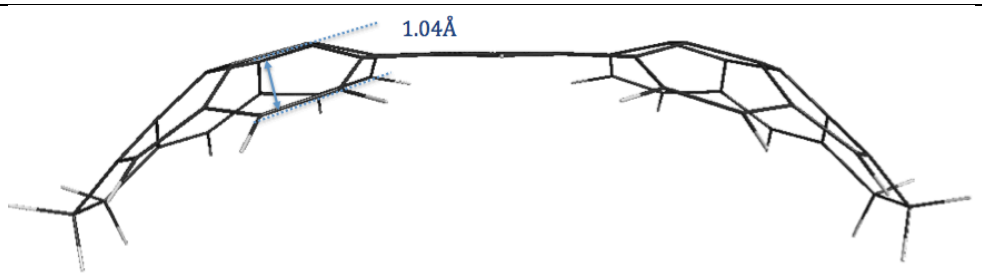
Set E n=1	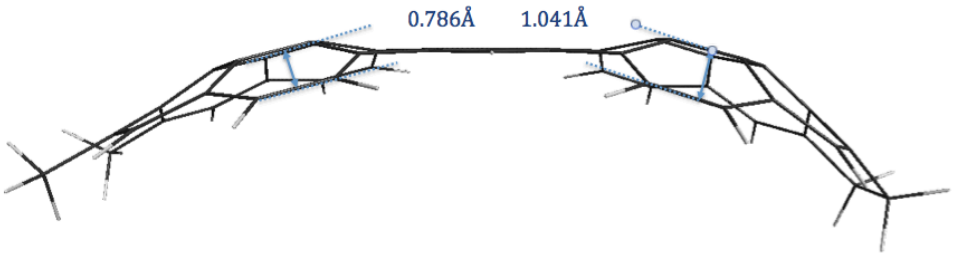

Figure 72. B3LYP/STO-3G optimized structure of sets B, E and A with n=1, with measured corannulene derivatives bowl depth.

For C-DFT calculations the donor and acceptor fragments were defined in the same manner as described before (Figure 59), and the distance between the donor and the acceptor is measured as the distance between the corannulene derivative end atoms connected to the bridge in the same manner as described for set A systems (Figure 60). Comparing the HOMO of set A and set B (Figure 73), one can see the resemblance of the orbitals, however, for set B, the corannulene bowl is deeper and more curved, as also observed in the orbitals.

HOMO set A, n=1	HOMO set B, n=1
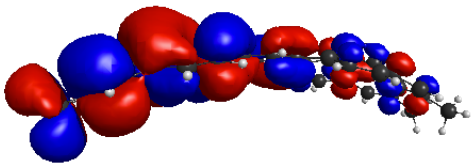	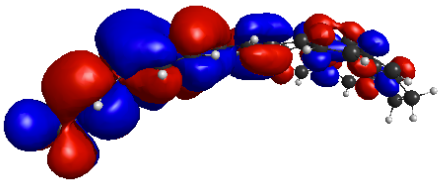

Figure 73. Calculated HOMO orbitals for set A and set B systems with n=1.

The affect of the HOMOs curvatures is reflected in the calculated overlap S_{AB} between the two diabatic states, as presented in Figure 74 for sets A, B and E systems. For both set B and set E systems, the overlap, S_{AB}, decreases exponentially (R^2= 0.962 for set B and R^2= 0.999 for set E). Comparison of the overlap values for the 3 sets of systems, one can see that, at short distance, there is a significant difference among the three sets, while in long distance the difference becomes much smaller. For n=1, the overlap S_{AB} between the two diabatic states for the symmetric system composed of annulated dimethyl-corannulene both for the donor and the acceptor (set B) is significantly higher than the value calculated for the symmetric system with D/A of dimethyl-corannulene (set A), while the value for the asymmetric system (set E) lies in between. The effect of the curvature depth seems to affect mostly in short-range, and this may be attributed to the short-range through space (TS) interactions between the donor and the acceptor orbitals, which is negligible beyond a separation greater than ≈3 Å. When the bowl is deeper and the curvature stronger, the atoms related to the donor and the atoms related to the acceptor lie relatively close to each other (Figure 75). The distances between the edge carbon atoms in each set for n=1 are calculated as ≈ 17.47 Å for set A, ≈ 16.45 Å for set B, and for the asymmetrical set E the distance lies in between with ≈16.95 Å.

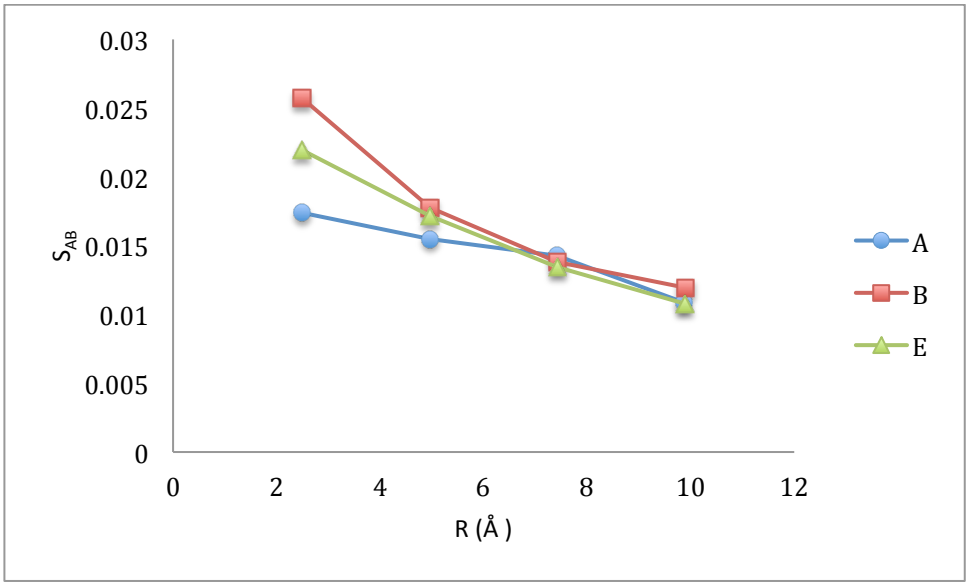

Figure 74. C-DFT calculated overlap S_{AB} as a function of the distance R between the donor and the acceptor for sets A, B and E.

A	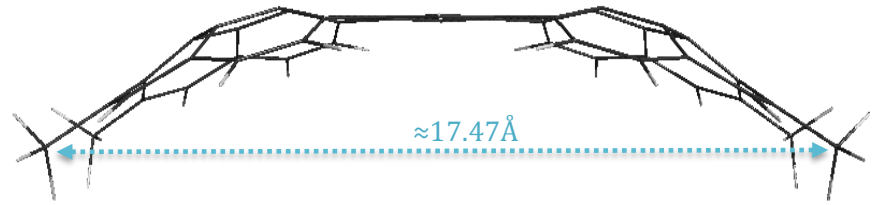
B	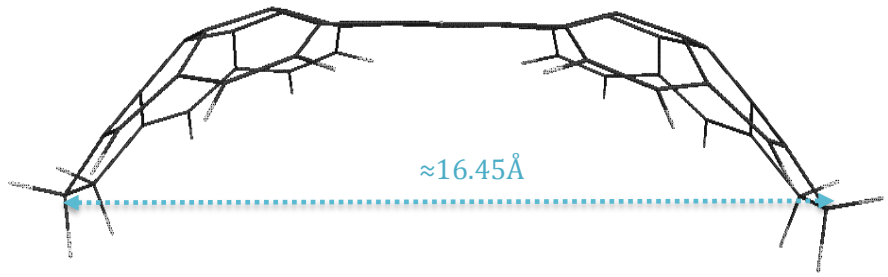
E	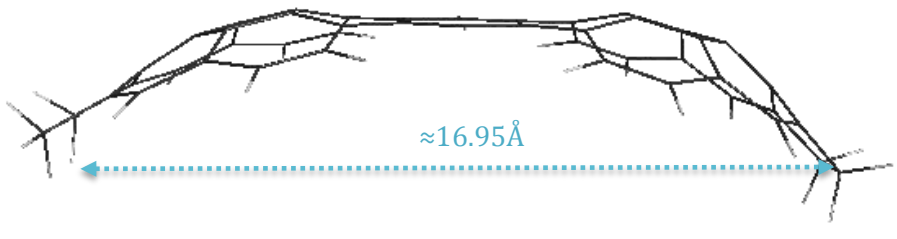

Figure 75. *f*-Cor-bridge-*f*-Cor system structures for n =1 for sets A, B and E.

The trend in overlap, S_{AB}, with increasing bridge units is reflected in the exponential results of calculated electronic coupling matrix element H_{AB} between the two diabatic

states in sets B and E (Figure 76). For both sets B and E, the calculated electronic coupling matrix elements show an exponential behavior (the curve fitting for set B is R^2= 0.972, and for set E R^2=0.989), with relatively small attenuation factor of ($\beta/2$)=0.087Å^{-1} for set B and ($\beta/2$)=0.092Å^{-1} for set E. The attenuation factor values are larger than in set A where the D/A are composed of dimethyl-corannulene. This is mostly due to the TS contribution to the short-distance interaction that occurs with the annulated dimethyl-corannulene based D/A systems. However, the value is still small enough to be in agreement with β range values of other unsaturated π-conjugate bridged systems.[50,65,66] The values of the electronic coupling matrix element for the symmetrical set B are in general higher than the values calculated for the asymmetrical set E.

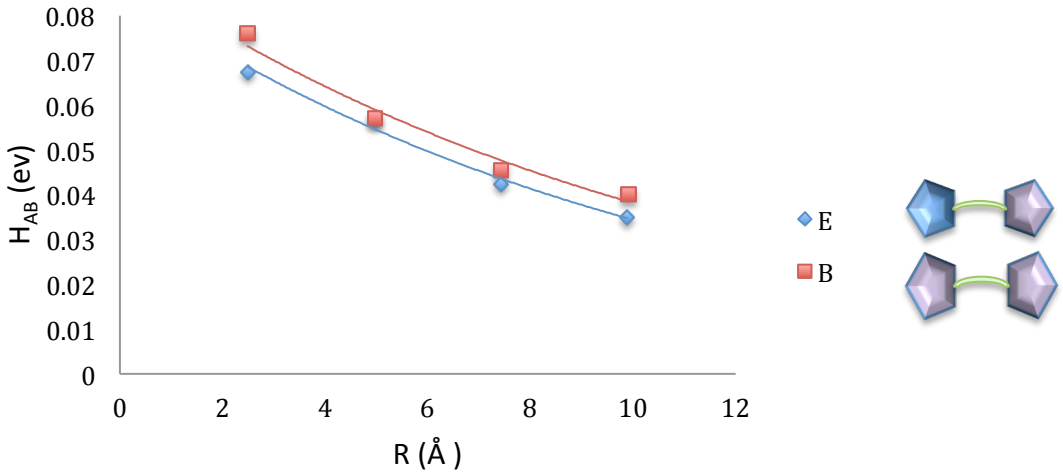

Figure 76. C-DFT calculated electronic coupling matrix elements, H_{AB} (ev), as a function of the distance between the donor and the acceptor calculated for the symmetrical B set (red) and asymmetrical E set (blue).

9.6 Symmetric and Unsymmetric 1,2-difluorocorannulene D/A

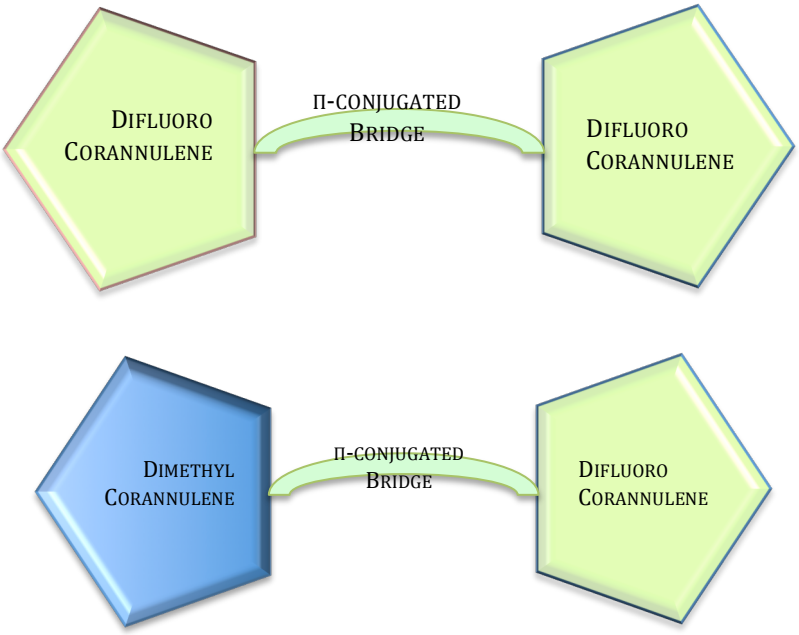

Figure 77. Schematic illustration for *f*-Cor-bridge-*f*-Cor for set C systems (top) and set F systems (bottom).

To examine the effect of electron withdrawing groups in the *f*-Cor-bridge-*f*-Cor system on the electronic coupling matrix element, two additional sets were investigated, set C and set F. These sets are characterized by difluorocorannulene D/A units with π-conjugated bridges of varying length, n=1-4 (Figure 77, Figure 58). In set C, the systems are symmetrical, with both donor and acceptor as difluorocorannulene, while in set F the systems are asymmetrical, with difluorocorannulene as the donor, and dimethylcorannulene as the acceptor. The donor and acceptor fragments were defined in the same manner as described before (Figure 59), and the distance between the donor and the acceptor is measured as the distance between the corannulene derivative end atoms connected to the bridge (Figure 60).

The dramatic effect of the withdrawing group on the overlap S_{AB} between the two diabatic states is shown in Figure 78. For both sets C and F, the overlap shows a dramatic decrease with increasing distance between the donor and the acceptor for the first three calculated points (for n=1-3). However, unexpectedly, at the forth point (n=4), the overlap increased sharply.

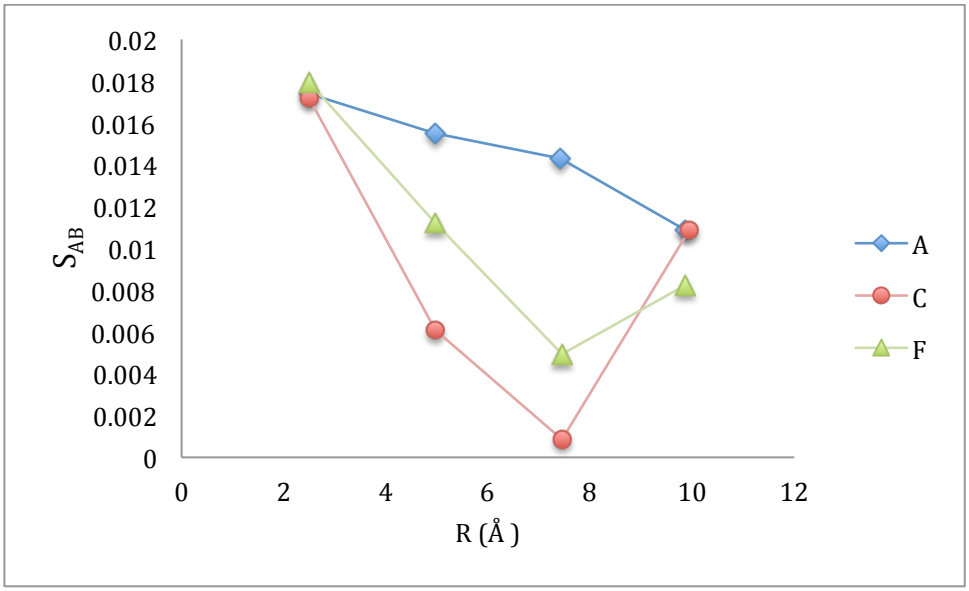

Figure 78. C-DFT calculated overlap, S_{AB}, as a function of the distance R between the donor and the acceptor for sets A, C and F.

For both sets C and F, the C-DFT calculated electronic coupling matrix element trends also show a dramatic decrease with increasing distance between the donor and the acceptor for the first three points (n=1-3) (Fig. 79). The effect is rather dramatic for the asymmetrical set F, which is effectively a hybridization between set A and set C. The calculated values lie in between the values for sets A and C. An unexpectedly sharp increase of the electronic coupling was found for the forth point (n=4).

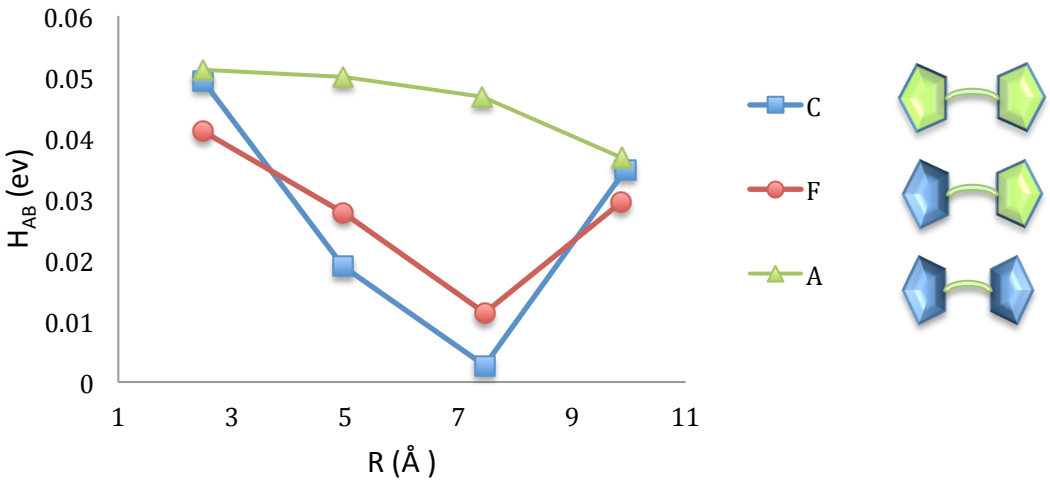

Figure 79. C-DFT electronic coupling matrix elements, H_{AB} (ev), as a function of the distance between the donor and the acceptor for sets C (blue), F (red) and A (green).

Results in Figure 79 show that the difference in H_{AB} values among the three sets is less significant in the short range than in the long-range. The short range differences may be attributed to the through space (TS) interactions, while the long range are related to the contribution of the bridge by through-bond (TB) interactions. As already shown, for the short range distance (n=1) for the three sets, one can see that the bowl depth and curvature is slightly different (Figure 80), where the bowl depth calculated for the symmetrical dimethylcorannulene derivative (0.786Å) is slightly lower than the symmetrical difluorinecorannulene derivative (0.806Å). For the unsymmetrical system F, the bowl depth of the dimethylcorannulene derivative is 0.786Å and of the difluorinecorannulene derivative is 0.806Å. A further look into the HOMOs of these systems (Figure 81) shows that, when the D/A is a difluorocorannulene derivative, the HOMO for n=1 is localized more at the edges towards the fluorine atoms, rather than in cases where the D/A is a dimethylcorannulene derivative. These results may explain the H_{AB} value difference for the three sets in the short-range. With respect to the long-range differences in H_{AB} values for n=1-3, this may be associated with the reduction in the bridge contribution when adding a withdrawing group to the D/A, as the electron density becomes larger at the D/A and smaller at the bridge.

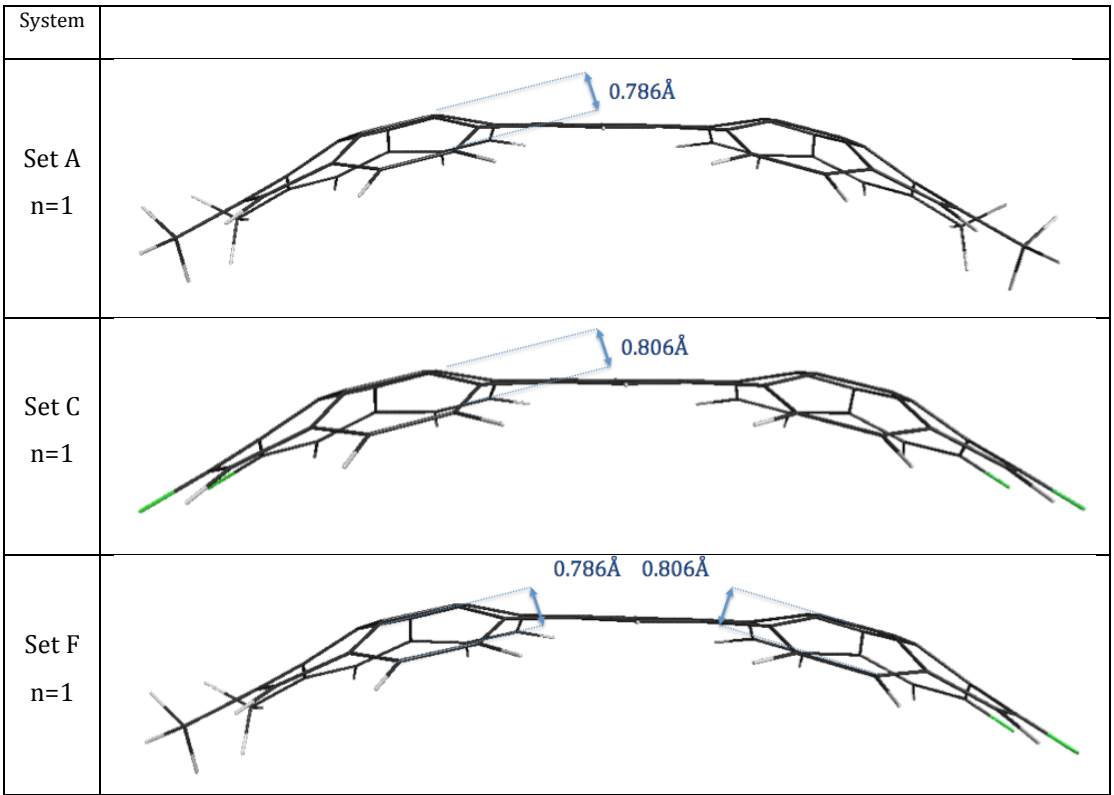

Figure 80. B3LYP/STO-3G optimized geometries for molecules of sets A, C and F for n=1, with calculated bowl depths of corannulene derivatives.

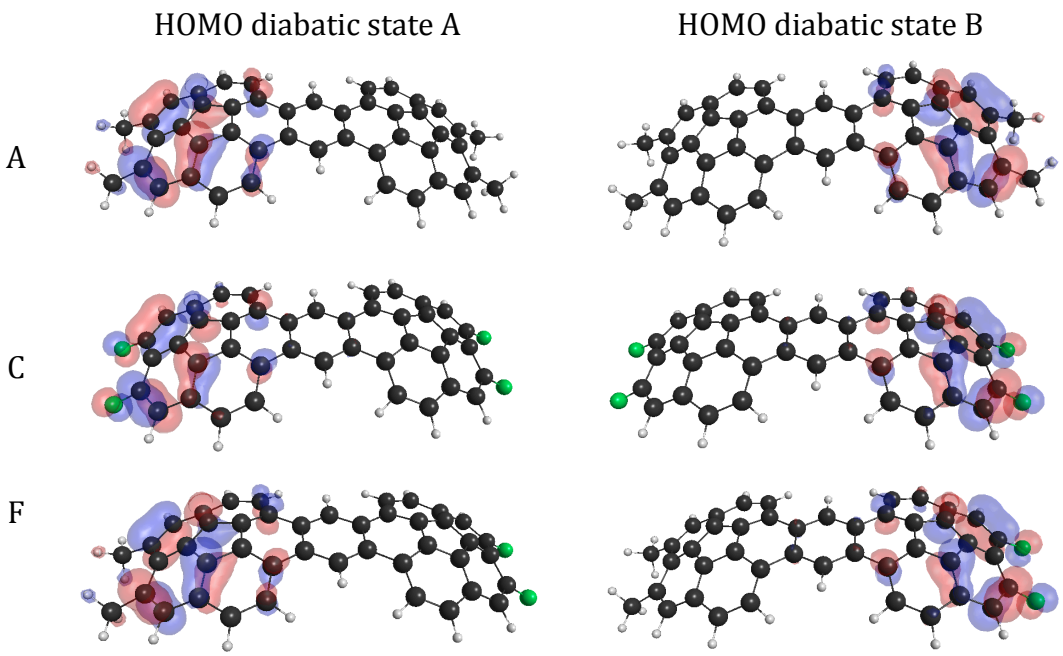

Figure 81. C-DFT calculated highest occupied molecular orbitals for n=1 systems of sets A, C and F.

The reasoning for the unexpected sharp increase both for the overlap and the resulting electronic coupling calculated values can be analyzed in terms of the HOMO-LUMO energy gap. Table 17 shows the HOMO-LUMO gap results calculated for the symmetric 1,2-difluorocorannulene D/A set, both for DFT and C-DFT methods. As one can see, while for DFT the gap gradually decreases with increasing bridge units for n=1-4, in C-DFT, the gap decreases for the first three systems (n=1-3), while in the fourth system (n=4), there is a slight increase. One expects a constant decrease in H/L gap with increase in length of the 'box' (here defined by the bridge length) as one learns with the model particle-in-a-box model. The fact that there is a sudden change in this phenomenon with the n=4, F-substituted system is an indication of something else going on.

n	**DFT HOMO-LUMO gap (ev)**	**C-DFT HOMO-LUMO gap (ev)**
1	-3.78232	-0.87075
2	-3.42858	-0.46258
3	-2.99321	-0.16326
4	-2.58504	-0.19047

Table 17. HOMO-LUMO gap values calculated for the symmetric 1,2-difluorocorannulene D/A set, for 1-4 number of bridge units, both for DFT and C-DFT.

The increase of the HOMO-LUMO gap in the case starting from the four-unit bridge system can be attributed to a further interaction between the HOMO and LUMO as these orbitals become very close in energy, as illustrated in Fig. 82. As the HOMO-LUMO gap decreases with increasing bridge units, the energy gap is decreased to a point where the HOMO and LUMO can mix to yield one lower energy HOMO and one higher energy LUMO, thereby giving a higher H/L gap then what an unmixed HOMO and unmixed LUMO gap would be. This can only happen in the cases where the orbitals are of the right symmetry to mix.

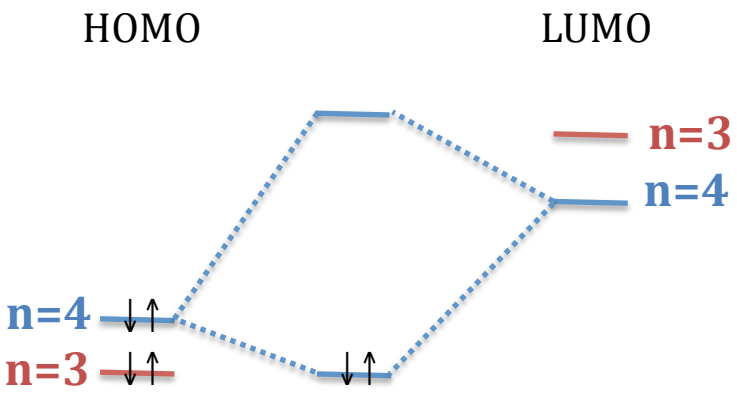

Figure 82. Illustration of the HOMO-LUMO gap results for n=3 and n=4 in C-DFT calculation for symmetric and asymmetric 1,2-difluorocoranulene D/A sets.

This further mixing of HOMO and LUMO orbitals is observed also with C-DFT. The HOMO and LUMO results for the symmetric 1,2-difluorocoranulene D/A set for n=1-4 are shown on Fig. 83. As one can see, for n=1-3, the HOMOs and LUMOs are symmetric, with the symmetry axis shown in green. However, the calculated HOMO and LUMO for n=4 appears to have lost this symmetry, which in this case is a consequence of the mixing of the HOMO and LUMO orbitals to produce a new set.

A further step in the development of the C-DFT methodology should involve further investigation into the control of the mixing. This can be done by enforcing symmetry restrictions to C-DFT calculations as appropriate for the particular system.

n	HOMO	LUMO
1	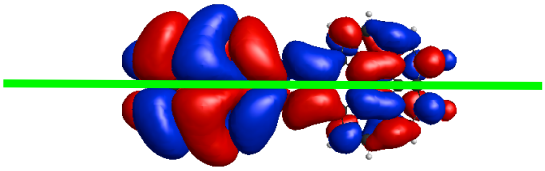	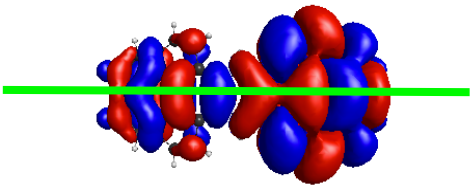
2	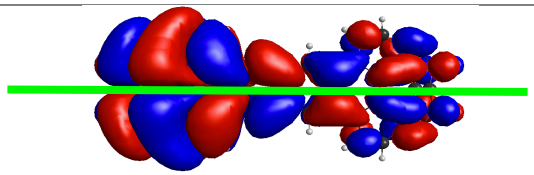	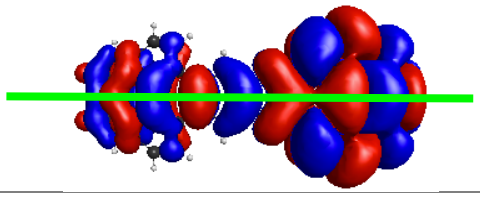
3	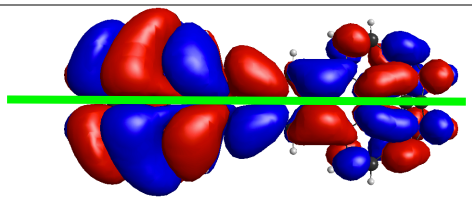	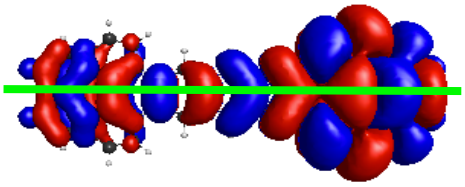
4	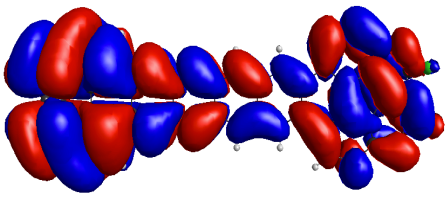	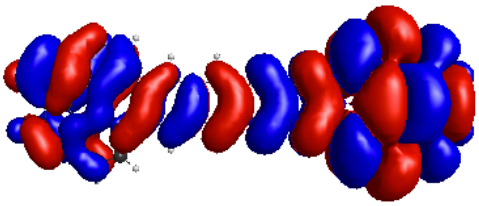

Figure 83. C-DFT HOMO and LUMO orbitals for symmetric 1,2-difluorocorannulene D/A set for n=1-4. Symmetry axes are shown in green.

9.7 Localization Schemes: *f*-Cor-bridge-*f*-Cor with unsaturated hydrocarbon bridge

D-B-A systems characterized by corannulene D/A with various bridges, in particular unsaturated π-type bridges, were extensively discussed previously. For examine the effect of LMO schemes on such systems, calculation were done with molecule belongs to set A with n=1. The calculations used the Becke's three-parameter hybrid functional[123] with Lee-Yang-Parr correlation[124] and a STO-3G basis set. The donor and the acceptor were defined as the whole corannulene derivative as was defined previously when investigating these systems. As one can see (Fig. 84), with regarding to the canonical orbitals, as expected, for the DFT the calculated HOMO is symmetrical and localized on the whole molecule, while the HOMO canonical orbital calculated with C-DFT is asymmetrical and localized mostly on the donor, with significant contribution also of the bridge. Localization with Pipek-Metzey scheme, further localized the orbitals and reduced dramatically the contribution of the bridge to the highest orbitals, where the LMOs acquired in DFT and with C-DFT are of high similarity. The LMOs received are

localized only on small fragment of the molecule, and apparently lead to much smaller overlap S_{AB} values. The HOMO LMOs characteristic can be reproduced in C-DFT calculation with defining the acceptor and the donor instead of the whole corannulene derivative only as a two-carbon-atom fragment as illustrated in Fig. 84.

	Canonical MOs	Pipek-Metzey LMOs
DFT	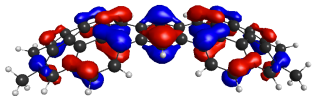	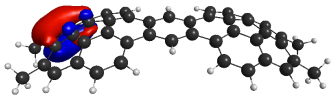
C-DFT with D/A fragments definition 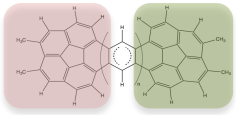	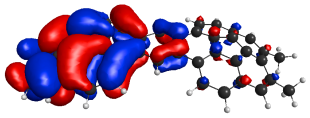	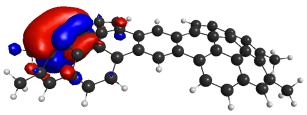
C-DFT with D/A fragments definition 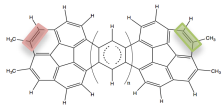	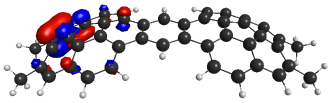	

Figure 84. Canonical and Pipek-Metzey MO for set A n=1, for C-DFT and DFT.

9.8 Conclusion remarks for D-B-A systems with corannulene D/A units systems

D-B-A corannulene D/A based systems enable investigation into various aspects related to electronic coupling matrix element H_{AB} values and behavior for designed *f*-Cor-bridge-*f*-Cor systems. Results of C-DFT calculated H_{AB} values of all calculated systems as well as the attenuation factor (β/2) values for all sets are presented in Figure 85 and Table 18, respectively. Overall, the sets show a decrease in the electronic coupling matrix element H_{AB} values as the distance between the donor and the acceptor gets larger. In general, for all three sets characterized with dimethylcorannulene D/A with unsaturated bridge (sets A, B and E), the attenuation factor (β/2) values are small and are within agreement with other unsaturated π-conjugate bridged systems.[50,65,66] The

only set tested with saturated bridge was found to be in agreement with β values characteristic for other saturated hydrocarbon bridged systems.[16, 60,61] A dramatic effect on the attenuation factor was determined with the addition of electron withdrawing groups to the donor and/or the acceptor fragments, resulting in significant increase of the attenuation factor value. This results aligns with a saturated bridge system rather then unsaturated bridge system. For both the two asymmetrical sets of systems (sets E and F), which may be referred to as hybridization of two symmetrical sets (set E as hybridization of sets A and B, set F as hybridization of sets A and C) the calculated behavior lies in between the behavior of the respective symmetrical systems.

Set	(β/2)
A	0.043Å^{-1}
B	0.087Å^{-1}
C	0.586Å^{-1}
D	0.66Å^{-1}
E	0.092Å^{-1}
F	0.26Å^{-1}

Table 18. C-DFT calculated attenuation factors (β/2) for systems A, B, C, D, E and F.

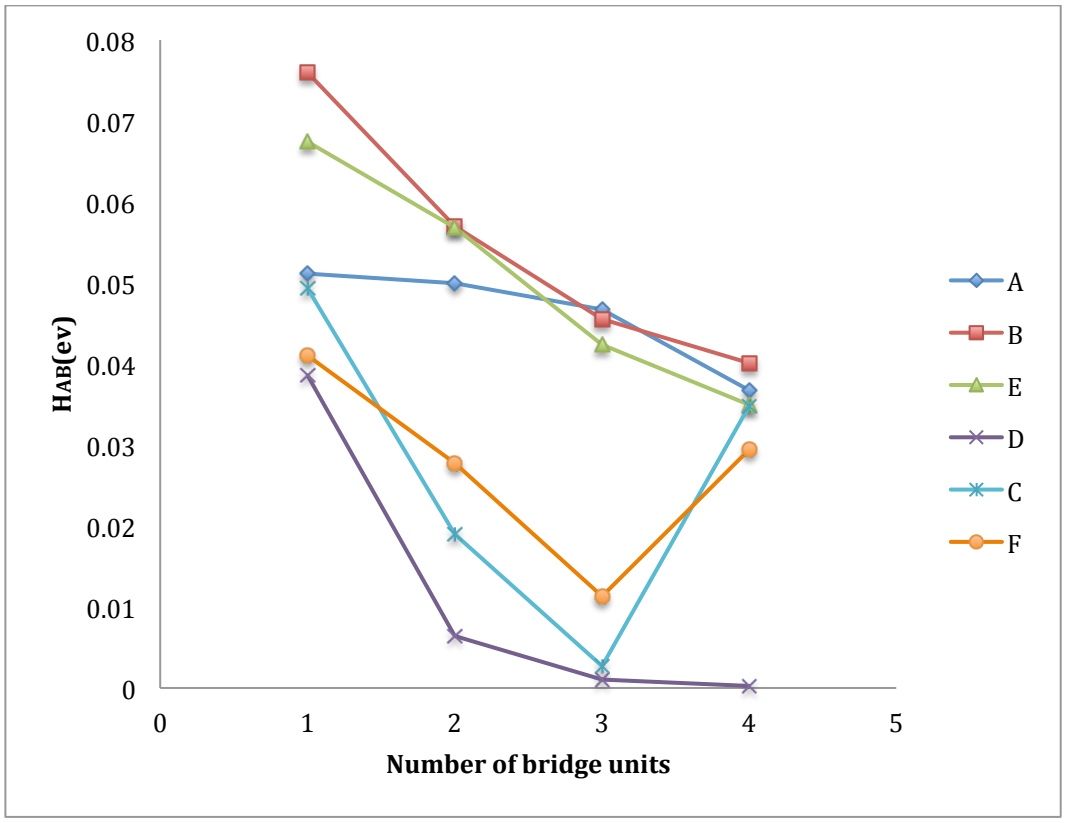

Figure 85. C-DFT calculated electronic coupling matrix elements, H_{AB} (ev), for various number of bridge units calculated for systems A, B, C, D, E and F for n=1-4.

10. Final Conclusions

10.1 Methodology for Electron Transfer Reactivity Predictions

This doctoral work has developed and evaluated a new C-DFT methodology that may be applied towards the calculation of electronic coupling and providing insight into the associated structural and mechanistic aspects of electron transfer reaction processes. This approach has been compared across various features of the underlying *ab initio* theory, such as wavefunction type, basis set extent, orbital localization scheme, and effects of solvation. The methodology is validated for a set of organic hydrocarbon molecules with characteristic TB and TS interactions coupling π donor and acceptor groups with known experimental values where available. The method is then used for investigation of a key application in the area of organic materials for electronic application based on a designed D-bridge-A system based on corannulene.

10.1.1 C-DFT Approach

A new charge-constraint C-DFT first-principles methodology has been implemented into the *ab initio* computational suite GAMESS for calculation of the electronic coupling, H_{AB}, between donor and acceptor states of organic molecular systems with electron transfer reactivity. The C-DFT methodology is developed using direct diabatic states construction. Through the development and associated validation, it is demonstrated that, with careful partitioning and choice of donor, acceptor, and spacer, the effective Hamiltonian is able to form diabats with localized molecular orbitals, representing the constraints in demand. The methods and implementations are demonstrated on model organic donor-acceptor systems, which provide a systematic comparison for through bond and through space interactions associated with electron transfer mechanisms. Calculated electronic coupling and associated decay attenuation factor results are shown to meet experimental expectations for bridgeless systems as well as for bridge-mediated systems, including saturated and unsaturated bridges.

Sensitivities of the implemented methodology with respect to the underlying quantum chemistry ansatz are discussed. In particular, choice of wave function type, basis set, and localization molecular orbital scheme, are characterized. In general, methodologies used for calculation of localized electron transfer reaction properties require a good quality basis set that does not involve diffuse functions.

Investigations into molecular orbital localization, using well-known localization schemes, through unitary transformation of the occupied orbitals, is enabled by special adaptation of the implemented C-DFT methodology. It is found that further orbital localization can dramatically reduce the contribution of the bridge and/or some D/A atoms to the dominant orbitals contributing to the electronic coupling. This then reduces the resulting value of the electronic coupling.

The inclusion of solvent effect in the developed methodology is shown to be particularly important for accurate predictions and improved understanding of electron transfer processes of realistic systems. It is found that in general, calculated systems in water solvent tend to maintain the decay attenuation factor characteristic for gas phase, with generally smaller values of evaluated electronic coupling.

Future work will be focused on coupling of the developed C-DFT methodology with the calculation of Franck-Condon density of states, for prediction of rate constants for ET reactions. Together, these theories provide the necessary underlying ability for better understanding of the details of the rate process in ET reactions, which ultimately aid in the development of future applications.

10.2 Structural Analysis

10.2.1 Test sets validation

Validation of results of simple experimentally known systems is essential for validation of the basic principles of new methodologies. In general, in C-DFT methodology for ET calculations, one expects larger values of constrained potential (V_c) when the charge separation demand is higher, and as the constraint demand is shared among fewer atoms. In addition, the molecular orbitals are expected to represent the constraints in demand. Simple ET-related systems tested using C-DFT methodology were shown to meet the expected constrained potential behavior. The calculated orbitals illustrate the electron density with regard to the constraints demand, that is, excess of electron density localized on the donor for one diabatic state, and excess of electron density localized on the acceptor for the other diabatic state.

10.2.2 Anthracene-dimer-anion

A set of bridgeless D/A systems, consisting of anthracene-dimer anions with distance separation R, is investigated for the dependence of the electronic coupling on the distance between the donor and the acceptor. It is found, that the overlap between the

diabatic states, and as a consequence, the electronic coupling, are decreased steeply with increasing donor-acceptor distance.

10.2.3 D-bridge-A with saturated hydrocarbon bridge

Two sets of D-bridge-A systems with saturated hydrocarbon bridge, one symmetrical consisting the same D/A, while the other is unsymmetrical, are investigated for the dependence of the electronic coupling on the mechanistic details of ET reactions through the bridge. In particular, the electronic coupling in the D-bridge-A systems is investigated with respect to bridge length and geometry. It is found, that for both sets, the overlap between the diabatic states, and as a consequence, the electronic coupling, are decreased exponentially with increasing donor-acceptor distance. For the two sets of saturated hydrocarbon bridge, the obtained decay attenuation factor values associated with the electronic coupling, are significantly lower than the values calculated for the set of bridgeless anthracene-dimer anions.

10.2.4 Application system : Corannulene-based D-bridge-A systems

A newly designed set of D-bridge-A systems based on functionalized corannulene derivatives as D and A is investigated in terms of the dependence of the electronic coupling on the mechanistic details of ET reactions through the bridge. In particular, the electronic coupling in the D-bridge-A systems is investigated with respect to bridge length, geometry and composition of bridge. It is found, that in general, the overlap between the diabatic states, and as a consequence, the electronic coupling, is decreased with increasing donor-acceptor distance. It is found that the obtained decay attenuation factor values associated with the electronic coupling in these systems is significantly lower than the values calculated for bridgeless systems, such as in the anthracene dimer anion case. The cases with the π-conjugated bridges show typically more efficient long-range transfer than do the cases with saturated bridge. As such, the π-conjugated bridge systems have smaller attenuation factor values relative to the values calculated for σ-bonds bridges. In addition, functionalized groups added to the D/A fragments show significant effect on the coupling, as a consequence of geometrical structural changes, as well as changes of the nature of the system as a whole. Effectively, structural changes are in turn associated with the characteristic through space and through bond interactions in these systems, thereby revealing important mechanistic information in these systems. These results should enable more focused design of effective D-bridge-A electron transfer systems based on the corannulene motif.

11 References

1. Kaduk, B., Kowalczyk, T. & Van Voorhis, T. Constrained Density Functional Theory. *Chem. Rev.* **112,** 321–370 (2012).
2. Wu, Q. & Van Voorhis, T. Extracting electron transfer coupling elements from constrained density functional theory. *J. Chem. Phys.* **125,** 164105 (2006).
3. Schmidt, M. W. *et al.* General atomic and molecular electronic structure system. *J. Comput. Chem.* **14,** 1347–1363 (1993).
4. Mori-Sánchez, P., Cohen, A. J. & Yang, W. Many-electron self-interaction error in approximate density functionals. *J. Chem. Phys.* **125,** 201102 (2006).
5. Tavernelli, I. Self-Interaction Corrected Density Functional Theory for the Study of Intramolecular Electron Transfer Dynamics in Radical Carbocations. *J. Phys. Chem. A* **111,** 13528–13536 (2007).
6. Pedrew, J. P. & Zunger, A. Self-interaction correction to density-functional approximations for many-electron systems. *Phys. Rev. B* **23,** 5048–5079 (1981).
7. Däne, M., Gonis, A., Nicholson, D. M. & Stocks, G. M. On a solution of the self-interaction problem in Kohn–Sham density functional theory. *J. Phys. Chem. Solids* **75,** 1160–1178 (2014).
8. Gidopoulos, N. I. & Lathiotakis, N. N. Constraining density functional approximations to yield self-interaction free potentials. *J. Chem. Phys.* **136,** 224109 (2012).
9. Becke, A. D. Real-space post-Hartree–Fock correlation models. *J. Chem. Phys.* **122,** 064101 (2005).

10. Mori-Sánchez, P., Cohen, A. J. & Yang, W. Self-interaction-free exchange-correlation functional for thermochemistry and kinetics. *J. Chem. Phys.* **124,** 091102 (2006).
11. d'Avezac, M., Calandra, M. & Mauri, F. Density functional theory description of hole-trapping in Si O 2 : A self-interaction-corrected approach. *Phys. Rev. B* **71,** (2005).
12. de la Lande, A. & Salahub, D. R. Derivation of interpretative models for long range electron transfer from constrained density functional theory. *J. Mol. Struct. THEOCHEM* **943,** 115–120 (2010).
13. Gilbert, M. & Albinsson, B. Photoinduced charge and energy transfer in molecular wires. *Chem Soc Rev* **44,** 845–862 (2015).
14. Wasielewski, M. R. Self-Assembly Strategies for Integrating Light Harvesting and Charge Separation in Artificial Photosynthetic Systems. *Acc. Chem. Res.* **42,** 1910–1921 (2009).
15. Gust, D., Moore, T. A. & Moore, A. L. Realizing artificial photosynthesis. *Faraday Discuss* **155,** 9–26 (2012).
16. Closs, G. L. & Miller, J. R. Intramolecular Long-Distance Electron Transfer in Organic Molecules. *Science* **240,** 440–447 (1988).
17. Van Voorhis, T. *et al.* The Diabatic Picture of Electron Transfer, Reaction Barriers, and Molecular Dynamics. *Annu. Rev. Phys. Chem.* **61,** 149–170 (2010).
18. Frauenfelder, H. & Wolynes, P. Rate Theories and Puzzle,S of HemeproteinKineltics. *Science* **229,** 337–345 (1985).
19. JORDAN, K. D. & Paddon-Row, M. N. Analysis of the Interactions Responsible for Long-Range Through-Bond-Mediated Electronic Coupling between

Remote Chromophores Attached to Rigid Polynorbornyl Bridges. **92,** 395–410 (1992).

20. Wasielewski, M. R. Photoinduced electron transfer in supramolecular systems for artificial photosynthesis. *Chem. Rev.* **92,** 435–461 (1992).
21. Gray, H. B. & Winkler, J. R. Long-range electron transfer. *Proc. Natl. Acad. Sci. U. S. A.* **102,** 3534–3539 (2005).
22. Berstis, L. & Baldridge, K. K. DFT-based Green's function pathways model for prediction of bridge-mediated electronic coupling. *Phys Chem Chem Phys* **17,** 30842–30853 (2015).
23. Marcus, R. A. On the Theory of Oxidation-Reduction Reactions Involving Electron Transfer. *J. Chem. Phys.* **24,** 966 (1956).
24. Heckmann, A. & Lambert, C. Organic Mixed-Valence Compounds: A Playground for Electrons and Holes. *Angew. Chem. Int. Ed.* **51,** 326–392 (2012).
25. Marcus, R. A. Electron transfer reactions in chemistry. Theory and experiment. *Rev. Mod. Phys.* **65,** 599 (1993).
26. Miller, J. R., Calcaterra, L. T. & Closs, G. L. Intramolecular long-distance electron transfer in radical anions. The effects of free energy and solvent on the reaction rates. *J. Am. Chem. Soc.* **106,** 3047–3049 (1984).
27. Yonemoto, E. H. *et al.* Photoinduced electron transfer in covalently linked ruthenium tris (bipyridyl)-viologen molecules: observation of back electron transfer in the Marcus inverted region. *J. Am. Chem. Soc.* **114,** 8081–8087 (1992).

28. Baldridge, K. K., Battersby, T. R., VernonClark, R. & Siegel, J. S. Does π-σ-π Through-Bond Coupling Significantly Increase C-C Bond Lengths? *J. Am. Chem. Soc.* **119,** 7048–7054 (1997).

29. NEWTON, M. D. Quantum Chemical Probes of Electron-Transfer Kinetics: The Nature of Donor-Acceptor Interactions. *Chem. Rev.* **91,** 767–792 (1991).

30. Hoffmann, R., Imamura, A. & Hehre, W. J. Benzynes, dehydroconjugated molecules, and the interaction of orbitals separated by a number of intervening sigma bonds. *J. Am. Chem. Soc.* **90,** 1499–1509 (1968).

31. Hoffmann, R. Interaction of orbitals through space and through bonds. *Acc. Chem. Res.* **4,** 1–9 (1971).

32. Paddon-Row, M. N. Some aspects of orbital interactions through bonds: Physical and chemical consequences. *Acc. Chem. Res.* **15,** 245–251 (1982).

33. McConnell, H. M. Intramolecular Charge Transfer in Aromatic Free Radicals. *J. Chem. Phys.* **35,** 508 (1961).

34. Miller, A. & Abrahams, E. Impurity Conduction at Low Concentrations. *Phys. Rev.* **120,** 745–755 (1960).

35. Mott, N. F. Conduction in glasses containing transition metal ions. *J. Non-Cryst. Solids* **1,** 1–17 (1968).

36. Kramers, H. A. L'interaction Entre les Atomes Magnétogènes dans un Cristal Paramagnétique. *Physica* **1,** 182–192 (1934).

37. ANDERsON, P. W. Antiferromagnetism. Theory of Suyerexchange Interaction. *Phys. Rev.* **79,** 350–356 (1950).

38. Halpern, J. & Orgel, L. E. The theory of electron transfer between metal ions in bridged systems. *Discuss. Faraday Soc.* **29,** 32–41 (1960).

39. Archer, M. D. & Nozik, A. J. *Nanostructured and Photoelectrochemical Systems for Solar Photon Conversion*. (World Scientific, 2008).

40. Harriman, A., Rostron, S. A., Khatyr, A. & Ziessel, R. The mechanism of long-range electron exchange in molecular-scale photonic wires. *Faraday Discuss* **131,** 377–391 (2006).

41. Nitzan, A. Electron transmission through molecules and molecular interfaces. *Annu. Rev. Phys. Chem.* **52,** 681–750 (2001).

42. Ricks, A. B. *et al.* Exponential Distance Dependence of Photoinitiated Stepwise Electron Transfer in Donor–Bridge–Acceptor Molecules: Implications for Wirelike Behavior. *J. Am. Chem. Soc.* **134,** 4581–4588 (2012).

43. Clayton, A. H., Scholes, G. D., Ghiggino, K. P. & Paddon-Row, M. N. Through-bond and through-space coupling in photoinduced electron and energy transfer: An ab initio and semiempirical study. *J. Phys. Chem.* **100,** 10912–10918 (1996).

44. Pettersson, K., Wiberg, J., Ljungdahl, T., Mårtensson, J. & Albinsson, B. Interplay between Barrier Width and Height in Electron Tunneling: Photoinduced Electron Transfer in Porphyrin-Based Donor−Bridge−Acceptor Systems. *J. Phys. Chem. A* **110,** 319–326 (2006).

45. Kilså, K., Kajanus, J., Macpherson, A. N., Mårtensson, J. & Albinsson, B. Bridge-Dependent Electron Transfer in Porphyrin-Based Donor−Bridge−Acceptor Systems. *J. Am. Chem. Soc.* **123,** 3069–3080 (2001).

46. Wiberg, J. *et al.* Charge Recombination versus Charge Separation in Donor−Bridge−Acceptor Systems. *J. Am. Chem. Soc.* **129,** 155–163 (2007).

47. Paddon-Row, M. N. *et al.* Factors affecting charge separation and recombination in photoexcited rigid donor-insulator-acceptor compounds. *J. Phys. Chem.* **92,** 6958–6962 (1988).

48. Roest, M. R., Oliver, A. M., Paddon-Row, M. N. & Verhoeven, J. W. Distance dependence of singlet and triplet charge recombination pathways in a series of rigid bichromophoric systems. *J. Phys. Chem. A* **101,** 4867–4871 (1997).

49. Closs, G. L., Piotrowiak, P., Maclnnis, J. M. & Fleming, G. R. Determination of Long Distance Intramolecular Triplet EnergyTransferRates. AQuantitativeComparison with Electron Transfer. *J. Am. Chem. Soc.* **110,** 2652–2653 (1988).

50. Davis, W. B., Svec, W. A., Ratner, M. A. & Wasielewski, M. R. Molecular-wire behaviour in p-phenylenevinylene oligomers. *Nature* **396,** 60–63 (1998).

51. Davis, W. B., Wasielewski, M. R., Ratner, M. A., Mujica, V. & Nitzan, A. Electron transfer rates in bridged molecular systems: a phenomenological approach to relaxation. *J. Phys. Chem. A* **101,** 6158–6164 (1997).

52. Weiss, E. A. *et al.* Making a Molecular Wire: Charge and Spin Transport through *p ara* -Phenylene Oligomers. *J. Am. Chem. Soc.* **126,** 5577–5584 (2004).

53. Comparison of V Values for Some Nitrogen- and Metal-Centered π-Bridged Mixed-Valence Compounds. *J. Am. Chem. Soc.* **120,** 298–304 (1998).

54. Moser, C. C., Keske, J. M., Warncke, K., Farid, R. S. & Dutton, P. L. Nature of biological electron transfer. *Nature* **355,** 796–802 (1992).

55. Lyshevski, S. E. *Nano and Molecular Electronics Handbook*. (CRC Press, 2007).

56. Winkler, J. R. & Gray, H. B. Electron transfer in ruthenium-modified proteins. *Chem. Rev.* **92,** 369–379 (1992).

57. Onuchic, J. N., Beratan, D. N., Winkler, J. R. & Gray, H. B. Pathway analysis of protein electron-transfer reactions. *Annu. Rev. Biophys. Biomol. Struct.* **21,** 349–377 (1992).

58. Vassilian, A., Wishart, J. F., Van Hemelryck, B., Schwarz, H. & Isied, S. S. Electron transfer across polypeptides. 6. Long-range electron transfer in osmium-ruthenium binuclear complexes bridged with oligoproline peptides. *J. Am. Chem. Soc.* **112,** 7278–7286 (1990).

59. Lewis, F. D. *et al.* Distance-Dependent Electron Transfer in DNA Hairpins. *Science* **277,** 673–676 (1997).

60. Johnson, M. D., Miller, J. R., Green, N. S. & Closs, G. L. Distance dependence of intramolecular hole and electron transfer in organic radical ions. *J. Phys. Chem.* **93,** 1173–1176 (1989).

61. Oevering, H. *et al.* Long-range photoinduced through-bond electron transfer and radiative recombination via rigid nonconjugated bridges: distance and solvent dependence. *J. Am. Chem. Soc.* **109,** 3258–3269 (1987).

62. Gilbert Gatty, M. *et al.* Hopping versus Tunneling Mechanism for Long-Range Electron Transfer in Porphyrin Oligomer Bridged Donor–Acceptor Systems. *J. Phys. Chem. B* **119,** 7598–7611 (2015).

63. Helms, A., Heiler, D. & McLendon, G. Electron transfer in bis-porphyrin donor-acceptor compounds with polyphenylene spacers shows a weak distance dependence. *J. Am. Chem. Soc.* **114,** 6227–6238 (1992).

64. Sachs, S. B. *et al.* Rates of interfacial electron transfer through π-conjugated spacers. *J. Am. Chem. Soc.* **119,** 10563–10564 (1997).

65. Miura, T., Carmieli, R. & Wasielewski, M. R. Time-Resolved EPR Studies of Charge Recombination and Triplet-State Formation within Donor–Bridge–Acceptor Molecules Having Wire-Like Oligofluorene Bridges. *J. Phys. Chem. A* **114,** 5769–5778 (2010).

66. de la Torre, G., Giacalone, F., Segura, J. L., Martin, N. & Guldi, D. M. Electronic Communication through pi-Conjugated Wires in Covalently Linked Porphyrin/C60 Ensembles. *Chem. - Eur. J.* **11,** 1267–1280 (2005).

67. Klamt, A. & Schüürmann, G. COSMO: a new approach to dielectric screening in solvents with explicit expressions for the screening energy and its gradient. *J. Chem. Soc. Perkin Trans. 2* 799–805 (1993).

68. Baldridge, K. K. & Jonas, V. Implementation and refinement of the modified-conductorlike screening quantum mechanical solvation model at the MP2 level. *J. Chem. Phys.* **113,** 7511 (2000).

69. Baldridge, K. & Klamt, A. First principles implementation of solvent effects without outlying charge error. *J. Chem. Phys.* **106,** 6622 (1997).

70. Gregerson, L. N. & Baldridge, K. K. Outlying Charge, Stability, Efficiency, and Algorithmic Enhancements in the Quantum-Mechanical Solvation Method, COSab-GAMESS. *Helv. Chim. Acta* **86,** 4112–4132 (2003).

71. Klamt, A. The COSMO and COSMO-RS solvation models. *Wiley Interdiscip. Rev. Comput. Mol. Sci.* **1,** 699–709 (2011).

72. Andzelm, J., Kölmel, C. & Klamt, A. Incorporation of solvent effects into density functional calculations of molecular energies and geometries. *J. Chem. Phys.* **103,** 9312 (1995).

73. Klamt, A. & Jonas, V. Treatment of the outlying charge in continuum solvation models. *J. Chem. Phys.* **105,** 9972 (1996).

74. Klamt, A. *COSMO-RS, From Quantum Chemistry to Fluid Phase Thermodynamics and Drug Design*. (Elsevier, 2005).

75. Pipek, J. & Mezey, P. G. A fast intrinsic localization procedure applicable for ab initio and semiempirical linear combination of atomic orbital wave functions. *J. Chem. Phys.* **90,** 4916 (1989).

76. Kleier, D. A. Localized molecular orbitals for polyatomic molecules. I. A comparison of the Edmiston-Ruedenberg and Boys localization methods. *J. Chem. Phys.* **61,** 3905 (1974).

77. Jensen, F. *Introduction to Computational Chemistry*. (Wiley, 2006).

78. Edmiston, C. & Ruedenberg, K. Localized atomic and molecular orbitals. *Rev. Mod. Phys.* **35,** 457 (1963).

79. Boys, S. . in *Quantum Theory of Atoms, Molecules, and the Solid State A Tribute to John C. Slater* 253–262 (Edited by Per-Olov Löwdin. New York: Academic Press, 1966).

80. Boughton, J. W. & Pulay, P. Comparison of the boys and Pipek–Mezey localizations in the local correlation approach and automatic virtual basis selection. *J. Comput. Chem.* **14,** 736–740 (1993).

81. Wu, Q. & Van Voorhis, T. Constrained Density Functional Theory and Its Application in Long-Range Electron Transfer. *J. Chem. Theory Comput.* **2,** 765–774 (2006).

82. Pulay, P. Convergence acceleration of iterative sequences. the case of scf iteration. *Chem. Phys. Lett.* **73,** 393–398 (1980).

83. Hamilton, T. P. & Pulay, P. Direct inversion in the iterative subspace (DIIS) optimization of open-shell, excited-state, and small multiconfiguration SCF wave functions. *J. Chem. Phys.* **84,** 5728 (1986).

84. Saha, S., Roy, R. K. & Ayers, P. W. Are the Hirshfeld and Mulliken population analysis schemes consistent with chemical intuition? *Int. J. Quantum Chem.* **109,** 1790–1806 (2009).

85. Sholl, D. S. & Steckel, J. A. *Density Functional Theory: A Practical Introduction*. (John Wiley & Sons, Inc., 2009).

86. DeKock, R. L. & Gray, H. B. *Chemical Structure and Bonding*. (University Science Books, 1989).

87. Kubas, A. *et al.* Electronic couplings for molecular charge transfer: benchmarking CDFT, FODFT and FODFTB against high-level ab initio calculations. II. *Phys Chem Chem Phys* **17,** 14342–14354 (2015).

88. JORDAN, K. D. & Paddon-Row, M. N. Long-Range Interactions in a Series of Rigid Nonconjugated Dienes. 1. Distance Dependenceofthe?T+,?T-andr+*,?r-S*pllttingsDeterminedbyabInitioCalculations. *J. Phys. Chem.* **96,** 1188–1 196 (1992).

89. Kim, K., Jordan, K. D. & Paddon-Row, M. N. Long-Range Interactions in a Series of Rigid Nonconjugated Polynorbornyl Dienes. 2. Role of Electron Correlation in Determining the Distance Dependence of the. pi.+,. pi.-and. pi.+,. pi.-Splittings. *J. Phys. Chem.* **98,** 11053–11058 (1994).

90. Balaji, V., Ng, L., Paddon-Row, M. N. & Patney, H. K. A Study of Long-Range T * , T * Interactions in Rigid Molecules Using Electron Transmission Spectroscopy. *J. Am. Chem. Soc.* **109,** 6957–6969 (1987).

91. Lee, S. *et al.* Effects of hydroxyl groups in polymeric dielectrics on organic transistor performance. *Appl. Phys. Lett.* **88,** 162109 (2006).

92. Shirota, Y. Organic materials for electronic and optoelectronic devices. *J. Mater. Chem.* **10,** 1–25 (2000).

93. Katz, H. E. & Huang, J. Thin-Film Organic Electronic Devices. *Annu. Rev. Mater. Res.* **39,** 71–92 (2009).

94. Kauffman, D. R. & Star, A. Carbon Nanotube Gas and Vapor Sensors. *Angew. Chem. Int. Ed.* **47,** 6550–6570 (2008).

95. Mowbray, D. J., Morgan, C. & Thygesen, K. S. Influence of O 2 and N 2 on the conductivity of carbon nanotube networks. *Phys. Rev. B* **79,** 195431–1 – 195431–6 (2009).

96. Zoppi, L., Siegel, J. S. & Baldridge, K. K. Electron transport and optical properties of curved aromatics. *Wiley Interdiscip. Rev. Comput. Mol. Sci.* **3,** 1–12 (2013).

97. Forrest, S. R. The path to ubiquitous and low-cost organic electronic appliances on plastic. *Nature* **428,** 911–918 (2004).

98. Burroughes, J. *et al.* Light-emitting diodes based on conjugated polymers. *Nature* **347,** 539–541 (1990).

99. Schwartz, G., Fehse, K., Pfeiffer, M., Walzer, K. & Leo, K. Highly efficient white organic light emitting diodes comprising an interlayer to separate fluorescent and phosphorescent regions. *Appl. Phys. Lett.* **89,** 083509 (2006).

100. Dumur, F. Carbazole-based polymers as hosts for solution-processed organic light-emitting diodes: Simplicity, efficacy. *Org. Electron.* **25,** 345–361 (2015).

101. Capelli, R. *et al.* Organic light-emitting transistors with an efficiency that outperforms the equivalent light-emitting diodes. *Nat. Mater.* **9,** 496–503 (2010).

102. Zhao, Y. & Liang, W. Charge transfer in organic molecules for solar cells: theoretical perspective. *Chem Soc Rev* **41,** 1075–1087 (2012).
103. Dimitrakopoulos, C. D. & Malenfant, P. R. Organic thin film transistors for large area electronics. *Adv. Mater.* **14,** 99 (2002).
104. Soldano, C. *et al.* ITO-Free Organic Light-Emitting Transistors with Graphene Gate Electrode. *ACS Photonics* **1,** 1082–1088 (2014).
105. Butterfield, A. M., Gilomen, B. & Siegel, J. S. Kilogram-Scale Production of Corannulene. *Org. Process Res. Dev.* **16,** 664–676 (2012).
106. Newman, M. S., Lutz, W. B. & Lednicer, D. A NEW REAGENT FOR RESOLUTION BY COMPLEX FORMATION; THE RESOLUTION OF PHENANTHRO-[3, 4-c] PHENANTHRENE1. *J. Am. Chem. Soc.* **77,** 3420–3421 (1955).
107. Martin, R. The Helicenes. *Angew. Chem. Int. Ed.* **13,** 649–660 (1974).
108. Luo, J., Xu, X., Mao, R. & Miao, Q. Curved Polycyclic Aromatic Molecules That Are π-Isoelectronic to Hexabenzocoronene. *J. Am. Chem. Soc.* **134,** 13796–13803 (2012).
109. Lovas, F. J. *et al.* Interstellar Chemistry: A Strategy for Detecting Polycyclic Aromatic Hydrocarbons in Space. *J. Am. Chem. Soc.* **127,** 4345–4349 (2005).
110. Baldridge, K. K. & Siegel, J. S. Corannulene-based fullerene fragments C20H10-C50H10: when does a buckybowl become a buckytube? *Theor. Chem. Acc. Theory Comput. Model. Theor. Chim. Acta* **97,** 67–71 (1997).
111. Zoppi, L., Martin-Samos, L. & Baldridge, K. K. Buckybowl superatom states: a unique route for electron transport? *Phys Chem Chem Phys* **17,** 6114–6121 (2015).

112. Zoppi, L., Ferretti, A. & Baldridge, K. K. Static and Field-Oriented Properties of Bowl-Shaped Polynuclear Aromatic Hydrocarbon Fragments. *J. Chem. Theory Comput.* **9,** 4797–4804 (2013).

113. Filatov, A. S., Scott, L. T. & Petrukhina, M. A. π−π Interactions and Solid State Packing Trends of Polycyclic Aromatic Bowls in the Indenocorannulene Family: Predicting Potentially Useful Bulk Properties. *Cryst. Growth Des.* **10,** 4607–4621 (2010).

114. Wu, Y.-T. *et al.* Multiethynyl Corannulenes: Synthesis, Structure, and Properties. *J. Am. Chem. Soc.* **130,** 10729–10739 (2008).

115. Zoppi, L., Martin-Samos, L. & Baldridge, K. K. Effect of Molecular Packing on Corannulene-Based Materials Electroluminescence. *J. Am. Chem. Soc.* **133,** 14002–14009 (2011).

116. Barth, W. E. & Lawton, R. G. Dibenzo [ghi, mno] fluoranthene. *J. Am. Chem. Soc.* **88,** 380–381 (1966).

117. Kobryn, L., Henry, W. P., Fronczek, F. R., Sygula, R. & Sygula, A. Molecular clips and tweezers with corannulene pincers. *Tetrahedron Lett.* **50,** 7124–7127 (2009).

118. Sygula, A., Fronczek, F. R., Sygula, R., Rabideau, P. W. & Olmstead, M. M. A Double Concave Hydrocarbon Buckycatcher. *J. Am. Chem. Soc.* **129,** 3842–3843 (2007).

119. Lu, R.-Q. *et al.* Corannulene derivatives as non-fullerene acceptors in solution-processed bulk heterojunction solar cells. *J Mater Chem A* **2,** 20515–20519 (2014).

120. Shi, K., Lei, T., Wang, X.-Y., Wang, J.-Y. & Pei, J. A bowl-shaped molecule for organic field-effect transistors: crystal engineering and charge transport switching by oxygen doping. *Chem Sci* **5,** 1041–1045 (2014).

121. Seiders, T. J., Baldridge, K. K., Grube, G. H. & Siegel, J. S. Structure/Energy Correlation of Bowl Depth and Inversion Barrier in Corannulene Derivatives: Combined Experimental and Quantum Mechanical Analysis. *J. Am. Chem. Soc.* **123,** 517–525 (2001).

122. Wu, Y.-T. & Siegel, J. S. Aromatic Molecular-Bowl Hydrocarbons: Synthetic Derivatives, Their Structures, and Physical Properties. *Chem. Rev.* **106,** 4843–4867 (2006).

123. Becke, A. D. Density-functional thermochemistry. III. The role of exact exchange. *J. Chem. Phys.* **98,** 5648 (1993).

124. Lee, C., Yang, W. & Parr, R. G. Development of the Colle-Salvetti correlation-energy formula into a functional of the electron density. *Phys. Rev. B* **37,** 785 (1988).

12 Appendices

Geometries and C-DFT D/A fragments

Set A n=1	
Donor fragment atoms	1-34
Acceptor fragment atoms	35-68

Atom	Atomic number	x	y	z
C	6	-3.672004668	0.725255227	-0.952607294
C	6	-3.672004668	-0.725255227	-0.952607294
C	6	-4.990858522	1.159187658	-1.297124461
C	6	-4.990858522	-1.159187658	-1.297124461
C	6	-5.813438398	0.000000000	-1.517245743
C	6	-2.536572602	1.503135272	-1.154559842
C	6	-2.536572602	-1.503135272	-1.154559842
C	6	-5.266328864	2.408061273	-1.863464286
C	6	-5.266328864	-2.408061273	-1.863464286
C	6	-6.972326441	0.000000000	-2.302919816
C	6	-1.247287494	0.737085673	-1.11537881
C	6	-1.247287494	-0.737085673	-1.11537881
C	6	-4.113114704	3.307767774	-1.906322924
C	6	-4.113114704	-3.307767774	-1.906322924
C	6	-6.582410394	2.480590597	-2.506461455
C	6	-6.582410394	-2.480590597	-2.506461455
C	6	-2.820481287	2.875817568	-1.574792634
C	6	-2.820481287	-2.875817568	-1.574792634
C	6	-7.40504874	1.363277314	-2.720611447
C	6	-7.40504874	-1.363277314	-2.720611447
H	1	-6.920357915	3.447520962	-2.906778064
H	1	-6.920357915	-3.447520962	-2.906778064
C	6	-8.733609194	1.590026996	-3.469882375
C	6	-8.733609194	-1.590026996	-3.469882375
H	1	-4.241147396	4.329842292	-2.292617543
H	1	-4.241147396	-4.329842292	-2.292617543
H	1	-1.987684185	3.579483023	-1.717371226
H	1	-1.987684185	-3.579483023	-1.717371226
H	1	-8.905581998	2.666675465	-3.61548055
H	1	-8.905581998	-2.666675465	-3.61548055
H	1	-8.721889642	1.108629555	-4.461653119
H	1	-8.721889642	-1.108629555	-4.461653119
H	1	-9.584056724	1.176876846	-2.903865924
H	1	-9.584056724	-1.176876846	-2.903865924
C	6	3.672004668	0.725255227	-0.952607294
C	6	3.672004668	-0.725255227	-0.952607294
C	6	4.990858522	1.159187658	-1.297124461
C	6	4.990858522	-1.159187658	-1.297124461

C	6	5.813438398	0.000000000	-1.517245743
C	6	2.536572602	1.503135272	-1.154559842
C	6	2.536572602	-1.503135272	-1.154559842
C	6	5.266328864	2.408061273	-1.863464286
C	6	5.266328864	-2.408061273	-1.863464286
C	6	6.972326441	0.000000000	-2.302919816
C	6	1.247287494	0.737085673	-1.11537881
C	6	1.247287494	-0.737085673	-1.11537881
C	6	4.113114704	3.307767774	-1.906322924
C	6	4.113114704	-3.307767774	-1.906322924
C	6	6.582410394	2.480590597	-2.506461455
C	6	6.582410394	-2.480590597	-2.506461455
C	6	2.820481287	2.875817568	-1.574792634
C	6	2.820481287	-2.875817568	-1.574792634
C	6	7.40504874	1.363277314	-2.720611447
C	6	7.40504874	-1.363277314	-2.720611447
H	1	6.920357915	3.447520962	-2.906778064
H	1	6.920357915	-3.447520962	-2.906778064
C	6	8.733609194	1.590026996	-3.469882375
C	6	8.733609194	-1.590026996	-3.469882375
H	1	4.241147396	4.329842292	-2.292617543
H	1	4.241147396	-4.329842292	-2.292617543
H	1	1.987684185	3.579483023	-1.717371226
H	1	1.987684185	-3.579483023	-1.717371226
H	1	8.905581998	2.666675465	-3.61548055
H	1	8.905581998	-2.666675465	-3.61548055
H	1	8.721889642	1.108629555	-4.461653119
H	1	8.721889642	-1.108629555	-4.461653119
H	1	9.584056724	1.176876846	-2.903865924
H	1	9.584056724	-1.176876846	-2.903865924
C	6	0.000000000	1.405550005	-1.127522171
C	6	0.000000000	-1.405550005	-1.127522171
H	1	0.000000000	2.503446883	-1.129308367
H	1	0.000000000	-2.503446883	-1.129308367

Set A n=2				
Donor fragment atoms	1-34			
Acceptor fragment atoms	35-68			

Atom	Atomic number	x	y	z
C	6	-4.923228661	0.727583488	-0.723185607
C	6	-4.923228661	-0.727583488	-0.723185607
C	6	-6.200483248	1.160012978	-1.200960287
C	6	-6.200483248	-1.160012978	-1.200960287
C	6	-6.994871825	0.000000000	-1.509188775
C	6	-3.775731264	1.507130603	-0.819207713
C	6	-3.775731264	-1.507130603	-0.819207713
C	6	-6.417163436	2.409224735	-1.794452799
C	6	-6.417163436	-2.409224735	-1.794452799
C	6	-8.059191791	0.000000000	-2.419938268
C	6	-2.48484357	0.747825203	-0.682434866
C	6	-2.48484357	-0.747825203	-0.682434866
C	6	-5.269952551	3.311233842	-1.720739142
C	6	-5.269952551	-3.311233842	-1.720739142
C	6	-7.65432578	2.480631238	-2.57733615
C	6	-7.65432578	-2.480631238	-2.57733615
C	6	-4.016258564	2.878550419	-1.264386975
C	6	-4.016258564	-2.878550419	-1.264386975
C	6	-8.44452864	1.362263037	-2.884675389
C	6	-8.44452864	-1.362263037	-2.884675389
H	1	-7.945578372	3.44757365	-3.012761408
H	1	-7.945578372	-3.44757365	-3.012761408
C	6	-9.676448088	1.587707342	-3.7842135
C	6	-9.676448088	-1.587707342	-3.7842135
H	1	-5.360358825	4.332925531	-2.118292665
H	1	-5.360358825	-4.332925531	-2.118292665
H	1	-3.172405813	3.580629892	-1.325590273
H	1	-3.172405813	-3.580629892	-1.325590273
H	1	-9.829405424	2.664085188	-3.951120989
H	1	-9.829405424	-2.664085188	-3.951120989
H	1	-9.548885761	1.104128712	-4.766691503
H	1	-9.548885761	-1.104128712	-4.766691503
H	1	-10.58771649	1.175889256	-3.321156264
H	1	-10.58771649	-1.175889256	-3.321156264
C	6	4.923228661	0.727583488	-0.723185607
C	6	4.923228661	-0.727583488	-0.723185607
C	6	6.200483248	1.160012978	-1.200960287
C	6	6.200483248	-1.160012978	-1.200960287
C	6	6.994871825	0.000000000	-1.509188775
C	6	3.775731264	1.507130603	-0.819207713
C	6	3.775731264	-1.507130603	-0.819207713

C	6	6.417163436	2.409224735	-1.794452799
C	6	6.417163436	-2.409224735	-1.794452799
C	6	8.059191791	0.000000000	-2.419938268
C	6	2.48484357	0.747825203	-0.682434866
C	6	2.48484357	-0.747825203	-0.682434866
C	6	5.269952551	3.311233842	-1.720739142
C	6	5.269952551	-3.311233842	-1.720739142
C	6	7.65432578	2.480631238	-2.57733615
C	6	7.65432578	-2.480631238	-2.57733615
C	6	4.016258564	2.878550419	-1.264386975
C	6	4.016258564	-2.878550419	-1.264386975
C	6	8.44452864	1.362263037	-2.884675389
C	6	8.44452864	-1.362263037	-2.884675389
H	1	7.945578372	3.44757365	-3.012761408
H	1	7.945578372	-3.44757365	-3.012761408
C	6	9.676448088	1.587707342	-3.7842135
C	6	9.676448088	-1.587707342	-3.7842135
H	1	5.360358825	4.332925531	-2.118292665
H	1	5.360358825	-4.332925531	-2.118292665
H	1	3.172405813	3.580629892	-1.325590273
H	1	3.172405813	-3.580629892	-1.325590273
H	1	9.829405424	2.664085188	-3.951120989
H	1	9.829405424	-2.664085188	-3.951120989
H	1	9.548885761	1.104128712	-4.766691503
H	1	9.548885761	-1.104128712	-4.766691503
H	1	10.58771649	1.175889256	-3.321156264
H	1	10.58771649	-1.175889256	-3.321156264
C	6	-1.256034966	1.416232904	-0.637291086
C	6	1.256034966	1.416232904	-0.637291086
C	6	-1.256034966	-1.416232904	-0.637291086
C	6	1.256034966	-1.416232904	-0.637291086
H	1	-1.24228074	2.514543245	-0.640858237
H	1	1.24228074	2.514543245	-0.640858237
H	1	-1.24228074	-2.514543245	-0.640858237
H	1	1.24228074	-2.514543245	-0.640858237
C	6	0.000000000	0.724309485	-0.615103252
C	6	0.000000000	-0.724309485	-0.615103252

Set A n=3

Donor fragment atoms	1-34
Acceptor fragment atoms	35-68

Atom	Atomic number	x	y	z
C	6	-6.111193204	0.728832863	-0.562210633
C	6	-6.111193204	-0.728832863	-0.562210633

C	6	-7.289114946	1.16058587	-1.250657628
C	6	-7.289114946	-1.16058587	-1.250657628
C	6	-8.017593648	0.000000000	-1.691217738
C	6	-4.964530794	1.509922846	-0.467868673
C	6	-4.964530794	-1.509922846	-0.467868673
C	6	-7.40174841	2.409610335	-1.874200192
C	6	-7.40174841	-2.409610335	-1.874200192
C	6	-8.904258054	0.000000000	-2.776751482
C	6	-3.705424802	0.752042182	-0.142705241
C	6	-3.705424802	-0.752042182	-0.142705241
C	6	-6.286536515	3.31363497	-1.606548247
C	6	-6.286536515	-3.31363497	-1.606548247
C	6	-8.480635088	2.480158111	-2.86325409
C	6	-8.480635088	-2.480158111	-2.86325409
C	6	-5.127498804	2.881019299	-0.946214693
C	6	-5.127498804	-2.881019299	-0.946214693
C	6	-9.201675937	1.360711779	-3.304921189
C	6	-9.201675937	-1.360711779	-3.304921189
H	1	-8.689381396	3.446163513	-3.345518815
H	1	-8.689381396	-3.446163513	-3.345518815
C	6	-10.24821566	1.582924261	-4.41553557
C	6	-10.24821566	-1.582924261	-4.41553557
H	1	-6.309344384	4.335064374	-2.014212247
H	1	-6.309344384	-4.335064374	-2.014212247
H	1	-4.28476287	3.582507262	-0.866280906
H	1	-4.28476287	-3.582507262	-0.866280906
H	1	-10.38186804	2.659511427	-4.597331122
H	1	-10.38186804	-2.659511427	-4.597331122
H	1	-9.932053497	1.113831256	-5.36197526
H	1	-9.932053497	-1.113831256	-5.36197526
H	1	-11.22415049	1.155078185	-4.135967696
H	1	-11.22415049	-1.155078185	-4.135967696
C	6	6.111193204	0.728832863	-0.562210633
C	6	6.111193204	-0.728832863	-0.562210633
C	6	7.289114946	1.16058587	-1.250657628
C	6	7.289114946	-1.16058587	-1.250657628
C	6	8.017593648	0.000000000	-1.691217738
C	6	4.964530794	1.509922846	-0.467868673
C	6	4.964530794	-1.509922846	-0.467868673
C	6	7.40174841	2.409610335	-1.874200192
C	6	7.40174841	-2.409610335	-1.874200192
C	6	8.904258054	0.000000000	-2.776751482
C	6	3.705424802	0.752042182	-0.142705241
C	6	3.705424802	-0.752042182	-0.142705241
C	6	6.286536515	3.31363497	-1.606548247
C	6	6.286536515	-3.31363497	-1.606548247

C	6	8.480635088	2.480158111	-2.86325409
C	6	8.480635088	-2.480158111	-2.86325409
C	6	5.127498804	2.881019299	-0.946214693
C	6	5.127498804	-2.881019299	-0.946214693
C	6	9.201675937	1.360711779	-3.304921189
C	6	9.201675937	-1.360711779	-3.304921189
H	1	8.689381396	3.446163513	-3.345518815
H	1	8.689381396	-3.446163513	-3.345518815
C	6	10.24821566	1.582924261	-4.41553557
C	6	10.24821566	-1.582924261	-4.41553557
H	1	6.309344384	4.335064374	-2.014212247
H	1	6.309344384	-4.335064374	-2.014212247
H	1	4.28476287	3.582507262	-0.866280906
H	1	4.28476287	-3.582507262	-0.866280906
H	1	10.38186804	2.659511427	-4.597331122
H	1	10.38186804	-2.659511427	-4.597331122
H	1	9.932053497	1.113831256	-5.36197526
H	1	9.932053497	-1.113831256	-5.36197526
H	1	11.22415049	1.155078185	-4.135967696
H	1	11.22415049	-1.155078185	-4.135967696
C	6	-2.497409582	1.418828203	0.048779081
C	6	2.497409582	1.418828203	0.048779081
C	6	-2.497409582	-1.418828203	0.048779081
C	6	2.497409582	-1.418828203	0.048779081
H	1	-2.482540249	2.517093714	0.044204928
H	1	2.482540249	2.517093714	0.044204928
H	1	-2.482540249	-2.517093714	0.044204928
H	1	2.482540249	-2.517093714	0.044204928
C	6	-1.236119542	0.730543988	0.181930235
C	6	1.236119542	0.730543988	0.181930235
C	6	-1.236119542	-0.730543988	0.181930235
C	6	1.236119542	-0.730543988	0.181930235
C	6	0.000000000	1.424479747	0.221412672
C	6	0.000000000	-1.424479747	0.221412672
H	1	0.000000000	2.523415615	0.212592465
H	1	0.000000000	-2.523415615	0.212592465

Set A n=4

Donor fragment atoms	1-34
Acceptor fragment atoms	35-68

Atom	Atomic number	x	y	z
C	6	-7.339227181	0.729193555	-0.603190138
C	6	-7.339227181	-0.729193555	-0.603190138
C	6	-8.522906743	1.160427133	-1.280237588

C	6	-8.522906743	-1.160427133	-1.280237588
C	6	-9.256636852	0.000000000	-1.711871494
C	6	-6.193072957	1.511027312	-0.515193848
C	6	-6.193072957	-1.511027312	-0.515193848
C	6	-8.64332405	2.410081723	-1.901219742
C	6	-8.64332405	-2.410081723	-1.901219742
C	6	-10.15906099	0.000000000	-2.783629342
C	6	-4.934391767	0.754570636	-0.180157149
C	6	-4.934391767	-0.754570636	-0.180157149
C	6	-7.524995843	3.31318937	-1.645332889
C	6	-7.524995843	-3.31318937	-1.645332889
C	6	-9.736607	2.480665944	-2.874853316
C	6	-9.736607	-2.480665944	-2.874853316
C	6	-6.359785673	2.880886887	-0.994251993
C	6	-6.359785673	-2.880886887	-0.994251993
C	6	-10.46465713	1.361439178	-3.305885131
C	6	-10.46465713	-1.361439178	-3.305885131
H	1	-9.953466658	3.446959971	-3.35298799
H	1	-9.953466658	-3.446959971	-3.35298799
C	6	-11.5295893	1.58403338	-4.398750478
C	6	-11.5295893	-1.58403338	-4.398750478
H	1	-7.550921984	4.334361072	-2.05341637
H	1	-7.550921984	-4.334361072	-2.05341637
H	1	-5.516480825	3.582573759	-0.92205464
H	1	-5.516480825	-3.582573759	-0.92205464
H	1	-11.66835278	2.660699628	-4.576166483
H	1	-11.66835278	-2.660699628	-4.576166483
H	1	-11.22774655	1.117338851	-5.35109071
H	1	-11.22774655	-1.117338851	-5.35109071
H	1	-12.49996611	1.153664092	-4.104310952
H	1	-12.49996611	-1.153664092	-4.104310952
C	6	7.339227181	0.729193555	-0.603190138
C	6	7.339227181	-0.729193555	-0.603190138
C	6	8.522906743	1.160427133	-1.280237588
C	6	8.522906743	-1.160427133	-1.280237588
C	6	9.256636852	0.000000000	-1.711871494
C	6	6.193072957	1.511027312	-0.515193848
C	6	6.193072957	-1.511027312	-0.515193848
C	6	8.64332405	2.410081723	-1.901219742
C	6	8.64332405	-2.410081723	-1.901219742
C	6	10.15906099	0.000000000	-2.783629342
C	6	4.934391767	0.754570636	-0.180157149
C	6	4.934391767	-0.754570636	-0.180157149
C	6	7.524995843	3.31318937	-1.645332889
C	6	7.524995843	-3.31318937	-1.645332889
C	6	9.736607	2.480665944	-2.874853316

C	6	9.736607	-2.480665944	-2.874853316
C	6	6.359785673	2.880886887	-0.994251993
C	6	6.359785673	-2.880886887	-0.994251993
C	6	10.46465713	1.361439178	-3.305885131
C	6	10.46465713	-1.361439178	-3.305885131
H	1	9.953466658	3.446959971	-3.35298799
H	1	9.953466658	-3.446959971	-3.35298799
C	6	11.5295893	1.58403338	-4.398750478
C	6	11.5295893	-1.58403338	-4.398750478
H	1	7.550921984	4.334361072	-2.05341637
H	1	7.550921984	-4.334361072	-2.05341637
H	1	5.516480825	3.582573759	-0.92205464
H	1	5.516480825	-3.582573759	-0.92205464
H	1	11.66835278	2.660699628	-4.576166483
H	1	11.66835278	-2.660699628	-4.576166483
H	1	11.22774655	1.117338851	-5.35109071
H	1	11.22774655	-1.117338851	-5.35109071
H	1	12.49996611	1.153664092	-4.104310952
H	1	12.49996611	-1.153664092	-4.104310952
C	6	-3.734652124	1.420779738	0.039648626
C	6	3.734652124	1.420779738	0.039648626
C	6	-3.734652124	-1.420779738	0.039648626
C	6	3.734652124	-1.420779738	0.039648626
H	1	-3.719990631	2.519144636	0.037664122
H	1	3.719990631	2.519144636	0.037664122
H	1	-3.719990631	-2.519144636	0.037664122
H	1	3.719990631	-2.519144636	0.037664122
C	6	-2.47330146	0.733191123	0.218038578
C	6	2.47330146	0.733191123	0.218038578
C	6	-2.47330146	-0.733191123	0.218038578
C	6	2.47330146	-0.733191123	0.218038578
C	6	-1.249427117	1.426181111	0.320511258
C	6	1.249427117	1.426181111	0.320511258
C	6	-1.249427117	-1.426181111	0.320511258
C	6	1.249427117	-1.426181111	0.320511258
H	1	-1.249317993	2.525129121	0.314198239
H	1	1.249317993	2.525129121	0.314198239
H	1	-1.249317993	-2.525129121	0.314198239
H	1	1.249317993	-2.525129121	0.314198239
C	6	0.000000000	0.735308178	0.357446136
C	6	0.000000000	-0.735308178	0.357446136

Set B n=1

Donor fragment atoms	1-32
Acceptor fragment atoms	33-64

Atom	Atomic number	x	y	z
C	6	-3.680463984	-0.732679912	-0.398517156
C	6	-3.680463984	0.732679912	-0.398517156
C	6	-4.996725251	-1.177096866	-0.774767714
C	6	-4.996725251	1.177096866	-0.774767714
C	6	-5.800707109	0.000000000	-0.958558255
C	6	-2.537853096	-1.491509417	-0.653330862
C	6	-2.537853096	1.491509417	-0.653330862
C	6	-5.236307575	-2.360778529	-1.509416184
C	6	-5.236307575	2.360778529	-1.509416184
C	6	-6.815292337	0.000000000	-1.89485843
C	6	-1.245772027	-0.734834135	-0.607845305
C	6	-1.245772027	0.734834135	-0.607845305
C	6	-4.07264498	-3.245818501	-1.579801884
C	6	-4.07264498	3.245818501	-1.579801884
C	6	-6.436325845	-2.381896387	-2.377027168
C	6	-6.436325845	2.381896387	-2.377027168
C	6	-2.79899364	-2.834959092	-1.167008407
C	6	-2.79899364	2.834959092	-1.167008407
C	6	-7.18521859	-1.218912199	-2.577840562
C	6	-7.18521859	1.218912199	-2.577840562
H	1	-6.625595789	-3.278994081	-2.985186488
H	1	-6.625595789	3.278994081	-2.985186488
C	6	-8.22252482	-0.800818132	-3.658941686
C	6	-8.22252482	0.800818132	-3.658941686
H	1	-4.173563535	-4.225914714	-2.069207103
H	1	-4.173563535	4.225914714	-2.069207103
H	1	-1.953548045	-3.514838248	-1.34525701
H	1	-1.953548045	3.514838248	-1.34525701
H	1	-9.230781194	-1.185083878	-3.416767149
H	1	-9.230781194	1.185083878	-3.416767149
H	1	-7.948606233	-1.193485545	-4.654331555
H	1	-7.948606233	1.193485545	-4.654331555
C	6	3.680463984	-0.732679912	-0.398517156
C	6	3.680463984	0.732679912	-0.398517156
C	6	4.996725251	-1.177096866	-0.774767714
C	6	4.996725251	1.177096866	-0.774767714
C	6	5.800707109	0.000000000	-0.958558255
C	6	2.537853096	-1.491509417	-0.653330862
C	6	2.537853096	1.491509417	-0.653330862
C	6	5.236307575	-2.360778529	-1.509416184
C	6	5.236307575	2.360778529	-1.509416184

C	6	6.815292337	0.000000000	-1.89485843
C	6	1.245772027	-0.734834135	-0.607845305
C	6	1.245772027	0.734834135	-0.607845305
C	6	4.07264498	-3.245818501	-1.579801884
C	6	4.07264498	3.245818501	-1.579801884
C	6	6.436325845	-2.381896387	-2.377027168
C	6	6.436325845	2.381896387	-2.377027168
C	6	2.79899364	-2.834959092	-1.167008407
C	6	2.79899364	2.834959092	-1.167008407
C	6	7.18521859	-1.218912199	-2.577840562
C	6	7.18521859	1.218912199	-2.577840562
H	1	6.625595789	-3.278994081	-2.985186488
H	1	6.625595789	3.278994081	-2.985186488
C	6	8.22252482	-0.800818132	-3.658941686
C	6	8.22252482	0.800818132	-3.658941686
H	1	4.173563535	-4.225914714	-2.069207103
H	1	4.173563535	4.225914714	-2.069207103
H	1	1.953548045	-3.514838248	-1.34525701
H	1	1.953548045	3.514838248	-1.34525701
H	1	9.230781194	-1.185083878	-3.416767149
H	1	9.230781194	1.185083878	-3.416767149
H	1	7.948606233	-1.193485545	-4.654331555
H	1	7.948606233	1.193485545	-4.654331555
C	6	0.000000000	-1.405807914	-0.622913266
C	6	0.000000000	1.405807914	-0.622913266
H	1	0.000000000	-2.503575972	-0.624077587
H	1	0.000000000	2.503575972	-0.624077587

Set B n=2

Donor fragment atoms 1-32

Acceptor fragment atoms 33-64

Atom	Atomic number	x	y	z
C	6	-4.921312893	-0.734807293	-0.369064663
C	6	-4.921312893	0.734807293	-0.369064663
C	6	-6.242887809	-1.177433976	-0.723647651
C	6	-6.242887809	1.177433976	-0.723647651
C	6	-7.049673430	0.000000000	-0.892621564
C	6	-3.785791167	-1.495379490	-0.642821146
C	6	-3.785791167	1.495379490	-0.642821146
C	6	-6.497871026	-2.361990310	-1.453175714
C	6	-6.497871026	2.361990310	-1.453175714
C	6	-8.082814994	0.000000000	-1.808220993
C	6	-2.484207588	-0.745660122	-0.604333909
C	6	-2.484207588	0.745660122	-0.604333909

C	6	-5.337207370	-3.246025432	-1.547442949
C	6	-5.337207370	3.246025432	-1.547442949
C	6	-7.715300486	-2.382394965	-2.296767129
C	6	-7.715300486	2.382394965	-2.296767129
C	6	-4.055415068	-2.835122718	-1.156685637
C	6	-4.055415068	2.835122718	-1.156685637
C	6	-8.467050816	-1.219199291	-2.483104304
C	6	-8.467050816	1.219199291	-2.483104304
H	1	-7.917319045	-3.279832887	-2.900310885
H	1	-7.917319045	3.279832887	-2.900310885
C	6	-9.525191077	-0.800852298	-3.543862507
C	6	-9.525191077	0.800852298	-3.543862507
H	1	-5.446020275	-4.224446452	-2.038478129
H	1	-5.446020275	4.224446452	-2.038478129
H	1	-3.212565354	-3.513084745	-1.353802064
H	1	-3.212565354	3.513084745	-1.353802064
H	1	-10.528618048	-1.185502336	-3.283058112
H	1	-10.528618048	1.185502336	-3.283058112
H	1	-9.269902808	-1.193061516	-4.544390069
H	1	-9.269902808	1.193061516	-4.544390069
C	6	4.921312893	-0.734807293	-0.369064663
C	6	4.921312893	0.734807293	-0.369064663
C	6	6.242887809	-1.177433976	-0.723647651
C	6	6.242887809	1.177433976	-0.723647651
C	6	7.049673430	0.000000000	-0.892621564
C	6	3.785791167	-1.495379490	-0.642821146
C	6	3.785791167	1.495379490	-0.642821146
C	6	6.497871026	-2.361990310	-1.453175714
C	6	6.497871026	2.361990310	-1.453175714
C	6	8.082814994	0.000000000	-1.808220993
C	6	2.484207588	-0.745660122	-0.604333909
C	6	2.484207588	0.745660122	-0.604333909
C	6	5.337207370	-3.246025432	-1.547442949
C	6	5.337207370	3.246025432	-1.547442949
C	6	7.715300486	-2.382394965	-2.296767129
C	6	7.715300486	2.382394965	-2.296767129
C	6	4.055415068	-2.835122718	-1.156685637
C	6	4.055415068	2.835122718	-1.156685637
C	6	8.467050816	-1.219199291	-2.483104304
C	6	8.467050816	1.219199291	-2.483104304
H	1	7.917319045	-3.279832887	-2.900310885
H	1	7.917319045	3.279832887	-2.900310885
C	6	9.525191077	-0.800852298	-3.543862507
C	6	9.525191077	0.800852298	-3.543862507
H	1	5.446020275	-4.224446452	-2.038478129
H	1	5.446020275	4.224446452	-2.038478129

H	1	3.212565354	-3.513084745	-1.353802064
H	1	3.212565354	3.513084745	-1.353802064
H	1	10.528618048	-1.185502336	-3.283058112
H	1	10.528618048	1.185502336	-3.283058112
H	1	9.269902808	-1.193061516	-4.544390069
H	1	9.269902808	1.193061516	-4.544390069
C	6	-1.256541550	-1.416727395	-0.616116074
C	6	1.256541550	-1.416727395	-0.616116074
C	6	-1.256541550	1.416727395	-0.616116074
C	6	1.256541550	1.416727395	-0.616116074
H	1	-1.243918429	-2.515148771	-0.614143843
H	1	1.243918429	-2.515148771	-0.614143843
H	1	-1.243918429	2.515148771	-0.614143843
H	1	1.243918429	2.515148771	-0.614143843
C	6	0.000000000	-0.724555115	-0.616959824
C	6	0.000000000	0.724555115	-0.616959824

Set B n=3

Donor fragment atoms	1-32
Acceptor fragment atoms	33-64

Atom	Atomic number	x	y	z
C	6	-6.162870951	-0.736053288	-0.221864737
C	6	-6.162870951	0.736053288	-0.221864737
C	6	-7.388969915	-1.177831627	-0.831813768
C	6	-7.388969915	1.177831627	-0.831813768
C	6	-8.143765227	0.000000000	-1.163381290
C	6	-4.996809077	-1.498380184	-0.274310253
C	6	-4.996809077	1.498380184	-0.274310253
C	6	-7.495178637	-2.363798747	-1.595945344
C	6	-7.495178637	2.363798747	-1.595945344
C	6	-8.966019756	0.000000000	-2.273309503
C	6	-3.716318419	-0.749744867	-0.029094756
C	6	-3.716318419	0.749744867	-0.029094756
C	6	-6.344112257	-3.252656287	-1.454713184
C	6	-6.344112257	3.252656287	-1.454713184
C	6	-8.511822644	-2.383688808	-2.672084126
C	6	-8.511822644	2.383688808	-2.672084126
C	6	-5.163402497	-2.840566887	-0.823857569
C	6	-5.163402497	2.840566887	-0.823857569
C	6	-9.204591756	-1.219084423	-3.012806437
C	6	-9.204591756	1.219084423	-3.012806437
H	1	-8.585033122	-3.282131839	-3.302849920
H	1	-8.585033122	3.282131839	-3.302849920
C	6	-10.015226407	-0.800442012	-4.272506476

C	6	-10.015226407	0.800442012	-4.272506476
H	1	-6.359141151	-4.233174222	-1.953188378
H	1	-6.359141151	4.233174222	-1.953188378
H	1	-4.298698064	-3.518797873	-0.848701860
H	1	-4.298698064	3.518797873	-0.848701860
H	1	-11.050374739	-1.187524717	-4.231418817
H	1	-11.050374739	1.187524717	-4.231418817
H	1	-9.552790990	-1.192425833	-5.196114551
H	1	-9.552790990	1.192425833	-5.196114551
C	6	6.162870951	-0.736053288	-0.221864737
C	6	6.162870951	0.736053288	-0.221864737
C	6	7.388969915	-1.177831627	-0.831813768
C	6	7.388969915	1.177831627	-0.831813768
C	6	8.143765227	0.000000000	-1.163381290
C	6	4.996809077	-1.498380184	-0.274310253
C	6	4.996809077	1.498380184	-0.274310253
C	6	7.495178637	-2.363798747	-1.595945344
C	6	7.495178637	2.363798747	-1.595945344
C	6	8.966019756	0.000000000	-2.273309503
C	6	3.716318419	-0.749744867	-0.029094756
C	6	3.716318419	0.749744867	-0.029094756
C	6	6.344112257	-3.252656287	-1.454713184
C	6	6.344112257	3.252656287	-1.454713184
C	6	8.511822644	-2.383688808	-2.672084126
C	6	8.511822644	2.383688808	-2.672084126
C	6	5.163402497	-2.840566887	-0.823857569
C	6	5.163402497	2.840566887	-0.823857569
C	6	9.204591756	-1.219084423	-3.012806437
C	6	9.204591756	1.219084423	-3.012806437
H	1	8.585033122	-3.282131839	-3.302849920
H	1	8.585033122	3.282131839	-3.302849920
C	6	10.015226407	-0.800442012	-4.272506476
C	6	10.015226407	0.800442012	-4.272506476
H	1	6.359141151	-4.233174222	-1.953188378
H	1	6.359141151	4.233174222	-1.953188378
H	1	4.298698064	-3.518797873	-0.848701860
H	1	4.298698064	3.518797873	-0.848701860
H	1	11.050374739	-1.187524717	-4.231418817
H	1	11.050374739	1.187524717	-4.231418817
H	1	9.552790990	-1.192425833	-5.196114551
H	1	9.552790990	1.192425833	-5.196114551
C	6	-2.501624082	-1.418968933	0.101352880
C	6	2.501624082	-1.418968933	0.101352880
C	6	-2.501624082	1.418968933	0.101352880
C	6	2.501624082	1.418968933	0.101352880
H	1	-2.487911476	-2.517241780	0.098819874

H	1	2.487911476	-2.517241780	0.098819874
H	1	-2.487911476	2.517241780	0.098819874
H	1	2.487911476	2.517241780	0.098819874
C	6	-1.236684686	-0.730724865	0.195531048
C	6	1.236684686	-0.730724865	0.195531048
C	6	-1.236684686	0.730724865	0.195531048
C	6	1.236684686	0.730724865	0.195531048
C	6	0.000000000	-1.424343962	0.224039924
C	6	0.000000000	1.424343962	0.224039924
H	1	0.000000000	-2.523276184	0.218663100
H	1	0.000000000	2.523276184	0.218663100

Set B n=4

Donor fragment atoms 1-32

Acceptor fragment atoms 33-64

Atom	Atomic number	x	y	z
C	6	-7.399104689	-0.736522815	-0.247103209
C	6	-7.399104689	0.736522815	-0.247103209
C	6	-8.628841495	-1.177831628	-0.848408580
C	6	-8.628841495	1.177831628	-0.848408580
C	6	-9.386416925	0.000000000	-1.173301371
C	6	-6.233915392	-1.499150313	-0.306077630
C	6	-6.233915392	1.499150313	-0.306077630
C	6	-8.741344717	-2.363820569	-1.611928862
C	6	-8.741344717	2.363820569	-1.611928862
C	6	-10.218886371	0.000000000	-2.275050919
C	6	-4.952673033	-0.752114627	-0.054402834
C	6	-4.952673033	0.752114627	-0.054402834
C	6	-7.588669289	-3.251547738	-1.480848223
C	6	-7.588669289	3.251547738	-1.480848223
C	6	-9.768979409	-2.383813147	-2.678013513
C	6	-9.768979409	2.383813147	-2.678013513
C	6	-6.403355719	-2.839706510	-0.857295314
C	6	-6.403355719	2.839706510	-0.857295314
C	6	-10.465443811	-1.219311870	-3.011567871
C	6	-10.465443811	1.219311870	-3.011567871
H	1	-9.849307919	-3.282544576	-3.307488023
H	1	-9.849307919	3.282544576	-3.307488023
C	6	-11.291371381	-0.800530609	-4.261271613
C	6	-11.291371381	0.800530609	-4.261271613
H	1	-7.606124228	-4.231130168	-1.981037356
H	1	-7.606124228	4.231130168	-1.981037356
H	1	-5.538298804	-3.517207597	-0.889700413
H	1	-5.538298804	3.517207597	-0.889700413

H	1	-12.326088207	-1.187259354	-4.207190898
H	1	-12.326088207	1.187259354	-4.207190898
H	1	-10.840940094	-1.192722276	-5.190634012
H	1	-10.840940094	1.192722276	-5.190634012
C	6	7.399104689	-0.736522815	-0.247103209
C	6	7.399104689	0.736522815	-0.247103209
C	6	8.628841495	-1.177831628	-0.848408580
C	6	8.628841495	1.177831628	-0.848408580
C	6	9.386416925	0.000000000	-1.173301371
C	6	6.233915392	-1.499150313	-0.306077630
C	6	6.233915392	1.499150313	-0.306077630
C	6	8.741344717	-2.363820569	-1.611928862
C	6	8.741344717	2.363820569	-1.611928862
C	6	10.218886371	0.000000000	-2.275050919
C	6	4.952673033	-0.752114627	-0.054402834
C	6	4.952673033	0.752114627	-0.054402834
C	6	7.588669289	-3.251547738	-1.480848223
C	6	7.588669289	3.251547738	-1.480848223
C	6	9.768979409	-2.383813147	-2.678013513
C	6	9.768979409	2.383813147	-2.678013513
C	6	6.403355719	-2.839706510	-0.857295314
C	6	6.403355719	2.839706510	-0.857295314
C	6	10.465443811	-1.219311870	-3.011567871
C	6	10.465443811	1.219311870	-3.011567871
H	1	9.849307919	-3.282544576	-3.307488023
H	1	9.849307919	3.282544576	-3.307488023
C	6	11.291371381	-0.800530609	-4.261271613
C	6	11.291371381	0.800530609	-4.261271613
H	1	7.606124228	-4.231130168	-1.981037356
H	1	7.606124228	4.231130168	-1.981037356
H	1	5.538298804	-3.517207597	-0.889700413
H	1	5.538298804	3.517207597	-0.889700413
H	1	12.326088207	-1.187259354	-4.207190898
H	1	12.326088207	1.187259354	-4.207190898
H	1	10.840940094	-1.192722276	-5.190634012
H	1	10.840940094	1.192722276	-5.190634012
C	6	-3.743732518	-1.420919985	0.095548828
C	6	3.743732518	-1.420919985	0.095548828
C	6	-3.743732518	1.420919985	0.095548828
C	6	3.743732518	1.420919985	0.095548828
H	1	-3.730142248	-2.519247320	0.094806121
H	1	3.730142248	-2.519247320	0.094806121
H	1	-3.730142248	2.519247320	0.094806121
H	1	3.730142248	2.519247320	0.094806121
C	6	-2.476030088	-0.733351111	0.221094618
C	6	2.476030088	-0.733351111	0.221094618

C	6	-2.476030088	0.733351111	0.221094618
C	6	2.476030088	0.733351111	0.221094618
C	6	-1.249792424	-1.426100317	0.293394517
C	6	1.249792424	-1.426100317	0.293394517
C	6	-1.249792424	1.426100317	0.293394517
C	6	1.249792424	1.426100317	0.293394517
H	1	-1.249821620	-2.525049446	0.289269545
H	1	1.249821620	-2.525049446	0.289269545
H	1	-1.249821620	2.525049446	0.289269545
H	1	1.249821620	2.525049446	0.289269545
C	6	0.000000000	-0.735377363	0.319181731
C	6	0.000000000	0.735377363	0.319181731

Set C n=1

Donor fragment atoms 1-28

Acceptor fragment atoms 29-56

Atom	Atomic number	x	y	z
C	6	-3.673090019	0.726531409	-0.946324533
C	6	-3.673090019	-0.726531409	-0.946324533
C	6	-4.992893810	1.164440483	-1.281140012
C	6	-4.992893810	-1.164440483	-1.281140012
C	6	-5.811491475	0.000000000	-1.489487299
C	6	-2.536385684	1.501518547	-1.155152726
C	6	-2.536385684	-1.501518547	-1.155152726
C	6	-5.269306473	2.411301315	-1.863436937
C	6	-5.269306473	-2.411301315	-1.863436937
C	6	-6.968034166	0.000000000	-2.270842179
C	6	-1.247227681	0.737066710	-1.119936950
C	6	-1.247227681	-0.737066710	-1.119936950
C	6	-4.111360148	3.307885062	-1.909581269
C	6	-4.111360148	-3.307885062	-1.909581269
C	6	-6.571978134	2.497140181	-2.521432180
C	6	-6.571978134	-2.497140181	-2.521432180
C	6	-2.820314275	2.873755312	-1.578228449
C	6	-2.820314275	-2.873755312	-1.578228449
C	6	-7.383447389	1.355876786	-2.718425263
C	6	-7.383447389	-1.355876786	-2.718425263
H	1	-6.911305631	3.443800662	-2.964765367
H	1	-6.911305631	-3.443800662	-2.964765367
F	9	-8.553681894	1.484454512	-3.419928321
F	9	-8.553681894	-1.484454512	-3.419928321
H	1	-4.237859976	4.328551096	-2.299654805
H	1	-4.237859976	-4.328551096	-2.299654805

H	1	-1.986996141	3.576217380	-1.724639957
H	1	-1.986996141	-3.576217380	-1.724639957
C	6	3.673090019	0.726531409	-0.946324533
C	6	3.673090019	-0.726531409	-0.946324533
C	6	4.992893810	1.164440483	-1.281140012
C	6	4.992893810	-1.164440483	-1.281140012
C	6	5.811491475	0.000000000	-1.489487299
C	6	2.536385684	1.501518547	-1.155152726
C	6	2.536385684	-1.501518547	-1.155152726
C	6	5.269306473	2.411301315	-1.863436937
C	6	5.269306473	-2.411301315	-1.863436937
C	6	6.968034166	0.000000000	-2.270842179
C	6	1.247227681	0.737066710	-1.119936950
C	6	1.247227681	-0.737066710	-1.119936950
C	6	4.111360148	3.307885062	-1.909581269
C	6	4.111360148	-3.307885062	-1.909581269
C	6	6.571978134	2.497140181	-2.521432180
C	6	6.571978134	-2.497140181	-2.521432180
C	6	2.820314275	2.873755312	-1.578228449
C	6	2.820314275	-2.873755312	-1.578228449
C	6	7.383447389	1.355876786	-2.718425263
C	6	7.383447389	-1.355876786	-2.718425263
H	1	6.911305631	3.443800662	-2.964765367
H	1	6.911305631	-3.443800662	-2.964765367
F	9	8.553681894	1.484454512	-3.419928321
F	9	8.553681894	-1.484454512	-3.419928321
H	1	4.237859976	4.328551096	-2.299654805
H	1	4.237859976	-4.328551096	-2.299654805
H	1	1.986996141	3.576217380	-1.724639957
H	1	1.986996141	-3.576217380	-1.724639957
C	6	0.000000000	1.405702046	-1.133286710
C	6	0.000000000	-1.405702046	-1.133286710
H	1	0.000000000	2.503569014	-1.134031092
H	1	0.000000000	-2.503569014	-1.134031092

Set C n=2

Donor fragment atoms 1-28

Acceptor fragment atoms 29-56

Atom	Atomic number	x	y	z
C	6	-4.924877909	0.728884603	-0.720907628
C	6	-4.924877909	-0.728884603	-0.720907628
C	6	-6.204950780	1.165520042	-1.186508132
C	6	-6.204950780	-1.165520042	-1.186508132
C	6	-6.997376456	0.000000000	-1.479283051

C	6	-3.775675289	1.505515147	-0.825063501
C	6	-3.775675289	-1.505515147	-0.825063501
C	6	-6.422307271	2.412144110	-1.796709057
C	6	-6.422307271	-2.412144110	-1.796709057
C	6	-8.064000025	0.000000000	-2.379569210
C	6	-2.484729104	0.747664234	-0.691701924
C	6	-2.484729104	-0.747664234	-0.691701924
C	6	-5.269250876	3.310344867	-1.729766136
C	6	-5.269250876	-3.310344867	-1.729766136
C	6	-7.648545782	2.496557054	-2.587573160
C	6	-7.648545782	-2.496557054	-2.587573160
C	6	-4.016524717	2.875812408	-1.274728728
C	6	-4.016524717	-2.875812408	-1.274728728
C	6	-8.431732543	1.354381880	-2.870357754
C	6	-8.431732543	-1.354381880	-2.870357754
H	1	-7.938251483	3.442814855	-3.065479399
H	1	-7.938251483	-3.442814855	-3.065479399
F	9	-9.519165211	1.478384485	-3.695104986
F	9	-9.519165211	-1.478384485	-3.695104986
H	1	-5.357806594	4.329832381	-2.132906416
H	1	-5.357806594	-4.329832381	-2.132906416
H	1	-3.171496786	3.576138673	-1.341865234
H	1	-3.171496786	-3.576138673	-1.341865234
C	6	4.924877909	0.728884603	-0.720907628
C	6	4.924877909	-0.728884603	-0.720907628
C	6	6.204950780	1.165520042	-1.186508132
C	6	6.204950780	-1.165520042	-1.186508132
C	6	6.997376456	0.000000000	-1.479283051
C	6	3.775675289	1.505515147	-0.825063501
C	6	3.775675289	-1.505515147	-0.825063501
C	6	6.422307271	2.412144110	-1.796709057
C	6	6.422307271	-2.412144110	-1.796709057
C	6	8.064000025	0.000000000	-2.379569210
C	6	2.484729104	0.747664234	-0.691701924
C	6	2.484729104	-0.747664234	-0.691701924
C	6	5.269250876	3.310344867	-1.729766136
C	6	5.269250876	-3.310344867	-1.729766136
C	6	7.648545782	2.496557054	-2.587573160
C	6	7.648545782	-2.496557054	-2.587573160
C	6	4.016524717	2.875812408	-1.274728728
C	6	4.016524717	-2.875812408	-1.274728728
C	6	8.431732543	1.354381880	-2.870357754
C	6	8.431732543	-1.354381880	-2.870357754
H	1	7.938251483	3.442814855	-3.065479399
H	1	7.938251483	-3.442814855	-3.065479399
F	9	9.519165211	1.478384485	-3.695104986

F	9	9.519165211	-1.478384485	-3.695104986
H	1	5.357806594	4.329832381	-2.132906416
H	1	5.357806594	-4.329832381	-2.132906416
H	1	3.171496786	3.576138673	-1.341865234
H	1	3.171496786	-3.576138673	-1.341865234
C	6	-1.255930449	1.416409733	-0.647458829
C	6	1.255930449	1.416409733	-0.647458829
C	6	-1.255930449	-1.416409733	-0.647458829
C	6	1.255930449	-1.416409733	-0.647458829
H	1	-1.242253666	2.514745271	-0.649970756
H	1	1.242253666	2.514745271	-0.649970756
H	1	-1.242253666	-2.514745271	-0.649970756
H	1	1.242253666	-2.514745271	-0.649970756
C	6	0.000000000	0.724460248	-0.625946948
C	6	0.000000000	-0.724460248	-0.625946948

Set C n=3

Donor fragment atoms	1-28
Acceptor fragment atoms	29-56

Atom	Atomic number	x	y	z
C	6	-6.156134052	0.729460091	-0.603140102
C	6	-6.156134052	-0.729460091	-0.603140102
C	6	-7.484199603	1.164868079	-0.898236799
C	6	-7.484199603	-1.164868079	-0.898236799
C	6	-8.308427407	0.000000000	-1.080812378
C	6	-5.030220137	1.508417140	-0.841383570
C	6	-5.030220137	-1.508417140	-0.841383570
C	6	-7.783014883	2.414138359	-1.466649942
C	6	-7.783014883	-2.414138359	-1.466649942
C	6	-9.491735602	0.000000000	-1.819918734
C	6	-3.728119499	0.752615220	-0.826256751
C	6	-3.728119499	-0.752615220	-0.826256751
C	6	-6.630470290	3.311265581	-1.548560303
C	6	-6.630470290	-3.311265581	-1.548560303
C	6	-9.108484685	2.498546343	-2.078403561
C	6	-9.108484685	-2.498546343	-2.078403561
C	6	-5.327884826	2.877350675	-1.256947647
C	6	-5.327884826	-2.877350675	-1.256947647
C	6	-9.924390636	1.356729061	-2.249542300
C	6	-9.924390636	-1.356729061	-2.249542300
H	1	-9.465037921	3.445957441	-2.506168321
H	1	-9.465037921	-3.445957441	-2.506168321
F	9	-11.119232071	1.485166496	-2.908247313

F	9	-11.119232071	-1.485166496	-2.908247313
H	1	-6.769135866	4.331898646	-1.934490350
H	1	-6.769135866	-4.331898646	-1.934490350
H	1	-4.499643333	3.579876421	-1.429872727
H	1	-4.499643333	-3.579876421	-1.429872727
C	6	6.156134052	0.729460091	-0.603140102
C	6	6.156134052	-0.729460091	-0.603140102
C	6	7.484199603	1.164868079	-0.898236799
C	6	7.484199603	-1.164868079	-0.898236799
C	6	8.308427407	0.000000000	-1.080812378
C	6	5.030220137	1.508417140	-0.841383570
C	6	5.030220137	-1.508417140	-0.841383570
C	6	7.783014883	2.414138359	-1.466649942
C	6	7.783014883	-2.414138359	-1.466649942
C	6	9.491735602	0.000000000	-1.819918734
C	6	3.728119499	0.752615220	-0.826256751
C	6	3.728119499	-0.752615220	-0.826256751
C	6	6.630470290	3.311265581	-1.548560303
C	6	6.630470290	-3.311265581	-1.548560303
C	6	9.108484685	2.498546343	-2.078403561
C	6	9.108484685	-2.498546343	-2.078403561
C	6	5.327884826	2.877350675	-1.256947647
C	6	5.327884826	-2.877350675	-1.256947647
C	6	9.924390636	1.356729061	-2.249542300
C	6	9.924390636	-1.356729061	-2.249542300
H	1	9.465037921	3.445957441	-2.506168321
H	1	9.465037921	-3.445957441	-2.506168321
F	9	11.119232071	1.485166496	-2.908247313
F	9	11.119232071	-1.485166496	-2.908247313
H	1	6.769135866	4.331898646	-1.934490350
H	1	6.769135866	-4.331898646	-1.934490350
H	1	4.499643333	3.579876421	-1.429872727
H	1	4.499643333	-3.579876421	-1.429872727
C	6	-2.505957351	1.419809308	-0.847348219
C	6	2.505957351	1.419809308	-0.847348219
C	6	-2.505957351	-1.419809308	-0.847348219
C	6	2.505957351	-1.419809308	-0.847348219
H	1	-2.492583747	2.518295557	-0.846440036
H	1	2.492583747	2.518295557	-0.846440036
H	1	-2.492583747	-2.518295557	-0.846440036
H	1	2.492583747	-2.518295557	-0.846440036
C	6	-1.237213846	0.730674107	-0.854934739
C	6	1.237213846	0.730674107	-0.854934739
C	6	-1.237213846	-0.730674107	-0.854934739
C	6	1.237213846	-0.730674107	-0.854934739
C	6	0.000000000	1.424047690	-0.856110088

C	6	0.000000000	-1.424047690	-0.856110088
H	1	0.000000000	2.523047433	-0.854305283
H	1	0.000000000	-2.523047433	-0.854305283

Set D n=1

Donor fragment atoms 1-34

Acceptor fragment atoms 35-68

Atom	Atomic number	x	y	z
C	6	-3.697521819	0.717715761	-0.958573759
C	6	-3.697521819	-0.717715761	-0.958573759
C	6	-5.035774021	1.159117126	-1.233020979
C	6	-5.035774021	-1.159117126	-1.233020979
C	6	-5.869706444	0.000000000	-1.411764609
C	6	-2.562791794	1.478007509	-1.250557213
C	6	-2.562791794	-1.478007509	-1.250557213
C	6	-5.326525956	2.400027020	-1.803982680
C	6	-5.326525956	-2.400027020	-1.803982680
C	6	-7.055201491	0.000000000	-2.159994171
C	6	-1.304973678	0.701962444	-1.346740120
C	6	-1.304973678	-0.701962444	-1.346740120
C	6	-4.167045978	3.295382877	-1.912186211
C	6	-4.167045978	-3.295382877	-1.912186211
C	6	-6.664289834	2.475818124	-2.397229402
C	6	-6.664289834	-2.475818124	-2.397229402
C	6	-2.863987766	2.859556916	-1.653449849
C	6	-2.863987766	-2.859556916	-1.653449849
C	6	-7.499143427	1.360354537	-2.571545023
C	6	-7.499143427	-1.360354537	-2.571545023
H	1	-7.010767511	3.440490184	-2.795678544
H	1	-7.010767511	-3.440490184	-2.795678544
C	6	-8.851080590	1.587325093	-3.277869677
C	6	-8.851080590	-1.587325093	-3.277869677
H	1	-4.313007727	4.317126819	-2.293189617
H	1	-4.313007727	-4.317126819	-2.293189617
H	1	-2.035994496	3.558240460	-1.841589897
H	1	-2.035994496	-3.558240460	-1.841589897
H	1	-9.028058539	2.664205479	-3.415927502
H	1	-9.028058539	-2.664205479	-3.415927502
H	1	-8.870860634	1.108043112	-4.270642555
H	1	-8.870860634	-1.108043112	-4.270642555
H	1	-9.683375650	1.173018723	-2.686460844
H	1	-9.683375650	-1.173018723	-2.686460844
C	6	3.697521819	0.717715761	-0.958573759
C	6	3.697521819	-0.717715761	-0.958573759

C	6	5.035774021	1.159117126	-1.233020979
C	6	5.035774021	-1.159117126	-1.233020979
C	6	5.869706444	0.000000000	-1.411764609
C	6	2.562791794	1.478007509	-1.250557213
C	6	2.562791794	-1.478007509	-1.250557213
C	6	5.326525956	2.400027020	-1.803982680
C	6	5.326525956	-2.400027020	-1.803982680
C	6	7.055201491	0.000000000	-2.159994171
C	6	1.304973678	0.701962444	-1.346740120
C	6	1.304973678	-0.701962444	-1.346740120
C	6	4.167045978	3.295382877	-1.912186211
C	6	4.167045978	-3.295382877	-1.912186211
C	6	6.664289834	2.475818124	-2.397229402
C	6	6.664289834	-2.475818124	-2.397229402
C	6	2.863987766	2.859556916	-1.653449849
C	6	2.863987766	-2.859556916	-1.653449849
C	6	7.499143427	1.360354537	-2.571545023
C	6	7.499143427	-1.360354537	-2.571545023
H	1	7.010767511	3.440490184	-2.795678544
H	1	7.010767511	-3.440490184	-2.795678544
C	6	8.851080590	1.587325093	-3.277869677
C	6	8.851080590	-1.587325093	-3.277869677
H	1	4.313007727	4.317126819	-2.293189617
H	1	4.313007727	-4.317126819	-2.293189617
H	1	2.035994496	3.558240460	-1.841589897
H	1	2.035994496	-3.558240460	-1.841589897
H	1	9.028058539	2.664205479	-3.415927502
H	1	9.028058539	-2.664205479	-3.415927502
H	1	8.870860634	1.108043112	-4.270642555
H	1	8.870860634	-1.108043112	-4.270642555
H	1	9.683375650	1.173018723	-2.686460844
H	1	9.683375650	-1.173018723	-2.686460844
C	6	0.000000000	1.489361713	-1.587465464
C	6	0.000000000	-1.489361713	-1.587465464
H	1	0.000000000	1.868904805	-2.631394868
H	1	0.000000000	-1.868904805	-2.631394868
H	1	0.000000000	2.385104308	-0.938844195
H	1	0.000000000	-2.385104308	-0.938844195

Set D n=2

Donor fragment atoms 1-34

Acceptor fragment atoms 35-68

Atom	Atomic number	x	y	z
C	6	-4.829105545	0.717277364	-0.990638943

C	6	-4.829105545	-0.717277364	-0.990638943
C	6	-6.196558165	1.158755332	-0.994773636
C	6	-6.196558165	-1.158755332	-0.994773636
C	6	-7.049855120	0.000000000	-1.005772522
C	6	-3.774043454	1.484487036	-1.499101145
C	6	-3.774043454	-1.484487036	-1.499101145
C	6	-6.595315928	2.400108658	-1.494537230
C	6	-6.595315928	-2.400108658	-1.494537230
C	6	-8.359377377	0.000000000	-1.506630089
C	6	-2.570294624	0.704952044	-1.841974657
C	6	-2.570294624	-0.704952044	-1.841974657
C	6	-5.481835312	3.299067047	-1.828223386
C	6	-5.481835312	-3.299067047	-1.828223386
C	6	-8.023396715	2.476128291	-1.812594573
C	6	-8.023396715	-2.476128291	-1.812594573
C	6	-4.153282191	2.866508187	-1.831535601
C	6	-4.153282191	-2.866508187	-1.831535601
C	6	-8.875723706	1.360046989	-1.822792007
C	6	-8.875723706	-1.360046989	-1.822792007
H	1	-8.441382099	3.441179182	-2.134117098
H	1	-8.441382099	-3.441179182	-2.134117098
C	6	-10.338206124	1.586021593	-2.256853317
C	6	-10.338206124	-1.586021593	-2.256853317
H	1	-5.703118117	4.320774517	-2.170827792
H	1	-5.703118117	-4.320774517	-2.170827792
H	1	-3.379511188	3.567019342	-2.178045237
H	1	-3.379511188	-3.567019342	-2.178045237
H	1	-10.539207197	2.662445562	-2.361568598
H	1	-10.539207197	-2.662445562	-2.361568598
H	1	-10.546124420	1.103557384	-3.226092259
H	1	-10.546124420	-1.103557384	-3.226092259
H	1	-11.042008059	1.173258632	-1.516206485
H	1	-11.042008059	-1.173258632	-1.516206485
C	6	4.829105545	0.717277364	-0.990638943
C	6	4.829105545	-0.717277364	-0.990638943
C	6	6.196558165	1.158755332	-0.994773636
C	6	6.196558165	-1.158755332	-0.994773636
C	6	7.049855120	0.000000000	-1.005772522
C	6	3.774043454	1.484487036	-1.499101145
C	6	3.774043454	-1.484487036	-1.499101145
C	6	6.595315928	2.400108658	-1.494537230
C	6	6.595315928	-2.400108658	-1.494537230
C	6	8.359377377	0.000000000	-1.506630089
C	6	2.570294624	0.704952044	-1.841974657
C	6	2.570294624	-0.704952044	-1.841974657
C	6	5.481835312	3.299067047	-1.828223386

C	6	5.481835312	-3.299067047	-1.828223386
C	6	8.023396715	2.476128291	-1.812594573
C	6	8.023396715	-2.476128291	-1.812594573
C	6	4.153282191	2.866508187	-1.831535601
C	6	4.153282191	-2.866508187	-1.831535601
C	6	8.875723706	1.360046989	-1.822792007
C	6	8.875723706	-1.360046989	-1.822792007
H	1	8.441382099	3.441179182	-2.134117098
H	1	8.441382099	-3.441179182	-2.134117098
C	6	10.338206124	1.586021593	-2.256853317
C	6	10.338206124	-1.586021593	-2.256853317
H	1	5.703118117	4.320774517	-2.170827792
H	1	5.703118117	-4.320774517	-2.170827792
H	1	3.379511188	3.567019342	-2.178045237
H	1	3.379511188	-3.567019342	-2.178045237
H	1	10.539207197	2.662445562	-2.361568598
H	1	10.539207197	-2.662445562	-2.361568598
H	1	10.546124420	1.103557384	-3.226092259
H	1	10.546124420	-1.103557384	-3.226092259
H	1	11.042008059	1.173258632	-1.516206485
H	1	11.042008059	-1.173258632	-1.516206485
C	6	-1.285634283	1.388157819	-2.347176085
C	6	1.285634283	1.388157819	-2.347176085
C	6	-1.285634283	-1.388157819	-2.347176085
C	6	1.285634283	-1.388157819	-2.347176085
H	1	-1.202522207	1.247227512	-3.442214142
H	1	1.202522207	1.247227512	-3.442214142
H	1	-1.202522207	-1.247227512	-3.442214142
H	1	1.202522207	-1.247227512	-3.442214142
H	1	-1.326007476	2.473499069	-2.158074778
H	1	1.326007476	2.473499069	-2.158074778
H	1	-1.326007476	-2.473499069	-2.158074778
H	1	1.326007476	-2.473499069	-2.158074778
C	6	0.000000000	0.792225291	-1.665324266
C	6	0.000000000	-0.792225291	-1.665324266
H	1	0.000000000	1.126318637	-0.611945089
H	1	0.000000000	-1.126318637	-0.611945089

Set D n=3

Donor fragment atoms	1-34
Acceptor fragment atoms	35-68

Atom	Atomic number	x	y	z
C	6	6.114957306	-0.717224678	-1.014377793
C	6	6.114957306	0.717224678	-1.014377793

C	6	7.482063164	-1.158638863	-1.006821228
C	6	7.482063164	1.158638863	-1.006821228
C	6	8.335308592	0.000000000	-1.009513690
C	6	5.063341521	-1.484777411	-1.528832697
C	6	5.063341521	1.484777411	-1.528832697
C	6	7.885441933	-2.400325411	-1.501761273
C	6	7.885441933	2.400325411	-1.501761273
C	6	9.650364660	0.000000000	-1.494883642
C	6	3.860324381	-0.705031284	-1.875018383
C	6	3.860324381	0.705031284	-1.875018383
C	6	6.774461588	-3.298981986	-1.844631912
C	6	6.774461588	3.298981986	-1.844631912
C	6	9.317090099	-2.476339023	-1.804183551
C	6	9.317090099	2.476339023	-1.804183551
C	6	5.445665085	-2.866678271	-1.858184169
C	6	5.445665085	2.866678271	-1.858184169
C	6	10.169946813	-1.360481635	-1.804112211
C	6	10.169946813	1.360481635	-1.804112211
H	1	9.738928209	-3.441488437	-2.120344868
H	1	9.738928209	3.441488437	-2.120344868
C	6	11.638191060	-1.586898171	-2.217943325
C	6	11.638191060	1.586898171	-2.217943325
H	1	6.998544588	-4.320678573	-2.185518961
H	1	6.998544588	4.320678573	-2.185518961
H	1	4.674813263	-3.567490911	-2.210633658
H	1	4.674813263	3.567490911	-2.210633658
H	1	11.840698217	-2.663463794	-2.318477673
H	1	11.840698217	2.663463794	-2.318477673
H	1	11.859856051	-1.105647091	-3.184769461
H	1	11.859856051	1.105647091	-3.184769461
H	1	12.331719166	-1.173171999	-1.468138115
H	1	12.331719166	1.173171999	-1.468138115
C	6	-6.114957306	-0.717224678	-1.014377793
C	6	-6.114957306	0.717224678	-1.014377793
C	6	-7.482063164	-1.158638863	-1.006821228
C	6	-7.482063164	1.158638863	-1.006821228
C	6	-8.335308592	0.000000000	-1.009513690
C	6	-5.063341521	-1.484777411	-1.528832697
C	6	-5.063341521	1.484777411	-1.528832697
C	6	-7.885441933	-2.400325411	-1.501761273
C	6	-7.885441933	2.400325411	-1.501761273
C	6	-9.650364660	0.000000000	-1.494883642
C	6	-3.860324381	-0.705031284	-1.875018383
C	6	-3.860324381	0.705031284	-1.875018383
C	6	-6.774461588	-3.298981986	-1.844631912
C	6	-6.774461588	3.298981986	-1.844631912

C	6	-9.317090099	-2.476339023	-1.804183551
C	6	-9.317090099	2.476339023	-1.804183551
C	6	-5.445665085	-2.866678271	-1.858184169
C	6	-5.445665085	2.866678271	-1.858184169
C	6	-10.169946813	-1.360481635	-1.804112211
C	6	-10.169946813	1.360481635	-1.804112211
H	1	-9.738928209	-3.441488437	-2.120344868
H	1	-9.738928209	3.441488437	-2.120344868
C	6	-11.638191060	-1.586898171	-2.217943325
C	6	-11.638191060	1.586898171	-2.217943325
H	1	-6.998544588	-4.320678573	-2.185518961
H	1	-6.998544588	4.320678573	-2.185518961
H	1	-4.674813263	-3.567490911	-2.210633658
H	1	-4.674813263	3.567490911	-2.210633658
H	1	-11.840698217	-2.663463794	-2.318477673
H	1	-11.840698217	2.663463794	-2.318477673
H	1	-11.859856051	-1.105647091	-3.184769461
H	1	-11.859856051	1.105647091	-3.184769461
H	1	-12.331719166	-1.173171999	-1.468138115
H	1	-12.331719166	1.173171999	-1.468138115
C	6	2.569774983	-1.385387811	-2.367561487
C	6	-2.569774983	-1.385387811	-2.367561487
C	6	2.569774983	1.385387811	-2.367561487
C	6	-2.569774983	1.385387811	-2.367561487
C	6	0.000000000	-1.377828625	-2.306939772
C	6	0.000000000	1.377828625	-2.306939772
H	1	2.467698919	-1.235490858	-3.459666598
H	1	-2.467698919	-1.235490858	-3.459666598
H	1	2.467698919	1.235490858	-3.459666598
H	1	-2.467698919	1.235490858	-3.459666598
H	1	0.000000000	-1.168609669	-3.390278026
H	1	0.000000000	1.168609669	-3.390278026
H	1	2.613351153	-2.472173155	-2.187742289
H	1	-2.613351153	-2.472173155	-2.187742289
H	1	2.613351153	2.472173155	-2.187742289
H	1	-2.613351153	2.472173155	-2.187742289
H	1	0.000000000	-2.475348335	-2.186430697
H	1	0.000000000	2.475348335	-2.186430697
C	6	1.297169632	-0.793075433	-1.657259897
C	6	-1.297169632	-0.793075433	-1.657259897
C	6	1.297169632	0.793075433	-1.657259897
C	6	-1.297169632	0.793075433	-1.657259897
H	1	1.324207205	-1.129701312	-0.604537538
H	1	-1.324207205	-1.129701312	-0.604537538
H	1	1.324207205	1.129701312	-0.604537538
H	1	-1.324207205	1.129701312	-0.604537538

Set D n=4

Donor fragment atoms 1-34

Acceptor fragment atoms 35-68

Atom	Atomic number	x	y	z
C	6	7.402745860	-0.717174219	-1.031685793
C	6	7.402745860	0.717174219	-1.031685793
C	6	8.769598175	-1.158521562	-1.018000705
C	6	8.769598175	1.158521562	-1.018000705
C	6	9.622796496	0.000000000	-1.016455594
C	6	6.352936698	-1.485004484	-1.549069586
C	6	6.352936698	1.485004484	-1.549069586
C	6	9.175429312	-2.400586732	-1.509753096
C	6	9.175429312	2.400586732	-1.509753096
C	6	10.940682648	0.000000000	-1.493541232
C	6	5.150270679	-0.705091725	-1.896741821
C	6	5.150270679	0.705091725	-1.896741821
C	6	8.065708867	-3.299229227	-1.856792771
C	6	8.065708867	3.299229227	-1.856792771
C	6	10.608893278	-2.476624225	-1.803787843
C	6	10.608893278	2.476624225	-1.803787843
C	6	6.736819432	-2.867061205	-1.876098110
C	6	6.736819432	2.867061205	-1.876098110
C	6	11.461836385	-1.360774533	-1.799008183
C	6	11.461836385	1.360774533	-1.799008183
H	1	11.032713332	-3.441924877	-2.116788203
H	1	11.032713332	3.441924877	-2.116788203
C	6	12.932761390	-1.587530666	-2.202795460
C	6	12.932761390	1.587530666	-2.202795460
H	1	8.291241997	-4.321243528	-2.195805637
H	1	8.291241997	4.321243528	-2.195805637
H	1	5.967507050	-3.568392035	-2.230796481
H	1	5.967507050	3.568392035	-2.230796481
H	1	13.136019821	-2.664217598	-2.300601429
H	1	13.136019821	2.664217598	-2.300601429
H	1	13.161375102	-1.107160263	-3.168355693
H	1	13.161375102	1.107160263	-3.168355693
H	1	13.621009793	-1.173235044	-1.448378719
H	1	13.621009793	1.173235044	-1.448378719
C	6	-7.402745860	-0.717174219	-1.031685793
C	6	-7.402745860	0.717174219	-1.031685793
C	6	-8.769598175	-1.158521562	-1.018000705
C	6	-8.769598175	1.158521562	-1.018000705

C	6	-9.622796496	0.000000000	-1.016455594
C	6	-6.352936698	-1.485004484	-1.549069586
C	6	-6.352936698	1.485004484	-1.549069586
C	6	-9.175429312	-2.400586732	-1.509753096
C	6	-9.175429312	2.400586732	-1.509753096
C	6	-10.940682648	0.000000000	-1.493541232
C	6	-5.150270679	-0.705091725	-1.896741821
C	6	-5.150270679	0.705091725	-1.896741821
C	6	-8.065708867	-3.299229227	-1.856792771
C	6	-8.065708867	3.299229227	-1.856792771
C	6	-10.608893278	-2.476624225	-1.803787843
C	6	-10.608893278	2.476624225	-1.803787843
C	6	-6.736819432	-2.867061205	-1.876098110
C	6	-6.736819432	2.867061205	-1.876098110
C	6	-11.461836385	-1.360774533	-1.799008183
C	6	-11.461836385	1.360774533	-1.799008183
H	1	-11.032713332	-3.441924877	-2.116788203
H	1	-11.032713332	3.441924877	-2.116788203
C	6	-12.932761390	-1.587530666	-2.202795460
C	6	-12.932761390	1.587530666	-2.202795460
H	1	-8.291241997	-4.321243528	-2.195805637
H	1	-8.291241997	4.321243528	-2.195805637
H	1	-5.967507050	-3.568392035	-2.230796481
H	1	-5.967507050	3.568392035	-2.230796481
H	1	-13.136019821	-2.664217598	-2.300601429
H	1	-13.136019821	2.664217598	-2.300601429
H	1	-13.161375102	-1.107160263	-3.168355693
H	1	-13.161375102	1.107160263	-3.168355693
H	1	-13.621009793	-1.173235044	-1.448378719
H	1	-13.621009793	1.173235044	-1.448378719
C	6	3.856366337	-1.384144286	-2.382116232
C	6	-3.856366337	-1.384144286	-2.382116232
C	6	3.856366337	1.384144286	-2.382116232
C	6	-3.856366337	1.384144286	-2.382116232
C	6	1.284555700	-1.376593114	-2.285977276
C	6	-1.284555700	-1.376593114	-2.285977276
C	6	1.284555700	1.376593114	-2.285977276
C	6	-1.284555700	1.376593114	-2.285977276
H	1	3.744160105	-1.229481242	-3.472520045
H	1	-3.744160105	-1.229481242	-3.472520045
H	1	3.744160105	1.229481242	-3.472520045
H	1	-3.744160105	1.229481242	-3.472520045
H	1	1.265602140	-1.164096930	-3.368476108
H	1	-1.265602140	-1.164096930	-3.368476108
H	1	1.265602140	1.164096930	-3.368476108
H	1	-1.265602140	1.164096930	-3.368476108

H	1	3.901438908	-2.471677325	-2.207143211
H	1	-3.901438908	-2.471677325	-2.207143211
H	1	3.901438908	2.471677325	-2.207143211
H	1	-3.901438908	2.471677325	-2.207143211
H	1	1.287167650	-2.474501980	-2.168877494
H	1	-1.287167650	-2.474501980	-2.168877494
H	1	1.287167650	2.474501980	-2.168877494
H	1	-1.287167650	2.474501980	-2.168877494
C	6	2.591847285	-0.793156853	-1.656156463
C	6	-2.591847285	-0.793156853	-1.656156463
C	6	2.591847285	0.793156853	-1.656156463
C	6	-2.591847285	0.793156853	-1.656156463
H	1	2.633296647	-1.129530639	-0.603860706
H	1	-2.633296647	-1.129530639	-0.603860706
H	1	2.633296647	1.129530639	-0.603860706
H	1	-2.633296647	1.129530639	-0.603860706
C	6	0.000000000	-0.793931876	-1.609225899
C	6	0.000000000	0.793931876	-1.609225899
H	1	0.000000000	-1.132161934	-0.556093144
H	1	0.000000000	1.132161934	-0.556093144

Set E n=1

Donor fragment atoms	1-34
Acceptor fragment atoms	35-66

Atom	Atomic number	x	y	z
C	6	-3.645716482	0.725310817	-0.720872851
C	6	-3.645716482	-0.725310817	-0.720872851
C	6	-4.950526899	1.159175714	-1.115921636
C	6	-4.950526899	-1.159175714	-1.115921636
C	6	-5.764125708	0.000000000	-1.368722146
C	6	-2.503305822	1.502989183	-0.880453647
C	6	-2.503305822	-1.502989183	-0.880453647
C	6	-5.203620596	2.408129506	-1.692554278
C	6	-5.203620596	-2.408129506	-1.692554278
C	6	-6.890460786	0.000000000	-2.200555389
C	6	-1.216063964	0.737221079	-0.795218348
C	6	-1.216063964	-0.737221079	-0.795218348
C	6	-4.049892510	3.308069614	-1.690693807
C	6	-4.049892510	-3.308069614	-1.690693807
C	6	-6.492992380	2.480696347	-2.387292131
C	6	-6.492992380	-2.480696347	-2.387292131
C	6	-2.770903307	2.875899366	-1.310437999
C	6	-2.770903307	-2.875899366	-1.310437999
C	6	-7.306092367	1.363339071	-2.635360719

C	6	-7.306092367	-1.363339071	-2.635360719
H	1	-6.814579074	3.447848828	-2.800346801
H	1	-6.814579074	-3.447848828	-2.800346801
C	6	-8.602476838	1.590458211	-3.439124428
C	6	-8.602476838	-1.590458211	-3.439124428
H	1	-4.163511366	4.330385699	-2.080814438
H	1	-4.163511366	-4.330385699	-2.080814438
H	1	-1.933163496	3.579501806	-1.420676130
H	1	-1.933163496	-3.579501806	-1.420676130
H	1	-9.476565152	1.179582877	-2.908270247
H	1	-9.476565152	-1.179582877	-2.908270247
H	1	-8.766808654	2.667079607	-3.593575361
H	1	-8.766808654	-2.667079607	-3.593575361
H	1	-8.550081359	1.106983954	-4.428585696
H	1	-8.550081359	-1.106983954	-4.428585696
C	6	3.700844219	-0.732649041	-0.408410134
C	6	3.700844219	0.732649041	-0.408410134
C	6	5.030228343	-1.177016693	-0.735864832
C	6	5.030228343	1.177016693	-0.735864832
C	6	5.840545705	0.000000000	-0.889506850
C	6	2.568329226	-1.491380965	-0.705753332
C	6	2.568329226	1.491380965	-0.705753332
C	6	5.296563927	-2.360433014	-1.461602044
C	6	5.296563927	2.360433014	-1.461602044
C	6	6.889532616	0.000000000	-1.787707632
C	6	1.275523168	-0.734667866	-0.706239570
C	6	1.275523168	0.734667866	-0.706239570
C	6	4.136124583	-3.245273545	-1.575719530
C	6	4.136124583	3.245273545	-1.575719530
C	6	6.527285504	-2.381638087	-2.284837840
C	6	6.527285504	2.381638087	-2.284837840
C	6	2.848044928	-2.834465661	-1.210282451
C	6	2.848044928	2.834465661	-1.210282451
C	6	7.283415954	-1.218806274	-2.457528651
C	6	7.283415954	1.218806274	-2.457528651
H	1	6.737947333	-3.278228057	-2.886673041
H	1	6.737947333	3.278228057	-2.886673041
C	6	8.357141825	-0.800747660	-3.502611616
C	6	8.357141825	0.800747660	-3.502611616
H	1	4.255059876	-4.225248640	-2.061409511
H	1	4.255059876	4.225248640	-2.061409511
H	1	2.009554343	-3.513937749	-1.420313027
H	1	2.009554343	3.513937749	-1.420313027
H	1	9.356657497	-1.186024225	-3.228068230
H	1	9.356657497	1.186024225	-3.228068230
H	1	8.115438169	-1.192607816	-4.506675108

H	1	8.115438169	1.192607816	-4.506675108
C	6	0.030717924	-1.405590791	-0.764263146
C	6	0.030717924	1.405590791	-0.764263146
H	1	0.031067534	-2.503427138	-0.765583413
H	1	0.031067534	2.503427138	-0.765583413

Set E n=2

Donor fragment atoms 1-34

Acceptor fragment atoms 35-66

Atom	Atomic number	x	y	z
C	6	-4.885068232	-0.727500128	-0.785707758
C	6	-4.885068232	0.727500128	-0.785707758
C	6	-6.171391221	-1.159842783	-1.237258151
C	6	-6.171391221	1.159842783	-1.237258151
C	6	-6.972226198	0.000000000	-1.528000308
C	6	-3.739775584	-1.507191693	-0.901219497
C	6	-3.739775584	1.507191693	-0.901219497
C	6	-6.400898392	-2.409510642	-1.824698855
C	6	-6.400898392	2.409510642	-1.824698855
C	6	-8.057662679	0.000000000	-2.412944700
C	6	-2.447230473	-0.748011417	-0.776112921
C	6	-2.447230473	0.748011417	-0.776112921
C	6	-5.251833894	-3.310879663	-1.774150181
C	6	-5.251833894	3.310879663	-1.774150181
C	6	-7.656142995	-2.480908115	-2.578813020
C	6	-7.656142995	2.480908115	-2.578813020
C	6	-3.989077467	-2.878395654	-1.342032536
C	6	-3.989077467	2.878395654	-1.342032536
C	6	-8.453797083	-1.362734546	-2.867482198
C	6	-8.453797083	1.362734546	-2.867482198
H	1	-7.958086086	-3.448087240	-3.006426456
H	1	-7.958086086	3.448087240	-3.006426456
C	6	-9.707800559	-1.588617345	-3.735849339
C	6	-9.707800559	1.588617345	-3.735849339
H	1	-5.349900043	-4.332765646	-2.169483058
H	1	-5.349900043	4.332765646	-2.169483058
H	1	-3.147059944	-3.581105222	-1.419386441
H	1	-3.147059944	3.581105222	-1.419386441
H	1	-9.864936854	-2.665018478	-3.898755650
H	1	-9.864936854	2.665018478	-3.898755650
H	1	-9.604987951	-1.104830848	-4.721043181
H	1	-9.604987951	1.104830848	-4.721043181
H	1	-10.607221954	-1.177154091	-3.249903092
H	1	-10.607221954	1.177154091	-3.249903092

C	6	4.965627333	0.734824735	-0.498103947
C	6	4.965627333	-0.734824735	-0.498103947
C	6	6.273523310	1.177592090	-0.901504167
C	6	6.273523310	-1.177592090	-0.901504167
C	6	7.072988472	0.000000000	-1.102739940
C	6	3.821206514	1.495753189	-0.731616162
C	6	3.821206514	-1.495753189	-0.731616162
C	6	6.501244587	2.362747535	-1.639239031
C	6	6.501244587	-2.362747535	-1.639239031
C	6	8.068008725	0.000000000	-2.059652740
C	6	2.521465847	0.745533662	-0.666240239
C	6	2.521465847	-0.745533662	-0.666240239
C	6	5.339264415	3.248780730	-1.687016535
C	6	5.339264415	-3.248780730	-1.687016535
C	6	7.683700450	2.382987858	-2.530811376
C	6	7.683700450	-2.382987858	-2.530811376
C	6	4.072856994	2.837367979	-1.250706347
C	6	4.072856994	-2.837367979	-1.250706347
C	6	8.425715800	1.219125053	-2.748955601
C	6	8.425715800	-1.219125053	-2.748955601
H	1	7.862020183	3.280797737	-3.141216986
H	1	7.862020183	-3.280797737	-3.141216986
C	6	9.440719374	0.800801843	-3.850783563
C	6	9.440719374	-0.800801843	-3.850783563
H	1	5.431040595	4.228410255	-2.179028860
H	1	5.431040595	-4.228410255	-2.179028860
H	1	3.223982096	3.516473516	-1.414533236
H	1	3.223982096	-3.516473516	-1.414533236
H	1	9.147173191	1.193757667	-4.840405257
H	1	9.147173191	-1.193757667	-4.840405257
H	1	10.453771644	1.184694732	-3.628634702
H	1	10.453771644	-1.184694732	-3.628634702
C	6	-1.218762487	-1.416290978	-0.727458323
C	6	-1.218762487	1.416290978	-0.727458323
C	6	1.293315520	1.416471876	-0.674392367
C	6	1.293315520	-1.416471876	-0.674392367
H	1	-1.205099916	-2.514665336	-0.729130972
H	1	-1.205099916	2.514665336	-0.729130972
H	1	1.280239549	2.514804910	-0.675419048
H	1	1.280239549	-2.514804910	-0.675419048
C	6	0.037239573	-0.724423810	-0.688642105
C	6	0.037239573	0.724423810	-0.688642105

Set E n=3

Donor fragment atoms 1-34

Acceptor fragment atoms 35-66

Atom	Atomic number	x	y	z
C	6	-6.079953414	-0.728797812	-0.603899671
C	6	-6.079953414	0.728797812	-0.603899671
C	6	-7.270177028	-1.160519466	-1.270474759
C	6	-7.270177028	1.160519466	-1.270474759
C	6	-8.006834852	0.000000000	-1.697250575
C	6	-4.931880066	-1.509867627	-0.529727147
C	6	-4.931880066	1.509867627	-0.529727147
C	6	-7.394806570	-2.409811685	-1.891093175
C	6	-7.394806570	2.409811685	-1.891093175
C	6	-8.914609057	0.000000000	-2.764985726
C	6	-3.668151261	-0.752136777	-0.221981752
C	6	-3.668151261	0.752136777	-0.221981752
C	6	-6.274731258	-3.313666464	-1.643829696
C	6	-6.274731258	3.313666464	-1.643829696
C	6	-8.492759586	-2.480370607	-2.858989828
C	6	-8.492759586	2.480370607	-2.858989828
C	6	-5.103683535	-2.880902298	-1.004898331
C	6	-5.103683535	2.880902298	-1.004898331
C	6	-9.222318555	-1.360966152	-3.286748267
C	6	-9.222318555	1.360966152	-3.286748267
H	1	-8.711133785	-3.446479243	-3.336768124
H	1	-8.711133785	3.446479243	-3.336768124
C	6	-10.289434299	-1.583220332	-4.377514993
C	6	-10.289434299	1.583220332	-4.377514993
H	1	-6.305404410	-4.335299566	-2.050426281
H	1	-6.305404410	4.335299566	-2.050426281
H	1	-4.259945513	-3.582706786	-0.939644815
H	1	-4.259945513	3.582706786	-0.939644815
H	1	-10.429174850	-2.659901567	-4.554014509
H	1	-10.429174850	2.659901567	-4.554014509
H	1	-9.988321508	-1.117504427	-5.330587245
H	1	-9.988321508	1.117504427	-5.330587245
H	1	-11.259091522	-1.151905951	-4.082302431
H	1	-11.259091522	1.151905951	-4.082302431
C	6	6.197488451	0.736093061	-0.338167908
C	6	6.197488451	-0.736093061	-0.338167908
C	6	7.413228914	1.177871137	-0.968867701
C	6	7.413228914	-1.177871137	-0.968867701
C	6	8.162233722	0.000000000	-1.313416025
C	6	5.030594494	1.498416458	-0.372301459
C	6	5.030594494	-1.498416458	-0.372301459

C	6	7.506041238	2.363431569	-1.735368120
C	6	7.506041238	-2.363431569	-1.735368120
C	6	8.964509112	0.000000000	-2.438154431
C	6	3.753661067	0.749640184	-0.110419268
C	6	3.753661067	-0.749640184	-0.110419268
C	6	6.357552468	3.252463225	-1.575631891
C	6	6.357552468	-3.252463225	-1.575631891
C	6	8.503236384	2.383473373	-2.829383111
C	6	8.503236384	-2.383473373	-2.829383111
C	6	5.187652784	2.840359643	-0.925269507
C	6	5.187652784	-2.840359643	-0.925269507
C	6	9.189648063	1.218810909	-3.182099881
C	6	9.189648063	-1.218810909	-3.182099881
H	1	8.564663668	3.281680377	-3.461702089
H	1	8.564663668	-3.281680377	-3.461702089
C	6	9.977352316	0.800400076	-4.456304365
C	6	9.977352316	-0.800400076	-4.456304365
H	1	6.363838881	4.232443511	-2.075383144
H	1	6.363838881	-4.232443511	-2.075383144
H	1	4.322200085	3.517998558	-0.936940797
H	1	4.322200085	-3.517998558	-0.936940797
H	1	9.498131056	1.192281588	-5.371344808
H	1	9.498131056	-1.192281588	-5.371344808
H	1	11.013115033	1.187635814	-4.434143824
H	1	11.013115033	-1.187635814	-4.434143824
C	6	-2.458800511	-1.418885694	-0.039983685
C	6	-2.458800511	1.418885694	-0.039983685
C	6	2.539903392	1.418910025	0.029231747
C	6	2.539903392	-1.418910025	0.029231747
H	1	-2.444068018	-2.517181841	-0.043959458
H	1	-2.444068018	2.517181841	-0.043959458
H	1	2.525977037	2.517148570	0.026236798
H	1	2.525977037	-2.517148570	0.026236798
C	6	-1.197181627	-0.730599220	0.091965527
C	6	-1.197181627	0.730599220	0.091965527
C	6	1.275337932	0.730666872	0.124539661
C	6	1.275337932	-0.730666872	0.124539661
C	6	0.038411602	-1.424395340	0.142279355
C	6	0.038411602	1.424395340	0.142279355
H	1	0.038462987	-2.523343321	0.135182331
H	1	0.038462987	2.523343321	0.135182331

Set E n=4

Donor fragment atoms	1-34
Acceptor fragment atoms	35-66

Atom	Atomic number	x	y	z
C	6	-7.306773247	-0.729165753	-0.641103569
C	6	-7.306773247	0.729165753	-0.641103569
C	6	-8.503280386	-1.160385649	-1.294871656
C	6	-8.503280386	1.160385649	-1.294871656
C	6	-9.245570192	0.000000000	-1.711712368
C	6	-6.159233052	-1.510957175	-0.574682892
C	6	-6.159233052	1.510957175	-0.574682892
C	6	-8.636090091	-2.410168806	-1.912978053
C	6	-8.636090091	2.410168806	-1.912978053
C	6	-10.169860336	0.000000000	-2.764488041
C	6	-4.895309726	-0.754633755	-0.259370793
C	6	-4.895309726	0.754633755	-0.259370793
C	6	-7.512858028	-3.313098263	-1.678891847
C	6	-7.512858028	3.313098263	-1.678891847
C	6	-9.749166518	-2.480807381	-2.863982639
C	6	-9.749166518	2.480807381	-2.863982639
C	6	-6.335204274	-2.880772097	-1.050347434
C	6	-6.335204274	2.880772097	-1.050347434
C	6	-10.486118120	-1.361637549	-3.280020430
C	6	-10.486118120	1.361637549	-3.280020430
H	1	-9.975833243	-3.447181251	-3.337391775
H	1	-9.975833243	3.447181251	-3.337391775
C	6	-11.572816118	-1.584269093	-4.351242753
C	6	-11.572816118	1.584269093	-4.351242753
H	1	-7.546636130	-4.334480773	-2.085915193
H	1	-7.546636130	4.334480773	-2.085915193
H	1	-5.490908546	-3.582655778	-0.993656673
H	1	-5.490908546	3.582655778	-0.993656673
H	1	-11.717570431	-2.661031976	-4.523251217
H	1	-11.717570431	2.661031976	-4.523251217
H	1	-11.287767121	-1.120790971	-5.310357592
H	1	-11.287767121	1.120790971	-5.310357592
H	1	-12.536267348	-1.150759418	-4.039320153
H	1	-12.536267348	1.150759418	-4.039320153
C	6	7.435045623	0.736549706	-0.355518953
C	6	7.435045623	-0.736549706	-0.355518953
C	6	8.650133285	1.177886800	-0.986514883
C	6	8.650133285	-1.177886800	-0.986514883
C	6	9.399237224	0.000000000	-1.330740609
C	6	6.268763790	1.499360975	-0.387627544
C	6	6.268763790	-1.499360975	-0.387627544

C	6	8.743684445	2.363888478	-1.752505448
C	6	8.743684445	-2.363888478	-1.752505448
C	6	10.202731983	0.000000000	-2.454335045
C	6	4.992545453	0.752021554	-0.113021851
C	6	4.992545453	-0.752021554	-0.113021851
C	6	7.595220673	3.252246181	-1.592961206
C	6	7.595220673	-3.252246181	-1.592961206
C	6	9.742501807	2.383823507	-2.845444586
C	6	9.742501807	-2.383823507	-2.845444586
C	6	6.425222149	2.840390123	-0.941558511
C	6	6.425222149	-2.840390123	-0.941558511
C	6	10.429286767	1.219145831	-3.197506079
C	6	10.429286767	-1.219145831	-3.197506079
H	1	9.805471341	3.282474846	-3.476982556
H	1	9.805471341	-3.282474846	-3.476982556
C	6	11.219564295	0.800501120	-4.470194533
C	6	11.219564295	-0.800501120	-4.470194533
H	1	7.601083652	4.232035635	-2.092990963
H	1	7.601083652	-4.232035635	-2.092990963
H	1	5.559717441	3.517880881	-0.952882544
H	1	5.559717441	-3.517880881	-0.952882544
H	1	10.741999405	1.192345934	-5.386140656
H	1	10.741999405	-1.192345934	-5.386140656
H	1	12.255286668	1.187622380	-4.445894333
H	1	12.255286668	-1.187622380	-4.445894333
C	6	-3.693222802	-1.420789993	-0.053185299
C	6	-3.693222802	1.420789993	-0.053185299
C	6	3.785250527	1.420793900	0.051148081
C	6	3.785250527	-1.420793900	0.051148081
H	1	-3.678783059	-2.519173256	-0.054489555
H	1	-3.678783059	2.519173256	-0.054489555
H	1	3.771363210	2.519098108	0.049578614
H	1	3.771363210	-2.519098108	0.049578614
C	6	-2.430668406	-0.733241153	0.117690094
C	6	-2.430668406	0.733241153	0.117690094
C	6	2.518407594	0.733304591	0.183931003
C	6	2.518407594	-0.733304591	0.183931003
C	6	-1.207011640	-1.426147168	0.221705262
C	6	-1.207011640	1.426147168	0.221705262
C	6	1.291991368	1.426175314	0.254417712
C	6	1.291991368	-1.426175314	0.254417712
H	1	-1.206945735	-2.525096962	0.216479270
H	1	-1.206945735	2.525096962	0.216479270
H	1	1.292027974	2.525115734	0.249256407
H	1	1.292027974	-2.525115734	0.249256407
C	6	0.042277215	-0.735354757	0.269275757

C	6	0.042277215	0.735354757	0.269275757

Set F n=1

Donor fragment atoms 1-34

Acceptor fragment atoms 35-62

Atom	Atomic number	x	y	z
C	6	-3.668185658	-0.725282074	-0.964748951
C	6	-3.668185658	0.725282074	-0.964748951
C	6	-4.988891865	-1.159139464	-1.301818797
C	6	-4.988891865	1.159139464	-1.301818797
C	6	-5.812862022	0.000000000	-1.516945607
C	6	-2.533819323	-1.503076500	-1.172435684
C	6	-2.533819323	1.503076500	-1.172435684
C	6	-5.267309281	-2.407903613	-1.866969714
C	6	-5.267309281	2.407903613	-1.866969714
C	6	-6.976183765	0.000000000	-2.295944913
C	6	-1.244237630	-0.737262400	-1.135596972
C	6	-1.244237630	0.737262400	-1.135596972
C	6	-4.114108317	-3.307380284	-1.916671546
C	6	-4.114108317	3.307380284	-1.916671546
C	6	-6.587318858	-2.480603793	-2.502090611
C	6	-6.587318858	2.480603793	-2.502090611
C	6	-2.819585610	-2.875518232	-1.591952778
C	6	-2.819585610	2.875518232	-1.591952778
C	6	-7.411396427	-1.363316590	-2.711265690
C	6	-7.411396427	1.363316590	-2.711265690
H	1	-6.927648858	-3.447528404	-2.900498029
H	1	-6.927648858	3.447528404	-2.900498029
C	6	-8.744253845	-1.590321442	-3.452897872
C	6	-8.744253845	1.590321442	-3.452897872
H	1	-4.243849532	-4.329340252	-2.302732775
H	1	-4.243849532	4.329340252	-2.302732775
H	1	-1.987488786	-3.579045367	-1.739571069
H	1	-1.987488786	3.579045367	-1.739571069
H	1	-8.917808119	-2.667034206	-3.596083954
H	1	-8.917808119	2.667034206	-3.596083954
H	1	-8.737748709	-1.109628877	-4.445104090
H	1	-8.737748709	1.109628877	-4.445104090
H	1	-9.591464957	-1.176327631	-2.882660135
H	1	-9.591464957	1.176327631	-2.882660135
H	1	1.991465367	3.575892339	-1.729455659
H	1	1.991465367	-3.575892339	-1.729455659
H	1	4.244343325	4.328469745	-2.297825685
H	1	4.244343325	-4.328469745	-2.297825685

F	9	8.564206077	1.484653580	-3.404042153
F	9	8.564206077	-1.484653580	-3.404042153
H	1	6.919636705	3.443592479	-2.954708546
H	1	6.919636705	-3.443592479	-2.954708546
C	6	7.391632171	1.355784216	-2.706477514
C	6	7.391632171	-1.355784216	-2.706477514
C	6	2.824613159	2.873636981	-1.580733657
C	6	2.824613159	-2.873636981	-1.580733657
C	6	6.579231319	2.496881825	-2.512380389
C	6	6.579231319	-2.496881825	-2.512380389
C	6	4.116607786	3.307810182	-1.908354978
C	6	4.116607786	-3.307810182	-1.908354978
C	6	1.250155532	0.736891462	-1.127826896
C	6	1.250155532	-0.736891462	-1.127826896
C	6	6.974728944	0.000000000	-2.260342413
C	6	5.274433293	2.411277846	-1.858637683
C	6	5.274433293	-2.411277846	-1.858637683
C	6	2.539335801	1.501365464	-1.158714434
C	6	2.539335801	-1.501365464	-1.158714434
C	6	5.815497686	0.000000000	-1.482976426
C	6	3.675501543	0.726494959	-0.946238978
C	6	3.675501543	-0.726494959	-0.946238978
C	6	4.996400991	1.164494272	-1.276946210
C	6	4.996400991	-1.164494272	-1.276946210
C	6	0.002856071	-1.405718647	-1.144893716
C	6	0.002856071	1.405718647	-1.144893716
H	1	0.002576214	-2.503611409	-1.145480158
H	1	0.002576214	2.503611409	-1.145480158

Set F n=2

Donor fragment atoms 1-34

Acceptor fragment atoms 35-62

Atom	Atomic number	x	y	z
C	6	-4.924736257	-0.727606226	-0.716288886
C	6	-4.924736257	0.727606226	-0.716288886
C	6	-6.201467092	-1.160066466	-1.195707043
C	6	-6.201467092	1.160066466	-1.195707043
C	6	-6.995160107	0.000000000	-1.505621431
C	6	-3.777164436	-1.507273697	-0.810914685
C	6	-3.777164436	1.507273697	-0.810914685
C	6	-6.417130409	-2.409344796	-1.789475776
C	6	-6.417130409	2.409344796	-1.789475776
C	6	-8.057228718	0.000000000	-2.419095317
C	6	-2.486217731	-0.747870921	-0.675438874

C	6	-2.486217731	0.747870921	-0.675438874
C	6	-5.270340848	-3.311718272	-1.713479591
C	6	-5.270340848	3.311718272	-1.713479591
C	6	-7.652325397	-2.480646468	-2.575399933
C	6	-7.652325397	2.480646468	-2.575399933
C	6	-4.017328582	-2.878926549	-1.255577516
C	6	-4.017328582	2.878926549	-1.255577516
C	6	-8.441397868	-1.362151535	-2.885111572
C	6	-8.441397868	1.362151535	-2.885111572
H	1	-7.942560342	-3.447618720	-3.011493278
H	1	-7.942560342	3.447618720	-3.011493278
C	6	-9.670255948	-1.587353062	-3.788870029
C	6	-9.670255948	1.587353062	-3.788870029
H	1	-5.360523002	-4.333616731	-2.110497549
H	1	-5.360523002	4.333616731	-2.110497549
H	1	-3.173519703	-3.581217587	-1.315136623
H	1	-3.173519703	3.581217587	-1.315136623
H	1	-9.824736916	-2.663844751	-3.953655745
H	1	-9.824736916	2.663844751	-3.953655745
H	1	-9.537577528	-1.106546590	-4.772068819
H	1	-9.537577528	1.106546590	-4.772068819
H	1	-10.582612988	-1.172574557	-3.330716923
H	1	-10.582612988	1.172574557	-3.330716923
C	6	4.923487218	0.728875204	-0.724186350
C	6	4.923487218	-0.728875204	-0.724186350
C	6	6.202655008	1.165479180	-1.192307028
C	6	6.202655008	-1.165479180	-1.192307028
C	6	6.994567848	0.000000000	-1.486627033
C	6	3.774007182	1.505411397	-0.826265336
C	6	3.774007182	-1.505411397	-0.826265336
C	6	6.418827119	2.412111465	-1.802928668
C	6	6.418827119	-2.412111465	-1.802928668
C	6	8.059530158	0.000000000	-2.388949893
C	6	2.483368881	0.747597751	-0.689729728
C	6	2.483368881	-0.747597751	-0.689729728
C	6	5.265884775	3.310251147	-1.733907394
C	6	5.265884775	-3.310251147	-1.733907394
C	6	7.643650576	2.496497671	-2.595957758
C	6	7.643650576	-2.496497671	-2.595957758
C	6	4.014025635	2.875653607	-1.276565965
C	6	4.014025635	-2.875653607	-1.276565965
C	6	8.426292307	1.354413006	-2.880329402
C	6	8.426292307	-1.354413006	-2.880329402
H	1	7.932416985	3.442863297	-3.074313704
H	1	7.932416985	-3.442863297	-3.074313704
F	9	9.512202758	1.478587647	-3.707206479

F	9	9.512202758	-1.478587647	-3.707206479
H	1	5.353688248	4.329727196	-2.137233875
H	1	5.353688248	-4.329727196	-2.137233875
H	1	3.168768671	3.575829077	-1.342300110
H	1	3.168768671	-3.575829077	-1.342300110
C	6	-1.257294317	-1.416275827	-0.633489702
C	6	-1.257294317	1.416275827	-0.633489702
C	6	1.254681825	1.416346022	-0.641862442
C	6	1.254681825	-1.416346022	-0.641862442
H	1	-1.243503073	-2.514590493	-0.636963331
H	1	-1.243503073	2.514590493	-0.636963331
H	1	1.240970925	2.514686502	-0.644781294
H	1	1.240970925	-2.514686502	-0.644781294
C	6	-0.001110268	-0.724391836	-0.615671755
C	6	-0.001110268	0.724391836	-0.615671755

Set F n=3

Donor fragment atoms	1-34
Acceptor fragment atoms	35-62

Atom	Atomic number	x	y	z
C	6	-6.091440060	-0.728202953	-0.886458919
C	6	-6.091440060	0.728202953	-0.886458919
C	6	-7.410120998	-1.159513429	-1.226515670
C	6	-7.410120998	1.159513429	-1.226515670
C	6	-8.233384970	0.000000000	-1.443097142
C	6	-4.960933608	-1.510082118	-1.087504896
C	6	-4.960933608	1.510082118	-1.087504896
C	6	-7.692541876	-2.410779545	-1.786986842
C	6	-7.692541876	2.410779545	-1.786986842
C	6	-9.398425778	0.000000000	-2.218715132
C	6	-3.659584345	-0.752890864	-1.033349514
C	6	-3.659584345	0.752890864	-1.033349514
C	6	-6.543134769	-3.311285461	-1.834051882
C	6	-6.543134769	3.311285461	-1.834051882
C	6	-9.013848287	-2.481956784	-2.420100774
C	6	-9.013848287	2.481956784	-2.420100774
C	6	-5.247257571	-2.879686481	-1.507577884
C	6	-5.247257571	2.879686481	-1.507577884
C	6	-9.836058810	-1.363945548	-2.630562059
C	6	-9.836058810	1.363945548	-2.630562059
H	1	-9.356882498	-3.449326912	-2.815042277
H	1	-9.356882498	3.449326912	-2.815042277
C	6	-11.171080626	-1.590247405	-3.368710367
C	6	-11.171080626	1.590247405	-3.368710367

H	1	-6.673201572	-4.333561146	-2.219065183
H	1	-6.673201572	4.333561146	-2.219065183
H	1	-4.415605979	-3.583943845	-1.653912427
H	1	-4.415605979	3.583943845	-1.653912427
H	1	-11.345354068	-2.666928204	-3.511567707
H	1	-11.345354068	2.666928204	-3.511567707
H	1	-11.167127403	-1.109775048	-4.361045717
H	1	-11.167127403	1.109775048	-4.361045717
H	1	-12.016703690	-1.175942205	-2.796267365
H	1	-12.016703690	1.175942205	-2.796267365
C	6	6.213536388	0.729464288	-0.517640967
C	6	6.213536388	-0.729464288	-0.517640967
C	6	7.550133715	1.164901249	-0.771500943
C	6	7.550133715	-1.164901249	-0.771500943
C	6	8.379636372	0.000000000	-0.928428621
C	6	5.095577611	1.508166165	-0.791818460
C	6	5.095577611	-1.508166165	-0.791818460
C	6	7.866147690	2.413905642	-1.331127094
C	6	7.866147690	-2.413905642	-1.331127094
C	6	9.584587906	0.000000000	-1.631784181
C	6	3.793605916	0.752535038	-0.816698488
C	6	3.793605916	-0.752535038	-0.816698488
C	6	6.716678005	3.310802749	-1.449666754
C	6	6.716678005	-3.310802749	-1.449666754
C	6	9.209621383	2.498382292	-1.902227270
C	6	9.209621383	-2.498382292	-1.902227270
C	6	5.405760433	2.876748592	-1.198810902
C	6	5.405760433	-2.876748592	-1.198810902
C	6	10.030157971	1.356514635	-2.048524570
C	6	10.030157971	-1.356514635	-2.048524570
H	1	9.578818142	3.445763150	-2.319279890
H	1	9.578818142	-3.445763150	-2.319279890
F	9	11.244140432	1.484713923	-2.671498539
F	9	11.244140432	-1.484713923	-2.671498539
H	1	6.867008845	4.331140023	-1.831940254
H	1	6.867008845	-4.331140023	-1.831940254
H	1	4.583094106	3.578722052	-1.398462531
H	1	4.583094106	-3.578722052	-1.398462531
C	6	-2.437355399	-1.419713178	-1.018534083
C	6	-2.437355399	1.419713178	-1.018534083
C	6	2.572657036	1.419732261	-0.874100235
C	6	2.572657036	-1.419732261	-0.874100235
H	1	-2.424093813	-2.518201896	-1.017469083
H	1	-2.424093813	2.518201896	-1.017469083
H	1	2.559276850	2.518230528	-0.873451211
H	1	2.559276850	-2.518230528	-0.873451211

C	6	-1.168706544	-0.730630778	-0.989494609
C	6	-1.168706544	0.730630778	-0.989494609
C	6	1.304698659	0.730627840	-0.918740955
C	6	1.304698659	-0.730627840	-0.918740955
C	6	0.067953376	-1.423997321	-0.955390020
C	6	0.067953376	1.423997321	-0.955390020
H	1	0.067888589	-2.522986656	-0.953581122
H	1	0.067888589	2.522986656	-0.953581122

Molecules 1-6

Molecule 6

Donor fragment atoms 1-4

Acceptor fragment atoms 12-15

Atom	Atomic number	x	y	z
C	6	-1.248295430	-0.498767170	-0.668978630
C	6	-1.248295430	-0.498767170	0.668978630
H	1	-1.938879250	-0.999407950	-1.340615510
H	1	-1.938879250	-0.999407950	1.340615510
C	6	0.000001310	0.293537800	-1.125253200
C	6	0.000001310	0.293537800	1.125253200
C	6	-0.000000870	1.381315350	0.000000000
H	1	-0.000000080	0.633220020	-2.164591550
H	1	-0.000000080	0.633220020	2.164591550
H	1	0.904234110	2.002678390	0.000000000
H	1	-0.904237870	2.002675530	0.000000000
C	6	1.248300080	-0.498763230	-0.668978690
C	6	1.248300080	-0.498763230	0.668978690
H	1	1.938878660	-0.999407650	-1.340618370
H	1	1.938878660	-0.999407650	1.340618370

Molecule 5

Donor fragment atoms 1-4

Acceptor fragment atoms 23-26

Atom	Atomic number	x	y	Z
C	6	-2.413944480	0.671404300	0.757408020
C	6	-2.413944480	-0.671404300	0.757408020
H	1	-2.947037460	1.330205320	1.437165260
H	1	-2.947037460	-1.330205320	1.437165260
C	6	0.000000000	0.788329780	0.414077370
C	6	0.000000000	-0.788329780	0.414077370
C	6	1.374406460	1.130739930	-0.272311060
C	6	-1.374406460	1.130739930	-0.272311060

C	6	1.374406460	-1.130739930	-0.272311060
C	6	-1.374406460	-1.130739930	-0.272311060
C	6	1.567090630	0.000000000	-1.315104250
C	6	-1.567090630	0.000000000	-1.315104250
H	1	0.000000000	1.206547740	1.425251600
H	1	0.000000000	-1.206547740	1.425251600
H	1	1.465725780	2.162371400	-0.625313100
H	1	-1.465725780	2.162371400	-0.625313100
H	1	1.465725780	-2.162371400	-0.625313100
H	1	-1.465725780	-2.162371400	-0.625313100
H	1	2.582526450	0.000000000	-1.727094050
H	1	-2.582526450	0.000000000	-1.727094050
H	1	0.857021270	0.000000000	-2.139964580
H	1	-0.857021270	0.000000000	-2.139964580
C	6	2.413944480	0.671404300	0.757408020
C	6	2.413944480	-0.671404300	0.757408020
H	1	2.947037460	1.330205320	1.437165260
H	1	2.947037460	-1.330205320	1.437165260

Molecule 4

Donor fragment atoms	1-4
Acceptor fragment atoms	34-37

Atom	Atomic number	x	y	Z
C	6	-3.538601400	0.671957370	1.097583060
C	6	-3.538601400	-0.671957370	1.097583060
H	1	-3.934170960	1.329352970	1.866853710
H	1	-3.934170960	-1.329352970	1.866853710
H	1	-1.063909770	-1.205852270	1.333949800
C	6	1.227082250	0.790673550	0.334001390
C	6	-1.227082250	0.790673550	0.334001390
C	6	1.227082250	-0.790673550	0.334001390
C	6	-1.227082250	-0.790673550	0.334001390
C	6	0.000000000	1.137064810	-0.565299510
C	6	0.000000000	-1.137064810	-0.565299510
C	6	0.000000000	0.000000000	-1.608678940
C	6	2.703883410	1.131217600	-0.101163800
C	6	-2.703883410	1.131217600	-0.101163800
C	6	2.703883410	-1.131217600	-0.101163800
C	6	-2.703883410	-1.131217600	-0.101163800
C	6	3.083953380	0.000000000	-1.090465070
C	6	-3.083953380	0.000000000	-1.090465070
H	1	1.063909770	1.205852270	1.333949800
H	1	-1.063909770	1.205852270	1.333949800
H	1	0.000000000	2.161071780	-0.955638710

H	1	0.000000000	-2.161071780	-0.955638710
H	1	2.856274370	2.162831540	-0.432389230
H	1	-2.856274370	2.162831540	-0.432389230
H	1	2.856274370	-2.162831540	-0.432389230
H	1	-2.856274370	-2.162831540	-0.432389230
H	1	4.158770080	0.000000000	-1.304090020
H	1	-4.158770080	0.000000000	-1.304090020
H	1	2.543165210	0.000000000	-2.035144570
H	1	-2.543165210	0.000000000	-2.035144570
H	1	-0.869065460	0.000000000	-2.260639910
H	1	0.869065460	0.000000000	-2.260639910
H	1	1.063909770	-1.205852270	1.333949800
C	6	3.538601400	0.671957370	1.097583060
C	6	3.538601400	-0.671957370	1.097583060
H	1	3.934170960	1.329352970	1.866853710
H	1	3.934170960	-1.329352970	1.866853710

Molecule 3

Donor fragment atoms 1-4

Acceptor fragment atoms 45-48

Atom	Atomic number	x	y	z
C	6	-4.551004890	-0.671976510	-1.689441320
C	6	-4.551004890	0.671976510	-1.689441320
H	1	-4.798581600	-1.329657670	-2.518856290
H	1	-4.798581600	1.329657670	-2.518856290
C	6	0.000000000	-0.793795820	-0.088609480
C	6	0.000000000	0.793795820	-0.088609480
C	6	1.367238160	-1.137556080	0.580586850
C	6	-1.367238160	-1.137556080	0.580586850
C	6	1.367238160	1.137556080	0.580586850
C	6	-1.367238160	1.137556080	0.580586850
C	6	2.416204210	-0.791034160	-0.522463980
C	6	-2.416204210	-0.791034160	-0.522463980
C	6	2.416204210	0.791034160	-0.522463980
C	6	-2.416204210	0.791034160	-0.522463980
C	6	1.560077070	0.000000000	1.605518700
C	6	-1.560077070	0.000000000	1.605518700
H	1	0.000000000	-1.204146390	-1.105282190
H	1	0.000000000	1.204146390	-1.105282190
H	1	2.078388210	-1.206431980	-1.478203890
H	1	-2.078388210	-1.206431980	-1.478203890
H	1	2.078388210	1.206431980	-1.478203890
H	1	-2.078388210	1.206431980	-1.478203890
H	1	1.437564020	-2.161850930	0.965642150

H	1	-1.437564020	-2.161850930	0.965642150
H	1	1.437564020	2.161850930	0.965642150
H	1	-1.437564020	2.161850930	0.965642150
H	1	2.538192510	0.000000000	2.079180240
H	1	-2.538192510	0.000000000	2.079180240
H	1	0.832964600	0.000000000	2.413367990
H	1	-0.832964600	0.000000000	2.413367990
C	6	3.947604420	-1.131268620	-0.359369840
C	6	-3.947604420	-1.131268620	-0.359369840
C	6	3.947604420	1.131268620	-0.359369840
C	6	-3.947604420	1.131268620	-0.359369840
C	6	4.501271250	0.000000000	0.544248640
C	6	-4.501271250	0.000000000	0.544248640
H	1	4.157498360	-2.163451910	-0.061099090
H	1	-4.157498360	-2.163451910	-0.061099090
H	1	4.157498360	2.163451910	-0.061099090
H	1	-4.157498360	2.163451910	-0.061099090
H	1	5.597698690	0.000000000	0.558684710
H	1	-5.597698690	0.000000000	0.558684710
H	1	4.141984940	0.000000000	1.572361830
H	1	-4.141984940	0.000000000	1.572361830
C	6	4.551004890	-0.671976510	-1.689441320
C	6	4.551004890	0.671976510	-1.689441320
H	1	4.798581600	-1.329657670	-2.518856290
H	1	4.798581600	1.329657670	-2.518856290

Molecule 2

Donor fragment atoms	1-4
Acceptor fragment atoms	56-59

Atom	Atomic number	x	y	Z
C	6	-5.416092400	0.672015730	-2.195575710
C	6	-5.416092400	-0.672015730	-2.195575710
H	1	-5.510353570	-1.329322460	-3.055623770
H	1	-5.510353570	1.329322460	-3.055623770
C	6	-1.227782490	0.794171090	0.197746010
C	6	1.227782490	0.794171090	0.197746010
C	6	-1.227782490	-0.794171090	0.197746010
C	6	1.227782490	-0.794171090	0.197746010
C	6	0.000000000	1.138143660	1.098915580
C	6	0.000000000	-1.138143660	1.098915580
C	6	0.000000000	0.000000000	2.141408210
C	6	2.693095920	1.137699600	0.611054960
C	6	-2.693095920	1.137699600	0.611054960
C	6	2.693095920	-1.137699600	0.611054960

C	6	-2.693095920	-1.137699600	0.611054960
C	6	3.069033620	0.000000000	1.583827730
C	6	-3.069033620	0.000000000	1.583827730
C	6	3.526557210	0.791110520	-0.662922200
C	6	-3.526557210	0.791110520	-0.662922200
C	6	3.526557210	-0.791110520	-0.662922200
C	6	-3.526557210	-0.791110520	-0.662922200
C	6	5.770178790	0.000000000	0.010293770
C	6	-5.770178790	0.000000000	0.010293770
H	1	5.322522160	2.162931920	-0.523059550
H	1	-5.322522160	2.162931920	-0.523059550
H	1	5.322522160	-2.162931920	-0.523059550
H	1	-5.322522160	-2.162931920	-0.523059550
H	1	6.850565910	0.000000000	-0.173731580
H	1	-6.850565910	0.000000000	-0.173731580
H	1	5.602896690	0.000000000	1.085895420
H	1	-5.602896690	0.000000000	1.085895420
C	6	5.062405590	1.131358860	-0.778489170
C	6	-5.062405590	1.131358860	-0.778489170
C	6	5.062405590	-1.131358860	-0.778489170
C	6	-5.062405590	-1.131358860	-0.778489170
H	1	1.047656180	1.203669670	-0.802401010
H	1	-1.047656180	1.203669670	-0.802401010
H	1	1.047656180	-1.203669670	-0.802401010
H	1	-1.047656180	-1.203669670	-0.802401010
H	1	3.022535320	-1.205938580	-1.541887640
H	1	-3.022535320	-1.205938580	-1.541887640
H	1	3.022535320	1.205938580	-1.541887640
H	1	-3.022535320	1.205938580	-1.541887640
H	1	0.000000000	-2.161495690	1.490990760
H	1	0.000000000	2.161495690	1.490990760
H	1	2.831708190	2.161351200	0.976981520
H	1	-2.831708190	2.161351200	0.976981520
H	1	2.831708190	-2.161351200	0.976981520
H	1	-2.831708190	-2.161351200	0.976981520
H	1	4.116725440	0.000000000	1.870371700
H	1	-4.116725440	0.000000000	1.870371700
H	1	2.502742530	0.000000000	2.510918140
H	1	-2.502742530	0.000000000	2.510918140
H	1	0.867844640	0.000000000	2.794458630
H	1	-0.867844640	0.000000000	2.794458630
C	6	5.416092400	0.672015730	-2.195575710
C	6	5.416092400	-0.672015730	-2.195575710
H	1	5.510353570	-1.329322460	-3.055623770
H	1	5.510353570	1.329322460	-3.055623770

Molecule 1				
Donor fragment atoms	1-4			
Acceptor fragment atoms	67-70			
Atom	Atomic number	x	y	z
C	6	-6.10241	-0.67202	-3.32618
C	6	-6.10241	0.67202	-3.32618
H	1	-6.03960	-1.32933	-4.18910
H	1	-6.03960	1.32933	-4.18910
C	6	0.00000	-0.79455	0.22545
C	6	0.00000	0.79455	0.22545
C	6	1.36981	-1.13824	0.89187
C	6	-1.36981	-1.13824	0.89187
C	6	1.36981	1.13824	0.89187
C	6	-1.36981	1.13824	0.89187
C	6	2.41541	-0.79425	-0.21578
C	6	-2.41541	-0.79425	-0.21578
C	6	2.41541	0.79425	-0.21578
C	6	-2.41541	0.79425	-0.21578
C	6	1.55935	0.00000	1.91688
C	6	-1.55935	0.00000	1.91688
H	1	0.00000	-1.20355	-0.79088
H	1	0.00000	1.20355	-0.79088
H	1	2.05822	-1.20367	-1.16718
H	1	-2.05822	-1.20367	-1.16718
H	1	2.05822	1.20367	-1.16718
H	1	-2.05822	1.20367	-1.16718
H	1	1.44059	-2.16154	1.27764
H	1	-1.44059	-2.16154	1.27764
H	1	1.44059	2.16154	1.27764
H	1	-1.44059	2.16154	1.27764
H	1	2.53189	0.00000	2.40029
H	1	-2.53189	0.00000	2.40029
H	1	0.82605	0.00000	2.71809
H	1	-0.82605	0.00000	2.71809
C	6	3.93134	-1.13772	-0.07368
C	6	-3.93134	-1.13772	-0.07368
C	6	3.93134	1.13772	-0.07368
C	6	-3.93134	1.13772	-0.07368
C	6	4.52099	-0.79111	-1.47728
C	6	-4.52099	-0.79111	-1.47728
C	6	4.52099	0.79111	-1.47728
C	6	-4.52099	0.79111	-1.47728
C	6	4.47711	0.00000	0.81498
C	6	-4.47711	0.00000	0.81498
H	1	3.86652	-1.20593	-2.25077

H	1	-3.86652	-1.20593	-2.25077
H	1	3.86652	1.20593	-2.25077
H	1	-3.86652	1.20593	-2.25077
H	1	4.13382	-2.16136	0.26119
H	1	-4.13382	-2.16136	0.26119
H	1	4.13382	2.16136	0.26119
H	1	-4.13382	2.16136	0.26119
H	1	5.55937	0.00000	0.90700
H	1	-5.55937	0.00000	0.90700
H	1	4.08823	0.00000	1.82934
H	1	-4.08823	0.00000	1.82934
C	6	6.01070	-1.13136	-1.86850
C	6	-6.01070	-1.13136	-1.86850
C	6	6.01070	1.13136	-1.86850
C	6	-6.01070	1.13136	-1.86850
C	6	6.84946	0.00000	-1.22071
C	6	-6.84946	0.00000	-1.22071
H	1	6.31270	-2.16293	-1.66429
H	1	-6.31270	-2.16293	-1.66429
H	1	6.31270	2.16293	-1.66429
H	1	-6.31270	2.16293	-1.66429
H	1	7.87874	0.00000	-1.59712
H	1	-7.87874	0.00000	-1.59712
H	1	6.87951	0.00000	-0.13260
H	1	-6.87951	0.00000	-0.13260
C	6	6.10241	-0.67202	-3.32618
C	6	6.10241	0.67202	-3.32618
H	1	6.03960	-1.32933	-4.18910
H	1	6.03960	1.32933	-4.18910

Molecules 7-10

Molecule 7	
b1 set	
Acceptor fragment atoms	5-6
Donor fragment atoms	25-34
b2 set	
Acceptor fragment atoms	1-6
Donor fragment atoms	25-48
b3 set	
Acceptor fragment atoms	5-6
Donor fragment atoms	29-30
b4 set	
Acceptor fragment atoms	5-6
Donor fragment atoms	39,44

Atom	Atomic number	x	y	z
C	6	-3.333579964	8.172398048	-1.235011529
C	6	-3.333579964	8.172398048	1.235011529
N	7	-3.745553192	8.555479528	-2.214408977
N	7	-3.745553192	8.555479528	2.214408977
C	6	-2.794019388	7.666664025	0.000000000
C	6	-1.827037575	6.755351626	0.000000000
C	6	-0.557384707	3.375934385	-1.139537463
C	6	-0.557384707	3.375934385	1.139537463
C	6	-0.958866494	6.078422110	-1.038961389
C	6	-0.958866494	6.078422110	1.038961389
C	6	0.486018796	3.294066309	0.000000000
C	6	0.161162294	6.386126489	0.000000000
H	1	-0.190656486	3.333587069	-2.155085308
H	1	-0.190656486	3.333587069	2.155085308
H	1	-0.917617737	6.434664364	-2.056806645
H	1	-0.917617737	6.434664364	2.056806645
H	1	0.989936594	2.335195562	0.000000000
H	1	0.407441979	7.441040330	0.000000000
H	1	1.240548757	4.059257160	0.000000000
H	1	1.070034570	5.816921438	0.000000000
C	6	-1.418951260	4.619091810	-0.784143090
C	6	-1.418951260	4.619091810	0.784143090
H	1	-2.410919715	4.502623878	-1.201431097
H	1	-2.410919715	4.502623878	1.201431097
C	6	-1.418483765	2.196013293	-0.715541534
C	6	-1.418483765	2.196013293	0.715541534
C	6	-2.072535655	1.251459007	-1.416266775
C	6	-2.072535655	1.251459007	1.416266775

C	6	-2.747981310	0.202545905	-0.704931834
C	6	-2.747981310	0.202545905	0.704931834
C	6	-3.383720479	-0.860243350	-1.389785130
C	6	-3.383720479	-0.860243350	1.389785130
C	6	-3.999199767	-1.862298978	-0.704495172
C	6	-3.999199767	-1.862298978	0.704495172
H	1	-4.476651628	-2.664691530	-1.237887507
H	1	-4.476651628	-2.664691530	1.237887507
H	1	-3.357018132	-0.872580285	-2.462284169
H	1	-3.357018132	-0.872580285	2.462284169
O	8	-2.056152789	1.223074122	-2.777444940
C	6	-3.086536380	1.934638713	-3.421607891
H	1	-4.064215500	1.596715389	-3.092489977
H	1	-2.979915759	1.747986061	-4.481137797
H	1	-2.999640434	3.000952051	-3.237589256
O	8	-2.056152789	1.223074122	2.777444940
C	6	-3.086536380	1.934638713	3.421607891
H	1	-4.064215500	1.596715389	3.092489977
H	1	-2.979915759	1.747986061	4.481137797
H	1	-2.999640434	3.000952051	3.237589256

Molecule 8

b1 set	
Acceptor fragment atoms	5-6
Donor fragment atoms	7-16
b2 set	
Acceptor fragment atoms	1-6
Donor fragment atoms	7-30
b3 set	
Acceptor fragment atoms	5-6
Donor fragment atoms	11-12
b4 set	
Acceptor fragment atoms	5-6
Donor fragment atoms	21-22

Atom	Atomic number	x	y	z
C	6	-3.655769304	7.599278041	-1.234738821
C	6	-3.655769304	7.599278041	1.234738821
N	7	-4.152884553	7.865544850	-2.213387375
N	7	-4.152884553	7.865544850	2.213387375
C	6	-1.836572994	6.614035961	0.000000000
C	6	-3.004655340	7.247307959	0.000000000
C	6	-0.650264186	-0.141388687	-0.715537631
C	6	-0.650264186	-0.141388687	0.715537631
C	6	-1.397873187	-1.014329843	-1.415411127

C	6	-1.397873187	-1.014329843	1.415411127
C	6	-2.180950280	-1.986145273	-0.704916470
C	6	-2.180950280	-1.986145273	0.704916470
C	6	-2.925913964	-2.975605296	-1.389541153
C	6	-2.925913964	-2.975605296	1.389541153
C	6	-3.644458049	-3.906907032	-0.704423210
C	6	-3.644458049	-3.906907032	0.704423210
H	1	-4.204334915	-4.654018146	-1.238132946
H	1	-4.204334915	-4.654018146	1.238132946
H	1	-2.900611335	-2.990609295	-2.462083937
H	1	-2.900611335	-2.990609295	2.462083937
O	8	-1.383213040	-1.048461987	-2.777837838
O	8	-1.383213040	-1.048461987	2.777837838
C	6	-2.322127573	-0.223679980	-3.423973621
C	6	-2.322127573	-0.223679980	3.423973621
H	1	-3.333238997	-0.443975191	-3.095302407
H	1	-3.333238997	-0.443975191	3.095302407
H	1	-2.237782770	-0.423492086	-4.483366147
H	1	-2.237782770	-0.423492086	4.483366147
H	1	-2.111316657	0.825720779	-3.242203167
H	1	-2.111316657	0.825720779	3.242203167
C	6	-0.391622909	2.278443708	-0.786550414
C	6	-0.391622909	2.278443708	0.786550414
C	6	0.330149300	0.942213692	-1.135848399
C	6	0.330149300	0.942213692	1.135848399
C	6	-0.822041906	6.184270282	-1.039263263
C	6	-0.822041906	6.184270282	1.039263263
C	6	1.360375386	0.740572291	0.000000000
C	6	0.174915367	6.781284914	0.000000000
H	1	-1.392410678	2.234214167	-1.195872140
H	1	-1.392410678	2.234214167	1.195872140
H	1	0.688715370	0.861742683	-2.152522386
H	1	0.688715370	0.861742683	2.152522386
H	1	-0.875664742	6.539281222	-2.056972861
H	1	-0.875664742	6.539281222	2.056972861
H	1	1.751275224	-0.270127822	0.000000000
H	1	0.121723057	7.863577357	0.000000000
H	1	2.199042280	1.413808592	0.000000000
H	1	1.206524790	6.488888894	0.000000000
C	6	0.234988414	3.657587771	-1.135926195
C	6	0.234988414	3.657587771	1.135926195
C	6	-0.898017571	4.655106456	-0.785510740
C	6	-0.898017571	4.655106456	0.785510740
C	6	1.249192962	3.869295483	0.000000000
H	1	-1.833765411	4.306690663	-1.205534513
H	1	-1.833765411	4.306690663	1.205534513

H	1	1.720219561	4.833104582	0.000000000
H	1	2.048993065	3.154040901	0.000000000
H	1	0.612676922	3.737108698	-2.148909508
H	1	0.612676922	3.737108698	2.148909508

Molecule 9	
b1 set	
Acceptor fragment atoms	5-6
Donor fragment atoms	7-16
b2 set	
Acceptor fragment atoms	1-6
Donor fragment atoms	7-30
b3 set	
Acceptor fragment atoms	5-6
Donor fragment atoms	11-12
b4 set	
Acceptor fragment atoms	5-6
Donor fragment atoms	21-22

Atom	Atomic number	x	y	z
C	6	-4.117406353	6.708174255	-1.234631986
C	6	-4.117406353	6.708174255	1.234631986
N	7	-4.660124533	6.863252666	-2.212990811
N	7	-4.660124533	6.863252666	2.212990811
C	6	-3.406295636	6.502519092	0.000000000
C	6	-2.130348701	6.131463942	0.000000000
C	6	-0.326192274	-2.588268734	-0.715672095
C	6	-0.326192274	-2.588268734	0.715672095
C	6	-1.205028393	-3.329408212	-1.414968231
C	6	-1.205028393	-3.329408212	1.414968231
C	6	-2.135990059	-4.160696540	-0.704915462
C	6	-2.135990059	-4.160696540	0.704915462
C	6	-3.033252042	-5.014516551	-1.389403608
C	6	-3.033252042	-5.014516551	1.389403608
C	6	-3.895005803	-5.815376427	-0.704453511
C	6	-3.895005803	-5.815376427	0.704453511
H	1	-4.570080172	-6.460404037	-1.238122774
H	1	-4.570080172	-6.460404037	1.238122774
H	1	-3.011015689	-5.032937992	-2.461996096
H	1	-3.011015689	-5.032937992	2.461996096
O	8	-1.197104842	-3.366503634	-2.777825697
O	8	-1.197104842	-3.366503634	2.777825697
C	6	-1.981057883	-2.393317002	-3.422819625
C	6	-1.981057883	-2.393317002	3.422819625
H	1	-3.014863496	-2.437876305	-3.093388533

H	1	-3.014863496	-2.437876305	3.093388533
H	1	-1.933385655	-2.604084597	-4.482500963
H	1	-1.933385655	-2.604084597	4.482500963
H	1	-1.594097163	-1.395456438	-3.240716395
H	1	-1.594097163	-1.395456438	3.240716395
C	6	0.314605371	-0.240993622	-0.786040500
C	6	0.314605371	-0.240993622	0.786040500
C	6	0.814991950	-1.675268353	-1.135629232
C	6	0.814991950	-1.675268353	1.135629232
C	6	-1.047666078	5.927049061	-1.039261525
C	6	-1.047666078	5.927049061	1.039261525
C	6	1.799419031	-2.040819190	0.000000000
C	6	-0.201960081	6.724224206	0.000000000
H	1	-0.680648477	-0.127903110	-1.195523185
H	1	-0.680648477	-0.127903110	1.195523185
H	1	1.156580607	-1.812490637	-2.152220274
H	1	1.156580607	-1.812490637	2.152220274
H	1	-1.176076689	6.262592890	-2.056947617
H	1	-1.176076689	6.262592890	2.056947617
H	1	2.022217902	-3.101691635	0.000000000
H	1	-0.487798812	7.769567763	0.000000000
H	1	2.735440511	-1.511671731	0.000000000
H	1	0.868480120	6.662509288	0.000000000
C	6	0.517605934	3.675791803	-1.135944998
C	6	0.517605934	3.675791803	1.135944998
C	6	-0.799245512	4.415923315	-0.785755264
C	6	-0.799245512	4.415923315	0.785755264
C	6	1.460943220	4.104223845	0.000000000
H	1	-1.641659490	3.880012464	-1.205663792
H	1	-1.641659490	3.880012464	1.205663792
H	1	1.700238264	5.149676077	0.000000000
H	1	2.403613188	3.592705669	0.000000000
H	1	0.870175148	3.833036046	-2.148953819
H	1	0.870175148	3.833036046	2.148953819
C	6	1.148304027	1.024228288	-1.132146332
C	6	1.148304027	1.024228288	1.132146332
C	6	0.186819359	2.195887291	-0.787849094
C	6	0.186819359	2.195887291	0.787849094
C	6	2.186925017	1.064523481	0.000000000
H	1	-0.787181111	1.963125255	-1.199425735
H	1	-0.787181111	1.963125255	1.199425735
H	1	2.814951142	1.935396727	0.000000000
H	1	2.855958116	0.225476440	0.000000000
H	1	1.531825283	1.043212564	-2.146533568
H	1	1.531825283	1.043212564	2.146533568

Molecule 10	
b1 set	
Acceptor fragment atoms	5-6
Donor fragment atoms	7-16
b2 set	
Acceptor fragment atoms	1-6
Donor fragment atoms	7-30
b3 set	
Acceptor fragment atoms	5-6
Donor fragment atoms	11-12
b4 set	
Acceptor fragment atoms	5-6
Donor fragment atoms	21-22

Atom	Atomic number	x	y	z
C	6	-4.609551548	5.843042593	-1.234574102
C	6	-4.609551548	5.843042593	1.234574102
N	7	-5.168685583	5.922660646	-2.212744238
N	7	-5.168685583	5.922660646	2.212744238
C	6	-3.876854253	5.736737210	0.000000000
C	6	-2.561928108	5.544478707	0.000000000
C	6	-0.881938179	-4.963325371	-0.715768809
C	6	-0.881938179	-4.963325371	0.715768809
C	6	-1.909670897	-5.479041678	-1.414760664
C	6	-1.909670897	-5.479041678	1.414760664
C	6	-3.009331380	-6.069451786	-0.704871568
C	6	-3.009331380	-6.069451786	0.704871568
C	6	-4.081871598	-6.689099686	-1.389336202
C	6	-4.081871598	-6.689099686	1.389336202
C	6	-5.107419077	-7.265552086	-0.704456668
C	6	-5.107419077	-7.265552086	0.704456668
H	1	-5.915045195	-7.734028433	-1.238223826
H	1	-5.915045195	-7.734028433	1.238223826
H	1	-4.064631892	-6.711964725	-2.461940178
H	1	-4.064631892	-6.711964725	2.461940178
O	8	-1.911406375	-5.516947831	-2.777787093
O	8	-1.911406375	-5.516947831	2.777787093
C	6	-2.444816164	-4.386410304	-3.421773332
C	6	-2.444816164	-4.386410304	3.421773332
H	1	-3.459637321	-4.186650141	-3.090737070
H	1	-3.459637321	-4.186650141	3.090737070
H	1	-2.449555757	-4.602284628	-4.481522656
H	1	-2.449555757	-4.602284628	4.481522656
H	1	-1.833740545	-3.507718281	-3.240393746

H	1	-1.833740545	-3.507718281	3.240393746
C	6	0.729101394	-0.429293491	-0.787435359
C	6	0.729101394	-0.429293491	0.787435359
C	6	0.440490143	-4.340964816	-1.135598215
C	6	0.440490143	-4.340964816	1.135598215
C	6	-1.461382928	5.492295961	-1.039313663
C	6	-1.461382928	5.492295961	1.039313663
C	6	1.312395002	-4.926230500	0.000000000
C	6	-0.735253230	6.399735558	0.000000000
H	1	-0.272183350	-0.431798185	-1.199277362
H	1	-0.272183350	-0.431798185	1.199277362
H	1	0.740827524	-4.554136782	-2.152171171
H	1	0.740827524	-4.554136782	2.152171171
H	1	-1.635237063	5.806884734	-2.056942537
H	1	-1.635237063	5.806884734	2.056942537
H	1	1.281700247	-6.009834792	0.000000000
H	1	-1.163984066	7.395153546	0.000000000
H	1	2.345839823	-4.629752066	0.000000000
H	1	0.333268512	6.487976038	0.000000000
C	6	0.402010208	3.480136819	-1.135992853
C	6	0.402010208	3.480136819	1.135992853
C	6	-1.005057265	4.030395285	-0.785801389
C	6	-1.005057265	4.030395285	0.785801389
C	6	1.275242377	4.037661095	0.000000000
H	1	-1.764837940	3.382727817	-1.205722428
H	1	-1.764837940	3.382727817	1.205722428
H	1	1.362273229	5.106451994	0.000000000
H	1	2.281846627	3.667717547	0.000000000
H	1	0.729238573	3.684999394	-2.149009304
H	1	0.729238573	3.684999394	2.149009304
C	6	1.389782301	0.936298092	-1.132140869
C	6	1.389782301	0.936298092	1.132140869
C	6	0.278258156	1.968351800	-0.788049153
C	6	0.278258156	1.968351800	0.788049153
C	6	2.411435821	1.127146558	0.000000000
H	1	-0.655151966	1.605963154	-1.199448228
H	1	-0.655151966	1.605963154	1.199448228
H	1	2.897931361	2.083936212	0.000000000
H	1	3.203598895	0.404002330	0.000000000
C	6	1.392730593	-1.792483256	-1.131909748
C	6	1.392730593	-1.792483256	1.131909748
C	6	0.287918966	-2.829481756	-0.786054123
C	6	0.287918966	-2.829481756	0.786054123
C	6	2.412174534	-1.996432983	0.000000000
H	1	3.225965084	-1.296402788	0.000000000
H	1	2.866865355	-2.968738020	0.000000000

H	1	-0.653898267	-2.487963718	-1.195188990
H	1	-0.653898267	-2.487963718	1.195188990
H	1	1.770408150	-1.863705426	-2.146404512
H	1	1.770408150	-1.863705426	2.146404512
H	1	1.767236742	1.007886840	-2.146576312
H	1	1.767236742	1.007886840	2.146576312

C_6H_8 molecule

C_6H_8 molecule	
Donor and acceptor defined as end C atoms	
Acceptor fragment atoms	2
Donor fragment atoms	12
Donor and acceptor defined as end CH_2 groups	
Acceptor fragment atoms	1-3
Donor fragment atoms	12-14
Donor and acceptor defined as end ethylene groups	
Acceptor fragment atoms	1-5
Donor fragment atoms	10-14

Atom	Atomic number	x	y	z
H	1	-3.9926071	-0.4250985	0.0000000
C	6	-3.0773443	0.1594221	0.0000000
H	1	-3.1888863	1.2416407	0.0000000
C	6	-1.8670459	-0.4234643	0.0000000
H	1	-1.8017188	-1.5123468	0.0000000
C	6	-0.6079620	0.2962234	0.0000000
C	6	0.6079620	-0.2962234	0.0000000
H	1	-0.6643885	1.3859510	0.0000000
H	1	0.6643885	-1.3859510	0.0000000
H	1	1.8017188	1.5123468	0.0000000
C	6	1.8670459	0.4234643	0.0000000
C	6	3.0773443	-0.1594221	0.0000000
H	1	3.1888863	-1.2416407	0.0000000
H	1	3.9926071	0.4250985	0.0000000

Anthracene-dimer

Anthracene-dimer R=3Å	
Acceptor fragment atoms	1-24
Donor fragment atoms	25-48

Atom	Atomic number	x	y	z
C	6	9.974744	7.224319	5.500548
C	6	11.22914	7.907745	5.499884
C	6	12.413696	7.212081	5.499204
C	6	12.413696	5.78792	5.499204
C	6	11.22914	5.092256	5.499884
C	6	9.974744	5.775682	5.500548
C	6	8.750001	5.09408	5.501297
C	6	7.525257	5.775682	5.500548
C	6	7.525257	7.224319	5.500548
C	6	8.750001	7.905921	5.501297
C	6	6.270862	5.092256	5.499884
C	6	5.086305	5.78792	5.499204
C	6	5.086305	7.212081	5.499204
C	6	6.270862	7.907745	5.499884
H	1	11.22805	8.999792	5.499829
H	1	13.363441	7.748887	5.498539
H	1	13.363441	5.251114	5.498539
H	1	11.22805	4.000209	5.499829
H	1	8.750001	4.000775	5.501422
H	1	8.750001	8.999226	5.501422
H	1	6.271952	4.000209	5.499829
H	1	4.13656	5.251114	5.498539
H	1	4.13656	7.748887	5.498539
H	1	6.271952	8.999792	5.499829
C	6	9.974744	7.224319	8.499453
C	6	11.22914	7.907745	8.500116
C	6	12.413696	7.212081	8.500797
C	6	12.413696	5.78792	8.500797
C	6	11.22914	5.092256	8.500116
C	6	9.974744	5.775682	8.499453
C	6	8.750001	5.09408	8.498705
C	6	7.525257	5.775682	8.499453
C	6	7.525257	7.224319	8.499453
C	6	8.750001	7.905921	8.498705
C	6	6.270862	5.092256	8.500116
C	6	5.086305	5.78792	8.500797
C	6	5.086305	7.212081	8.500797
C	6	6.270862	7.907745	8.500116

H	1	11.22805	8.999792	8.500173
H	1	13.363441	7.748887	8.501461
H	1	13.363441	5.251114	8.501461
H	1	11.22805	4.000209	8.500173
H	1	8.750001	4.000775	8.498579
H	1	8.750001	8.999226	8.498579
H	1	6.271952	4.000209	8.500173
H	1	4.13656	5.251114	8.501461
H	1	4.13656	7.748887	8.501461
H	1	6.271952	8.999792	8.500173

Anthracene-dimer R=3.5Å

Acceptor fragment atoms	1-24
Donor fragment atoms	25-48

Atom	Atomic number	x	y	z
C	6	9.974865	7.224319	5.750546
C	6	11.229261	7.907745	5.749879
C	6	12.413817	7.212081	5.749201
C	6	12.413817	5.78792	5.749201
C	6	11.229261	5.092256	5.749879
C	6	9.974865	5.775682	5.750546
C	6	8.750001	5.09408	5.7513
C	6	7.525136	5.775682	5.750546
C	6	7.525136	7.224319	5.750546
C	6	8.750001	7.905921	5.7513
C	6	6.270741	5.092256	5.749879
C	6	5.086184	5.78792	5.749201
C	6	5.086184	7.212081	5.749201
C	6	6.270741	7.907745	5.749879
H	1	11.228171	8.999792	5.749822
H	1	13.363563	7.748887	5.748535
H	1	13.363563	5.251114	5.748535
H	1	11.228171	4.000209	5.749822
H	1	8.750001	4.000775	5.751429
H	1	8.750001	8.999226	5.751429
H	1	6.271831	4.000209	5.749822
H	1	4.136439	5.251114	5.748535
H	1	4.136439	7.748887	5.748535
H	1	6.271831	8.999792	5.749822
C	6	9.974865	7.224319	9.249454
C	6	11.229261	7.907745	9.250121
C	6	12.413817	7.212081	9.2508
C	6	12.413817	5.78792	9.2508

C	6	11.229261	5.092256	9.250121
C	6	9.974865	5.775682	9.249454
C	6	8.750001	5.09408	9.248701
C	6	7.525136	5.775682	9.249454
C	6	7.525136	7.224319	9.249454
C	6	8.750001	7.905921	9.248701
C	6	6.270741	5.092256	9.250121
C	6	5.086184	5.78792	9.2508
C	6	5.086184	7.212081	9.2508
C	6	6.270741	7.907745	9.250121
H	1	11.228171	8.999792	9.250179
H	1	13.363563	7.748887	9.251467
H	1	13.363563	5.251114	9.251467
H	1	11.228171	4.000209	9.250179
H	1	8.750001	4.000775	9.248572
H	1	8.750001	8.999226	9.248572
H	1	6.271831	4.000209	9.250179
H	1	4.136439	5.251114	9.251467
H	1	4.136439	7.748887	9.251467
H	1	6.271831	8.999792	9.250179

Anthracene-dimer R=3.8Å

Acceptor fragment atoms	1-24
Donor fragment atoms	25-48

Atom	Atomic number	x	y	z
C	6	9.974865	7.224319	5.450546
C	6	11.229261	7.907745	5.449879
C	6	12.413817	7.212081	5.449201
C	6	12.413817	5.78792	5.449201
C	6	11.229261	5.092256	5.449879
C	6	9.974865	5.775682	5.450546
C	6	8.750001	5.09408	5.4513
C	6	7.525136	5.775682	5.450546
C	6	7.525136	7.224319	5.450546
C	6	8.750001	7.905921	5.4513
C	6	6.270741	5.092256	5.449879
C	6	5.086184	5.78792	5.449201
C	6	5.086184	7.212081	5.449201
C	6	6.270741	7.907745	5.449879
H	1	11.228171	8.999792	5.449822
H	1	13.363563	7.748887	5.448535
H	1	13.363563	5.251114	5.448535
H	1	11.228171	4.000209	5.449822
H	1	8.750001	4.000775	5.451429

H	1	8.750001	8.999226	5.451429
H	1	6.271831	4.000209	5.449822
H	1	4.136439	5.251114	5.448535
H	1	4.136439	7.748887	5.448535
H	1	6.271831	8.999792	5.449822
C	6	9.974865	7.224319	9.249454
C	6	11.229261	7.907745	9.250121
C	6	12.413817	7.212081	9.2508
C	6	12.413817	5.78792	9.2508
C	6	11.229261	5.092256	9.250121
C	6	9.974865	5.775682	9.249454
C	6	8.750001	5.09408	9.248701
C	6	7.525136	5.775682	9.249454
C	6	7.525136	7.224319	9.249454
C	6	8.750001	7.905921	9.248701
C	6	6.270741	5.092256	9.250121
C	6	5.086184	5.78792	9.2508
C	6	5.086184	7.212081	9.2508
C	6	6.270741	7.907745	9.250121
H	1	11.228171	8.999792	9.250179
H	1	13.363563	7.748887	9.251467
H	1	13.363563	5.251114	9.251467
H	1	11.228171	4.000209	9.250179
H	1	8.750001	4.000775	9.248572
H	1	8.750001	8.999226	9.248572
H	1	6.271831	4.000209	9.250179
H	1	4.136439	5.251114	9.251467
H	1	4.136439	7.748887	9.251467
H	1	6.271831	8.999792	9.250179

Anthracene-dimer R=3.9Å

Acceptor fragment atoms	1-24
Donor fragment atoms	25-48

Atom	Atomic number	x	y	Z
C	6	9.974865	7.224319	5.350546
C	6	11.229261	7.907745	5.349879
C	6	12.413817	7.212081	5.349201
C	6	12.413817	5.78792	5.349201
C	6	11.229261	5.092256	5.349879
C	6	9.974865	5.775682	5.350546

C	6	8.750001	5.09408	5.3513
C	6	7.525136	5.775682	5.350546
C	6	7.525136	7.224319	5.350546
C	6	8.750001	7.905921	5.3513
C	6	6.270741	5.092256	5.349879
C	6	5.086184	5.78792	5.349201
C	6	5.086184	7.212081	5.349201
C	6	6.270741	7.907745	5.349879
H	1	11.228171	8.999792	5.349822
H	1	13.363563	7.748887	5.348535
H	1	13.363563	5.251114	5.348535
H	1	11.228171	4.000209	5.349822
H	1	8.750001	4.000775	5.351429
H	1	8.750001	8.999226	5.351429
H	1	6.271831	4.000209	5.349822
H	1	4.136439	5.251114	5.348535
H	1	4.136439	7.748887	5.348535
H	1	6.271831	8.999792	5.349822
C	6	9.974865	7.224319	9.249454
C	6	11.229261	7.907745	9.250121
C	6	12.413817	7.212081	9.2508
C	6	12.413817	5.78792	9.2508
C	6	11.229261	5.092256	9.250121
C	6	9.974865	5.775682	9.249454
C	6	8.750001	5.09408	9.248701
C	6	7.525136	5.775682	9.249454
C	6	7.525136	7.224319	9.249454
C	6	8.750001	7.905921	9.248701
C	6	6.270741	5.092256	9.250121
C	6	5.086184	5.78792	9.2508
C	6	5.086184	7.212081	9.2508
C	6	6.270741	7.907745	9.250121
H	1	11.228171	8.999792	9.250179
H	1	13.363563	7.748887	9.251467
H	1	13.363563	5.251114	9.251467
H	1	11.228171	4.000209	9.250179
H	1	8.750001	4.000775	9.248572
H	1	8.750001	8.999226	9.248572
H	1	6.271831	4.000209	9.250179
H	1	4.136439	5.251114	9.251467
H	1	4.136439	7.748887	9.251467
H	1	6.271831	8.999792	9.250179

Anthracene-dimer R=4.5Å

Acceptor fragment atoms	1-24
Donor fragment atoms	25-48

Atom	Atomic number	x	y	z
C	6	9.974623	7.224319	5.25055
C	6	11.229019	7.907745	5.249887
C	6	12.413575	7.212081	5.249206
C	6	12.413575	5.78792	5.249206
C	6	11.229019	5.092256	5.249887
C	6	9.974623	5.775682	5.25055
C	6	8.750001	5.09408	5.251294
C	6	7.525378	5.775682	5.25055
C	6	7.525378	7.224319	5.25055
C	6	8.750001	7.905921	5.251294
C	6	6.270982	5.092256	5.249887
C	6	5.086426	5.78792	5.249206
C	6	5.086426	7.212081	5.249206
C	6	6.270982	7.907745	5.249887
H	1	13.36332	7.748887	5.248543
H	1	13.36332	5.251114	5.248543
H	1	11.227929	4.000209	5.249834
H	1	8.750001	4.000775	5.251418
H	1	8.750001	8.999226	5.251418
H	1	6.272073	4.000209	5.249834
H	1	4.136681	5.251114	5.248543
H	1	4.136681	7.748887	5.248543
H	1	6.272073	8.999792	5.249834
H	1	11.227929	8.999792	5.249834
C	6	9.974623	7.224319	9.749452
C	6	11.229019	7.907745	9.750113
C	6	12.413575	7.212081	9.750796
C	6	12.413575	5.78792	9.750796
C	6	11.229019	5.092256	9.750113
C	6	9.974623	5.775682	9.749452
C	6	8.750001	5.09408	9.748707
C	6	7.525378	5.775682	9.749452
C	6	7.525378	7.224319	9.749452
C	6	8.750001	7.905921	9.748707
C	6	6.270982	5.092256	9.750113
C	6	5.086426	5.78792	9.750796
C	6	5.086426	7.212081	9.750796
C	6	6.270982	7.907745	9.750113
H	1	11.227929	8.999792	9.750167
H	1	13.36332	7.748887	9.751459
H	1	13.36332	5.251114	9.751459
H	1	11.227929	4.000209	9.750167

H	1	8.750001	4.000775	9.748584
H	1	8.750001	8.999226	9.748584
H	1	6.272073	4.000209	9.750167
H	1	4.136681	5.251114	9.751459
H	1	4.136681	7.748887	9.751459
H	1	6.272073	8.999792	9.750167

Ethylen-dimer

Ethylene-dimer R=3.5Å	
Acceptor fragment atoms	1-6
Donor fragment atoms	7-12

C	6	4.99966000	5.92942926	5.57336774
C	6	4.99966000	5.92942929	6.90462036
H	1	4.99966000	6.85326897	4.99902950
H	1	4.99966000	5.00559174	4.99902606
H	1	4.99966000	6.85326442	7.47896647
H	1	4.99966000	5.00559632	7.47896987
C	6	8.49966000	5.92942926	5.57336774
C	6	8.49966000	5.92942929	6.90462036
H	1	8.49966000	6.85326897	4.99902950
H	1	8.49966000	5.00559174	4.99902606
H	1	8.49966000	6.85326442	7.47896647
H	1	8.49966000	5.00559632	7.47896987